

# Neutron scattering by Polymers using spin polarized neutrons with polarization analysis.

O.Schärfp  
Berchmanskolleg  
Kaulbachstr. 31a  
80539 München  
und TU Braunschweig  
Barbara Gabrys  
Department of Materials  
University of Oxford Parks Road, Oxford OX1 3PH UK

München, March 24, 2008

# Contents

<b>1</b>	<b>Some fundamental concepts of polymer physics.</b>	<b>1</b>
1.1	Introduction . . . . .	1
1.2	Description of polymers as long flexible chains . . . . .	2
1.3	Spatial configurations of polymers . . . . .	4
1.3.1	Mathematical description of the configuration of some simplified model chains. . . . .	4
1.3.1.1	Average square of the distance of the chain ends . . . . .	5
1.3.1.2	SPECIAL chain models . . . . .	5
1.4	Elasticity in polymers: entropy and enthalpy . . . . .	8
1.5	Elastic scattering from polymers: Structure of polymers. . . . .	10
1.5.1	Small angle scattering. . . . .	10
1.5.2	Wide angle scattering . . . . .	13
<b>2</b>	<b>Long history of short range order in polymers</b>	<b>17</b>
2.1	Introduction . . . . .	17
2.2	The gist of the debate . . . . .	18
2.3	Where do we stand? . . . . .	19
2.4	Scattering from polymers . . . . .	19
2.5	Future prospects . . . . .	20
2.6	A decade later . . . . .	21
<b>3</b>	<b>Short range-order in amorphous polystyrene</b>	<b>25</b>
3.1	Abstract . . . . .	25
3.2	Contents . . . . .	26
3.3	Introduction . . . . .	26
3.4	Sample characterization . . . . .	28
3.5	Sample preparation . . . . .	30
3.6	Measurement . . . . .	30
3.7	Results and interpretation of the wide angle scattering. . . . .	36
<b>4</b>	<b>Crystalline powder pattern</b>	<b>39</b>
4.1	Visualisation of the crystal structures . . . . .	39
4.2	Powder pattern: broadening by resolution and grain size . . . . .	40
4.3	Comparison with IHH, grain size etc. . . . .	42
4.4	Comparison with selectively deuterated materials . . . . .	48
<b>5</b>	<b>The random chain orientation. Calculation of <math>F_M</math></b>	<b>57</b>
5.1	$ F_M $ of ordered structure of different size . . . . .	59
5.2	$ F_M $ for amorphous regions. . . . .	64
5.3	Comparison with measurements . . . . .	73

<b>6</b>	<b>Paracrystallinity, Amorphous State</b>	<b>83</b>
6.1	a) Isotactic Material . . . . .	83
6.2	b) atactic material . . . . .	88
6.3	c) different definitions of amorphicity applied to our samples . . . . .	89
6.4	CONCLUSIONS . . . . .	90
<b>7</b>	<b>Partial structure factor</b>	<b>95</b>
7.1	The fundamental equations . . . . .	95
7.2	Application to the polymers . . . . .	98
7.3	Discussion of the results . . . . .	99
7.4	Spherical Fourier Transform . . . . .	100
7.5	Maximum entropy method to determine the $g_{ij}(r)$ . . . . .	101
7.6	Conclusions . . . . .	103
<b>8</b>	<b>SANS with polarization analysis on polystyrene</b>	<b>107</b>
8.1	Measurement . . . . .	107
8.2	Results and interpretation of the small angle scattering. . . . .	108
8.2.1	General outline . . . . .	109
8.2.2	Guinier plots . . . . .	110
8.2.3	Kratky plots . . . . .	113
8.2.4	Zimm plots . . . . .	115
8.2.5	Porod plots . . . . .	117
8.3	Discussion . . . . .	119
<b>9</b>	<b>Multiple Scattering Correction</b>	<b>123</b>
9.1	Overview of multiple scattering corrections . . . . .	123
9.1.1	Method of Blech and Averbach . . . . .	123
9.1.2	Method of Sears . . . . .	125
9.1.3	Monte Carlo method . . . . .	126
9.2	Detailed description of MC for scattering . . . . .	126
9.2.1	Some fundamental concepts of mathematical statistics . . . . .	126
9.2.2	Random number!generator . . . . .	127
9.2.2.1	Generation of random numbers with rectangular distribution . . . . .	127
9.2.2.2	Test for sequential correlation . . . . .	127
9.2.3	Simulation of a trace of particles with collisions . . . . .	128
9.2.4	Neutron histories . . . . .	130
9.2.4.1	Neutron history in single scattering . . . . .	130
9.2.4.2	Probability that the neutron arrives in the energy channel $\omega$ of the detector in angle $\vartheta$ . . . . .	132
9.2.4.3	Double and n-fold scattering . . . . .	132
9.2.5	Remarks: The subroutines. . . . .	133
9.2.5.1	Subroutines to determine the distance of the sample boundary. . . . .	133
9.2.5.2	Different problems connected with $S(Q, \omega)$ . . . . .	135
9.2.5.3	Monte Carlo program with spin dependent scattering . . . . .	139
9.2.5.4	How one can determine a standard deviation? . . . . .	139
9.3	Example Monte Carlo multiple scattering program in C. . . . .	141
<b>10</b>	<b>Origin for spherical average</b>	<b>157</b>
10.1	Abstract . . . . .	157
10.2	Introduction . . . . .	157
10.3	Discussion . . . . .	159

# Index

- $F_M$ 
  - equation, 59
  - for one monomer, 59
  - visualization, 59
- $F_M$  by summing includes shape, 58
- $F_M$  molecular form factor, 58
- Bragg peaks
  - voids, 43
- absolute calibration, 107
- affine deformation, 48
- amorphicity
  - integral over non-peak structured part, 90
  - lack of periodicity
    - tendency to order, 89
  - only randomly oriented chains, 90
- amorphous
  - local structure, 17
- amorphous transition regions
  - look for, 83
- amorphous halo, 19
  - assignment of distances, 19
- amorphous scatterin
  - chain periodicities, 69
- amorphous transition regions
  - not needed if paracrystalline, 83
- atactic, 2
- atacticity
  - paracrystallinity, 89
- atomic coordinates, 4
  - table, 40
- atomic force microscope, 1
  - force on one chain, 10
- atomic form factor, 57
- average density, 101
- average end to end distance, 4
- Bathia-Thornton definition, 97
- benzene rotation, 42
- biopolymers, 1
- Blech-Averbach method
  - elastic only, 123
- block copolymer, 2
- boson peak, 1
- broadening of second peak in IHH, 87
- bundles, 18, 74
- center of gravity
  - artefact peak, 66
  - weighed by scattering amplitude, 66
- chain periodicities
  - spherical averaged, 69
- chain end distance, 5
- chain length
  - DH peak, 81
- cluster, 27
- coherent
  - see separation, 30
  - separation from incoherent, 27
- combination iso- syndio-tactic, 54
- compare grain size and bundles, 74
- compare with measurements, 74
- concepts of mathematical statistics, 126
- configuration, 4, 27
- conformation, 4, 26
- convergence factor, 100
- coordination number, 97
- coordination numbers, 26
- copolymer, 2
- correctio
  - comparison with V standard, 32
- correction
  - multiple scatter
    - change of peak height, 33
  - background
    - incoherent, 31
  - Debye-Waller factor, 34
  - energy dependence, 34
  - for finite flipping R, 31
  - incoherent background, 31
  - internal calibration
    - problem from  $H_2O$ , 32
    - problem in DD-sample, 32
  - multiple scatter, 33

- Monte Carlo, 33
  - incoherent twice flipped, 33
  - multiple scattering
    - approximate, 33
  - sample shape, 32
  - time of flight measurement, 34
  - twice flipped resembles no flip, 33
- correlation
  - between chains and chains, 95
  - between rings and chains, 95
  - between rings and rings, 95
  - no angular correlation, 65
- correlation function
  - uncorrelated monomers, 65
- correlation coefficient, 127
- correlation function, 95
- correlation functions, 95
- covariance, 126
- cross-linked network, 2
- crystal
  - visualization, 39
- crystalline structure, 25
- crystallinity, 39
  - overview, 39
  - peak widths
    - pro and contra, 55
  - peaks
    - pro and contra, 55
  - pro and contra, 54
  - transition iso-syndio, 56
- data correction, 107
- Debye function
  - discussion, 12
  - Kratky plot, 12
- Debye function for scattering, 11
- Debye-Waller factor, 66
- depolarized light scattering
  - structural information, 10
- determine  $r_j$ , 66
- diffraction by chain of different length, 61
- diffuse scattering
  - amorphous part of samples, 65
  - Kuhn length, 66
  - long segments
    - peak at small Q, 69
  - random orientation, 65
  - randomly oriented chain pieces, 25
  - weakly dependent on size, 69
- disorder
  - in regular manner, 85
- disappearance of 110, 44
- disorder
  - peak width, 84
- disposition function, 57
- distinguish  $S(Q)$  from  $F_M$ , 58
- distribution, 127
  - continuous, 127
  - discrete
    - Poisson, 127
  - exponential, 127
  - rectangular, 127
- distribution of chain end distance, 4
- distribution of nearest distances, 85
- double scattering, 132
- effect of heating, 112
- elastic and diffuse
  - by grain size, 88
- elastic constants, 17
- elasticity
  - enthalpy, 10
  - entropy as source of, 8
- electron microscopy
  - no support by light, 19
  - problems, 18
  - support by polarised neutron, 19
- entropy
  - elasticity in polymers, 8
- equipartition, 126
- excluded volume exponent, 6
- expectation value, 126
- external calibration, 108
- Faber-Ziman definition, 96, 97
- Faraday conference, 17
- flat plate, 135
- flipper, 30, 107
- flipping ratio
  - measurement
    - Vycor glass, 32
    - with quartz, 32
- Flory
  - gaussian coil, 18
- Flory parameter, 6
- Flory school
  - gaussian down to atomic, 18
- Fourier pairs, 100
- Fourier transform, 100
  - convergence factor, 100
  - factors in crystallography, 57

- Fourier transform of single chains, 62
- fractals, 1
- Fraunhofer approximation, 57
- freely jointed chain, 5, 95
  - end to end square dist., 5
  - radius of gyration, 6
- freely rotating chain, 7
- from crystal to disorder, 57
- from one monomer to small clusters, 57
- gaussian coil, 27, 115
  - end to end distance, 7
  - excluded volume effect, 6
  - SANS, 18
- genes as memory, 1
- glass transition
  - long time scale, 17
- glass transitions, 1
- glassy state, 17
- grain size, 42, 74
  - selective deuteration, 50
- grain size and shape factor, 43
- grain size effects, 25
- groups of parallel chains, 69
- Guinier plot, 110
  - number of monomers, 110
- Guinier plots
  - normalized, 110
- hexagonal dense packing, 25
- high polymer, 2
- high Q
  - calculated intensity correct, 77
- history
  - chain, 18
  - chains in matter, 18
  - polymer structure, 17
  - polymers as associations, 18
  - statistical methods, 18
- homopolymer, 2
- how to correct by a factor, 130
- include disorder in chain position, 85
- incoherent
  - separation from coherent, 27
  - SANS, 107
- instrument, 27
  - D7, 30
  - resolution function, 40
- interaction radius, 85, 86
- interchain correlation
  - Miller indices, 54
- internal calibration, 31
- internal calibration, 108
- internal standard, 107
- interpretation
  - correlation between peaks, 36
  - crystalline
    - overview, 39
  - IHH sample, 37
  - methods, 36
  - model free, 36
  - paracrytal, 39
  - peak positions, 36
  - peak widths, 36
- ionomers, 27
- isostructural supposition, 81
  - partial structure factors, 81
- isostructurality, 89, 110
- isotactic, 2, 25, 39
  - chains no inversion symmetry, 44
  - diffuse background, 83
  - disappeared 110, 44
  - peak intensity, 83
  - powder pattern, 42
    - measured, 44
  - structural consequences, 44
  - third Miller indices, 48
- isotactic at small Q, 54
- isotactic sample, 83
- isotacticity
  - ultra pure, 30
- Kratky plot, 12, 114
  - Debye function, 12
  - generalized, 115
  - two different plateaus, 115
- Kuhnlength, 6, 95
  - correlation length, 66
  - gaussian coil, 6
- Langevin function
  - entropy, 9
- Laue diffuse scattering, 33
- light polarization
  - parallel chain correlations, 10
- light scattering
  - selected frequencies, 10
- macromolecule, 2
- maximum entropy
  - advantage in Fourier transform, 102

- proper probability density, 102
- maximum entropy method, 101
  - method of Collins, 102
- measured disorder in isotactic
  - same as atacticity, 89
- melts, 1
- methods to improve variance, 130
- Miller indices
  - interchain correlations, 54
- molecular form factor, 58
  - range of  $Q$ -dependent scattering, 77
- monomer, 2
- monomers as scattering units, 95
- Monte Carlo
  - how to include elastic scattering, 135
  - introduction to neutron scattering, 2
  - main program, 144
  - program in C, 141
  - spin dependent scattering, 139
  - subroutines
    - DIST, 142
    - NEWV, 141
    - RONE, 143
    - SINT, 144
  - variance, 141
- Monte Carlo method, 126
- Monte Carlo simulation
  - conditions, 128
- Monte Carlo integration, 136
- multiple scattering, 27, 108
  - changes of the pattern, 128
  - correction experimentally impossible, 123
  - extrapolation to zero thickness not correct, 123
  - overview, 123
  - why, 123
- multiple scattering correction
  - three reliable methods, 123
- neutron history, 130
- nodules, 18
- normalization of  $Q \cdot S(Q, \omega)$ , 136
- one-dimensional metals, 1
- organic superconductors, 1
- packing
  - disordered hexagonal dense, 27
- packing of polymers, 27
- pair correlation function
  - maximum entropy method, 102
- pair distribution, 4
- parabola fit, 98
- paracrystal
  - difficulties, 39
  - fundamental description, 39
  - tail at higher  $Q$ , 87
- paracrystal in two dimensions, 85
- paracrystall
  - broad peak, 87
- paracrystallinity, 2, 25, 28, 58, 80
  - atacticity, 89
  - no need of transition regions, 88
- paracrystals, 18
- parallel chains
  - randomly oriented, 69
  - scattering of groups of, 69
- parallelly arranged chains needed, 80
- partial coordination number, 97
- partial distribution functions, 97
- partial pair correlation, 26
- partial structure factors, 26, 96
  - isostructural supposition, 81
- partials
  - discussion of peak positions, 99
  - discussion of peak widths, 99
  - Fourier transform, 100
- peak broadening
  - interaction region, 25
- peak broadening
  - grain size, 25, 27
  - interaction region, 27
- peak width increasing
  - disorder, 84
- Pechold, 18
- polarizer, 30
- polydispersity, 28
- polymer
  - solid state
    - no theory, 1
- polymers
  - in solid state, 27
- Porod plot, 117
  - inner surface, 117
- powder averaging
  - visualization, 64
- powder pattern, 27, 40
  - instrument resolution, 40
  - isotactic, 42
  - syndiotactic, 42
- problems with  $S(Q, \omega)$ , 135

- quadratic interpolation, 139
- qualitative interpretation insufficient, 48
- quartz, 108
- radial density functions, 103
- radius of gyration, 5
- random orientation
  - correlation length, 66
- random chain orientation, 64
- random chain orientation
  - comparison with measurement, 70
  - discussion of calculation, 70
- random number
  - generation, 127
  - sequential correlation test, 127
- Random number generator, 127
- random number with exponential distribution, 131
- random orientation, 56
- random oriented chains
  - no sharp peaks, 77
- random variable, 126
- Renormalization group, 1, 7
- Rietveld refinement, 48
- role of polarization analysis, 19
- rotation of benzene, 42
- sample
  - $\sigma_{inc}$ , 28
  - characterization, 28
  - identification code, 28
  - molecular weight, 28
  - polydispersity, 28
    - chromatography, 30
  - preparation, 30
    - atactic, 30
    - DH, 30
    - high molecular, 30
    - isotactic, 30
    - no chain transfer agents, 30
  - table, 28, 30
    - description, 36
  - weight, 28
- sample preparation, 27
- SANS
  - aim of our task, 109
  - Bragg peaks
    - convolution with shape factor, 109
  - comparison with Higgins and Stein, 109
  - comparison with Rawiso, 109
  - D11, 109
  - D7 cannot give chain length, 108
  - DD sample calibration, 108
  - degree of order, 109
  - disposition function, 109
  - Guinier plot
    - radius  $R_g$ , 110
  - Guinier plot
    - degree of polymerization, 110
  - Guinier plots
    - laws to be used, 110
    - results on D11, 110
    - results on D7, 110
  - instrument, 107
  - molecular form factor, 109
  - multiple scattering, 108
  - origin in a solid, 109
  - overview of integral characteristics, 108
  - plots possible, 108
  - range of regularly arranged pieces, 108
  - sample form, 108
  - shape function, 109
  - side peaks
    - clustering, 113
  - wide angle scattering, 109
- SANS peaks in pure samples, 113
- SANS solid polymer
  - not the right method, 110
- scattering amplitude, 95
- scattering geometries, 133
- Scherrer formula, 42
- Sears method
  - also inelastic, 125
- selective deuteration, 25
  - grain size, 50
- self organization, 1
- semicrystalline, 30
- separation
  - coherent, 30
  - incoherent, 30
- shape factor
  - finite number of monomers, 73
  - width of Bragg peaks, 58
- shape and size
  - width of Bragg scattering, 58
- shape factor, 43, 58, 73
  - Bragg peaks, 109
  - if atomic positions known, 73
  - Scherrer formula, 58
  - small angle scattering, 58
- shape function, 84



- short range order
  - begin again, 19
  - PMMA, 20
  - polycarbonate, 20
  - universally present, 27
- short range order parameters, 26
- simulation of trace with collisions, 128
- single chain
  - collection of chains, 18
- single chains, 40
- single random oriented chains
  - disagreement, 72
- single scattering
  - with absorption, 132
  - without absorption, 132
- small angle scattering, 10, 26, 30, 32
- solid polymer
  - all questions open, 1
- solitons, 1
- Soxhlet extraction, 30
- spherical average, 95
  - object not spherical, 66
- spherical Fourier transform, 100
  - discretisation of the problem, 102
  - maximum entropy method, 102
- standard deviation, 126
- structure
  - atomic positions, 40
  - visualization, 39
- structure amplitude, 58
- Structure factors
  - calculated with partials, 99
- structure information
  - only at  $Q < 2$ , 77
- subroutines, 133
- syndiotactic, 2, 25, 40
  - powder pattern, 42
- syndiotactic at higher  $Q$ , 54
- tacticity, 2
- theta solvent, 115
- transform hexagonal to rectangular, 60
- variance, 126
- visualization
  - crystal
    - isotactic, 39
  - single chains, 40
  - unit cell, 40
- void scattering
  - Bragg peaks, 58
- voids
  - Bragg peaks, 43
  - broadening, 43
- Vycor glass, 108
- Warren-Cowley parameters, 97
- wide angle scattering, 26
- wide angle scattering, 13
- Zimm plot, 110, 115
  - results correspond to Guinier plot, 117

# Chapter 1

## Some fundamental concepts of polymer physics.

### 1.1 Introduction

Polymers are technically very important materials, and their production and applications underpins a vast industrial sector. Since the last decade biopolymers play an increasing role both in technology and fundamental research. In the genes they form memory structures of nearly unbeatable miniaturization. A special form of polymerisation - self organization - provides very useful means for deliberately changing even such complicated structures as ribosomes as for example by introducing at a specific point a protonated aminoacid simultaneously in the same way on many ( $10^{14}$ ) originally deuterated individual units [1]. Many very modern concepts such as fractals [2], glass transitions [3], boson peaks [4], one-dimensional metals [6], solitons [6], organic superconductors [6], or renormalization group theoretic concepts [7] apply very naturally to descriptions of phenomena occurring in polymers. The last decade has witnessed an application of the atomic force microscope to measure forces as a function of extension on single chains [5]. And this list is not comprehensive! Polymer physics permeates so many branches of advanced science that it is impossible to give a complete overview of any of them. Since polymers may well replace metals and even storage devices based on silicon in near future it is certainly worth the effort to learn about them. At the very least they will feature centrally in fundamental investigations in materials science.

Theory and experiment of *polymers in solution* is quite advanced, and rarely a discrepancy between theory and experiment can be found. Hence many books, reviews and summer schools about polymer physics concentrate on clear results obtained so far. The physics of melts is more difficult, and many questions about the structure and dynamics are open for solid polymers. As recently as 1991, the 22nd Ferienkurs about the physics of polymers, (Jülich) did not mention anything about physics of solid polymers. In the 1992 edition of the classic polymer text by Sperling [8] the author writes "The interpretation of diffraction data on amorphous polymers is currently a subject of debate." He then shows examples of data interpretation of diffraction in the bulk amorphous state which go from "considerable order" to "little or no order fits the data best". There were two symposia about this topic, as early as in 1976 [9] and 1979 [10]. Since that time, there were no dedicated symposia - but progress in computer simulations, as outlined in a recent review ([18]).

The scattering experiments on polymers are typically made in solution. Measurements in the solid state are tricky: they yield results which can hardly be compared to any theory. To begin with, not even a structure factor for the amorphous state can be calculated satisfactorily. The method of partial structure factors seems not really applicable; it is also difficult to find measured and fitted spectra for crystalline polymers even if structural refinements have been made. All

published spectra show the broadening of the peaks with increasing value of  $\vec{Q}$ , the momentum transfer vector, and a disappearance of peaks at higher  $Q$ . Such a behaviour of the scattering pattern is always an indication of paracrystallinity, i.e. a lack of real long-range order. In the absence of the long-range order one cannot apply the standard crystallographic extinction rules - there are more peaks present than expected for a perfect crystalline structure. It then depends on the sample size or the taste of investigator which peaks are considered essential, and which are not.

We begin by a short description of theory of chain molecules, and indicate how this theory is applied to polymers in solution. There we signal how the problems, encountered in the description of polymers in the bulk, are avoided. In the following chapters of this treatise we describe neutron diffraction studies performed on carefully synthesised polystyrene samples. These are four selectively deuterated atactic, one isotactic and one syndiotactic sample. We investigate the structure using wide angle neutron scattering (WANS) and by small angle neutron scattering (SANS), both with polarization analysis. The advantage of the polarization analysis over the standard neutron scattering experiment lies in the experimental separation of the coherent and incoherent scattering. Since for a correct description of the structure purely coherent scattering is required, we are starting with the advantage of having it as well as the absolute cross section. The latter is provided by normalisation to the internal standard. By measuring the scattering with flip and without flip, we have all the needed information for the internal standard, the separation of coherent and incoherent scattering on the same sample.

In order to elucidate problems encountered in data analysis, we apply different existing methods to describe the results obtained. Half of the solution of any problem is to state it clearly: not only can we learn these methods but by comparing and contrasting their results we shed light on potential problems. We hope that this pedagogical approach will provide an encouragement for a keen reader to solve problems posed.

One of the serious problems in the scattering from the bulk is the presence of the multiple scattering. In the latter part of this book we provide description of a Monte Carlo program to calculate multiple scattering corrections for an isotropic scatterer (with polarisation analysis). This description provides a compact introduction to neutron scattering where all processes present in the measurement must be described - this is necessary for the program to model the measurement faithfully. We hope that in this way the most compact and simultaneously complete introduction to neutron scattering is given.

## 1.2 Description of polymers as long flexible chains

Let us begin with recalling relevant nomenclature. The term *macromolecule* is an all-embracing term. It covers all large molecules. *High polymer* is restricted to structures that are at least approximately multiples of a low-molecular-weight unit (a *monomer*). In a *homopolymer* one has a single monomer type. A *copolymer* consists of two different monomer units in irregular sequence. A *block copolymer* is a sequence of one unit followed by a sequence of a second unit in the same chain.

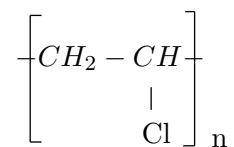
Polymerisation is a statistical process with the consequence of certain defects: Polymer chains are not all of the same length. Other defects are: they can have short or long branches. If these branches bridge two chains they form a *cross-linked network*. If the monomers are asymmetric with respect to the chain axis the resulting disturbance in regularity is the *tacticity*. If the sequence is random, the polymer is *atactic* and will generally not crystallize. In the case of polystyrene or polypropylene one can have two different regular tacticities, which are called *syndiotactic* and *isotactic*. The above can be visualized as follows:

POLYMER: repeating chemical unit      MONOMER

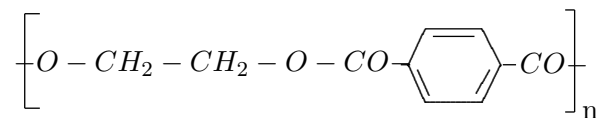
Number of monomers in the macromolecule:

$n$  = DEGREE of polymerisation.

Example: polyvinyl chloride



polyethylene terephthalate

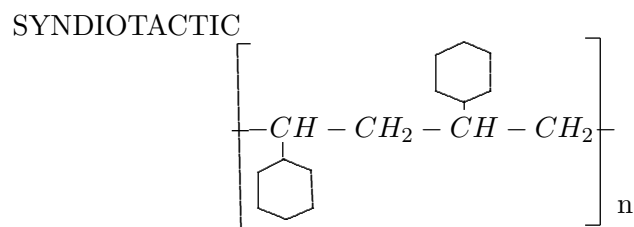
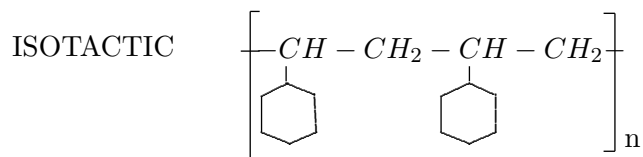


TACTICITY in the case of asymmetric monomers

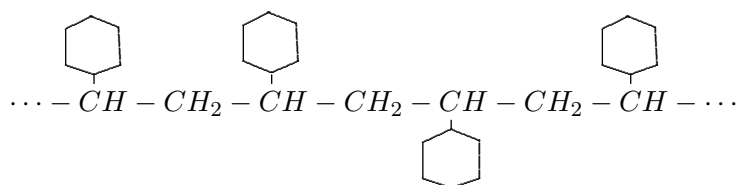
RANDOM sequence: atactic

REGULAR sequence: tactic (isotactic or syndiotactic)

Example: Polystyrene



ATACTIC



COPOLYMER: two different monomer units in irregular sequence

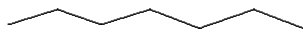
alternating copolymer: two units in alternating sequence

block copolymer: sequence of one unit alternating with sequence of the other

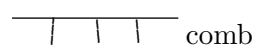
### 1.3 Spatial configurations of polymers

CONFORMATION: can be

LINEAR CHAIN



Regular or irregular branching chains



SPATIAL crosslinked NETWORKS (vulcanized rubber)

CONFORMATION: depends on forces

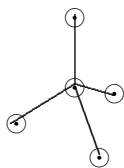
**Intra molecular forces**

**Inter molecular forces**

} both of the same origin

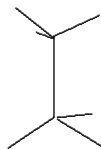
#### Intra molecular forces

Limiting case: only bond length fixed



$CH_4$

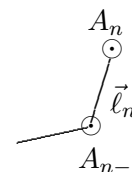
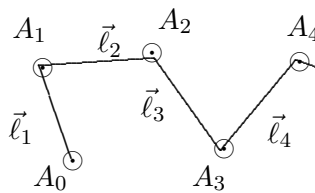
very rigid form



$C_2H_6$

rotation around bond  
between  $CH_3$  groups

possible without demand of bonds



freely bound chain

monomer about all bounds

completely free rotatable

#### 1.3.1 Mathematical description of the configuration of some simplified model chains.

In what follows we use the terms *configuration* and *conformation*. Configuration is the more general term, conformation connotes form and symmetrical arrangement of parts. Configuration refers to the disposition of the parts of the object without regard for shape and symmetry. The following is very clearly described in the book of Flory [12], which despite being published in 1969 remains a classical source for description of polymer physics. The question posed is: how can one describe the spatial configuration of chain molecules?

- **Pair distribution function** is not adapted. Would only give the most probable distance of two groups in the macromolecule. But for wide angle scattering it is very well adapted as it yields the order information in the region where the polymer chains are correlated.
- **Time average of distance squared of the ends of the molecule** is better adapted to describe a property of the whole chain form.
- **Distribution function of the distance of chain ends** As the number of configurations of a long chain molecule is very large, one has to use statistical methods. This characterizes the spatial configuration of the chain, albeit indirectly. It allows to determine expectation values.
- **Giving all coordinates of all atoms** Can only be done in idealized cases of perfect long-range order (i.e. crystals).

## 1.3.1.1 Average square of the distance of the chain ends

Expressions of general validity:

$$\vec{r} = \sum_{i=1}^n \vec{\ell}_i \quad (1.1)$$

$$r^2 = \sum_{i,j=1}^n \vec{\ell}_i \cdot \vec{\ell}_j \quad (1.2)$$

$$= \sum_{i=1}^n \ell_i^2 + 2 \sum_{0 < i < j \leq n} \vec{\ell}_i \cdot \vec{\ell}_j \quad (1.3)$$

Statistical average with equal, fixed bond length  $\ell$

$$\langle r^2 \rangle = n\ell^2 + 2 \sum_{i < j} \langle \vec{\ell}_i \cdot \vec{\ell}_j \rangle \quad (1.4)$$

**Radius of gyration**  $R_g = \sqrt{\langle r^2 \rangle}$  is defined by coordinates  $s_i$  of the  $i^{th}$  atom in the center of gravity system of the chain. (Definition of center of gravity:  $\sum_i s_i = 0$ )

$$s^2 = \frac{1}{n+1} \sum_{i=0}^n s_i^2 \quad (1.5)$$

$$= \frac{1}{(n+1)^2} \sum_{0 \leq i < j \leq n} r_{ij}^2 \quad \text{with } \vec{r}_{ij} = \vec{s}_i - \vec{s}_j \quad (1.6)$$

$$\langle s^2 \rangle = \frac{1}{(n+1)^2} \sum_{0 \leq i < j \leq n} \langle r_{ij}^2 \rangle \quad (1.7)$$

## 1.3.1.2 SPECIAL chain models

1. **Freely jointed chain** ( $\varphi$  and  $\vartheta$  uniformly distributed)  $n$  bonds of fixed length, jointed in linear succession, the angles at the bond junctions being free to assume all values with equal probability. Rotations about bonds are likewise free.

- **End to end square distance**

$$\langle \vec{\ell}_i \cdot \vec{\ell}_j \rangle = 0 \quad (1.8)$$

$$\boxed{\langle r^2 \rangle_0 = n\ell^2} \quad (1.9)$$

This is a GENERAL RELATION for the end-to-end square distance. Improved models give only corrections to this relation. This fact is expressed by

$$\boxed{c_n = \frac{\langle r^2 \rangle_0}{n\ell^2}} \quad (1.10)$$

which is the **characteristic ratio of a chain**. It is unity for the freely jointed chain.

- **Mean-square radius of gyration** From eq.(1.9) it follows (used together with eq. (1.7))

$$\langle r_{ij}^2 \rangle_0 = |j - i| \cdot \ell^2 \quad (1.11)$$

$$\langle s^2 \rangle_0 = \frac{\ell^2}{(n+1)^2} \sum_{0 \leq i < j \leq n} (j-i) \quad (1.12)$$

$$\frac{\langle s^2 \rangle_0}{n\ell^2} = \frac{1}{6} \frac{n+2}{n+1} \xrightarrow{n \rightarrow \infty} \frac{1}{6} \quad (1.13)$$

$$(1.14)$$

$$\boxed{\langle s^2 \rangle_0 = \frac{1}{6} \langle r^2 \rangle_0} \quad (1.15)$$

which goes back to Debye [11].

- **The Kuhn bond length** The correlation between bonds  $i$  and  $i+k$  in a real chain with finite degree of flexibility must vanish with increasing  $k$ . Representing the real chain of  $n$  bonds of length  $\ell$  by an equivalent chain consisting of  $n'$  hypothetical bonds of length  $\ell'$  results then in a chain connected by free joints as in the simplest model.

$$n'\ell' = r_{max} = n\ell \quad \text{fully extended length of real chain} \quad (1.16)$$

$$n'(\ell')^2 = \langle r^2 \rangle_0 \quad \text{the actual unperturbed mean square end-to-end length} \quad (1.17)$$

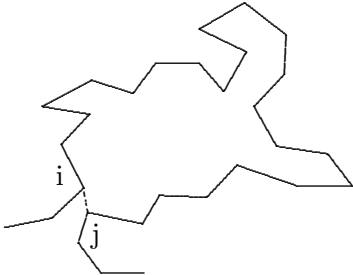
For example for a polymethylene chain  $r_{max} = 0.83n\ell$  and  $\langle r^2 \rangle_0 = 6.7n\ell^2$ , resulting in  $\ell' \approx 8\ell$  and  $n' \approx \frac{1}{10}n$ .

#### Some remarks concerning this grouping into subunits:

- As the new vectors  $\ell'$  are now uncorrelated, they are uniformly distributed and this is termed Gaussian coil.
- The **weak point in this approach** is the neglect of interactions between monomers  $i$  and  $j$  with  $|j-i|$  very large (see sketch below!). When these are included the chain is **not** gaussian. This is sometimes treated as excluded volume effect, [7] which results in a scaling law with an exponent  $\nu$  in the relation for the mean square end to end distance  $R_F^2$  and the degree of polymerization  $N$

$$R_F = aN^\nu \quad (1.18)$$

where  $\nu$  is a universal exponent  $\nu = \frac{3}{5}$  in three dimensions.



large loop interactions are not included

- This problem of the **excluded volume** depends also on the interaction with the solvent. The  **$\theta$ -solvent** is a solvent where the excluded volume effect is just zero and the polymer chain behaves as an ideal chain molecule. (It corresponds to the Boyle temperature for a real gas, where the repulsion is exactly compensated by the mutual attraction.) At the  $\theta$ -point the perturbation of the configuration must vanish. At the  $\theta$ -temperature the solution is on the threshold of precipitation. [12],[13]. Flory derives the exponent  $\nu$  by using the Flory parameter  $\chi$  to describe the interaction analogously as in the van der Waals gas.

- The above theories about polymers are limited to solutions and the melt: nothing about solid polymers. Our measurements described in chapters 2 and 3 are on solid polymers.
- The use of grouping of monomers into subunits is the coarse graining followed by a change of scale, which are the basic ingredients of the Renormalization Group, if applied to the determination of the energy. In [7] you can find an introduction into the application of this method to problems in polymers, mainly in connection with excluded volume effects. If you remember that by increasing the size of the subunits you come to a description which is independent of the structure and properties of the subunit: the gaussian coil, you have something like a universality in the Renormalization group theory and a fixed point behaviour like in critical phenomena. The Renormalization group theory is well described in [14, 15, 16].

**2. Freely rotating chain ( $\vartheta$  fixed,  $\varphi$  uniformly distributed)** This is the case of fixed bond angles, but free rotation. The correlations between bond directions are imposed by fixing the angle  $\vartheta$ . It then follows:

$$\langle \vec{\ell}_i \cdot \vec{\ell}_{j+k} \rangle = \ell^2 \cos^k \vartheta \quad (1.19)$$

$$\langle r^2 \rangle_0 = n\ell^2 + 2 \sum_{i < j} \cos^{j-i} \vartheta \quad (1.20)$$

$$\sum_{0 < i < j \leq n} \vec{\ell}_i \cdot \vec{\ell}_j = \frac{2}{n} \sum_{k=1}^{n-1} (n-k) \cos^k \vartheta \quad (1.21)$$

as  $n-k$  terms exist with equal  $j-i=k$ . Thus we get

$$\langle r^2 \rangle_0 = n\ell^2 \left( 1 + 2 \sum_{k=1}^{n-1} \cos^k \vartheta - \frac{2}{n} \sum_{k=1}^{n-1} k \cos^k \vartheta \right) \quad (1.22)$$

$$c_n = \frac{\langle r^2 \rangle}{n\ell^2} = \frac{1+\alpha}{1-\alpha} - \frac{2\alpha}{n} \frac{1-\alpha^n}{(1-\alpha)^2} \quad (1.23)$$

$$\alpha = \cos \vartheta \quad (1.24)$$

$$c_\infty = \frac{1+\alpha}{1-\alpha} \quad (1.25)$$

$$= \frac{1+\cos \vartheta}{1-\cos \vartheta} = 2 \quad \text{with } \cos \vartheta = \frac{1}{3} \quad (1.26)$$

**3. Distribution function for the end-to-end distance for long chains unperturbed by self-interactions of long range and by external constraints**

Let  $W_{ij}(\vec{r}_{ij})$  denote the probability distribution to find chain members  $i, j$  in the distance  $\vec{r}_{ij}$ .



unperturbed chain  
infinite length  
without long-range interaction  
without excluded volume effect( $\theta$  solvent)

} for large  $j-i$   

gaussian

$$W_{i,j}(\vec{r}_{ij}) = W_0 e^{-\alpha r_{ij}^2}$$

$$W_0 = \frac{3}{2\pi \langle r_{ij}^2 \rangle}$$

$$\alpha = \frac{3}{2 \langle r_{ij}^2 \rangle}$$

$x, y, z$  components of  $\vec{r}_{ij}$

After many steps the components  $w(x), w(y), w(z)$  of  $W_{ij}(\vec{r}_{ij})$  are uncorrelated

$$W_{ij}(r_{ij}) = w(x) \cdot w(y) \cdot w(z)$$

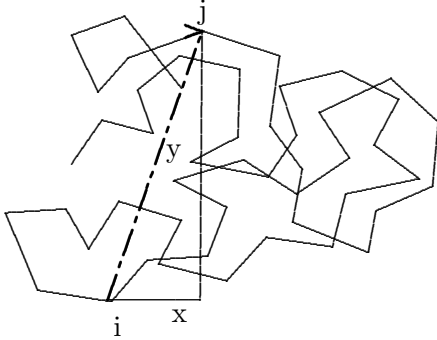
Isotropy:  $w(x) \cdot w(y) \cdot w(z) = \Phi(r_{ij}^2)$   
shows that  $w(x)$  has the form

$$w(x) = c e^{-\alpha x^2}$$

For the end-to-end distance  $r$  we need the radial distribution function

$$W(r)dr = W_0 4\pi r^2 dr = \left( \frac{\beta}{\sqrt{\pi}} \right)^3 e^{-\beta^2 r^2} 4\pi r^2 dr$$

with  $\beta^2 = \frac{3}{2n\ell^2}$



$w(x), w(y)$  are the probabilities (for  $i$  and  $j$  many steps apart) to find in the distance  $x$  from  $i$  and  $y$  from  $i$  the number  $j$  chain member

## 1.4 About the elastic behaviour of polymers: Entropy and enthalpy as origin of the forces.

The length of the bonds and the angles  $\vartheta$  between bonds of a polymer are nearly impossible to change without destruction of the polymer. Rotations  $\varphi$  around bond directions are easy to achieve, provided the chain is in a solvent, and is not hindered by its neighbors. These rotations make possible a large number of configurations, which have all the same thermodynamic energy  $U$ , and the same a-prioric probability. In the non deformed state the mean square averaged end-to-end distance is given by (see e.1.9 or 1.22)

$$\langle r^2 \rangle_0 = n\ell^2 \quad (1.27)$$

$$\langle r^2 \rangle_0 = n\ell^2 \left( 1 + 2 \sum_{k=1}^{n-1} \cos^k \vartheta - \frac{2}{n} \sum_{k=1}^{n-1} k \cos^k \vartheta \right) \quad (1.28)$$

This distances can be obtained by a large number of chain configurations. The probability of this state is correspondingly large. Under stress the strain of the chain and of  $\langle r^2 \rangle$  gets larger and the number of configurations to achieve this becomes smaller. In the extreme case of the completely stressed chain one has only one configuration. So under stress the entropy is diminished and we get an elastic force:

$$dF = dU - TdS - SdT \quad (1.29)$$

$$dU = TdS - dW \quad (1.30)$$

$$dW = -fdL - SdT \quad (1.31)$$

$$dF = fdL - SdT \quad (1.32)$$

$$f = \left( \frac{\partial F}{\partial L} \right)_{T,V} \quad (1.33)$$

$$= \left( \frac{\partial U}{\partial L} \right)_{T,V} - T \left( \frac{\partial S}{\partial L} \right)_{T,V} \quad (1.34)$$

$$= f_U + f_S \quad \text{conventional elasticity } f_U \text{ and entropy elasticity } f_S \quad (1.35)$$

$f_U$  is obtained by conservation of internal energy,  $f_S$  is obtained by diminished disorder. To determine  $f_U$  one recalls that

$$f_U = \left. \frac{\partial U}{\partial L} \right|_{T,V} = f - T \left. \frac{\partial f}{\partial T} \right|_{L,V} \quad (1.36)$$

In section 3 on page 7 we derived the mean square end-to-end distribution function for the freely jointed chain. By using the Kuhn length this distribution function can be used for real polymers. For example for the Kuhn length  $\ell = 2.5\sqrt{6} \text{ \AA}$  and  $n = 667$  we have a distribution function statistically equivalent to a polyethylene chain with 1000 monomer units and unhindered rotation about tetrahedrally directed -C-C- bonds of length  $2.5 \text{ \AA}$ .

The entropy  $S(r)$  associated with this distribution is given by this distribution by the logarithm:

$$S(r) = k_B \ln(W(r)) = S_0 - k_B \frac{3r^2}{2n\ell^2} \quad \text{for 3 dimensions} \quad (1.37)$$

The free energy  $F(r)$  is then

$$F(r) = U - TS = F(0) + \frac{3}{2} \frac{Tr^2}{n\ell^2} \quad (1.38)$$

$$\frac{\partial F}{\partial r} = f = \frac{3Tr}{n\ell^2} \quad (1.39)$$

$$\langle \vec{r} \rangle_f = \vec{f} \frac{n\ell^2}{3T} \quad (1.40)$$

This is valid whenever  $n\ell \ll \langle \vec{r} \rangle$ . If the strain is strong then the supposition for the gaussian that  $\langle \vec{r} \rangle \approx 0$  is not fulfilled. Then a better approximation for the distribution function for high values of  $r/(n\ell)$  is the inverse Langevin function (see Kuhn et al. [17]).

$$\ln W(r) = L^{-1}\left(\frac{r}{n\ell}\right) \quad (1.41)$$

or

$$\frac{r}{n\ell} = \coth(\ln W(r)) - \frac{1}{\ln(W(r))} \quad (1.42)$$

By expansion into a series this gives

$$\ln W(r) = \text{const} - n \left[ \frac{3}{2} \left( \frac{r}{n\ell} \right)^2 + \frac{9}{20} \left( \frac{r}{n\ell} \right)^4 + \left( \frac{99}{350} \frac{r}{n\ell} \right)^6 + \dots \right] \quad (1.43)$$

The first expression in this series is a gaussian. It can be measured with an atomic force microscope (AFM) if one pulls on one polymer chain [5]. One can see that the deformation with small forces corresponding to the entropy change is proportional to the overall length  $n\ell$ . If one has stretched the polymer to its maximum length then it is much stiffer corresponding then to deformations by changing bond angles or bond length, a change in enthalpy.

## 1.5 Elastic scattering from polymers: Structure of polymers.

Experimentally the spatial configuration of the polymer chain molecule can be determined by light scattering, X-ray scattering and neutron scattering. *Light scattering* uses Infrared and Raman scattering. These can give structural information even during the polymerisation process e.g. by observing special energy peaks, which are indications of C=C double bonds. By using polarized light and observing the depolarized component information about parallel correlations of chains is obtained, as the chain direction is a preferred polarization direction of a beam scattered by a chain molecule. This gives a polarization component other than the incident beam, if the chain direction is not parallel to the incident polarization. The principle of the determination of the chain structure by neutron scattering is described below.

### 1.5.1 Small angle scattering.

In X-ray and neutron scattering one has to distinguish SMALL ANGLE scattering and WIDE ANGLE scattering. For small angle scattering one can neglect the phase difference of elementary waves scattered by different atoms in a monomer. Single chain links can be treated as point scatterer. For the calculation of the scattering amplitude one has to add the contributions of the single chain links with the correct phase in the detector (i.e. with long distances for parallel beams). The structure factor gives a desired link:

$$F(\vec{Q}) = \frac{1}{N^2} \left| \sum_{j=1}^N e^{i\vec{Q} \cdot \vec{r}_j} \right|^2 \quad (1.44)$$

where  $\vec{Q}$  is the scattering vector. For an ensemble of molecules we take the average

$$F(\vec{Q}) = \left\langle \frac{1}{N^2} \left| \sum_{j=1}^N e^{i\vec{Q} \cdot \vec{r}_j} \right|^2 \right\rangle \quad (1.45)$$

$$= \frac{1}{N^2} \sum_{i,j=1}^N \left\langle e^{i\vec{Q} \cdot \vec{r}_{ij}} \right\rangle \quad \vec{r}_{ij} = \vec{r}_i - \vec{r}_j \quad (1.46)$$

$$= \int g(\vec{r}) e^{i\vec{Q} \cdot \vec{r}} d\vec{r} \quad (1.47)$$

because (exact for Gaussian distribution)

$$\left\langle e^{i\vec{Q} \cdot \vec{r}_{ij}} \right\rangle = e^{-\frac{1}{2} \langle (\vec{Q} \cdot \vec{r}_{ij})^2 \rangle} \quad (1.48)$$

$$\left\langle e^{i\vec{Q} \cdot \vec{r}_{ij}} \right\rangle = \left\langle 1 + \frac{1}{1!} i(\vec{Q} \cdot \vec{r}_{ij}) + \frac{1}{2!} (i\vec{Q} \cdot \vec{r}_{ij})^2 + \frac{1}{3!} (i\vec{Q} \cdot \vec{r}_{ij})^3 + \dots \right\rangle \quad (1.49)$$

$$\text{with } \langle r_{ij} \rangle = 0 \text{ odd powers disappear i.e.} \quad (1.50)$$

$$= 1 + \frac{1}{2!} i^2 \langle (\vec{Q} \cdot \vec{r}_{ij})^2 \rangle + \frac{1}{4!} i^4 \langle (\vec{Q} \cdot \vec{r}_{ij})^4 \rangle + \dots \quad (1.51)$$

$$e^{-\frac{1}{2}(\vec{Q} \cdot \vec{r}_{ij})^2} = 1 - \frac{1}{2} \langle (\vec{Q} \cdot \vec{r}_{ij})^2 \rangle + \frac{1}{3!} \left( -\frac{1}{2} \langle (\vec{Q} \cdot \vec{r}_{ij})^2 \rangle \right)^2 + \dots \quad (1.52)$$

Isotropy of  $\vec{Q}$  gives then

$$e^{-\frac{1}{2} \langle (\vec{Q} \cdot \vec{r}_{ij})^2 \rangle} = e^{-\frac{1}{6} Q^2 \langle r_{ij}^2 \rangle} \quad (1.53)$$

$$F(Q) = \frac{1}{N^2} \sum_{i,j=1}^N e^{-\frac{1}{6} Q^2 \langle r_{ij}^2 \rangle} \quad (1.54)$$

$\langle r_{ij}^2 \rangle$  depends only on  $j - i$ . Let  $j - i = k$ . Then  $j - i$  occurs  $N - k$  times in the double sum. We put  $\langle r_k^2 \rangle = \langle r_{i,i+k}^2 \rangle$  and get

$$F(Q) = \frac{1}{N} + \frac{2}{N} \sum_{k=1}^N \left( 1 - \frac{k}{N} \right) e^{-\frac{1}{6} Q^2 \langle r_k^2 \rangle} \quad (1.55)$$

Applying this relation to the freely jointed chain with  $\langle r_k^2 \rangle = k\ell^2$  gives the DEBYE function D(Q)

$$\left. \begin{aligned} z &= \frac{1}{6} Q^2 N \ell^2 \\ x &= \frac{k}{N} \\ \frac{1}{N} \sum_{k=1}^N &\longrightarrow \int_{\frac{1}{N}}^1 dx \end{aligned} \right\} \begin{aligned} D(Q) &= 2 \int_{1/N}^1 (1-x)^{-zx} dx + \frac{1}{N} \\ &\approx 2 \int_0^1 (1-x) e^{-zx} dx \end{aligned}$$

$$zx = u \quad (1.56)$$

$$dx = \frac{1}{z} du \quad (1.57)$$

$$D(Q) = \frac{2}{z} \int_0^z e^u du - \frac{2}{z^2} \int_0^z u e^{-u} du \quad (1.58)$$

$$= \frac{2}{z} (1 - e^{-z}) + \frac{2}{z^2} (z e^{-z}) - \frac{2}{z^2} (1 - e^{-z}) \quad (1.59)$$

$$(1.60)$$

$$\boxed{D(Q) = \frac{2}{z^2} (e^{-z} - 1 + z)} \quad (1.61)$$

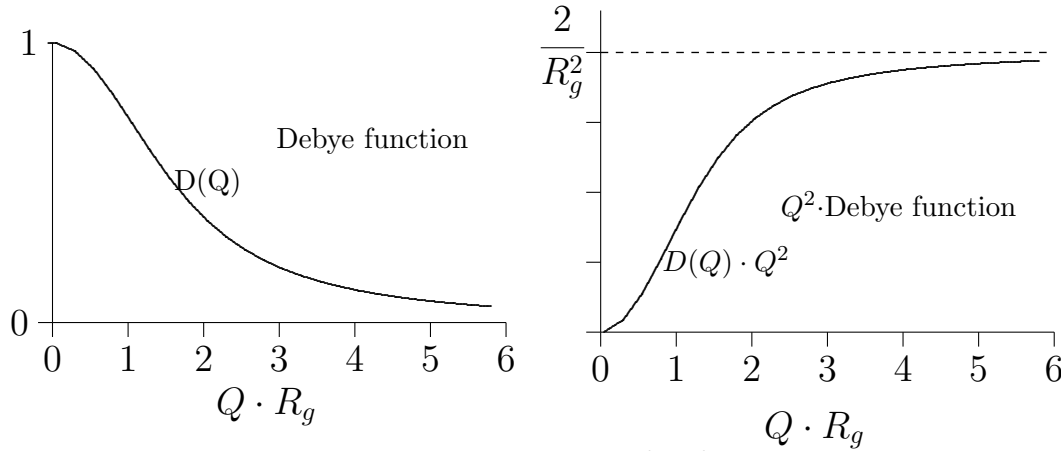
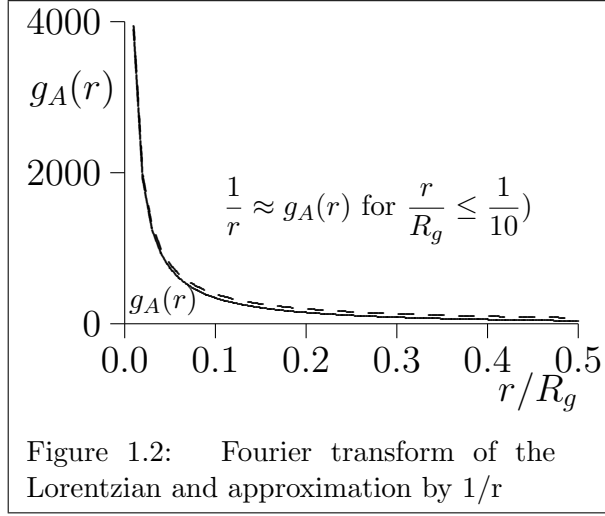
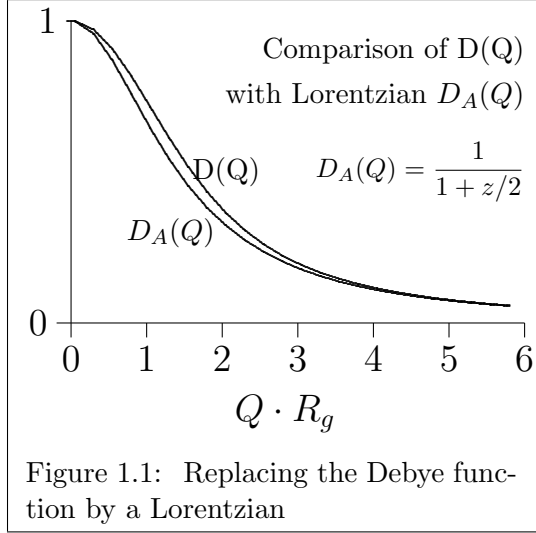
In order to obtain the radius of gyration  $R_g$ , we use

$$z = \frac{1}{6} Q^2 N \ell^2 = Q^2 \langle s^2 \rangle_0 \quad (1.62)$$

$$= Q^2 R_g^2 \quad (1.63)$$

$$R_g = \sqrt{\langle s^2 \rangle} \quad (1.64)$$

The Debye function also describes in good approximation the scattering by real polymer chains.



The Debye function behaves for small  $Q$  as  $(1 - Q^2 \cdot R_g^2/3)$  and for large  $Q$  (i.e.  $Q \cdot R_g \ll 1$ ) as  $2/(Q^2 R_g^2)$ . The Fourier transform of the Debye function gives the probability density to find two chain segments in the distance  $r$ . To see this behaviour we replace  $D(Q)$  by a Lorentzian  $D_A(Q)$  (see the fig.1.1) with

$$D_A(z) = \frac{1}{1+z/2} \quad (1.65)$$

The Fourier transform of this function is easy to determine. It is

$$g_A(r) = \frac{4\pi^2}{R_g^2} \frac{1}{r} e^{-\frac{r}{R_g}\sqrt{2}} \quad (1.66)$$

This function behaves in a large region like  $1/r$  (see fig.1.2). Hence we can get some insight into the meaning of the pair correlation function. We calculated it previously for a gaussian coil. In this case in a sphere of radius  $r$  around a chain segment one has a number of  $n$  other chain segments. For small  $r$  these segments belong in general to the same piece of the chain as the chain segment at  $r = 0$ . Then we must have  $r^2 = n\ell^2$  as in the freely jointed chain or  $n = r^2/\ell^2$ . The density  $n/r^3$  is then proportional to  $1/(r\ell^2)$  and this is roughly proportional to  $g(r)$ . For larger  $r$  this approximation cannot be valid, as this would result in  $n > N$ .

The behaviour of the Debye function is the basis for the *Kratky plot* (see fig.1.3)

The scattering curve of a gaussian coil has then three different ranges of behaviour:

- A Guinier range,  $Q < 1/R_g$ , the whole chain determines the scattering, result: degree of polymerisation  $n$ ,  $R_g$

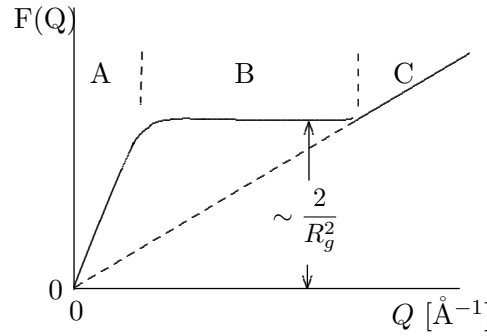


Figure 1.3: Schematic scattering curve for a gaussian coil in the Kratky plot representation:  $F(Q) \propto (n+1)Q^2 I_D$  over  $Q$ , with  $I_D$ =scattered intensity (for more details see chapter 8 on page 107 especially 8.2.3 on page 113 and fig.8.4 on page 115)

- *B* Plateau,  $F(Q)=\text{const.}$   $I_D \sim Q^{-2}$ , result  $R_g^2$
- *C* Scattering from smaller units,  $F(Q) \sim Q$ ,  $I_D \sim Q^{-1}$

With neutrons one can investigate sizes  $D \sim 2\pi/Q$  of 1000 - 0.5 Å. In the figure 1.3 the real behaviour of the curve depends essentially on the chain configuration. (In the case of non gaussian behaviour one needs numerical calculations). For other plots see the chapter on small angle neutron scattering 8 on page 107.

### 1.5.2 Wide angle scattering

In this part the different methods applied for wide angle scattering will be shown as crystal diffraction, powder pattern and its dependence of the size of the crystallites. Diffuse scattering of randomly oriented scatterers, paracrystallinity and its consequences for the scattering, partial structure factors applied to polymers.



# Bibliography

- [1] W.Knop, M.Hirai, H.B.Stuhrmann, R.Wagner, J.Zhao, O.Schärpf, R.R.Crichton, M.Krumpolc, K.H.Nierhaus, A.Rijllart, T.O.Ninikoski: J.Appl. Cryst. **25** (1992) 155-165
- [2] R.Jullien, From Guinier to fractals. Journal de physique I, **2** (1992) 759-770, J.Teixeira, Small angle scattering by fractal systems: J.Appl. Cryst. **21** (1988) 781-785
- [3] W.Götze, Aspects of structural glass transitions, in: Liquids, Freezing and Glass Transitions, J.P.Hansen, D.Levesque, J.Zinn-Justin, eds., Les Houches, Session LI, 1989, course 5, p.292-503. Elsevier Science publishers 1991.
- [4] A.P.Sokolov, U.Buchenau, W.Steffen, B.Frick, A.Wischnewski, Phys.Rev.B **52** (1995) R9815-R9818
- [5] Florin, Thesis (1995) (Inst. Prof. Gaub) LMU-München, Florin, E.L., M.Rief, et al.: Sensing specific molecular interactions with the atomic force microscop, Biosensors Bioelectr. **10** (9-10), 895-901, 1995
- [6] S.Roth, One-dimensional Metals, VCH Verlagsgesellschaft, Weinheim, New York, 1995.
- [7] P.-G. de Gennes, Scaling Concepts in Polymer Physics, Cornell University Press, Ithaca and London, 1979
- [8] Sperling, Introduction to Physical Polymer Science, John Wiley & Sons, New York 1992
- [9] Symposion on "Physical Structure of the Amorphous State", J.Macromol. Sci. Phys. **B12** (1976)
- [10] Organization of Macromolecules in the Condensed Phase, Faraday Discuss., Chem.Soc. **68** (1979)
- [11] J.Chem.Phys., **14** 636 (1946)
- [12] P.J.Flory, Statistical mechanics of chain molecules, Interscience Publishers, a division of John Wiley, New York 1969.
- [13] R.A.Fava, Polymers, Part A:Molecular Structure and Dynamics, L.Marton and C.Marton eds., Methods of Experimental Physics, Vol.16, Academic Press, London 1980.
- [14] Shang-Keng Ma, Modern Theory of Critical Phenomena, W.A.Benjamin, Reading, Massachusetts, 1976
- [15] Yu.A.Izyumov, V.N.Syromyatnikov, Phase transitions and crystal symmetry, Kluwer Academic Publishers, London 1990.
- [16] K.G.Wilson, Rev.Mod.Phys. **47** (1975) 773-840



- [17] W.Kuhn, F.Grün, *Kolloid Z.* **101** (1942) 248
- [18] Paul W. and Smith G.D. *Rep. Prog. Phys.* 2004, **67**, 1117-1185

## Chapter 2

# Long history of short range order in polymers

The problem of existence of a short range order in amorphous polymers has been controversial for decades. It is only with the advent of fast computers and cheap computing power that serious efforts have been made to address this problem numerically. This however should not make us complacent, and here we investigate methodologies proposed by various authors. Firstly, a historical perspective is on order, as presented by us in 1994 ([1]).

### 2.1 Introduction

The determination of a local structure in amorphous polymers remains a fundamental problem in polymer science. Its importance stems from the fact that in order to understand physical properties at the molecular level one has also to know the polymer morphology at this level. The link to the macroscopic dimension, relevant eg for mechanical measurements, occurs through 3-D elastic constants [2]. The latter are calculable for crystalline polymers which possess regular structure, hence their physical properties and mechanical behaviour can be understood. Naturally a question arises: what can be estimated for non-crystalline polymers? This amounts to a description of amorphous polymers on a local scale and is a subject of many studies conducted in the last few decades.

It is frequently observed that amorphous polymers form glasses in the solid state and resemble liquids in the melt. The 'glassy state' is usually understood as a lack of ordering on a short - a few nanometers - scale. This general statement has obvious drawbacks: firstly, there are polymers which form mixtures of amorphous and crystalline phases spontaneously, hence ordering is not an unusual phenomenon for macromolecules. Secondly, the present poor understanding of a 'ground state' in glasses results in an ambiguity about permanent structural properties of the amorphous phase. The evolution of a structure can happen on a very long time-scale. An example is provided by the glassy polyethylene bottles, which lose their quality after a few months due to ordering of polymer chains. Many experimental techniques supported by theoretical considerations were engaged in studies of ordering of macromolecules and these efforts even became topics for symposia, for example the Faraday Discussion in 1979 [3]. In comparison with earlier [4, 5] and more recent reviews of this subject [6, 7] the Faraday conference volume entails the arguments brought for and against short range order in the most comprehensive way.

What is this debate about? The idea of polymers being 'organised' on a local level had a difficult birth. Already in 1860 Lourenço [8] has realised that the synthesised polyethylene glycols were complex and could have 'different degree of condensation' (in modern parlance, the number of repeating units). However, Kekulé's formula of the benzene ring (1865) has overshadowed all

attempts to describe constitution of polymers in terms other than 'colloidal associations', where several cyclic units were held together by some forces. It took about sixty years of researches until Staudinger has specifically proposed the chain formulas for polymers like polystyrene [9]. Even then it took several years of struggle, before the hypothesis of long, linear chains was finally accepted and the concept of isolated polymeric chains gained legitimacy. The next question was about the behaviour of these chains in different states of matter and the validity of statistical methods being applied to evaluate physico - chemical properties of polymers. Kuhn was the first to apply the statistical methods to treat the molecular weight distribution in degraded cellulose [10]. The dominance of statistical methods in polymer science is largely due to Flory [11, 12], with the resulting quantification of the experimental results in both polymer chemistry and physics. It is difficult to imagine, how would one otherwise be able to quantify these experimental results. There was however one side effect of such an uncritical universal application of statistical methods: that of stultifying the growth of understanding of packing of polymers in dense matter. One does wonder, to which extent strong personalities of the scientists involved in the studies of ordering of macromolecules have shaped the debate...

## 2.2 The gist of the debate

Flory calculated [13] that a single chain forms a gaussian coil in a  $\theta$ -solvent and suggested that this result can be extended to melts and solid polymers. Again this hypothesis proved debatable for more than two decades before the small angle neutron scattering technique (SANS) was invented and called to aid [14]. By then the ground was prepared and the first SANS experiments on amorphous polymers in bulk [15, 16, 17] were accepted as the needed support for this hypothesis. Since the radius of gyration found (which is a measure of an overall conformation of the molecule) agreed with that expected from calculations it was naturally assumed that chain monomers are arranged in a random fashion. However, there remained an uncomfortable evidence of some local order provided eg by electron microscopy [4]. In the ensuing debate most participants have overlooked that the question is not how a *single polymer chain* behaves in a solid, but how a *collection* of such chains is packed [4].

In his lecture on levels of order in amorphous polymers, Flory has said that 'no significant order (exists) down to dimensions commensurate with the diameter of the chain' [3]. This statement epitomises the standpoint of one school of thought, where a polymer chain would assume a random gaussian coil configuration *in the solid state* [12]. According to Flory, the random gaussian coil approximation is difficult to reconcile with a local (short range) order [3], p.15. The other viewpoint was expressed by Yeh [18] and Pechold [19], who looked for an evidence of order on a scale of 5 - 10 nm in the form of nodules, meander arrays, bundles and paracrystals not only in the solid state, but also in *polymeric melts* [3]. These ideas clearly acknowledge a need of compatibility with the principle of dense packing, but their origins are too firmly set in the arrangements of crystalline structures e.g. the 'bundle model'. Chains were required to have their segments folded in a nearly parallel fashion within ordered clusters and were separated by amorphous domains of similar sizes. This model was based on the 'cluster-entropy hypothesis', which has also come under attack as not being sufficiently justified [3].

At the Faraday conference, the validity of experimental evidence obtained from various techniques used was questioned. There was however general agreement that the scattering techniques would provide the direct evidence of ordering needed (see in particular General Discussion in ref. [3]). If they are to provide a *direct evidence* then electron microscopy should deliver the most illuminating data. The limit of this method lies in the physical dimension of specially prepared thin samples, surface scattering and in short lived structures created due to beam damage [4, 20]. The structures appearing on the surface may not be representative of the bulk. However, if similar in size (about 3 nm) structures are found by wide angle neutron scattering of polarized neutrons

with polarization analysis [21] then the hypothesis of the short range order concluded from electron microscopy results is definitely strengthened. If the results obtained from light scattering do not seemingly corroborate these findings, one has to bear in mind that light wavelengths used do not allow direct conclusions to be drawn about small distances.

## 2.3 Where do we stand?

Nearly twenty years ago (1976) Geil has lucidly stated [4]: "We suggest that it is now appropriate to reexamine critically the interpenetrating, random coil model for amorphous polymers (as well as the models proposed here).[...] It is important, moreover, that at this time one keep(s) a relatively open mind, whether one is concerned with the morphology per se or with the properties of amorphous polymers, since it is obvious that all of the answers are not yet in. In a sense the subject of morphology of amorphous polymers is in about the same position as the morphology of the crystalline polymers was in 1957 with the descriptions of chain folding in single crystals; now as then it may be necessary to strip away 30 years or so of interpretations based on incorrect model and begin again."

Has the situation changed a nearly two decades later? There is a major progress in computer modelling techniques which has resulted in accessibility of molecular modelling software, such as supplied by 'Biosym', 'Polygraf', 'Cerius' or 'Chem-Ex'. These are invaluable for visualisation of structures and are based on algorithms available at present, supported by traditional Monte Carlo or molecular dynamics simulations. Both techniques rely on the interatomic potential chosen as an input and its goodness is judged by an agreement of predicted radial distribution function  $g(r)$  with that obtained from experiment. However, there are pitfalls in this approach even if the experimental data is good: for instance,  $\mathbf{r}$  space comparison is good for the short range structure, yielding splendid agreement for  $g(r)$  at *small values of  $r$*  while distinct features appearing at low  $Q$  in the structure factor  $S(Q)$  (indicating particular intermediate or short range ordering) can be grossly wrong or even missing [22]. For amorphous polymers, the 'amorphous cell' model, based on the random gaussian coil [23] is extensively used. Therefore the subsequent model fitting using commercially available software amounts to the comparison of this model with experimental curves [24]. Experimentally, a progress has been achieved in the wide angle neutron scattering with spin polarisation analysis. Here the major gain is the separation of the coherent and incoherent scattering, and the absolute intensity, which allows for detailed comparison of experimental data and a model. Once the purely coherent scattering has been obtained, different model functions can be tested. Data obtained for polycarbonates have been compared with the 'amorphous cell' model [25], whereas these for polystyrene have been analysed by a combination of crystallographic approach and scattering from randomly oriented chains [26].

## 2.4 Scattering from polymers

The final test for the goodness of fit of a model must come in the agreement of the measured and modelled curves. However, a typical wide angle X-ray pattern from a non-crystalline polymer [27] - [29] would show only an 'amorphous halo', *resembling* the pattern obtained from liquids (which lack long-range ordering). An assignment of interatomic distances to particular halos is difficult due to the mixture of intra- and inter-molecular contributions to this halo. Hence the importance of experimental separation of purely coherent scattering from the incoherent part and an absolute intensity; this may be obtained with scattering of spin polarized neutrons with spin polarization analysis. The determination of partial structure factors helps then to approach the solution of this problem.

If the repeating units of the chain are optically anisotropic [7], a mutual order of chain segments

(the conformational order) can be assessed by depolarized light scattering. From such measurements, no indication of parallel ordering of neighbouring chains was found in amorphous polymers, like poly (methyl methacrylate) or polystyrene [7].

Amorphous polycarbonate was investigated by both wide angle X-ray and neutron scattering by several groups [34] - [36, 25] (and references therein). From results obtained on oriented samples, correlations up to the third nearest neighbouring chains were deduced [35] (although the number of participating monomers was not specified). Regions of enhanced order, which were 'possibly' due to a preferential packing of a few oriented layers, have also been reported [34]. Selectively deuterated polycarbonates have also been studied using wide angle neutron scattering [36]. Experimental patterns were compared with calculated patterns and the main features were reproduced. Lamers et al. investigated the wide angle scattering of polarised neutrons with spin polarisation analysis [25] from three different chemical modifications of polycarbonate and were able to describe quantitatively the short range order found, in terms of spacings and correlation lengths for the packing of neighbouring chains. They have also used the 'amorphous cell' method [23] to simulate the scattered intensity obtained and found that this method reproduces well the interatomic spacings. Significant discrepancies were present at the order peaks representing interatomic distances. This was thought likely to arise from the finite size of the cell and the periodic boundary conditions as well as insufficient relaxation of the initial configuration.

PMMA is a fascinating polymer and several attempts have been made to resolve its local structure, as can be followed in several papers [3, 29] - [32]. However, a detailed model has yet to be proposed. Remarkably, the numerous small angle scattering measurements on PMMA have shown a very strong deviation from the scattering expected from a random coil [33].

Polystyrene, a model 'amorphous' polymer, has also been a subject of several studies. Most recent data were obtained from wide angle scattering with spin polarisation analysis [21, 26, 37] work where we were involved and which is represented in the following, and from wide angle neutron scattering [24] experiments. In the latter, the best agreement with models was found for 'a simulation of the polymer chain through growth of the amorphous material in a cubic box, subject to periodic boundary conditions and to statistical constraints on the allowed values for the bond torsional angles'. The authors stated [24] that there is not yet a quantitative agreement between experimental and calculated curves, especially at low Q values. It is at these values that the influence of ordering between chains would show and this result clearly calls for revision of the procedures used.

Spin polarisation has allowed us to obtain the relevant short range order parameters for a series of selectively deuterated non-crystalline polystyrenes and describe it consistently for all samples used. The diffraction pattern of PS can be interpreted assuming a structure which is determined by an average distance between neighbouring chains. This distance is not sharply determined but can be given in terms of distance distributions, characterised by a mean distance between chains, an interaction radius, distribution width and a degree of disorder. A self-convolution of this distribution gives a pattern comprising further neighbour distances. Then a picture of pseudo-crystallites, with a 2-D ordering in the x-y plane, randomly oriented with respect to each other, emerges for atactic polystyrene [26]. For isotactic polystyrene ordering is 3-D, with considerably larger correlations [37].

## 2.5 Future prospects

During the past decade it became obvious that, although many authors pay at least a lip service to the random gaussian coil approximation, the number of papers showing an evidence of short range order (and being recognised as such) steadily increases. There are new developments in the understanding of the structure of liquids and glasses [22], where Reverse Monte Carlo (RMC) modelling, based on experimental data, makes full use of the available information. RMC uses an

algorithm similar to that of Metropolis Monte Carlo, in the RMC one minimises the difference between structure factors calculated from the model and those measured experimentally, rather than minimising the potential energy of the system. This approach offers several advantages over Monte Carlo calculations: for instance no interatomic potential is required and data sets from different experimental techniques can be combined. RMC has been so far very successfully applied to liquids like molten metals and salts [22] and its application to polymers is underway.

This information is now more accessible due to computerised information search systems. Many polymer scientists are aware of the evidence coming from SANS. And on the large scale accessed by this technique the random coil model seems to describe reality quite well. The space region where this model does not fit is accessed by wide angle X-ray and neutron scattering and it is only recently that this information started to be disseminated. There is a scope for both more experiments on 'glassy' polymers and for revision and the expansion of the existing algorithms. One cannot help wondering: would the presence of the short range order in amorphous polymers be generally accepted, how many papers appearing in this field would have to change?

## 2.6 A decade later

As we have predicted, there is increasing awareness of the existence of the short range order in amorphous polymers. However it came more from the modelling than experimental side, as described in a recent review article ([38]).



# Bibliography

- [1] Gabrys B., Trends in Polymer Science 1994, **2**, 2
- [2] Tashiro K., Kobayashi M. and Tadokoro H. *Macromolecules* 1978, **11**, 908
- [3] 'Organization of Macromolecules in the Condensed Phase', Faraday Disc. Royal Soc. Chem. 1979, **68**, pp 14-141
- [4] Geil, P.H. *J. Macromol.Sci.-Phys.* 1976, **B12**, 173
- [5] Fischer, E.W. and Dettenmaier, M. *J. Non-Cryst. Solids* 1978, **31**, 181
- [6] Wendorf J.H. *Polymer* 1982, **23**, 543
- [7] Fischer E.W. and Voigt-Martin I.G. (1991) Ch.17 in '*Chemistry and Physics of Macromolecules*', Fischer, E.W., Schulz, R.C. and Sillescu, H., Eds.; Sonderforschungsbereiche, VCH, Weinheim, p. 477
- [8] Lourenço, A.-V. *Compt.rend.* 1860, **51**, 365; *Ann. chim. phys.* 1863, **67**, 273
- [9] Staudinger, H. *Ber.* 1920, **53**, 1073
- [10] Kuhn, W. *Ber.* 1930, **63**, 1503
- [11] Flory, P.J. 'Principles of Polymer Chemistry', Cornell University Press, New York, 1953
- [12] Flory, P.J. 'Statistical mechanics of chain molecules', Interscience Publishers, New York, 1969
- [13] Flory, P.J. *J. Chem. Phys.* 1949, **17**, 303
- [14] Higgins, J.S. and Stein, R.S. *J. Appl. Cryst.* 1978, **11**, 346
- [15] Kirste, R.G. Kruse, W.A., Schelten, J. *Makromol.Chem.* 1972, **162**, 299
- [16] Benoit, H., Cotton, J.P., Decker, D., Farnoux, B., Higgins, J.S., Jannink, G., Ober, R. and Picot, C. *Nature* 1973, **245**, 13
- [17] Wignall, G.D., Schelten, J. and Ballard, D.G.H. *Eur. Polym. J.* 1973, **9**, 965
- [18] Yeh, G.S.Y. *J.Macrom.Sci.Phys.B* 1972, **6**, 465
- [19] Pechold, W.R. *Kolloid Z.Z. Polym.* 1968, **228**, 1; idem 1969 **231**, 418
- [20] Vesely, D. and Downing, K.H. 'Electron beam damage of PE single crystals', in 'Electron beam crystallography of organic molecules', Kluwer Acad. Publ., 1990
- [21] Gabryś, B. and Schärpf, O. (1992) *Physica B* **180&181**, 495
- [22] McGreevy, R.L. (1991) *J. Phys.: Condens. Matter* **3**, F9



- [23] Theodoru, D.N. and Suter, U.W. *Macromolecules* 1985, **18**, 1467
- [24] Rosi-Schwartz B., Mitchell, G.R. and Soper, A.K. (1992) *Polymer* **33**, 3744
- [25] Lamers, C., Schärpf, O., Schweika, W., Batoulis, J., Sommer, K. and Richter, D. (1992) *Physica B* **180 & 181**, 515
- [26] Schärpf, O., Gabryś, B. and Peiffer, D.G. (1990) ILL Report **90SC26T**, Part A; Institute Laue-Langevin, Grenoble, France
- [27] Miller, R.L. and Boyer, R.F. (1984) *J.Polym.Sci.: Polym.Physics Ed.* **22**, 2021
- [28] Miller, R.L. and Boyer, R.F. (1984) *J.Polym.Sci.: Polym.Physics Ed.* **22**, 2043
- [29] Lovell, R., Mitchell, G.R. and Windle, A.H., p.46 in ref.[2]
- [30] Lovell, R. and Windle, A.H. (1981) *Polymer* **22**, 175
- [31] Sundararajan, P.R. and Flory, P.J. (1974) *J.Amer.Chem.Soc.* **96**, 5025
- [32] Gabryś, B., Higgins, J.S. and Schärpf, O. (1986) *J.Chem.Soc. Far.Trans.I* **82**, 1929
- [33] Dettenmaier, M., Maconnachie, A., Higgins, J.S., Kausch, H.H. and Nguyen, T.Q. (1986) *Macromolecules* **19**, 77
- [34] Mitchell, G.R. and Windle, A.H. (1985) *Colloid & Polymer Sci* **263**, 280
- [35] Schubach, H.R. and Heise, B. (1986) *Colloid & Polymer Sci* **264**, 335
- [36] Červinka, L. et al. (1987) *Polymer* **28**, 1287
- [37] Gabryś, B., Schärpf, O. and Peiffer, D.G. (1993) *J. Polym. Sci.: Part B: Polymer Physics* **31**, 1891
- [38] Paul W. and Smith G.D. *Rep. Prog. Phys.* 2004, **67**, 1117-1185

## Chapter 3

# Short range-order in amorphous polystyrene using polarized neutron scattering: a demonstration and detailed description.

Otto Schärpf, Physik Department E13

T.U.München

D-85747 Garching

Barbara Gabrys, Brunel Univ. of West London

Uxbridge, Middlesex UB83PH UK

Dennis G. Peiffer, EXXON Research and Engineering Co

Route 22 East, Annandale, N.J., U.S.A.

### 3.1 Abstract

We describe a new technique of polarization analysis with a multidetector for wide angle scattering to separate quantitatively the coherent part of the neutron spectra from selectively deuterated atactic polystyrene and protonated isotactic polystyrene. The method of the internal standard used is especially effective. The data are analysed by comparing them quantitatively with peak heights, widths, Bragg angles with the results of different models namely: 1. the crystalline structure of Greis et al. *Z. Kristallographie* 182,58(1988) , 2. a hexagonal dense packing of chains, both by calculating the respective powder patterns and using peak broadening by grain size effects , 3. by comparing with calculated diffuse scattering from randomly oriented chain pieces of different lengths and conformations of up to ten parallel chains of isotactic and syndiotactic chains of different lengths. Assuming that all selectively deuterated samples have the same structure allows us to decide in the ambiguous case of a model with three nearest neighbors and of hexagonal dense packing of the chain deuterated sample allowing for a more exact determination of the effective chain length, 4. Comparison with the paracrystalline picture (where the necessary fundamental concepts are shortly described). By these approaches we obtain in the case of the isotactic sample a very detailed description of the observed short range order giving the degree of disorder (for isotactic material in 33% of the sample the distance between the chains has a distribution with a width of 7% of the distance) and also the interaction region or the grain sizes depending on which factor dominates the peak broadening . These factors can clearly be distinguished by Q-dependent peak broadening. The selective deuteration in these different samples selectively increases the height of

diffraction peaks corresponding to the respective order (of chains or rings). The scattering from randomly oriented single chains cannot describe the observed scattering in detail. 5. Description of the measurements by partial structure factors, which we apply for the selectively deuterated parts of the polymer. The spherical Fourier transform of these partial structure factors yields the partial pair correlation functions  $g_{cc}(R)$ ,  $g_{rr}(R)$  and  $g_{cr}(R)$  for the chain parts  $c$  and the ring parts  $r$  of the polymer and makes possible to give quantitatively the partial coordination numbers  $Z_{\mu\nu}$  for the different coordination shells and in principle even the Warren-Cowley short range order parameters. Small angle scattering measurements simultaneously carried out show the weakness of the latter method in comparison with the wide angle scattering. The former is very valuable as a complementary method. The paper concludes in an exact description of the order or disorder in the conformation of the chains in atactic polystyrene. It then remains a matter of semantics whether one wants to call this short range order or random orientation of the chains.

## 3.2 Contents

- Introduction
- Sample characterization
- Sample preparation
- Measurements
- Results and interpretation of wide angle scattering
  1. Crystalline powder pattern
    - a. Crystal structures
    - b. powder pattern
    - c. comparison with measurements: isotactic sample
    - d. Comparison with measurement for selectively deuterated materials
  2. The random chain orientation. Calculation of  $F_M$ 
    - a.  $F_M$  of an ordered structure
    - b.  $F_M$  of amorphous regions
    - c. Comparison with measurements
  3. Real polymer and paracrystallinity. Description of amorphous state
    - a. Isotactic material
    - b. Atactic material
    - c. different definitions of amorphicity
- Conclusions
- References

## 3.3 Introduction

Experimentation with polarized neutrons using spin polarization analysis is not restricted to the investigation of magnetic phenomena but with the use of many analyzers distributed over a wide angular range allows for an unambiguous separation and analysis of the coherent and incoherent diffuse scattering from amorphous and liquid materials [1, 2]. In a usual neutron scattering experiment one always measures the total scattered intensity which is a sum of the coherent and

incoherent parts [2, 3]. Polarization analysis can separate experimentally the coherent and incoherent components and thus a purely coherent diffraction pattern for further analysis is obtained. The virtue of this technique is further amplified by an internal calibration yielding the absolute intensity as described below. The spectrum can then be directly compared with the calculated model curves.

The strength of this approach is evident and we have used it to tackle the problem of the packing of polymers in the solid state. Although recognized as a fundamental question with no general agreement it was considered as less important than the problem of the whole chain configuration [4]. The selective use of statistical methods and small angle X-ray and neutron scattering [5] which both probe large distances only has resulted in establishing a picture of a polymer chain forming a Gaussian coil. This result was consistent with the image of a polymer chain in dilute solution. However the idea of many Gaussian coils brought together to form a solid and still preserving their randomness over the whole length violates the principle of dense packing, well established for other amorphous and crystalline materials. The question of the existence of short range order and its impact on the macroscopic physical properties like elasticity and viscosity then arises. The answer is of not only academic interest, but is essential in understanding solid state properties of speciality polymers, for example, associating-type polymers. For example we have detected a short range order in amorphous poly(methyl methacrylate) (PMMA) [3]. In conjunction with the conclusions from other investigations like X-ray scattering short range order could be universally present in glassy polymers.

It is widely believed that the change in physical properties of ionomers is related to the change in a random structure of a precursor upon introduction of a small percentage of ionic groups. It is further assumed that this results in the attraction of ionic charges, which form pairs and higher multiplets, a process referred to as a microphase separation. Their size and distribution throughout the material is assumed to be such that they cause an appearance of an order peak at low values of the scattering vector  $Q$  in a small angle X-ray and neutron scattering experiment [6, 7]. The values of the multiplets (or cluster) sizes were estimated to be of the order of several Å, which should then be visible either in wide angle or small angle scattering.

It then became clear that before assigning of the origin of a low  $Q$  peak in ionomers as due to ionic charges grouped together one has to eliminate the structural effects present already in the parent polymer. Hence we decided to carry out a comparative study of a series of sodium sulfonated polystyrene ionomers (NaSPS) and its corresponding unsulphonated precursors. We always simultaneously measured small angle scattering with polarization analysis. The results of these measurements will be presented. The first concerns the structure of selectively deuterated atactic and isotactic polystyrene. The measurements on the ionomers are published in [21]

This seems interesting in itself because of the very detailed description of the structure of these materials resulting from our measurements. It is also of interest in view of the highly investigated physical properties, e.g. glass transition of glassy polymers such as atactic polystyrene. If one needs to describe a polymer's properties one should understand the underlying structural information.

Our approach also shows the strength of the wide angle scattering with polarization analysis in comparison to small angle scattering. The former will allow us to determine the width of the statistical distribution of distances of the parallelly arranged chains i.e. the degree of disorder in the isotactic sample and their percentage contributing from different grain sizes and subsequently distinguish beam broadening from grain sizes and disorder in the atactic samples.

In what follows we describe the sample preparation, the instrument and the new method of measurement and the correction for multiple scattering in the first section. Subsequently in "results and interpretation of the wide angle scattering" in the first section the scattering is regarded as resulting from a powder pattern of crystalline material. Then we relax the conditions of the crystalline order more and more arriving at disordered hexagonal dense packing and add the necessary grain size to explain the peak broadening. This is done initially with the isotactic sample

and then the results are applied to the atactic samples. This section greatly clarifies the structure of the isotactic sample and the selectively deuterated atactic samples.

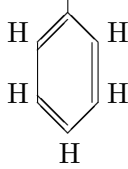
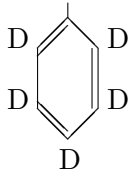
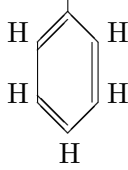
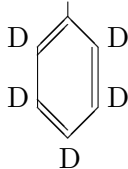
The next chapter treats the interpretation of the results of the wide angle scattering by firstly investigating the scattering of one monomer and adding more and more monomers in different order to get the necessary size of the units that scatter like the real polymer. This will guide us first to an ambiguous interpretation of two different structures, which can be the reason of the observed scattering pattern for different samples. Then we make use of the fact that we have the same samples, only differing in the selective deuteration, but of equal preparation, so that they must have the same structure. This helps us decide between the two possibilities. This allows then also to determine the chain length very sensitively in the case of the DH sample, which should then also be valid for the other polymers. This section clarifies the understanding of the scattering from the atactic samples.

The chapter following this tries to treat the remaining discrepancies first as a combination of short range order and randomly oriented chains and finally by paracrystallinity. This will give us a complete description of the isotactic and atactic structure underlying the observed structure. It remains then a question of semantics which is the proper name one wants to give to this structure, whether one wants to call it short range order or whether one prefers to call it amorphous or randomly structured. Independent of nomenclature, we describe the polymer structure by assigning numbers to the degree of disorder.

### 3.4 Sample characterization

We report in this paper on measurements on five different polystyrene samples i.e. the isotactic (IHH) and the atactic (HH) fully protonated one, the atactic chain deuterated (DH), the atactic ring deuterated (HD) and the fully deuterated (DD) sample. In the table below all samples used in the study are listed with regard to their molecular weight, structure of the monomer, polydispersity  $M_w/M_n$ . This quantity  $M_w/M_n$  is a measure of polydispersity because with  $M_n = \sum n_i M_i / \sum n_i$  and  $M_w = \sum w_i M_i / \sum w_i = \sum n_i M_i^2 / \sum n_i M_i$  and  $n_i$ =number of molecules of the  $i$ th fraction and  $w_i$ =weight of the  $i$ th fraction,  $M_n/M_w$  is always larger than one and only in monodisperse systems  $M_i$  can be factored out and one obtains one. Furthermore, our short identification code for each sample, incoherent cross section (in barn and in barn/sr), and measured transmission for  $\lambda=5.7 \text{ \AA}$ , sample weight (or total weight including aluminium foil) is given. Some samples were heated for 24 hours (HH run number 23040-52; DD).

**Table 1. STRUCTURE & CROSS SECTIONS OF PURE POLYSTYRENE (PS)**

SAMPLE Mol.weight	CODE $M_w/M_n$	STRUCTURE of Monomer	$\sigma_{inc}$ [b] Transm.,weight	file	time hours
Neutral PS: Polystyrene 600,000 HH	$C_8H_8$ (hydro- geneous) 1.06	$-(CH_2-CH)-$ 	639.28 b 50.87 b/sr $0.8459 = Tr_{old}$ $0.880093 = Tr_{new}$ 0.2162 g sample	ATACTIC 22913 22973 23037-9 23053-5	2x1 2x2 2x6 2x6
IHH			639.28 b 0.351 g sample $\lambda = 5.7 \text{ \AA}$ $\lambda = 4.8 \text{ \AA}$ $\Theta$ angle scan	ISOTACTIC $0.8378 = T_r$ 26553-5 26707-9 26711-16	2x6 2x9 2x6
Perdeutero- polystyrene 1.39 million DD	$C_8D_8$ 4.6	$-(CD_2-CD)-$ 	16.4 b 1.305 b/sr 0.9099 old 0.8798364 new 0.98259 g total	22914 22979 23057-9 23072-6	2x1 2x2 2x6 2x5.5
$\alpha, \alpha, \beta$ -D <sub>3</sub> PS 2.107 million DH	$C_8D_3H_5$ 2.4	$-(CD_2-CH)-$ 	405.7 b 32.28 b/sr 0.8149 0.750124 new 0.80227 g total	22915 22983 23012-4	2x1 2x2 2x6
RING-D5 PS 1.171 million HD	$C_8D_5H_3$ 6.6	$-(CH_2-CH)-$ 	249.98 b 19.89 b/sr 0.87385 0.8062185 new 0.81483 g total	22916 22986 22997-9	2x1 2x2 2x6

values taken:  $\sigma_{inc}^H = 79.9$  b,  $\sigma_{inc}^C = .01$  b,  $\sigma_{inc}^D = 2.04$  b,  $\sigma_{inc}^{Na} = 1.627$  b,  
 $\sigma_{inc}^S = .007$  b,  $\sigma_{inc}^O = 0$

### 3.5 Sample preparation

A typical polymerization procedure for the preparation of the various hydrogenous, deuterated and selectively deuterated polystyrenes for the neutron scattering experiments is given below. The unfunctionalized polymers are prepared through the emulsion polymerization of the appropriate styrene monomer using potassium persulfate as the initiator and sodium laurylsulfate as the surfactant. To ensure a high molecular product no chain transfer agents were used. All polystyrenes were prepared in 500 ml -4 neck flask equipped with an argon gas feed, a thermometer, and an air driven stirrer. For example, into the flask were added 90.0 ml of distilled water, 10.0 g  $\alpha, \alpha, \beta - D_3$  styrene, 0.5 g sodium laurylsulfate, and 0.1 g potassium persulfate. This mixture was vigorously agitated, degassed with argon gas, and heated to 50<sup>0</sup> C for 24 hours. The mixture was continuously blanketed with argon gas during the entire polymerization sequence. The polymer was isolated from the emulsion with the addition of a large excess of acetone and subsequently dried in a vacuum oven at 65<sup>0</sup> C for 48 hours. This particular polymer is designated DH. As noted previously in Table 1, the structures and appropriate designations of all unfunctionalized atactic polystyrenes are listed. The isotactic and syndiotactic chains of polystyrene are shown in fig.4.1 and 4.2 on page 42. The atactic chain consists of a random sequence of syndiotactic and isotactic units.

Isotactic polystyrene was prepared according to the well-known procedure of Natta [8]. The polymer obtained from the procedure is crystalline but contains still 6%-7% atactic chains. Semicrystalline isotactic polystyrene (IPS) was difficult to solubilize in the solvent used for the subsequent sulphonation reaction. The semicrystallinity was eliminated via quenching from the melt (260<sup>0</sup>C). After being quenched, the polymer was dissolved in boiling toluene, filtered, and subsequently precipitated into vigorously stirred methanol. The atactic polystyrene component was eliminated via Soxhlet extraction for 96 hours with methylethylketone. The polymer was then dried in a vacuum oven at 60<sup>0</sup>C for 24 hours. The Soxhlet extraction guarantees an ultra pure isotacticity (99.9% isotactic). We used in our measurements the material treated by the Soxhlet extraction to have a sample with an isotacticity as high as possible .

The materials were further characterised in terms of their molecular weight distribution with gel permeation chromatography. The molecular weights and the  $M_w/M_n$  ratio are listed in table 1.

### 3.6 Measurement

For all measurements the D7 instrument at the Institut Laue Langevin, Grenoble equipped with a polarization analysis option was used. Fig.3.1 shows its general lay-out. The small angle scattering set-up with spin analysis is shown schematically in fig.3.2. We emphasize the small angle scattering was carried out simultaneously with the wide angle measurement. The small angle apparatus consists of one analyzer with supermirrors [9] arranged horizontally lying also in a horizontal magnetic field arranged near the sample. This allows an angular range of 9<sup>0</sup> to be "scanned" by measuring simultaneously with 16 detectors of 1.2 cm width at a 1.68 m distance from the sample. This corresponds to an angular resolution of 0.01 Å<sup>-1</sup> for the incident wavelength of 5.72 Å.

In an actual experiment the neutrons doubly focused by a triple pyrolytic graphite monochromator are subsequently polarized vertically with a bender type supermirror polarizer [9] as shown in fig.3.1. The neutrons subsequently traverse a Mezei-type flipper, which serves to change the polarization direction of the neutrons relative to the magnetic guide field. After scattering by the sample the neutrons are detected by an array of detectors equipped with supermirror analyzers which transmit neutrons with only spin up component. In order to distinguish between the coherent  $\sigma_{coh}$  and the incoherent scattering  $\sigma_{inc}$  as described below, the measurement is carried out by alternating the spin-flip and non-spin-flip modes and counting the respective neutrons separately. In this way it is possible to measure separately the scattering of neutrons which are flipped by the

scattering process in the sample e.g. neutrons scattered by the nuclear spin of the proton. This spin-flip scattering results from  $2/3$  of the spin incoherent cross section and this cross-section  $\sigma_{inc}$  is known for each polymer sample for the formula unit of one monomer; the corresponding values calculated for each polymer sample are given in table 1. In this way measuring alternatively every minute separately the scattering with and without spin flip an internal calibration for each sample

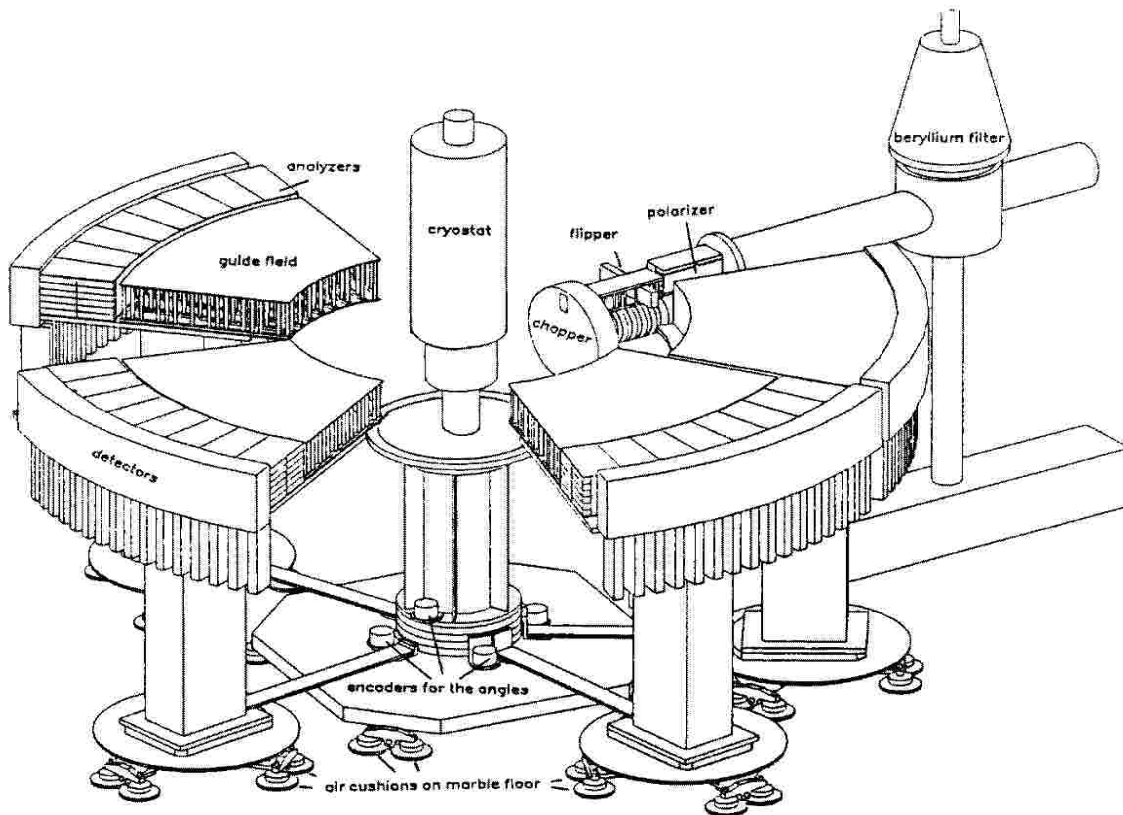


Figure 3.1: Lay-out of the D7 instrument showing the Be-filter, polarizer, flipper, chopper for time of flight measurement, guide fields, central part with sample space allowing for an oven or a cryostat. Four detector arms are attached to this part and each of them bears eight analyzers in permanent magnetic fields with guide fields in front of them and these arms can be moved independently on air-cushions around the sample in the angular range from  $-160^\circ$  to  $+160^\circ$ .

is obtained since the incoherent scattering is isotropic and only this cross section is measured in the spin-flip mode. The non-spin flip mode measures the sum of the coherent scattering,  $1/3$  of the incoherent scattering and the isotope related part of the incoherent scattering. Therefore the coherent part of the scattering  $\sigma_{coh}$  can be determined by subtracting half of the spinflip scattering from the non-spinflip scattering. If one relates  $\sigma_{coh}$  (after subtraction of the background and correction for a finite flipping ratio [2]) to the incoherent scattering  $\sigma_{inc}$ , one obtains an absolute calibration of the coherent scattering in barn/formula unit. In the discussion that follows it will transpire how important this calibration is and why it is very useful. It helps to identify and correct systematic errors and serves especially for comparison with model calculations and for the determination of the coordination numbers in chapter 7 on page 95. This is due to the fact that normally neutron scattering without polarization analysis cannot separate the coherent from incoherent scattering and, therefore, one has to resort to subtracting some arbitrarily assumed backgrounds whereas using spin polarization analysis both components can be separated experimentally. Subsequently the



coherent scattering component can be directly determined using the previously determined incoherent part as an internal calibration, which otherwise must be determined in a separate measurement using an incoherent scattering standard [e.g. vanadium, water]. The latter procedure impedes an exact determination of the absolute scattering per monomer because of beam inhomogeneities and sample inhomogeneities or uncertainties about the part of the sample in the beam or the cross section and thickness of the standard.

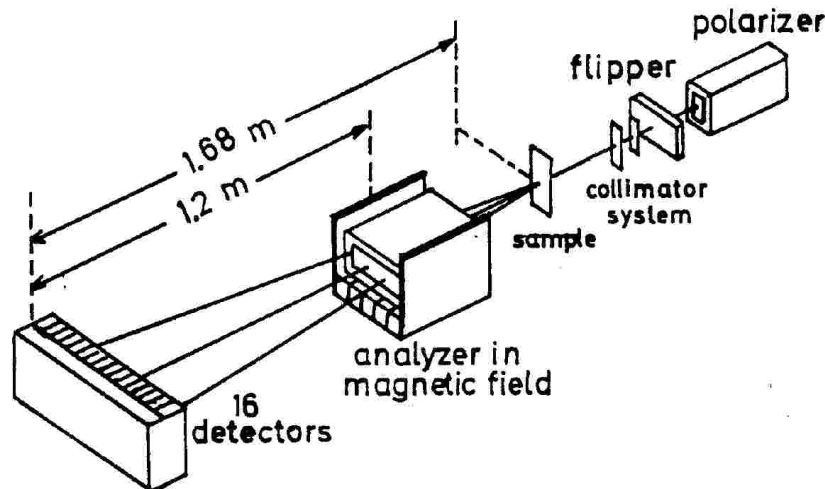


Figure 3.2: Sketch of the small angle scattering arrangement with analysis (see text)

The finite flipping ratio for small angle scattering was measured with a strong small angle scattering Vycor glass sample which scatters without flip. Quartz was used to determine the flipping ratio at wide angles. The number of flipped neutrons transmitted in this case as compared to those transmitted without flip yields a finite flipping ratio,  $R = (I^{\uparrow\uparrow}/I^{\uparrow\downarrow})$ , because of the imperfection of the polarizer. Typically, this ratio is approximately 30 to 40.

The fully deuterated sample (DD) has only a small  $\sigma_{inc}$  and shows a behavior deviating from the other samples, i.e. showing much less scattering than the others. The simplest reason for this behavior is the contamination by water or incomplete deuteration. This would give the wrong internal calibration standard, which would be in reality much higher due to an amount of absorbed water or hydrogen.

To exclude this possibility, we also made a vanadium calibration measurement for both the small and wide angle scattering. This vanadium calibration measurement shows in the case of the DD sample that there is 2.6 % contamination of hydrogen due to incomplete deuteration. Fig.3.4 shows the results with the internal calibration with the  $\sigma_{inc}$  already corrected for this hydrogen contamination. Figs.5.14 and 5.15 show another possibility of correction by relating the wide angle scattering to the calculated gas scattering at  $Q > 2 \text{ \AA}^{-1}$ . This gives the same results as the comparison with vanadium.

Due to the geometry of our instrument the ideal sample shape should be cylindrical for wide angle scattering and flat for small angle scattering. This is due to the fact that it is difficult to calibrate the scattered intensity for the form of the sample if one has a standard scatterer of another form. We tested the behavior of some samples using both geometries. Cylindrical and flat sample geometries gave similar results if a) the measurement was related to the internal calibration, and b) the measured transmission (given in table 1) was of the order of 80%-90%. Due to multiple scattering a sample with the transmission of 68% showed the behavior visible in fig.3.3 (circles) in

comparison with a thinner sample of 81% transmission (crosses).

The two curves of fig.3.3 give us the opportunity to show the importance of the multiple scattering correction and also how easy it is resolved in the case of polarization analysis. We did it by Monte Carlo calculations 9.1.3 on page 126, but one can draw some simple conclusions from the Monte Carlo calculations [2] which are easy to apply in general cases using only measured physical quantities. For example, for the fully hydrogenated sample (IHH and HH)  $\sigma_{inc} = 50.87$  b/(sr.mon.). Then the scattering with spin flip corresponds to  $2/3 \cdot 50.87 = 33$  b/(sr.mon.). Double scattering from a 10% scatterer gives then 3.3 b/(sr.mon.). Those doubly scattered neutrons are again incoherently scattered and  $2/3$  of it with a second spin flip (2.2 b/(sr.mon.)) appear additionally in the non spin flip part of the scattering and hence are interpreted as coherent scattering. As the incoherent scattering is flat in Q, the double scattering with twice flip is also flat. This flat background without flip must then be subtracted from the "coherent" part because it is only apparently coherent resulting from double scattering with flip, and twice flipped resembles no flip. This is quite an important correction in our case, orders of magnitude larger than the respective Laue diffuse scattering from disordered coherent atoms with strong difference in the coherent scattering lengths. If the absorption can be neglected, the incoherent scattering power of the diffuse coherently scattering sample can be determined from the measured transmission  $T_r$  given in table 1 for each sample by using the average  $\langle \sigma_{coh} \rangle$ . These values are from the uncorrected measurement of fig.3.4. The resulting  $\sigma_{coh}^{apparent}$  from double scattering is then determined by iterative repetition of these steps using the following formula: (all per steradian and monomer)

$$\sigma_{coh}^{apparent}(twice\,flipped) = \frac{2}{3} \frac{2}{3} (1 - T_r) \frac{\sigma_{inc}}{\langle \sigma_{coh} \rangle + \sigma_{inc} + \sigma_a} \sigma_{inc} \quad (3.1)$$

If absorption plays a role it has to be included in the denominator as  $\sigma_a$  related to one monomer. This denominator should include factors that lower the intensity of the transmitted beam i.e. absorption, incoherent scattering and integral over the whole angular range of the coherent scattering (therefore we have to take the average  $\langle \sigma_{coh} \rangle$  in this case).

The scattering curves of figs.3.3 and 3.4 allow an estimation of this part in comparison to the incoherent part which is estimated taken as flat of the height given in table 1. In fig.3.3  $\langle \sigma_{coh} \rangle = 9$  b/(sr.monomer) for the thick sample and 7 b/(sr.monomer) for the thin sample whereas  $\sigma_{inc} = 50$  b/(sr.mon.) and a  $T_r = 68\%$ . Using eq.(3.1) we obtain a 27% incoherent and 5% coherent scatterer for the thick sample. Accordingly the thin sample represents a 16.7% incoherent and 2.3% coherent scatterer. Eq.(1) gives then a double scattered flat background with double flip of 5.6 b/(sr.mon.) for the thick sample and 3.7 b/(sr.mon.) for the thin sample. This corresponds exactly to the minima of the measured curves in fig.3.3, which are then of zero cross section.

The other effect of multiple scattering is to diminish the peak height in the coherent scattering curve i.e. to flatten peaks. This effect is enhanced as the peaks narrow. The Monte Carlo calculations show that this effect is smaller than 5% if the transmission is 90%. This is visible in fig.3.3, where two samples with very different transmission are compared. Only a small reduction in the coherent peak is observed.

To avoid this effect the amount of material in some samples in the incident beam was reduced in order to obtain higher transmission values and thus diminishing the multiple scattering effect.

The measured scattering patterns shown in fig.3.4 are corrected for the following double scattering for the coherent scattering, which has been subtracted from the curves in fig.3.4 as a flat (Q independent) contribution:

HH	2.5 b/(sr.mon.)	IHH	2.5 b/(sr.mon.)
DD	0.02 b/(sr.mon.)	DH	2.87 b/(sr.mon.)
HD	1.29 b/(sr.mon.)		

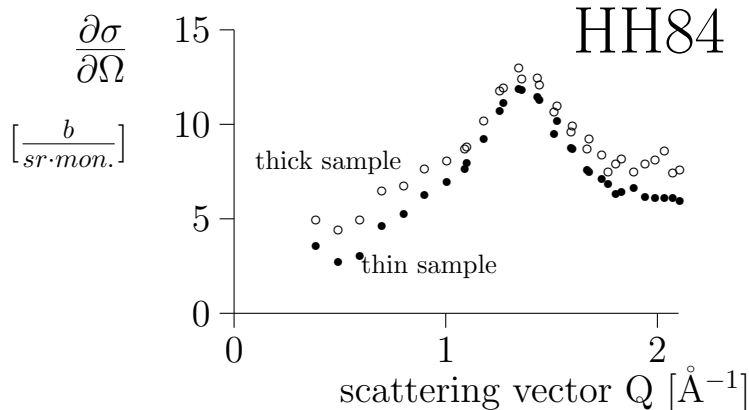


Figure 3.3: Comparison of scattering by a thick (circles) (Tr=68%) (HH84068) and a thin sample (crosses x) (Tr=81%).

Measurements were taken mainly at room temperature and without energy analysis. As is typical in diffraction work, all neutrons scattered into the respective detector at the respective angle  $\Theta$  were counted.

For one measurement we used time of flight energy analysis, to exclude errors by an eventual contamination by higher order reflection of the monochromator and also to see eventual contributions of the inelastic scattering of the sample. Such effects could contribute in an unexpected manner to the observed structure measurements. The result was that there is no contamination of second or higher order wavelengths. The observed inelasticity, which could diminish the peak height by the Debye-Waller factor, was negligibly small (in contrast to our observations in PMMA) and was consequently not taken into account. Debye-Waller factors would also cancel in the internal calibration method, as they are the same for coherent and incoherent scattering.

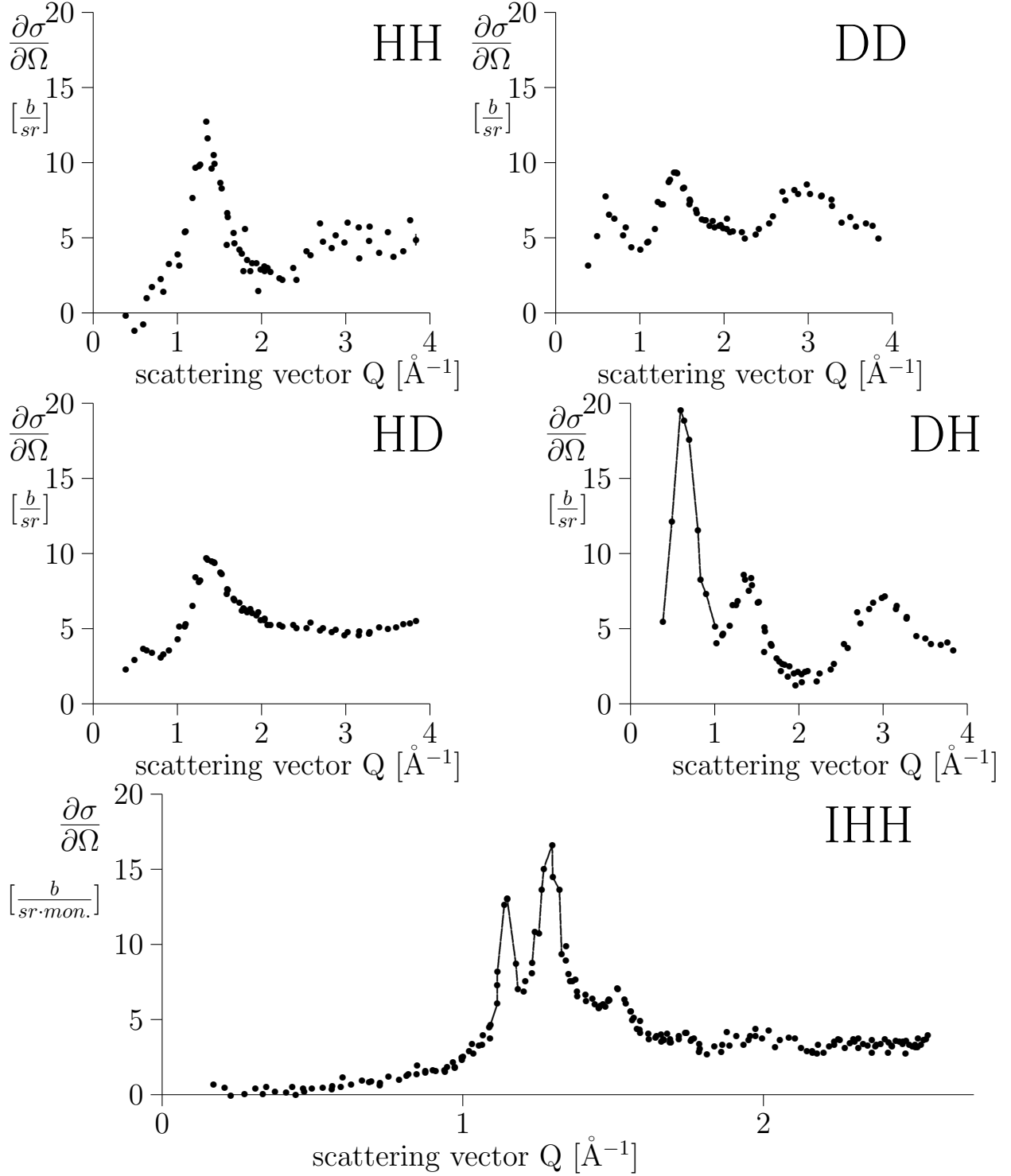


Figure 3.4: Measured coherent scattering cross section  $d\sigma/d\Omega$  (in absolute units) internally calibrated by relating the measured and known incoherent scattering for the selectively deuterated unfunctionalized polystyrene materials. Note that the error bars are vanishingly small. The figures include measurements using two wavelengths (5.715  $\text{\AA}$  and 3.1  $\text{\AA}$ ). Only the wide angle results are shown. For the IHH sample only measurements with  $\lambda = 4.8$   $\text{\AA}$  are shown.

### 3.7 Results and interpretation of the wide angle scattering.

In order to understand the effect of suphonation on the structure of polystyrene [21], first the unfunctionalized parent polymer samples with selective deuteration were investigated and this is the objective of what we describe here. The different selectively deuterated polystyrene structures are shown in table 1. The chemical constitution of each type of monomer unit is displayed in column 2 with their corresponding names: fully protonated, fully deuterated, chain and ring deuterated listed in column 1. The corresponding abbreviations (HH, DD, DH, HD) are listed in column 3. The resulting wide angle scattering  $d\sigma/d\Omega$  (in barn/sr/monomer) versus scattering vector,  $Q$ , (in  $\text{\AA}^{-1}$ ) for all parent polymer samples are shown in fig.3.4. The sample code abbreviated IHH indicates the isotacticity. The other samples are fully atactic.

The interpretation of these data can now be undertaken in several very different ways each of them leading to interesting conclusions. We will discuss the following methods: 1.crystalline powder pattern calculations 2.calculation of the scattering of the randomly oriented chain. Combining these calculations results in a third step 3.real polymer as a combination of short range order and random chain orientation. 4.partial structure factor determination. To each of these interpretations we consacrate a separate chapter.

We first try to interpret directly the observed peaks, i.e. their position, width, relative order and height change which can immediately give the following information:

1. **i) Regarding the individual peak positions and widths:** all samples show a peak at  $Q=1.33 \text{ \AA}^{-1}$  with a width of  $0.46 \text{ \AA}^{-1}$  corresponding to a period of  $4.71 \text{ \AA}$  and a correlation length of  $13.65 \text{ \AA}$ . In addition DH and DD have a peak at  $0.60 \text{ \AA}^{-1}$  with a width of  $0.34 \text{ \AA}^{-1}$  corresponding to a period of  $10.5 \text{ \AA}$  with a correlation length of  $18.5 \text{ \AA}$ . HD and HH have there only a slight blip. The third peak for DH and DD at  $3.0 \text{ \AA}^{-1}$  with a width of  $0.60 \text{ \AA}^{-1}$  corresponds to a period of  $2.09 \text{ \AA}$  with a correlation length of  $10.4 \text{ \AA}$ . It is broader in the HH polymer and is only slightly marked in the HD material. The IHH sample shows high narrow peaks at  $1.15 \text{ \AA}^{-1}$  of the width  $0.06 \text{ \AA}^{-1}$  corresponding to a period of  $5.5 \text{ \AA}$  and a correlation length  $105 \text{ \AA}$  and at  $1.28 \text{ \AA}^{-1}$  of the width  $0.08 \text{ \AA}^{-1}$  yielding a period of  $4.9 \text{ \AA}$  and the correlation length of  $79 \text{ \AA}$ . There are two lower peaks at  $1.51 \text{ \AA}^{-1}$  and at  $1.73 \text{ \AA}^{-1}$ , where one cannot give the width and some less clear peaks at  $1.9$ ,  $1.98$ ,  $2.08$  and  $2.3 \text{ \AA}^{-1}$ .
2. **ii) Regarding the correlations between the different peaks:** if one assumes that the peaks all result from one dimensional order along the chain direction, one would expect to see four equidistant peaks mainly in the chain deuterated polymers DH and DD. Indeed both DH and DD show regularly arranged peaks with the same  $Q$ -distances, but the regularity is not perfect the third peak being absent and the fourth peak shifted. (We will understand this better in the chapter about partial structure factors 7 on page 95.) In addition the fact that the second peak has already a much lower intensity than the first peak can imply some degree of one dimensional order along the chains. The first and second peaks show a periodicity of  $\approx 0.6 \text{ \AA}^{-1}$  in  $Q$  ( $1.33$  being roughly the double of  $0.6 \text{ \AA}^{-1}$ ), and their height should decrease with the form factor  $|F_M|^2$  of the monomer (see below, Random chain orientation). This form factor is the square of the structure amplitude of the monomer or monomers i.e. the atomic arrangement in the unit within one repeat distance of the chain. That the third peak is absent, and the fourth peak at  $3 \text{ \AA}^{-1}$  is shifted from its expected value of  $2.67 \text{ \AA}^{-1}$ , broader and higher than expected for a one dimensional chain lattice shows only that the peak at  $3 \text{ \AA}^{-1}$  is caused by some other effect than chain regularity. That the HH and HD samples do not show this behavior would confirm the one dimensional chain lattice. Their chains are hydrogenous and the proton cross section is smaller than that of the deuterion thus giving lower intensity which causes these peaks to vanish. The period  $0.6 \text{ \AA}^{-1}$  would give a chain period of  $10.5 \text{ \AA}$ , corresponding to one isotactic plus one syndiotactic unit, which should

then be very regularly arranged along the chain to give such a high peak. However, this seems very improbable. In the section on 'Random chain orientation' we calculate such form factors  $|F_M|^2$  as the square of the scattering amplitude for sequences of several selectively deuterated monomer units. These periodicities shown in figures 5.5 and 5.7 in all samples, are not observed in the experiment in all but the DH sample (see also fig. 5.9). The crystal structure method predicts the high intensity of the peak at  $Q=0.6 \text{ \AA}^{-1}$  only for the DH sample. Hence we have to abandon the one dimensional order hypothesis as reason for the high peaks. However as we shall see later, this cannot be abandoned totally.

3. iii) **The IHH sample** shows very narrow peaks, but broader than the resolution of the instrument, which seems to correspond to powder pattern peaks broadened by the effect of grain size. This is what one expects for isotactic material as this has crystalline character. It is shown below that the structure is not the perfect crystal structure as that reported by Greis et al.[10]. This could result from the fact that our isotactic material is much better by the Soxhlet extraction of the 6% remaining atactic material which guarantees the ultra pure isotacticity of our sample. The DH sample shows the peak at 110, which the IHH sample does not show, i.e. the order in the IHH sample shows smaller ordered distances than the atactic material, which seems plausible, as the helices of IHH can approach each other much more, if they are not disturbed by other chains in between.



## Chapter 4

# Crystalline powder pattern

Otto Schärpf, Physik Department E13  
T.U. München  
D-85747 Garching  
Barbara Gabrys, Brunel Univ. of West London  
Uxbridge, Middlesex UB83PH UK  
Dennis G. Peiffer, EXXON Research and Engineering Co  
Route 22 East, Annandale, N.J., U.S.A.

### 4.1 Visualization of the crystal structures of isotactic and syndiotactic polystyrene

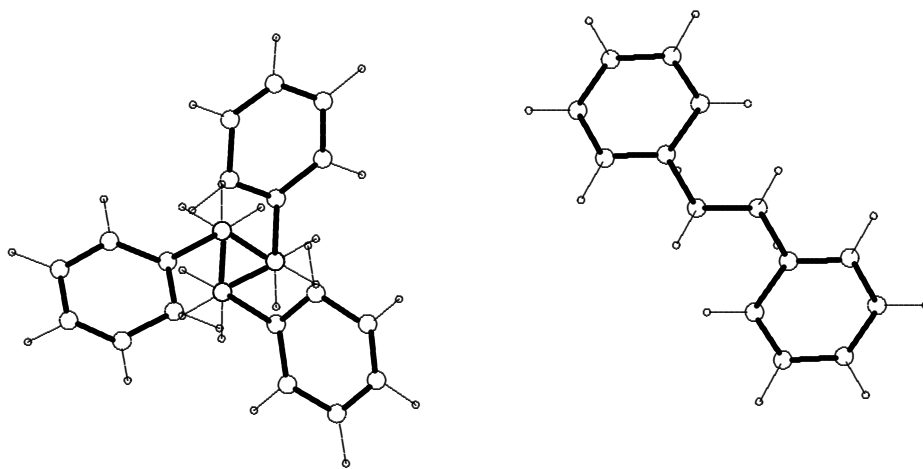
One could assume that the peaks present in all the scattering spectra represent powder pattern peaks in an analogous fashion to peaks obtained from crystalline powders as in the IHH material and as in conventional crystallography, and that in this instance the peaks are broadened due to the minute size of the ordered regions. We know very well that crystalline regions of small size scarcely occur in pure form in chain molecules; it is certainly difficult to imagine that chain molecules would form small ideal crystals and that these would be collected into a specimen without transition regions of lower order. In fact, disorder in the transition zones would cause disturbances in the crystalline regions, since these are very small. An exception could perhaps be thought for a set of folded crystals, each consisting of their "own" molecules, which do not pass into other crystals through transition zones. It is nevertheless reasonable to consider diffraction by small crystalline regions, for this will enable us to draw some conclusions about the size and shape of the crystalline zones and to identify the presence of two different grain sizes. Finally we will have to relax the crystalline order more and more in order to understand the measurements. This will lead us straight away to the paracrystallinity for the IHH sample and to the description with the partial structure factors for the atactic materials.

One could also imagine that the paracrystallinity is the fundamental description. But to treat all the relative questions in the paracrystalline nomenclature would be too difficult. The methods of paracrystalline description are not yet so evaluated and not at all generally known. Even such simple things as the determination of Miller indices or the determination of two different grain sizes from a powder pattern is much easier using generally known crystallographic methods.

In a first step it is informative to visualize the two crystallographic structures, in which polystyrene can crystallize namely the iso- and syndiotactic forms. The first should correspond to the structure of the IHH material and both are likely to give a certain approximation to the atactic structure too. The most complete information about crystalline structure is available on isotactic polystyrene.



Putting together the interpretation of the x-ray data given by Greis et al. [10] and the chain description by Bunn and Howells [11] it is possible to calculate the atomic positions (see table 2) and to plot the complete unit cell of isotactic polystyrene (figure 4.1 and 4.2). In addition Greis et al. gave information on the structure of syndiotactic polystyrene, but it is not as complete as for the isotactic form. They stated only that a cluster of three macromolecules with the zigzag backbone chains close to the threefold axis of the  $P3c1$  space group was in agreement with their results. Utilizing their lattice constants with one zigzag chain situated at  $(1/3,0,0)$  the atomic positions of one syndiotactic zigzag unit were determined and are shown in table 2. Applying the equivalent positions of  $P3c1$  :  $x,y,z$   $-y,x-y,z$   $-x+y,-x,z$  (but not the remaining three equivalent positions (see [12]), because the zigzag unit already comprises two monomer units) all other positions follow. This enables one to plot the complete unit cell of syndiotactic polystyrene using the program STRUPLO [13]. This program is not necessary but it helps. The resulting structures are shown in fig.4.1 and 4.2 directly plotted by using the atomic positions and the symmetry relations, not using STRUPLO but PICTEX. Fig.4.1 presents a view of a single isotactic and single syndiotactic chain projected along the (001) direction, while fig. 4.2 gives a perspective view of two neighboring isotactic chains related to each other by inversion symmetry and a perspective view of a syndiotactic chain. In fig. 4.3 the top view of the cell is shown with all chains belonging to the identical unit cell for the isotactic and syndiotactic case .



isotactic

syndiotactic polystyrene

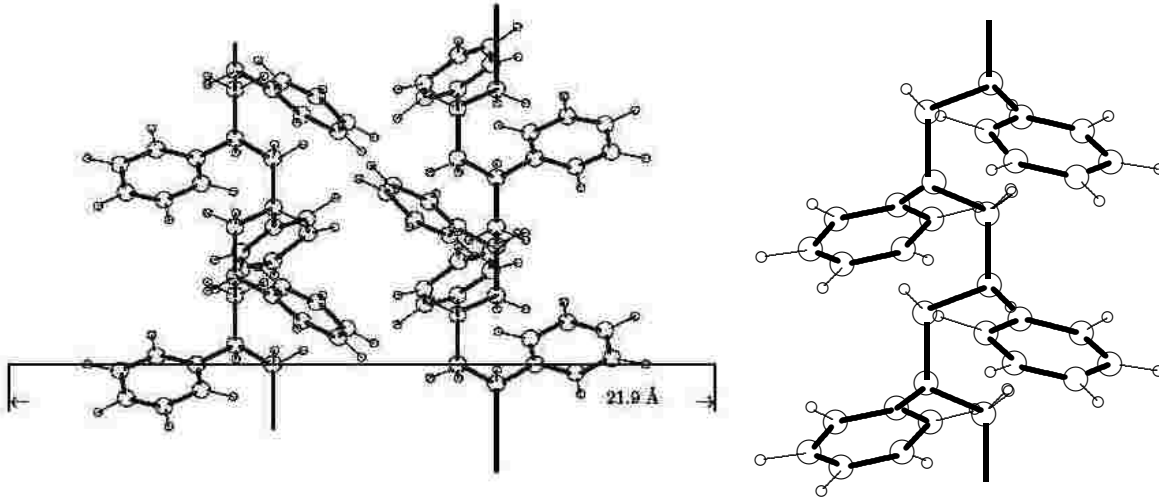
Figure 4.1: Top view of one chain projected along the (001)-direction. (The apparent carbon valence of 6 in the left part is an artefact due to the superposition of two atoms in the projection.)

## 4.2 powder pattern including the instrumental resolution and broadening by grain size

Furthermore using the atomic coordinates which produced this figure (see table 2), one obtains the powder patterns of figure 4.4 for isotactic and syndiotactic polystyrene using the LAZY-PULVERIX program [14]. In fig.4.4 the measured angular dependence of the resolution of the instrument is

Table 2. Fractional atomic coordinates used in calculations (in hexagonal system, see text eq.5.7 on page 60)

isotactic structure (1 monomer) with a=b=21.9 Å and c=6.65 Å				syndiotactic structure (2 monomers) with a=b=15.16 Å and c=5.045 Å			
Atom	x/a	y/b	z/c	Atom	x/a	y/b	z/c
C1	0.03606	0.00000	0.00000	C1	0.04459	0.00000	0.07309
C2	0.00000	0.03606	0.09234	C2	0.04459	0.00000	0.37834
C3	-0.07257	0.00000	0.00000	C3	0.13378	0.08919	0.52447
C4	-0.11872	0.02374	0.04060	C4	0.21991	0.08363	0.58973
C5	-0.18585	-0.00867	-0.03158	C5	0.12822	0.17532	0.58973
C6	-0.20659	-0.06833	-0.16670	C6	0.20872	0.25582	0.72230
C7	-0.16438	-0.09132	-0.20301	C7	0.30041	0.16413	0.72230
C8	-0.09498	-0.05799	-0.12331	C8	0.29478	0.25019	0.78824
H1	0.08952	0.02659	0.06596	H1	0.04459	-0.06371	-0.03128
H2	0.00974	-0.05319	0.06596	H2	0.10829	0.06371	-0.03128
H3	0.02659	0.08952	0.02638	H3	0.04459	-0.06371	0.48272
H4	-0.26028	-0.09380	-0.23265	H4	0.21991	0.01332	0.52040
H5	-0.18219	-0.13836	-0.30075	H5	0.05791	0.17532	0.52040
H6	-0.05982	-0.07763	-0.15910	H6	0.20872	0.32613	0.75666
H7	-0.22329	0.01096	0.00000	H7	0.37072	0.16413	0.75666
H8	-0.10046	0.07260	0.14135	H8	0.35849	0.31390	0.89262
the second monomer is generated by $x_{i+16} = -y_i$ $y_{i+16} = x_i - y_i$ $z_{i+16} = z_i + 1/3$  the third monomer is generated by $x_{i+32} = y_i - x_i$ $y_{i+32} = -x_i$ $z_{i+32} = z_i + 2/3$				C9	-0.04459	0.00000	-0.42691
				C10	-0.04459	0.00000	-0.12166
				C11	-0.13378	-0.08919	0.02447
				C12	-0.21991	-0.08363	0.08973
				C13	-0.12822	-0.17532	0.08973
				C14	-0.20872	-0.25582	0.22230
				C15	-0.30041	-0.16413	0.22230
				C16	-0.29478	-0.25019	0.28824
				H9	-0.04459	0.06371	-0.53128
				H10	-0.10829	-0.06371	-0.53128
				H11	-0.04459	0.06371	-0.01728
				H12	-0.21991	-0.01332	0.02040
				H13	-0.05791	-0.17532	0.02040
				H14	-0.20872	-0.32613	0.25666
				H15	-0.37072	-0.16413	0.25666
				H16	-0.35849	-0.31390	0.39262



two neighbouring inversionally symmetric isotactic chains at  $(1/3,0,0)$  and  $(2/3,0,0)$

one syndiotactic chain

Figure 4.2: Side view of the isotactic and syndiotactic chains

included by the half width of the gaussian  $H_k^2 = U \cdot \tan^2 \Theta_k + V \cdot \tan \Theta_k + W$  with  $U=2768$ ,  $V=20805$ ,  $W=16872$  and the resolution function for the  $k^{th}$  Bragg peak at the Bragg angle  $\Theta_k$  given by

$$R(\Theta) = \frac{2\sqrt{\ln 2}}{(H_k \sqrt{\pi})} \exp\left(\frac{-4 \ln 2 (\Theta - \Theta_k)^2}{H_k^2}\right) \quad (4.1)$$

All theoretical powder patterns are given in the same scale with the cross section in barns/sterad units related to one monomer as a function of scattering vector  $Q$  (incident wavelength 3.1 Å) for a direct comparison with the measurements shown in fig.3.4. For the highest peaks the crystallographic indices are given. Fig.4.4 shows a clear difference between the powder patterns of syndiotactic and isotactic polystyrene and our atactic material could be assumed to show a pattern which is an intermediate between these two polymer structures of Greis et al.[10]. The structural information about the syndiotactic material is not complete, the major hindrance being a lack of information on the position of the chains in the cell and on the rotation of the benzene ring around its axis along its valence bond to the chain. This information is more fully known for isotactic polystyrene [11]. As seen in fig.4.1,4.2 and 4.3 and from table 2 we used no rotation of the benzene ring for the syndiotactic polystyrene, only a tilt corresponding to the valence angle of carbon and for the isotactic polystyrene a rotation of 30 degrees around the axis along its valence bond to the chain.

### 4.3 Comparison with measurement for IHH: grain size and other structural information with dense packing of chains

Fig.4.5 shows the comparison of the measurement of the isotactic sample IHH with the respective calculated spectrum of figure 4.4 including the instrumental resolution (fig.4.5a). One sees immediately that the peak width of the measurement is broader than the instrumental  $Q$ -resolution. It is known from crystallography that the reason for such broadening can be the finite grain size (ref.[15] p.143). In this case one can use the Scherrer formula to describe the width dependence on the grain size  $L$

$$\Delta'(2\Theta) = \frac{0.9\lambda}{L \cdot \cos(\Theta_0)} \quad (4.2)$$

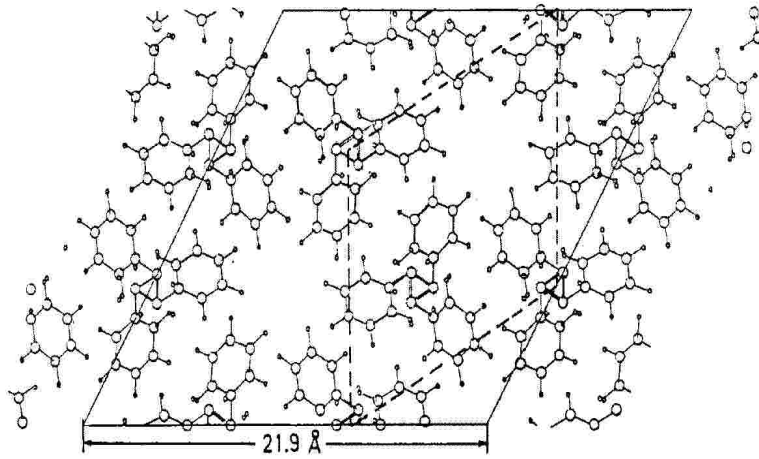
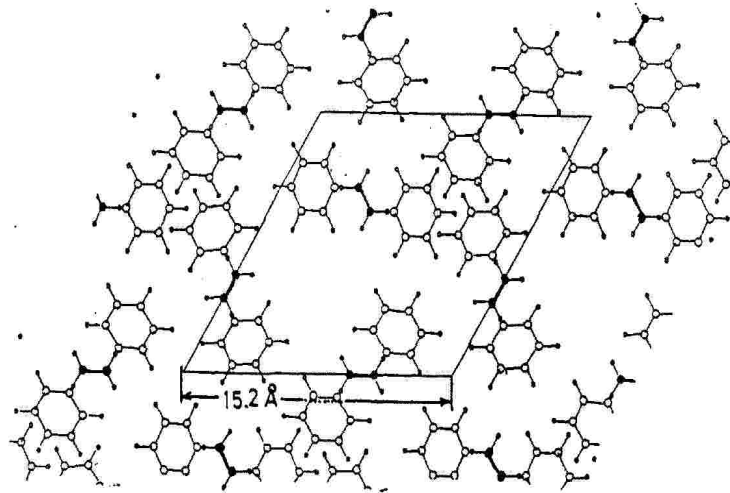
a) isotactic, symmetry  $R\bar{3}c$ b) syndiotactic, symmetry  $P3c1$ 

Figure 4.3: a) isotactic, symmetry  $R\bar{3}c$  b) syndiotactic, symmetry  $P3c1$  Top view (along (001)) of all the chains in the isotactic and syndiotactic unit cell.

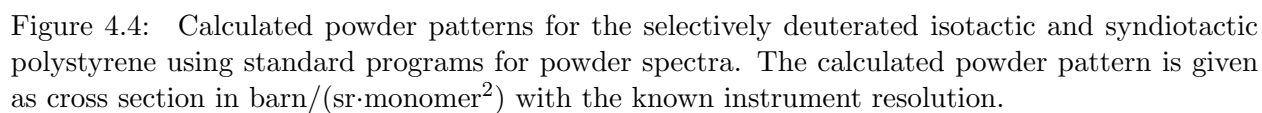
with  $\Delta' = \sqrt{(\Delta'_1)^2 - (\Delta'_0)^2}$ ,  $\Delta'_1$  = measured width and  $\Delta'_0$  = broadening of a theoretically infinite narrow line for the Bragg angle  $\Theta_0$ . This broadening effect of the grain size corresponds to the shape factor treated in the section "Random chain orientation", which gives in forward direction the small angle scattering and broadening around the Bragg peaks. Other reasons could be internal stresses in the grains or an imperfect crystal lattice i.e. paracrystallinity, or voids. Voids can only broaden diffraction lines, if they are situated in an ordered structure, which has such Bragg peaks, i.e. in this case the ordered regions must even be much larger than the voids. The small grains are a more economic way to obtain line broadening, it needs less order than voids [16]. Paracrystallinity will be further investigated in the third part of this paper. Fig.4.5b shows the powder pattern broadened by grain size of 100 Å. Figure 4.5 also shows other interesting features of the observed powder pattern, different from the calculated one:

- i) the measurement does not show all peaks
- ii) the peak heights do not correspond to the calculated ones
- iii) there is a diffuse background scattering, which must also be understood. (Note this is already purely coherent scattering in absolute intensity scale, but see also multiple scattering corrections in connection with fig. 3.3.)

Problem ii) giving percentage of ordered material and iii) giving percentage of amorphous material will be treated later in chapter 6 on page 83.

The fact that the measured spectrum does not show all peaks is fundamental. One could interpret it as a disappearance of peaks due to the effect of paracrystallinity. But this would only be possible for the peaks at higher  $Q$ : it cannot cause the disappearance of the first two peaks. The assumption that (110) disappears because of the anisotropy of the grain size would also be valid for the (220) reflection. Since in this case the disappearance of the peak (110) cannot result from grain size anisotropy, it must result from a change in the structure.

To arrive at a correct structure one needs a simple arrangement of the chains which would account for nearly all peculiarities of the observed diffraction pattern. As some peaks are coincident with those resulting from the structure of figs. 4.1, 4.2 and 4.3, the (220)-lattice planes must also belong to the structure to be determined. But the distance between the respective planes must be halved so that these old (220)-reflections become the new (110). The only simple arrangement yielding such an additional plane is obtained by lifting the condition of chains having inversion symmetry inherent in the  $R\bar{3}C$  group and, additionally to fill up the holes in the structure of fig. 4.3a. In the structure  $R\bar{3}C$  as given in fig. 4.3a each chain has only three nearest neighbor chains. Changing in this way the original structure  $R\bar{3}C$  is only possible, if one creates the chains in the structure independently of the crystal symmetry. In the structure  $R\bar{3}C$  the relations for the equivalent positions  $(-y, x-y, z+1/3; y-x, x, z+2/3)$  generate the isotactic structure of the chains at the symmetry positions possessing threefold axis. One can generate the chain structure in advance out of the atomic coordinates of one isotactic monomer from table 2 and using these coordinates of the atoms of three monomers of an isotactic chain piece in an analogous manner to the procedure used for the syndiotactic structure. This results in a structure different from that shown in fig. 4.3a, which corresponds to hexagonal dense packing. This is shown in fig. 4.6 in a smaller cell corresponding to that given by the broken line in fig. 4.3 with  $a=b=12.64$  and  $c=6.65$  Å and  $\gamma = 120^\circ$ . In fig. 4.6 the chains are drawn for clarity with smaller diameter to see them without overlap in the figure. In real structure they must be enlarged in diameter by a factor given by the lattice constant ratio  $21.9/11=1.99$  (for the result  $a=b=11$  Å). Putting the chains also into the holes of figure 4.3 namely at (000),  $(1/3, 2/3, 0)$ ,  $(2/3, 1/3, 0)$  of the smaller cell and fitting the lattice constants, one obtains a desired simple model, which reflects the observed diffraction pattern. This is shown in fig. 4.7 for different approximations. It corresponds to more densely packed chains (hexagonal with  $a=b=11$  Å instead of 12.64 Å) and an increased period along the chains of 9.65 Å instead of 6.65 Å.



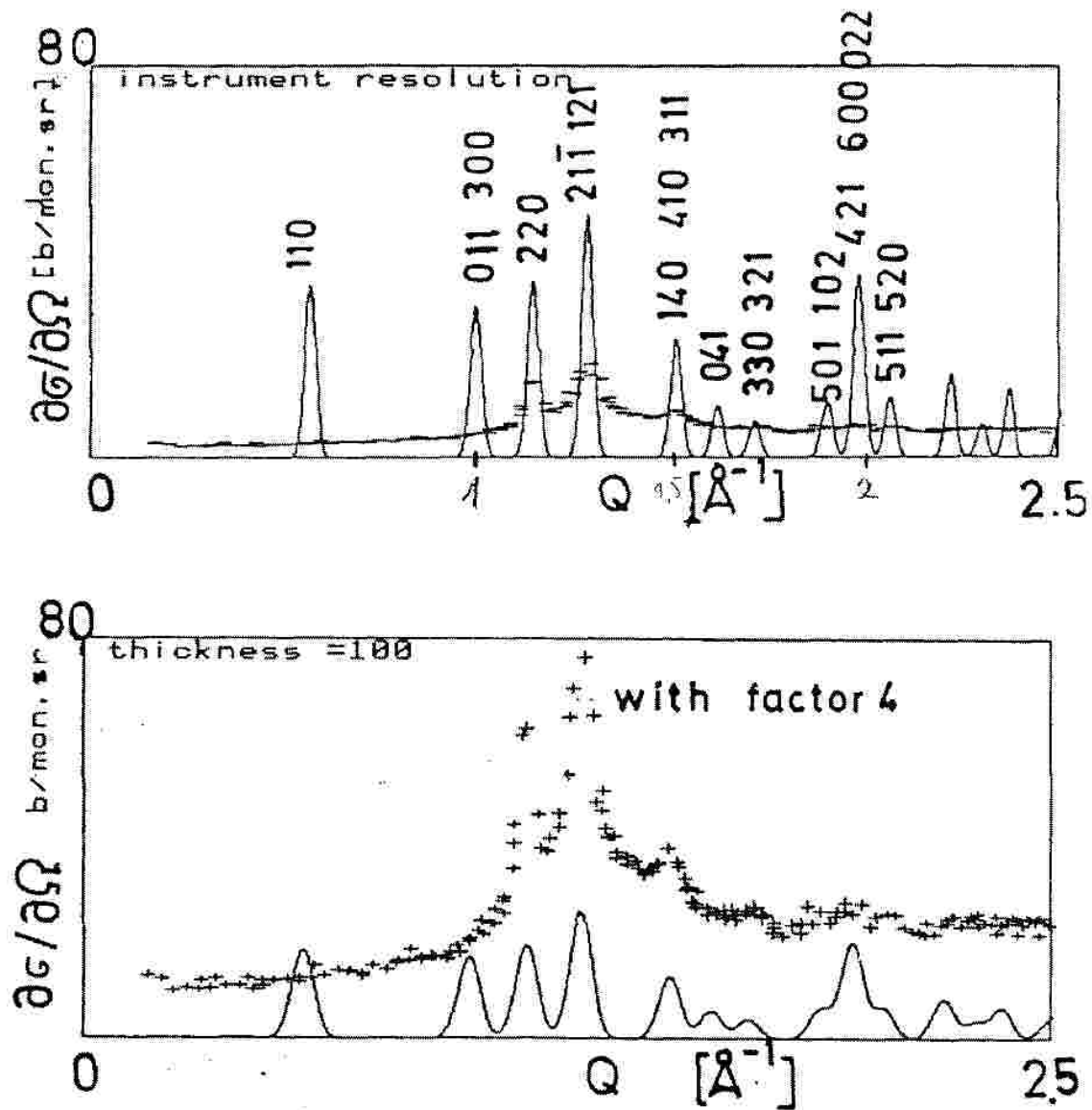


Figure 4.5: a) Comparison of the measured pattern for the isotactic sample IHH and the calculated powder pattern for the structure given by Greis et al. [10] b) The same but broadened by a grain size of 100  $\text{\AA}$ , the ordinate of the measured curve is multiplied by 4.



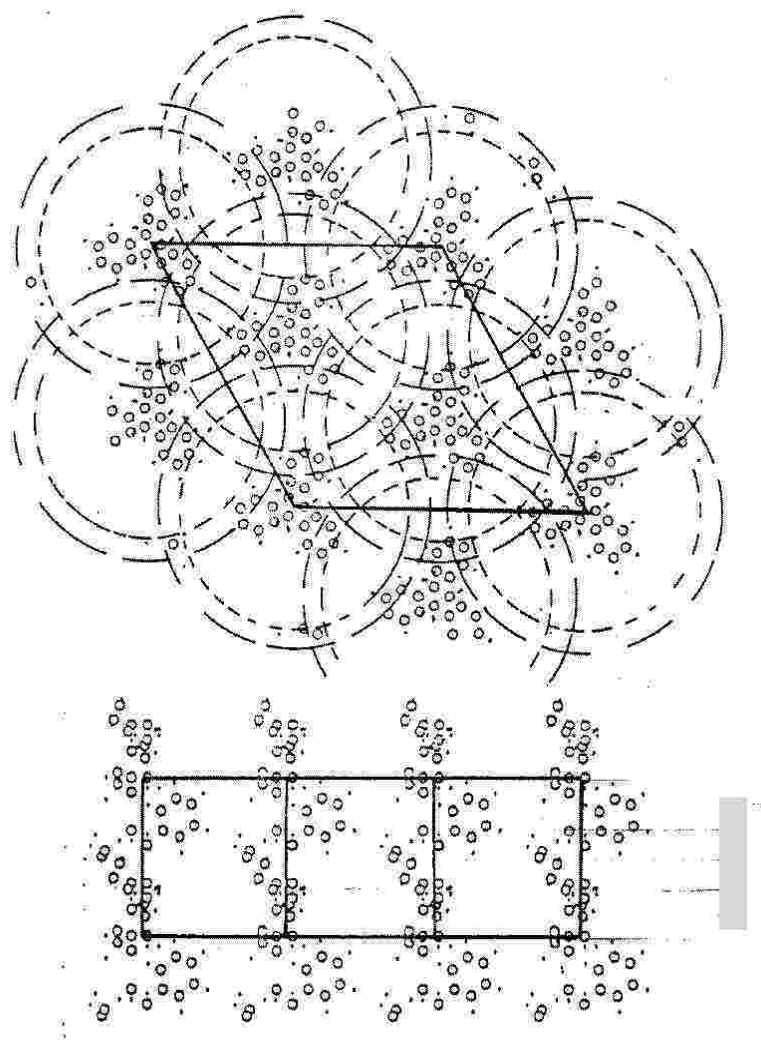


Figure 4.6: The structure of the isotactic sample as resulting from the fit, top and side views. The chains are drawn with smaller diameter to see them without overlap. The enlargement factor 21.9/11 is indicated by the larger circles, that of V3 by the smaller circles.



This indicates an affine deformation of the chains to compensate the prolongation for the crowding in the x-y plane due to very close packing. The smaller peaks appear as deviations of the chain positions which in our case is given by (000), (1/4,2/3,0), (3/4,1/3,0) included in the fit: each regular small deviation of the hexagonal closest packing of the chains produces these small peaks also at the position where we experimentally observe them.

Fig.4.8 shows how this behavior changes if one changes the diameter of the chains by the factor  $\sqrt{3/1.99} = 0.87$  compared to that of fig.4.7 and corresponding to the smaller diameter circle of fig.4.6. One sees that such a change alters the relative height of the peaks: the first and second peak are of equal height in fig.4.7 and different height in fig.4.8. The latter corresponds more closely to experiment (fig.3.4). In addition higher peaks in the Q-region above  $1.66 \text{ \AA}^{-1}$  appear for the larger diameter chain, whereas these peaks are smaller for the smaller diameter chain (fig.4.8). This demonstrates that the chains are stretched in the c-direction and contracted in the a and b direction i.e. one has an affine deformation of the chains in the solid .

The procedure followed here in connection with figs.4.5 to 4.11 corresponds to a Rietveld refinement [17] but governed by physical considerations instead of only mathematical optimizations.

This simple model yields all features of the observed spectra and is very plausible. That is to say that our isotactic material is not crystallized in the  $R\bar{3}C$  system, i.e. that the atoms in the chain do fulfill other symmetries than those corresponding to the global symmetry of the whole crystal and in this sense our isotactic material is not perfectly crystallized. But it shows also periodicities along the chains (in c-direction or in the direction of the third Miller index) correlated with the periodicities normal to the chains in the a-b plane as one can see from the indices of the reflections of the second peak. The grain size is  $\approx 120 \text{ \AA}$  normal to the chains. In the direction of the chains the peak seems to be broader and lower than calculated. This corresponds to a grain size of  $\approx 80 \text{ \AA}$  in the direction along the chains. From fig.4.6b) we observe why the close packing gives also correlations along the chains appearing as reflections with a third Miller index  $\neq 0$ : the reason is the helical structure. This keeps the chain molecules along the chain in the densely packed chains correlated so that peaks with the third index  $\pm 1$  appear. This is even the strongest peak in fig.4.5 but it is more broadened than the other high peak, apparently by a smaller thickness in this direction.

The procedure of comparing the measurements with the calculated powder pattern in the IHH material highlights some major features of neutron scattering results on polymer chains. They necessitate a complicated procedure because of the problems specific to an assembly of chain molecules. One always has scattering effects from isolated molecules in addition to the effects caused by deviations from the ideal molecular structure due to variations in molecular orientation, size and mutual dispositions of the ordered regions. The large number of parameters describing an assembly of chain molecules and their overlapping makes the pattern relatively poor even more so in the non crystallized materials. Interpretation of such patterns has to be made with great care, although experimental data sometimes seem to allow a simple interpretation. We can say already and reiterate in what follows that only by quantitative analysis it can be decided whether the assumed structure is true. Only qualitative interpretations can be very misleading.

## 4.4 Comparison with measurements of selectively deuterated materials

As discussed for the isotactic samples, the grain size determines the width of the reflections. We could now ask how the different grain sizes change the pattern of the selectively deuterated samples. The correlation lengths determined above from the width of the respective peaks indicate that the interesting grain size region lies somewhere between 20 and 100  $\text{\AA}$ . Fig.4.9 gives the calculated powder pattern broadened by grain sizes of 100, 80, 50, 30 and 20  $\text{\AA}$  for the samples HH, DH,

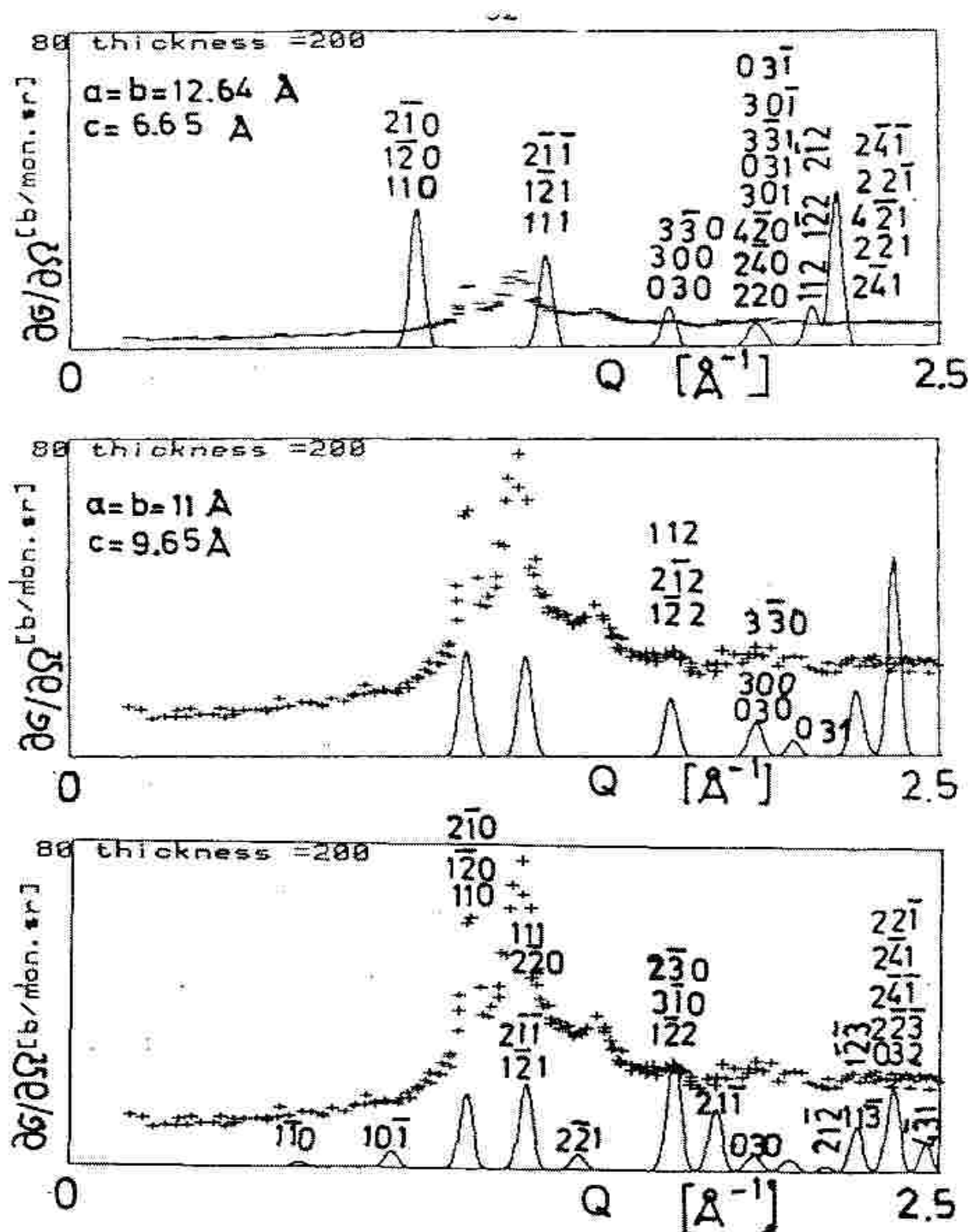


Figure 4.7: a) Comparison of the measured powder pattern with the model of the hexagonal densely packed chains with the cell size given by Greis et al.[10] (the cell is that marked by broken lines in fig.4.3 on page 43a; the chain diameter marked by the larger circles of fig.4.6 on page 47) b) comparison with the pattern resulting from changed cell size c) comparison with the cell size of b) but including a small deviation of the chains inside the cell from the symmetric position.

HD and DD respectively. Fig. 4.9 shows the effect of grain size for the isotactic crystal with the symmetry  $R\bar{3}C$  and fig.4.10 gives it for the hexagonal densely packed chains with the smaller chain

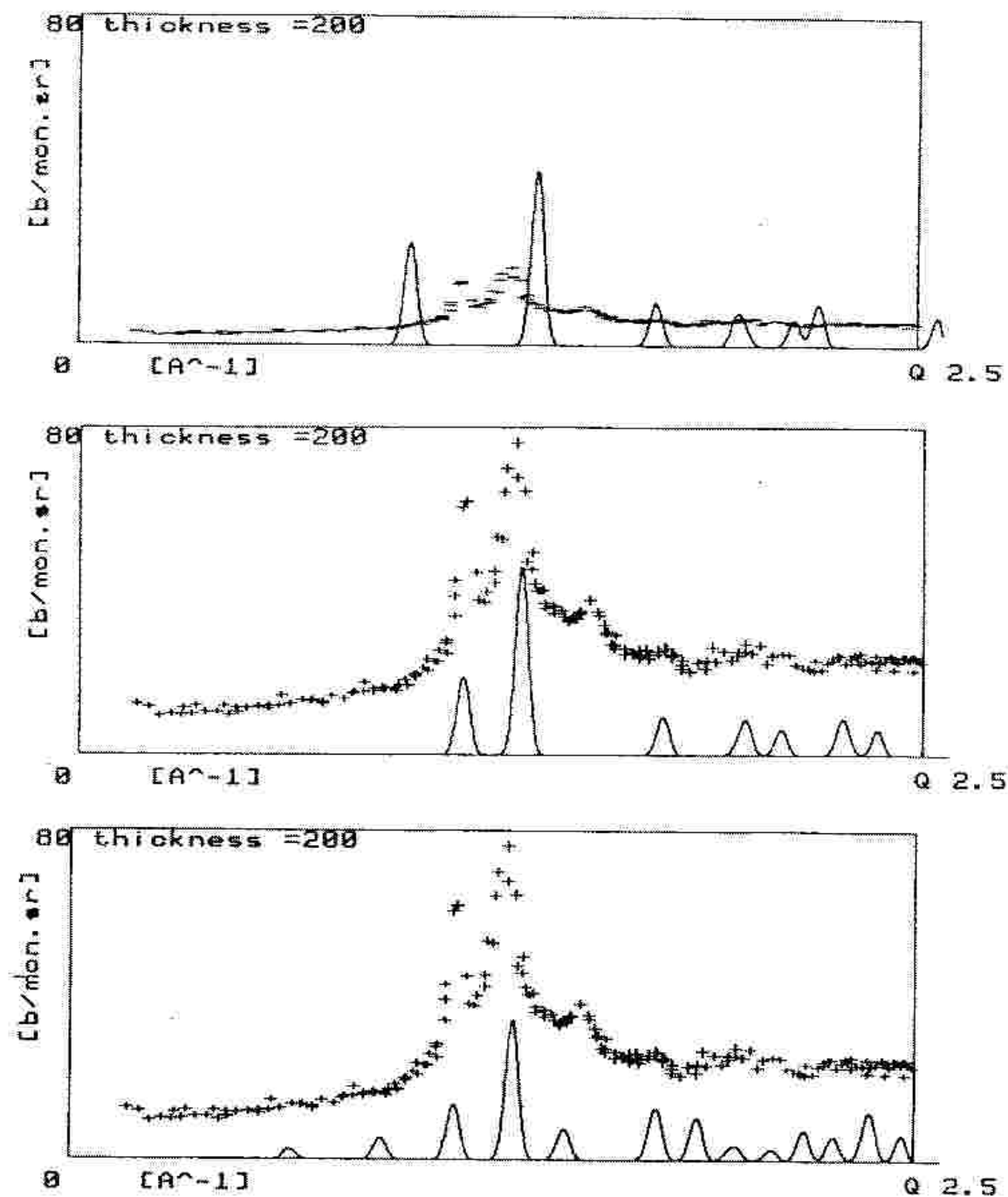


Figure 4.8: As figure 4.7 but for the smaller chain diameter corresponding to the smaller circles of fig.4.6.

diameter of fig.4.8 for the different selective deuterations (calculated for the wavelength  $5.7 \text{ \AA}$ ). This was the wavelength used for the measurements in the  $Q$ -range up to  $2 \text{ \AA}^{-1}$  (the wavelength must be specified because of the Lorentz factors). The decrease of the grain size results in patterns where with smaller grains the peaks correspond roughly to very high peaks in the calculated powder patterns of fig.4.4 and the diffuse scattering to many very densely spaced lower peaks.

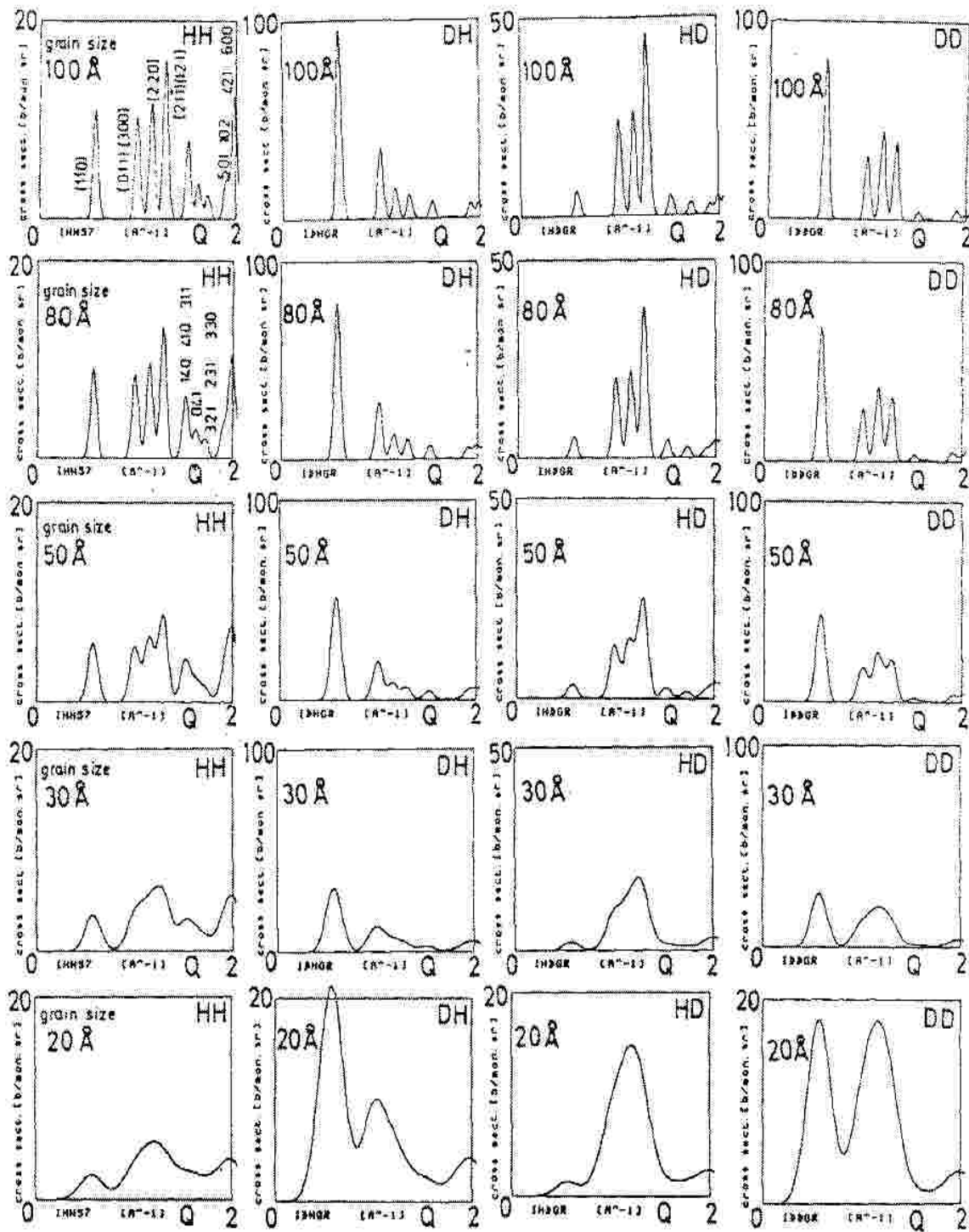


Figure 4.9: Change of the powder pattern of the isotactic structure of Greis et al.[10] with grain size for the selectively deuterated samples

From figs. 4.9 and 4.10 we can conclude that we have to use  $\approx 20$  Å grain size to understand our measurements and that for the atactic samples the results of the hexagonal densely packed version does not fit for DH but fits for HH, HD and DD. The structure of Greis et al. [10], which is



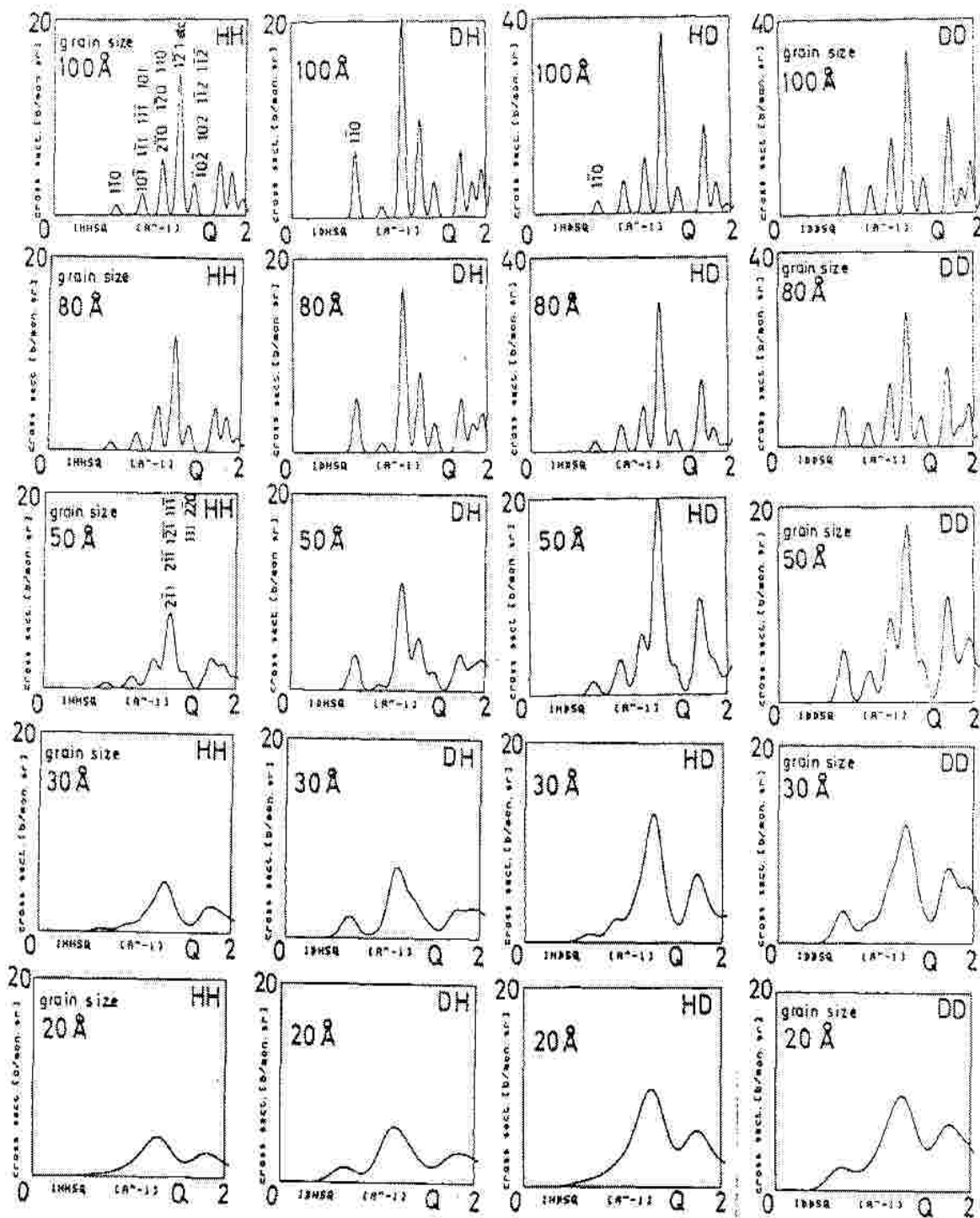
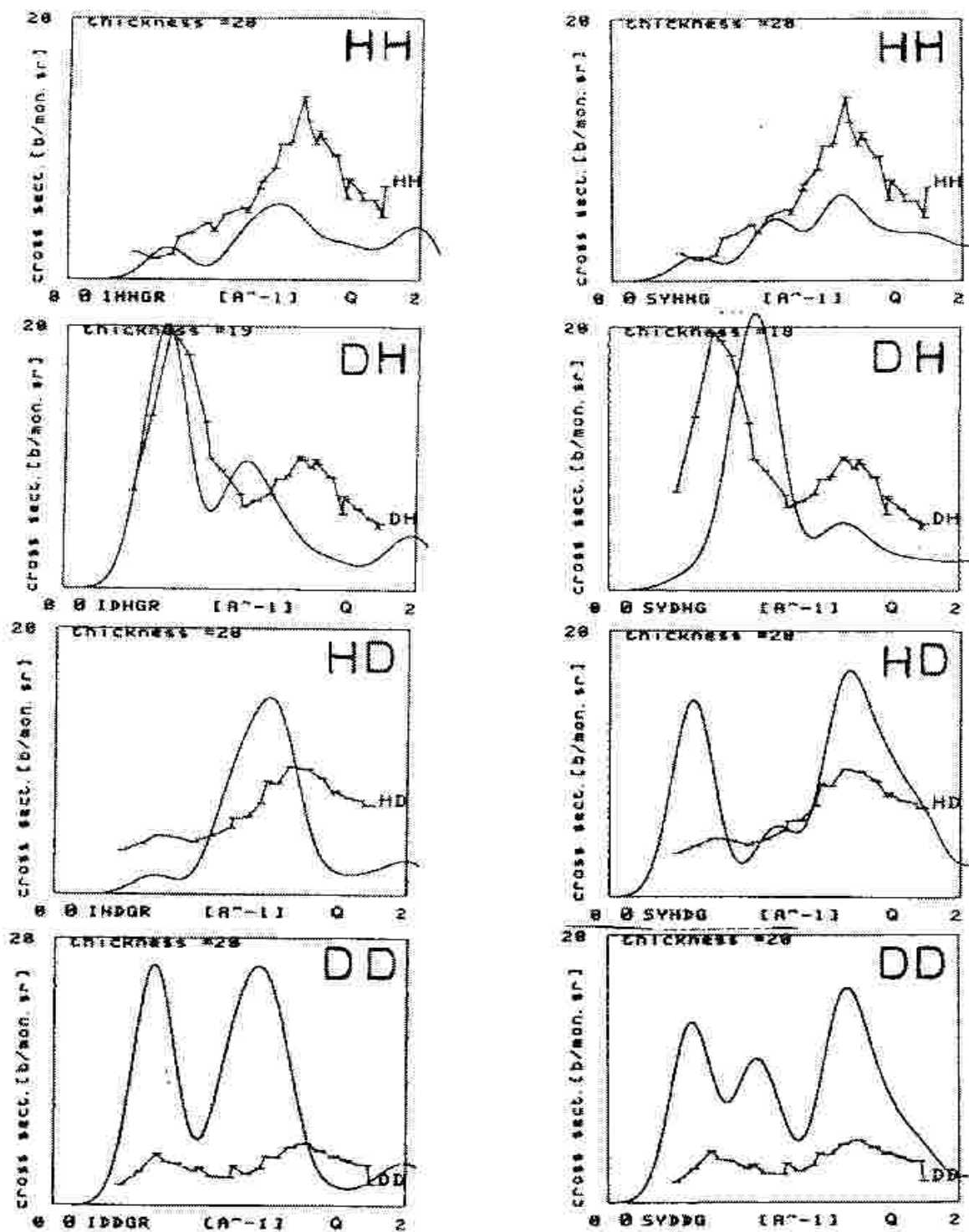


Figure 4.10: Change of the powder pattern of the isotactic hexagonal densely packed structure of fig.4.6.

less densely packed (only three nearest neighbors) is better adapted for both DH and HH but not at all for HD and DD. Fig.4.11 shows the results of the measurements together with the calculated powder patterns - the cross sections for all normalized to one monomer, including the instrumental



isotactic

syndiotactic

Figure 4.11: The comparison of the calculated powder patterns with the measured curves of fig.3.4 for selectively deuterated polystyrenes. The calculated powder pattern is given in barn/(sr.monomer<sup>2</sup>) with the known resolution of the instrument and a grain size broadening of 20 Å grains.

resolution increased by a grain size of 20 Å. (See also fig.5.14 third column). Note that the cross sections are not fitted by any factors or parameters. The good correspondence between the isotactic model of Greis et al.[10] and the measurements for DH and also for HH after subtracting the double scattering contribution already at this stage is unexpected. Fig.4.11 displays these comparisons for the calculated isotactic and syndiotactic spectra for the grain size 20 Å. In fig.5.15 also the results of the hexagonal dense packing of the grain size broadened peaks are included for comparison with the measured points.

From fig.4.11 we can conclude that the atactic selectively deuterated samples are better described by the isotactic structure for small  $Q < 1 \text{ Å}^{-1}$  and the syndiotactic structure for  $Q > 1 \text{ Å}^{-1}$  but eventually with a slightly different cell size, yielding a shift of the peaks.

It is always the peak at  $Q=1.33 \text{ Å}^{-1}$  that is shifted in the measurements to higher  $Q$ . In view of results obtained for the isotactic sample IHH one would expect this i.e. that also in the atactic samples the chains have a more dense packing than in the crystal structure of Greis. Another possibility would be that it is a sign of syndiotactic order in the chains, which follows from the indices of this second peak always including a third index  $l \neq 0$ .

Fig.4.11 deserves a more detailed interpretation. The scattering patterns of all the samples display a high peak at  $Q=1.33 \text{ Å}^{-1}$  (the second peak of the DH sample), which corresponds to the  $(2\ 1\ \bar{1})$  peak in the calculated powder patterns of the isotactic unit cell at  $Q_{theor} = 1.52 \text{ Å}^{-1}$  or to the  $(101)$  peak of the syndiotactic unit cell. The very high peak appearing at  $Q = 0.60 \text{ Å}^{-1}$  corresponds to the  $(110)$  peak of the isotactic unit cell and is very pronounced in the DH polymer at exactly the observed position and with the theoretically predicted intensity. The syndiotactic ordering shows a corresponding high peak but it is shifted to higher  $Q$  at  $(110)$  for DH and lower  $Q$  at  $(100)$  for HD and DD, respectively. The third peak can be attributed to the  $(1\ 1\ \bar{2})$  peak of syndiotactic structure at  $Q_{theor} = 2.88 \text{ Å}^{-1}$ . The isotactic structure does not have a corresponding peak at that position.

These observations seem point to a transition from isotactic - like behavior in the regions of small  $Q$  (i.e. large  $r$ ) to a more syndiotactic type structure in the regions of large  $Q$  (i.e. small  $r$ ). The region around  $Q \approx 1.5 \text{ Å}^{-1}$  where both structures have a high peak could then be considered a transition region. This manifests itself as a better fit with the isotactic structure for the first peak below  $Q = 1 \text{ Å}^{-1}$  and for the  $Q$  values higher than  $1 \text{ Å}^{-1}$  by a better fit with the syndiotactic model calculations related to the peak positions and peak heights .

A great advantage of this approach is that it allows for an interpretation of the patterns observed in terms of intra- and inter-chain contributions by determining the  $(hkl)$  indices of the peaks. The intra-chain correlations lying in the  $z$ -direction are indicated by the third index and inter-chain correlations in the  $x$ - $y$  plane are marked by the first two Miller indices . An examination of the data shows that most of the indices of the observed peaks demonstrate that the peaks belong to lattice planes lying nearly parallel to the  $c$  direction, i.e. periodicities resulting from parallel chains. Thus the very high peak at  $0.60 \text{ Å}^{-1}$  belongs clearly to indices  $(110)$  or  $(100)$  which contain only interchain interference effects, since these planes are parallel to the chains. Those  $(hkl)$  indices with a third index  $= 0$  will be shown later as resulting from other interference effects.

We can summarize the above statements: all have something true to them but do not fit completely. The above tentative interpretation of the first two peaks in the DH sample with one dimensional order along the chains (the first section of "results and interpretation") fits well with many features dicussed in ii) but as discussed further (cf. fig.5.5), these peaks should then be visible in all atactic samples (HH, HD, DH, DD), whereas the calculated structural results from crystallinity show the peaks only there where they really are measured, namely in DH (small in HD and DD) and also with the right intensity. Therefore the one dimensional order hypothesis proposed to explain the high intensity peaks was abandoned in favor of the three dimensional crystallinity. But the latter results of the three dimensional powder pattern show a shift of the peaks corresponding to a less dense packing than that of the hexagonal dense packing of the real

IHH sample. It is more like a threefold neighbor packing that lets enough space for the irregular chains resulting from atacticity. Finally the results are consistent with a two dimensional order of dense packing of chains, which have some correlations also along the chains because of the grooves arising by the helicity of the isotactic structure with correlations of 100 Å in the IHH sample and at least piecewise also in the atactic case with correlation length of 20 Å.

Including consequences from the observed widths related to the correlation lengths (see also the discussion in connection with fig.5.5), one can conclude that the observed correlation lengths or grain sizes are larger than or equal to a lattice constant  $a$  or  $b$  in the  $x$ - $y$  plane of fig.4.3 or fig.4.6. One dimensional order would imply [18] that the observed peaks in atactic polystyrene could all be understood as corresponding to periods of 10.5 Å with a correlation length of 18.5 Å along the chains. Such periods would have to include two to three repeating blocks of one isotactic and one syndiotactic unit. Apriori, due to its atacticity, this is unlikely.

In the crystalline model one needs one crystallite comprising at least some unit cells of the structure  $R\bar{3}C$  in order to get interference effects. (See also discussion in connection with figs.5.10-5.13 where we investigate the growing of the interferences by adding more - up to 90 monomers - as scattering centers.) This is very well fulfilled for the structure given by Greis et al.[10] with  $a=b=21.9$  Å,  $c=6.65$  Å in the IHH sample with a grain size of 100 Å in the plane and 80 Å in the direction of the chain. It holds even better for the structure found by us with hexagonal dense packing and a cell size with  $a=b=11$  Å and  $c=9.65$  Å.



In the isotactic structure one unit cell contains six symmetry related chains, whereas in the syndiotactic structure one unit cell  $a=b=15.16$  Å,  $c=5.045$  Å [10] contains three symmetry related chains. Perfect order implies order along the chains in the  $c$  direction correlated with order between the chains in the  $x$ - $y$  plane and the symmetry within the chain corresponding to the symmetry of its position in the cell. Since our chains are atactic, perfect order along the chains is not possible.

From figs. 4.1, 4.2 and 4.3 we can see that isotactic chains are bulky helices whereas syndiotactic chains are flat. For the perfectly atactic chains one can expect that neighboring chains need the space necessary for isotactic order and thus prefer the isotactic conformation of fig. 4.3a to the syndiotactic one of fig. 4.3b. This could explain the observed transition from isotactic to syndiotactic arrangement yielding the better agreement of the isotactic peaks for the smaller  $Q$ 's in fig. 4.11 and that of the syndiotactic peaks for the higher  $Q$ 's. This discussion will be resumed below in connection with the amorphous scattering by randomly distributed linear molecules and will help us clarify the amorphous character in the atactic polystyrene by comparing the scattering by crystal patterns broadened by grain size i.e. by small crystallinely packed pieces of chains with the amorphous scattering calculated from equation (10) with and without such packing (cf. figs. 5.9-5.14).

In what follows we investigate the consequences from conformations along the chains by inspecting the structure amplitude  $F_M$  for different chain lengths. This will show us that the interpretation of our observations (fig. 3.4) is still more complicated as it involves a mixture of diffraction by crystallinity and randomly distributed linear molecules. In the case of the IHH sample we will then be able to determine the percentage of the sample that is ordered with 100-200 Å grain size, the percentage of the part with smaller grain size of 30 Å and the amorphous part with randomly distributed linear molecules of two monomers without parallel packing of chains. But, as discussed in 6 on page 83, the introduction of paracrystallinity circumvents the latter. In the atactic samples it allows us to show that we have regions of 20 Å with short range order and we do not need the part with amorphous scattering by single chains.

## Chapter 5

# The random chain orientation. Calculation of $F_M$

In the first part of the results and interpretation we begin the analysis with perfect crystalline order and subsequently relax its conditions stepwise thus increasing the possible disorder. We first remove the condition that the chains fulfill the symmetry condition of the crystallographic site also with their internal structure, introducing hexagonal dense chain packing. This needs chains on positions which have no threefold axial symmetry. Then we introduce a "short range order" by a "small grain size" including an anisotropic shape. Finally we relax the condition of perfect hexagonal dense packing thus arriving at what will be recognized in part 3 as paracrystallinity. This procedure yields an increasingly diffuse scattering i.e. a more and more amorphous state. We had even different representatives of these different states of order in IHH, DH, HH and HD. And we found that even the chain in the solid polymer has to be affinely deformed by changing at least the bond angles and perhaps even the bond lengths.

In the second step in the present chapter, we reverse the order of proceeding. Here initially the only order is the chemical structure of the monomer and we construct from this the scattering of randomly oriented chains and then increase the order slowly by increasing the number of monomers in the chains, which are randomly oriented. In this case no packing of chains at all is included in a first step. This way we can distinguish features in the scattering pattern that come from intrachain correlations as opposed to those which result from interchain correlations. Finally we include into the calculations the packing of chains.

To this end the properties of the Fourier transforms have to be used more extensively than in the powder pattern case. It is known that the intensity scattered by a distribution of matter in the Fraunhofer approximation of diffraction can be described by a Fourier transform with respect to this distribution [18]. Then the properties of the convolution integral permit the separation of the influence of different structural parts into separate factors. For example, a regular distribution of atoms in a molecule or a monomer can be Fourier-transformed separately and taken as a factor  $F_M$ ; the structure amplitude  $F_{hkl}$  used in the powder pattern calculation (as done in the first part with the program LAZY) represents a similar quantity in crystallography. Also the electron distribution in an atom is taken out as a factor in the Fourier transform of the whole crystal (the atomic form factor). In this way we can represent the polymer as the convolution of the distribution  $Z(r_j)$  of the points on which the monomers sit and the monomers themselves. The arrangement in space  $Z(\mathbf{r})$  is termed the disposition function. This leads to the factors  $Z(\mathbf{Q})$  and  $F_M(Q)$  in the Fourier transform. As it is conventional in crystallography to assume that the atoms fill the whole space, the disposition function fills the whole space and its Fourier transform is infinitely sharp and is described by a series of true  $\delta$  - functions in forward direction and at the Bragg reflections.

The general formula for the scattered intensity can be written in the form

$$I(\mathbf{Q}) = N \cdot |F_M(\mathbf{Q})|^2 \cdot \overbrace{Z(\mathbf{Q})|S(\mathbf{Q})|^2} \quad (5.1)$$

where the overbrace indicates convolution,  $N$  is the number of monomers or of the units for which  $F_M$  is calculated,  $Z(\mathbf{Q})$  is the Fourier transform of the point distribution of the points where the scattering units lie and  $F_M(\mathbf{Q})$  is the structure amplitude of these units given by eq.(5.6 on page 59) . As we have already seen in connection with figs.4.5 to 4.11 the shape factor plays a role in our case as the scattering units are small .

Convolution of the shape factor  $|S(Q)|^2$  with a  $\delta$ -function leaves the shape factor unchanged, therefore one measures in the small angle scattering around the forward direction and in wide angle scattering around the Bragg peaks the following shape function:

$$I_0(\mathbf{Q}) = k|S(\mathbf{Q})|^2 \quad (5.2)$$

$$\mathbf{Q} = 0, \mathbf{Q}_{Bragg} \quad (5.3)$$

with  $k$  a constant proportional to  $|F_M(\mathbf{Q})|^2$  which is different for the selectively deuterated samples and for the different Bragg peaks and  $N$  the number of monomers or units for which  $F_M$  is calculated. Here  $I_0(Q)$  is the intensity of the scattering. If the order is crystalline then the shape factor is reproduced at any crystalline reflection i.e. it appears as convoluted with the  $\delta$ -functions corresponding to the crystalline reflections. This corresponds to the observed broadening of the Bragg peaks treated above by the Scherrer formula (eq.(4.2 on page 42)). For the (000) reflex this gives the small angle scattering. Thus the shape of the Bragg peaks and small angle scattering enables us to determine the shape of the scattering regions from the  $|S(Q)|^2$  curves. They have the same width at each Bragg position in contrast to disorder (paracrystallinity) as will be evident later. The scattering around the Bragg peaks allows to determine the shape and size of the ordered regions from the shape function and from the integral intensity one obtains an information about  $N$ , the number of contributing units with the scattering amplitude  $F_M$ . In the small angle scattering this is independent of the degree of order in these regions. But one has to pay for this because also in solids there is unavoidable void scattering which contributes to this scattering. This fact can disturb the measurements very strongly if the void sizes are the same as the grain sizes. The presence of voids is normally not known, one tries to find it by such a measurement. If the degree of order is low then  $|S(Q)|^2$  is zero for wide angle scattering. If the matrix is ordered and includes voids, then the Bragg peaks show also a broadening by voids. But this approach has to assume an ordered matrix [16].

In contrast to  $|S(Q)|^2$  the function  $|F_M|^2$  is a factor, it is not convoluted with the  $\delta$ -function but only multiplied with it. It can be seen in figs.5.6 and 5.7 that as the number of monomers is reduced, the broader  $|F_M(Q)|^2$  becomes. The function  $|F_M(Q)|^2$  has the effect of a molecular form factor like the magnetic or electronic form factors of atoms. Normally in the small angle scattering region it can be assumed constant. But if there are units or domains of fourteen monomers or more, then  $|F_M(Q)|^2$  already changes in the  $Q$  region of small angle scattering. For wide angular Bragg reflections  $|F_M(Q)|^2$  corresponds to the structure factor and gives the height of the Bragg peaks whereas the  $Q$  of the Bragg peaks is determined by the Fourier transform of the disposition function.  $N$  is always unity because of our method of normalization.

If the scattering units are small that they can be summed up in the  $F_M$  then the shape factor is already included in this sum and  $Z(Q)$  then needs no further convolution with another shape factor (e.g.in fig.5.5 or 5.10) . If  $Z(Q)$  is an infinite point lattice as assumed in crystallography than the finite size of the scattering object must be included by the convolution of  $Z(Q)$  with a shape factor  $|S(Q)|^2$ . The Debye-Waller factor will be included later. The internal calibration gives immediately an expression for the scattered intensity corrected for the Debye-Waller factor:

$(d\sigma/d\Omega)$  per monomer

$$\frac{d\sigma_{coh}}{d\Omega}/monomer = |F_M(Q)| \cdot \overbrace{Z(Q) \cdot |S(Q)|^2}. \quad (5.4)$$

Upon inspection of fig.3.4 we can presume that our polymer consists of ordered and amorphous regions. Therefore we have to know both

- **a) the scattering amplitude from the actual building block unit**, which consists of several monomers forming a regular linear structure, and
- **b) the scattering amplitude of such units, that are randomly distributed.**
- **This can then give further clarification** of the features of the spectra obtained (c).

## 5.1 $|F_M|$ of an ordered structure of isotactic and syndiotactic chains of different lengths

In order to gain an understanding of the procedure to find  $F_M$  for ordered and disordered systems we have performed Fourier transforms of one, three and up to fifteen monomers possessing isotactic and syndiotactic order and subsequently representing these transforms in the reciprocal (Q) space. In figs.5.1 and 5.2 we display the modulus  $|F_M|$  of these transforms for the samples HH,DH,HD and DD as a "mountain structure" and as a contour plot over different cross-sectioning planes in Q-space, namely over the  $Q_x - Q_y$  plane, the  $Q_x - Q_z$  plane or the  $Q_y - Q_z$  planes, respectively. The  $Q_x$ ,  $Q_y$ ,  $Q_z$  ranges are given in these figures. It is aesthetically pleasing to see the behavior of the monomer form factor  $|F_M|$  which also enters the powder pattern calculations at the position of diffraction peaks (e.g. for  $Q_x = 1, Q_y = 1, Q_z = 0$  for the (110) reflex). The powder pattern (fig.4.4) is essentially the same calculation not continuously but only for the spots where Bragg reflection occurs multiplied by the crystallographic multiplicity factor and the Lorentz factor. Figs.5.1 and 5.2 give these values for continuously varying Q. Figure 5.1 shows the behavior of  $|F_M(Q)|$  as a function of  $(Q_x, Q_y, Q_z)$  for the different samples HH, DH, HD, DD calculated for the isotactic structure, one monomer. The term  $|F_M(Q)|$  for one monomer is given by the following formula (we use Q if the structure factor is spherically symmetric and  $\mathbf{Q}$  where this assumption is not made):

$$\begin{aligned} |F_M(\mathbf{Q})| &= \left| \sum_{j=1}^M b_j \exp(i(\mathbf{r}_j \mathbf{Q})) \right| & (5.5) \\ &= \left( \left[ \sum_{j=1}^N b_j \cos(x_j Q_x + y_j Q_y + z_j Q_z) \right]^2 + \left[ \sum_{j=1}^N b_j \sin(x_j Q_x + y_j Q_y + z_j Q_z) \right]^2 \right)^{1/2} & (5.6) \end{aligned}$$

The fractional coordinates of the atoms forming the monomer are listed above in table 2 for the isotactic and the syndiotactic structure (two monomers). For eq.(5.6) one has to multiply these values with 21.9 for x and y and with 6.65 for z in the isotactic case and with 15.16 (x and y) or 5.045 (z) in the syndiotactic case. The coordinates of the table are for the monomer in the coordinate (0,0,0) and in the hexagonal coordinate system with  $120^\circ$  between a and b axis, c being orthogonal to the a-b plane. For the calculation in eq. (5.6) with Q in rectangular coordinates one also has to transform  $r_{hex}$  in the rectangular coordinates e.g. with

$$x_{rect} = x_{hex} - \frac{y_{hex}}{2}$$

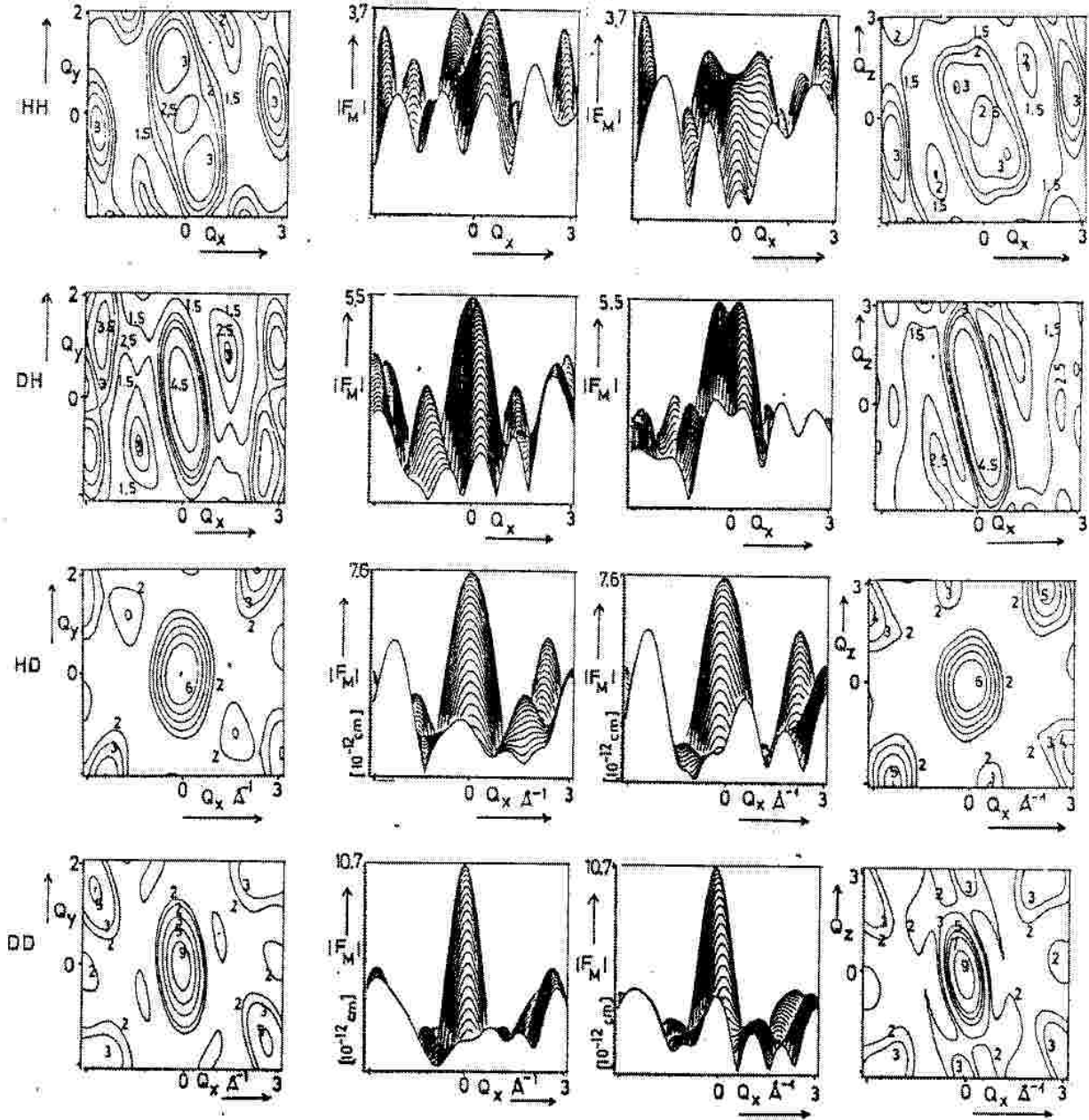


Figure 5.1: Representation of the modulus of the monomer form factor  $|F_M|$  for one monomer over the  $Q_x - Q_y$  and the  $Q_x - Q_z$  planes for the different samples HH, DH, HD, DD in the "mountain representation" and as contour plot.

$$\begin{aligned} y_{rect} &= y_{hex} * \sqrt{\frac{3}{2}} \\ z_{rect} &= z_{hex} \end{aligned} \quad (5.7)$$

(in figs.5.1-5.5). Fig.5.2 shows the behavior of the form factor for three monomers. Over the  $Q_x - Q_y$  plane the  $|F_M|$  for three monomers has approximately cylindrical symmetry. Increasing the number of monomers as shown in fig.5.3 leads to the increase in the height of the central peak at  $Q=(0,0,0)$  because it is the sum of all scattering lengths of all atoms contained in the structural unit. In the pattern corresponding to the  $Q_x$ - $Q_y$  plane the pattern remains unchanged, only the values become proportionally higher, the form remains the same because the x and y coordinates



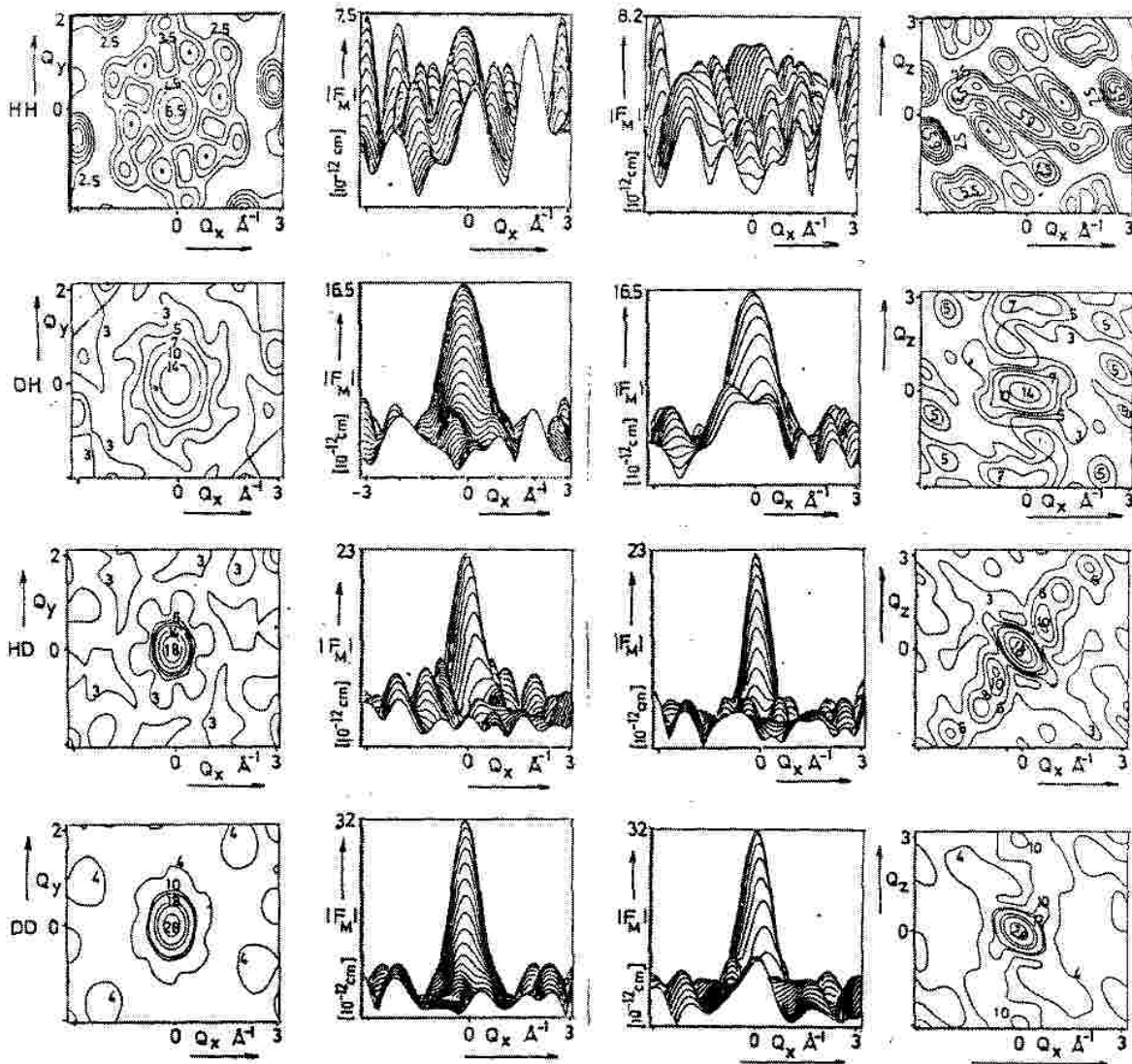


Figure 5.2: Representation of the modulus of the form factor  $|F_M|$  over the  $Q_x - Q_y$  plane and the  $Q_x - Q_z$  plane for three isotactically arranged monomers; mountain and contour plots.

of the atoms in the period remain the same. No characteristic pattern of  $|F_M|$  calculated for one isotactic unit (which comprises three monomers) over the  $Q_x - Q_z$  plane is evident in fig.5.2. But if one looks along  $Q_y$  in the  $Q_y - Q_z$  plane as done in the first image of fig.5.3 one sees the precursors of peaks. If one increases the number of isotactic units (6, 9, 12, 15 monomers) in the chain then one gets periodic behavior in the  $z$ -direction, cf. fig.5.3 for the isotactic case, and  $|F_M|$  becomes periodic in  $Q_z$ . Calculating the sum of eq.(5.6) for a larger number of monomers as shown in fig.5.3 for isotactic and in fig.5.4 for syndiotactic ordering, one obtains a new behavior of  $|F_M|$  in the  $Q_x - Q_z$  plane. A clear periodicity of about  $1 \text{ \AA}^{-1}$  in the  $Q_z$  direction emerges with an increasing number of isotactic units (each comprising three monomers). The more units one includes in the calculation, the narrower are the resulting peaks in the  $Q_z$  direction. This is clearly visible in fig.5.3. This figure shows the respective images for the sample HD for 3, 6, 9, 12, 15 isotactic monomers in the same representation as fig.5.1 and 5.2, but with the  $Q_z$  axis as abscissa in the mountain

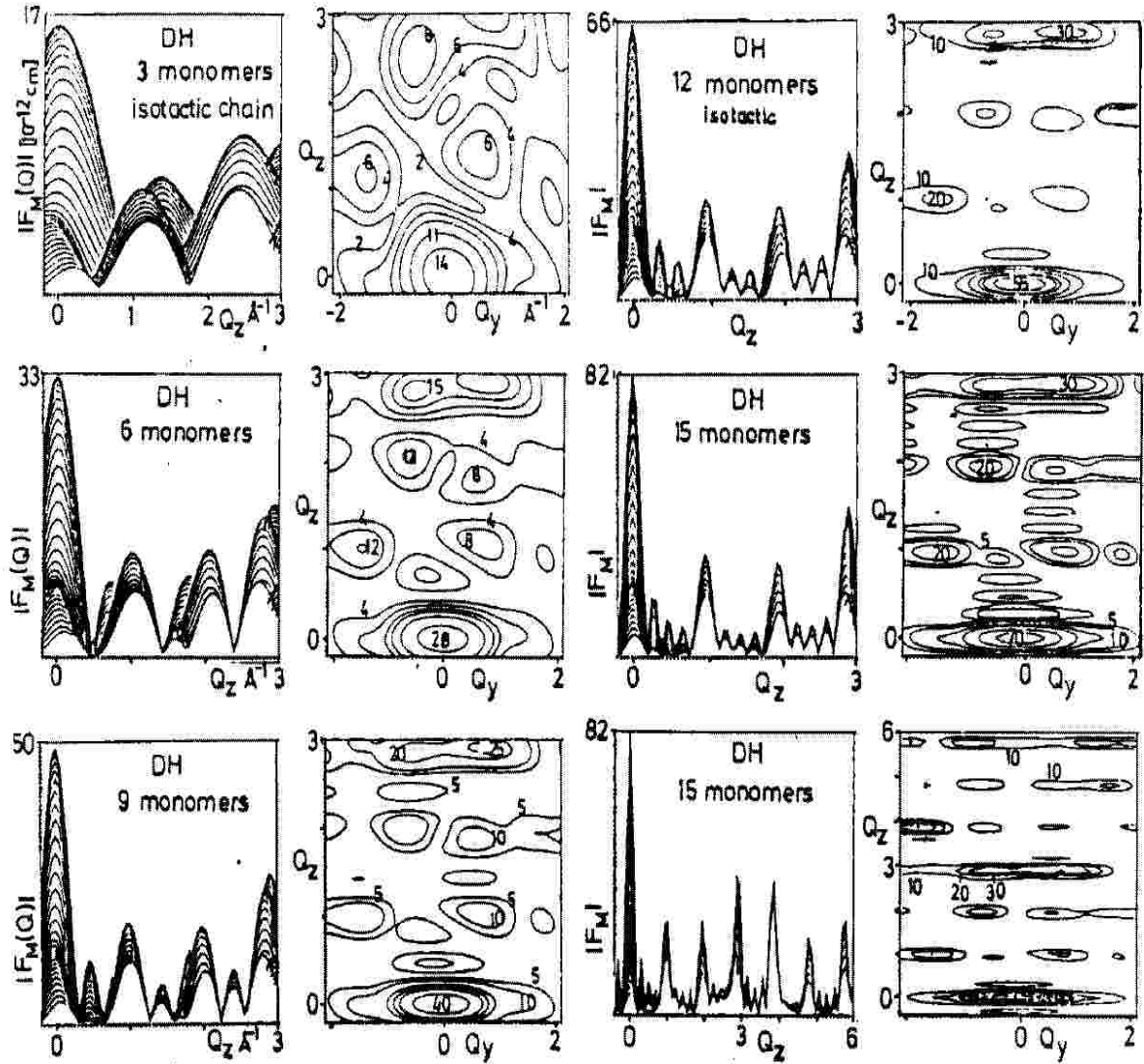


Figure 5.3: Behavior of  $|F_M(0, Q_y, Q_z)|$  with increasing chain length for isotactic structure of the sample DH (chain deuterated).

representation. Note that the last two images in fig. 5.3 show how the pattern repeats beyond  $Q = 3 \text{ \AA}^{-1}$ , preserving its character (here shown for up to  $Q_z = 6 \text{ \AA}^{-1}$ ). It is also evident that the peaks have a certain width in the  $Q_y$  (and also in the  $Q_x$ ) direction. That shows that they are not an infinitely thin line but a linear chain of a finite width. Thus the Fourier transform is not an infinite plane but a disk with a radius corresponding to  $2\pi/d_{chain} = 1.8^{-1}$  (half width), which yields for our calculated curves a chain diameter  $d_{chain}$  of  $3.5 \text{ \AA}$ . Fig. 5.5 shows the resulting peaks of  $|F_M|$  for all samples with assumed isotactic (with fifteen monomers) or syndiotactic (with fourteen monomers) structure. The pattern for the HH sample implies some ring structure corresponding to a ring of radius  $4.5 \text{ \AA}$  and a ring width of  $3.5 \text{ \AA}$ . The DD sample shows the structure of rings and plane disks for each third peak. This could explain why the third peak of fig. 3.4 is broader and has a different periodicity in  $Q$  than the first peaks. In order to understand this let us discuss how the diffraction pattern follows from this  $|F_M|$ . The powder reflection pattern from an  $|F_M|$  which is a ring or a

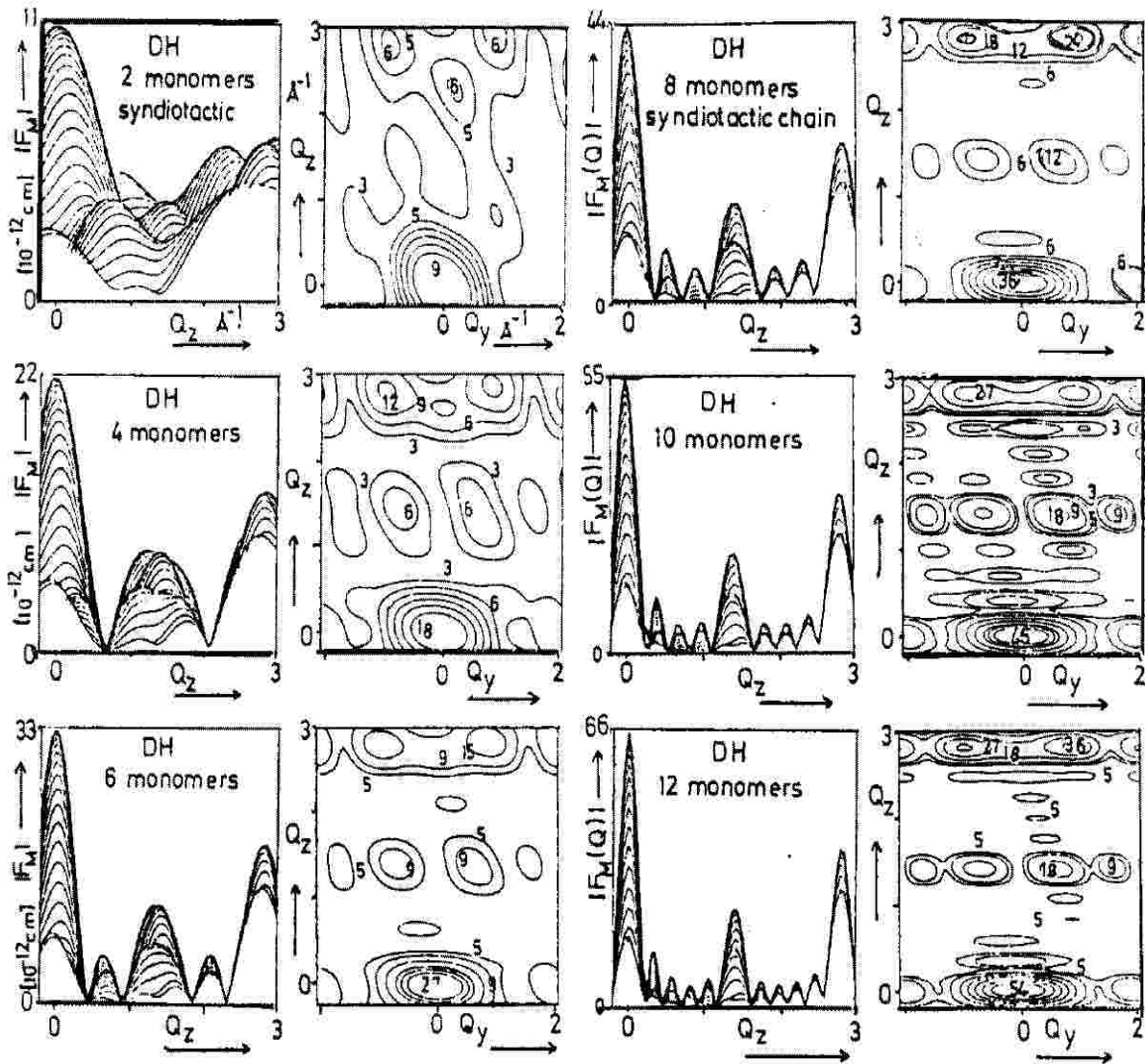


Figure 5.4: Behavior of  $|F_M(0, Q_y, Q_z)|$  with increasing chain length for syndiotactic structure of the sample DH (chain deuterated).

disk in the reciprocal lattice can be understood by considering a  $Q$  scan which over this region is achieved by rotating the sample. One obtains diffraction only if  $Q$  ends in the region of this disk or ring. Such a rotation of a crystal is not necessary in a powder: the crystallites are isotropically distributed and there are always some crystallites in the direction where the above condition is fulfilled. The intensity of the peaks corresponds to the  $|F_M|^2$  value at the respective point and is proportional to the volume of the region in reciprocal space (which fulfills the condition for the respective angle) weighted with the density in that region and the Lorentz factor as discussed above. The width of the peaks corresponds to the angular range, which corresponds with the condition that the  $Q$  arrow ends in the disk or ring region. Therefore a disk gives a broader peak than a ring and an infinite plane gives broader peaks than a disk, but a disk gives broader peaks than a sharp point from a three dimensional ordered crystal. This discussion shows how problematic it is in interpreting the peak width correctly. It is clear that if some reflex stems from a linear chain then



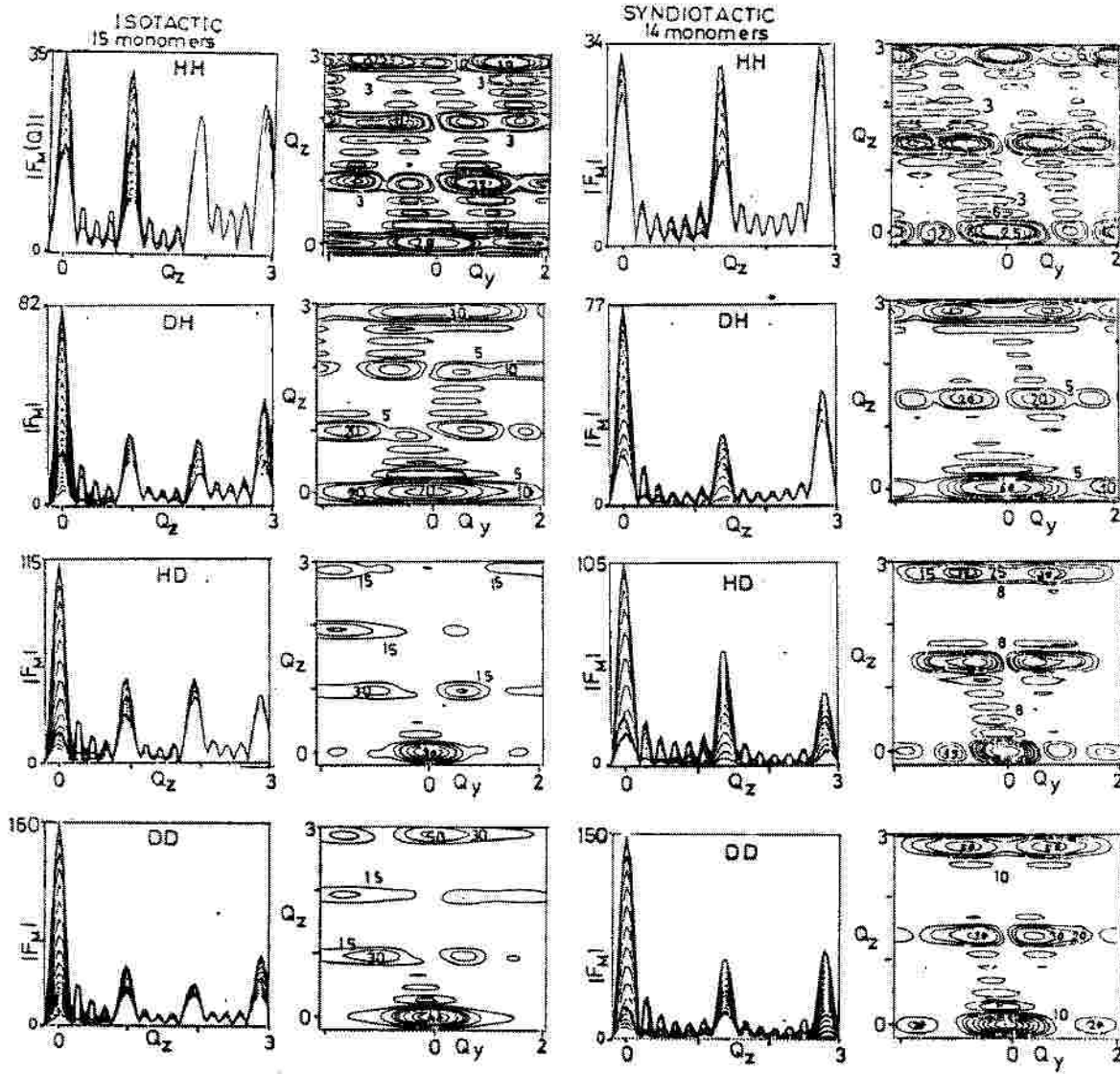


Figure 5.5: Behavior of  $|F_M(0, Q_y, Q_z)|$  with chain length 15 monomers for isotactic and 14 monomers for syndiotactic structure of all the samples i.e. HH,DH,HD,DD (differently selectively deuterated polystyrene).

it must be interpreted in a different way than if it comes from a three dimensional order. The effect of powder averaging on these peaks can be seen in figs.5.6 and 5.7 showing the diffuse scattering of the whole sample.

We can also conclude from these observations that diffraction from randomly oriented chain molecules can further our understanding of the observed scattering pattern. But presently we have to understand what effect the random orientation has on the spectral analysis.

## 5.2 $|F_M|$ for amorphous regions.

For the atactic sample the common assumption is that only random chain orientation is present [19]. Therefore it is interesting to compare the results obtained directly with calculations resulting from

this assumption. In part 5.1 on page 59 we examined the monomers or chains as ordered structures. The measurements shown in fig.3.4, especially the figure presenting the isotactic sample, also display a strong diffuse part which can result from an amorphous part of the sample. To calculate this quantity we follow mainly the approach outlined in reference [15, 18]. The intensity in a scattering experiment is generally given by the correlation function

$$I(Q) = \sum_j \sum_k F_{M_j} F_{M_k}^* e^{iQ \cdot R_j} e^{-iQ \cdot R_k} \quad (5.8)$$

with  $F_{M_j}$  = structure amplitude of monomer number  $j$  and  $R_j$ ,  $R_k$  the position of the "center of gravity weighted by the scattering length" of the respective arbitrarily oriented monomer, molecule or unit for which  $F_M$  is taken. The arbitrary orientation of the molecules requires the mean intensity and this comprises the calculation of  $\overline{F_{M_j}(Q) F_{M_k}^*(Q)}$  averaged over all  $j$  and  $k$ . Each  $F_{M_j}(Q)$  has at  $Q$  its own value. Averaging over pairs  $j \neq k$  the changes are independent and  $\overline{F_{M_j} F_{M_k}^*} = |\overline{F_{M_j}}| |\overline{F_{M_k}}| = |\overline{F_M}|^2$ . For terms with  $j=k$  the amplitude refers to the same molecule and we get

$$\overline{F_{M_j} F_{M_k}^*} = |\overline{F_M}|^2 \quad (5.9)$$

with the average over all orientations of the molecule. Hence one gets

$$I(Q) = N |\overline{F_M}|^2 + |\overline{F_M}|^2 \sum_{j \neq k} \sum_k e^{iQ \cdot R_j} e^{-iQ \cdot R_k} \quad (5.10)$$

or

$$I(Q) = N(|\overline{F_M}|^2 - |\overline{F_M}|^2) + |\overline{F_M}|^2 \sum_j \sum_k e^{iQ \cdot R_j} e^{-iQ \cdot R_k}. \quad (5.11)$$

In eq. (5.11) the first term describes the diffuse scattering from the disorder in orientation and the second part yields the diffraction pattern of the disposition of the single randomly oriented molecules, which can again be in a single crystal or in a powder (in the latter case of a powder it also has to be spherically averaged). The second term in eq. (5.11) corresponds to a system of averaged molecules having an amplitude  $\overline{F_M(Q)}$  and located at  $R_j$ ,  $R_k$ . The  $F_M(Q)$  term has the effect of an average form factor that changes the intensities of a diffraction pattern described by

$$Z(Q) = \sum_j \sum_k e^{iQ \cdot (R_j - R_k)} = \sum_j \sum_k \cos(Q \cdot (R_j - R_k)) \quad (5.12)$$

as a function of  $Q$ . Notice that the  $R_j$ ,  $R_k$  are not the atom positions in the monomers or chains but the "centers of gravity weighed by the scattering lengths" of the units themselves. If the units are large, they need much space and the periods in  $Z(R)$  are large. Therefore  $Z(Q)$  has many peaks at small angles. We will see that our units consist of 6-10 chain pieces comprising 6 monomers each i.e. units of 36 to 60 monomers. Then  $\langle F_M \rangle^2$  will be very narrow and we can disregard the scattering from the ordering of these large units, described by  $Z(Q)$ , giving small angle scattering only. So our scattering at large angles will be described by the first part of eq.(5.11).  $Z(Q)$  is what we observe in the small angle measurements. If there is order in  $Z(R)$  we will see peaks in the small angle scattering. Any disorder of  $Z(R)$  makes the small angle diffraction pattern increasingly more diffuse and hence deprives one of many details of value in analysis, but information (for example by a Guinier plot) about the average distance between the centers of the units for which the first part in eq.(5.11) is calculated or seen in the wide angular region can still be obtained.

We assume the monomers or groups of monomers are randomly oriented and randomly distributed in the uncorrelated or amorphous part of the sample. From the chapter about the physics of the polymers we know that the Kuhnlength is a measure of the size of correlated regions within the chains. But the excluded volume effect can also cause further distant parts of chains to be effectively parallel like spaghetti. This would increase the correlated part of scattering with small

correlation length but still there is no reason for large correlation lengths. The scattering from uncorrelated units is obtained by a spherical average over the structure amplitude of the monomer or the larger units given in figs.5.1 to 5.5 or in fig.5.10. This average amounts to an average over the cosine part of  $F_M(\mathbf{Q})$  because the averaged sine part is zero. This analysis gives [13]

$$\overline{\cos(\mathbf{Q} \cdot \mathbf{r}_{jk})} = \frac{\sin |\mathbf{Q}| |\mathbf{r}_{jk}|}{|\mathbf{Q}| |\mathbf{r}_{jk}|} \quad (5.13)$$

Then the spherical average of  $\langle F_M \rangle$  equals

$$\langle F_M \rangle = \sum_{j=1}^n b_j \frac{\sin(QR_j)}{QR_j} \quad (5.14)$$

whereas its squared amplitude is given by

$$\overline{|F_M|^2} = \sum_{j=1}^n \sum_{k=1}^n b_j b_k \frac{\sin Qr_{jk}}{Qr_{jk}} \quad (5.15)$$

Under these assumptions, the intensity is given by eq.(5.11).

Here it is noteworthy to explain how to determine  $r_j$  and  $r_{ij}$ . For  $\langle F_M \rangle$  the location of the center of the sphere plays a role if one does spherical averaging for an object which is not spherically symmetric. If the molecule has no symmetry center (as the polystyrene monomer) one has to determine first a "center of gravity" of the atoms weighed by their scattering lengths  $\mathbf{r}_0 = \sum r_i b_i / \sum b_i$ . If one ignores the "center of gravity" one obtains different patterns for one monomer in the syndiotactic and isotactic case. The reason for this is that the spherical averaging sees a broader "mass" distribution and  $\langle F_M \rangle$  becomes narrower.  $\langle |F_M|^2 \rangle$  remains the same because only the relative distances  $|r_j - r_k| = r_{jk}$  between the atoms enter the calculation, which do not depend on the center of gravity. If these two are than subtracted from each other one gets an artefact peak at low  $Q$  values. If one relates the scattering to the "center of gravity", the results for  $\langle F_M \rangle^2$ ,  $\langle |F_M|^2 \rangle$ , and  $\langle |F_M|^2 \rangle - \langle F_M \rangle^2$  for the syndiotactic and the isotactic chains for short chains as one or two monomers are identical, as anticipated. This "center of gravity" has to be determined for the whole unit which is randomly oriented. In contrast to this  $r_{ij}$  is the distance between atom  $i$  and  $j$  and does not depend on the location of the center. The Debye-Waller factor  $e^{-2W}$  can be included in the following way

$$I(\mathbf{Q}) = N(\overline{|F_M|^2} - \overline{|F_M|^2} e^{-2W}) + \overline{|F_M|^2} Z(\mathbf{Q}) e^{-2W} \quad (5.16)$$

with

$$Z(\mathbf{Q}) = \sum_j \sum_k e^{i\mathbf{Q} \cdot \mathbf{R}_j} e^{-i\mathbf{Q} \cdot \mathbf{R}_k}. \quad (5.17)$$

In the first column of fig. 5.6 the spherically averaged form factors  $\langle F_M \rangle$ , in the second column the spherically averaged  $\langle |F_M|^2 \rangle$  and in the third column the difference  $\langle |F_M|^2 \rangle - \langle F_M \rangle^2$  calculated for 1,2,3,6 and 12 monomers are shown for the isotactic structure. All three quantities are calculated for all samples HH,DH,HD and DD. Fig. 5.7 shows the similar trends for the syndiotactic order also calculated for 1,2,3,6 and 12 monomers, respectively. Comparison of figs.5.6 and 5.7 shows that there is no difference for the averaged physical quantities represented for chains with small numbers of monomers. Only if the chains get longer than four monomers do they show different behavior. But this can be understood by the effect of the different chain periodicities from fig.5.5, spherically averaged as in eqs. (5.13)-(5.16).

The difference  $\langle |F_M|^2 \rangle - \langle F_M \rangle^2$  in the third column of figs.5.6 and 5.7 represents a measure of the diffuse scattering by spherical averaging (it must still be multiplied by  $N$ , the number of monomers

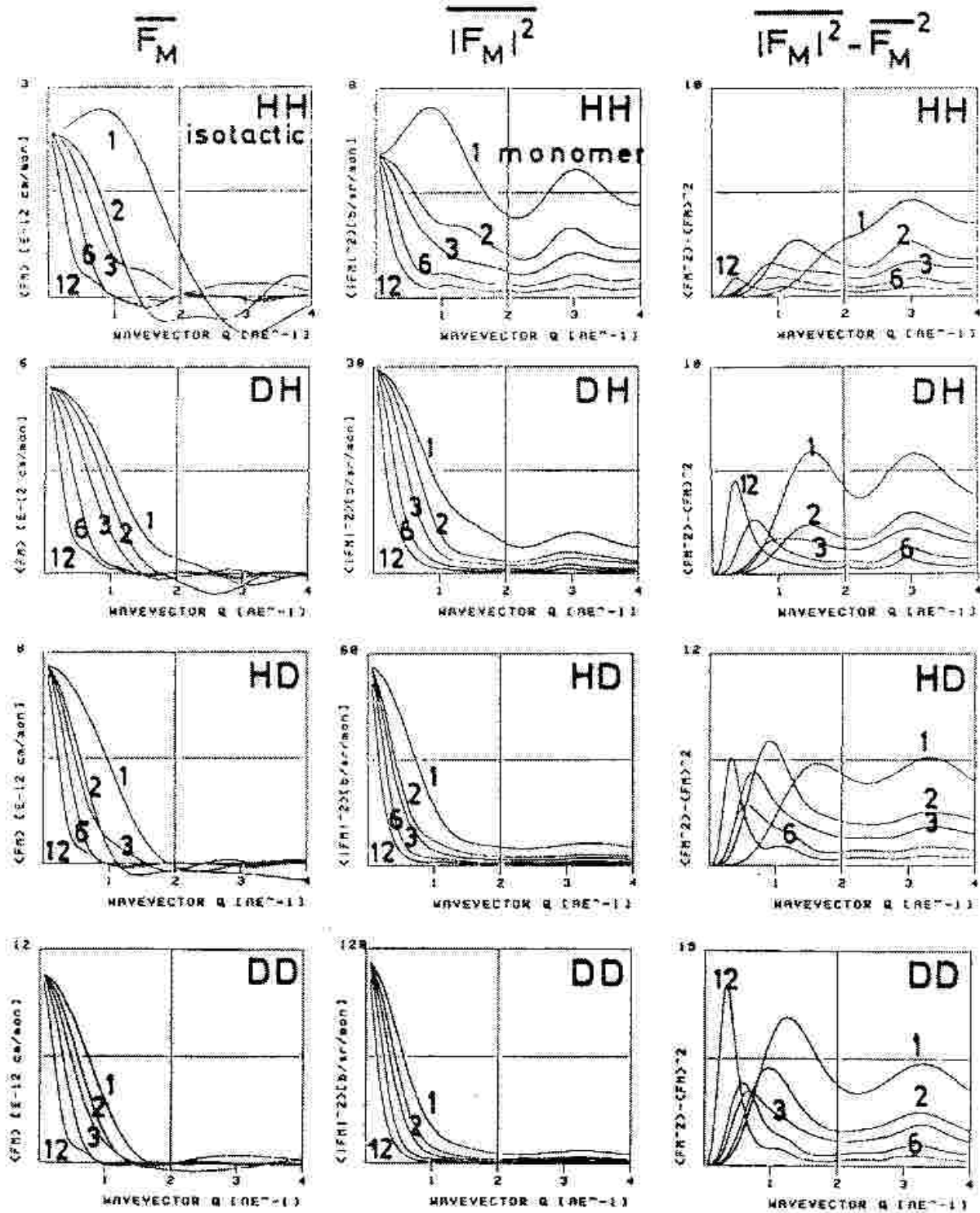


Figure 5.6: The characteristic averages for the isotactic structure. First column: calculated  $\langle F_M \rangle$  in  $10^{-12}$  cm/monomer, second column: calculated  $\langle |F_M|^2 \rangle$  in  $10^{-24}$   $\text{cm}^2/\text{monomer}^2$ , and third column: difference  $\langle |F_M|^2 \rangle - \langle F_M \rangle^2$  for the different parent polymers HH, DD, DH, HD for one, two, three, six and twelve monomers. The  $Q$  range is 0 to 4  $\text{\AA}^{-1}$ .

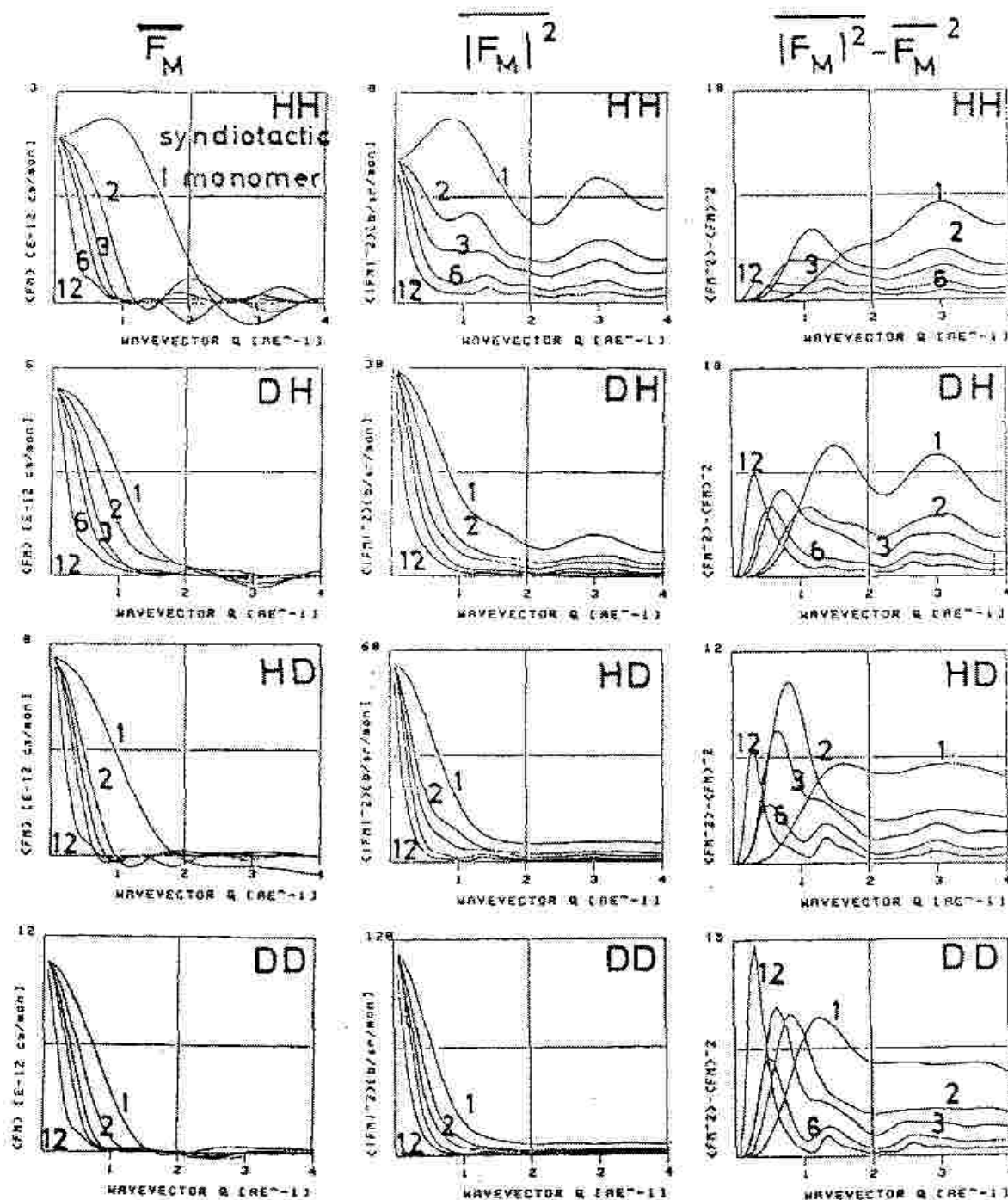


Figure 5.7: The characteristic averages calculated for the syndiotactic structure, with the center of the molecule at "center of gravity". First column: calculated  $\langle F_M \rangle$  in  $10^{-12}$  cm/monomer, second column: calculated  $\langle |F_M|^2 \rangle$  in  $10^{-24}$  cm<sup>2</sup>/monomer<sup>2</sup>, and third column: difference  $\{ \langle |F_M|^2 \rangle - \langle F_M \rangle^2 \}$ /monomer<sup>2</sup> for the different parent polymers HH, DD, DH, HD for one, two, three, six and twelve monomers. The Q range is 0 to 4  $\text{\AA}^{-1}$ .



in the unit, if  $F_M$  is normalized to one monomer by division by  $N$  and  $\langle |F_M|^2 \rangle$  by division by  $N^2$ . The influence of averaging shows as weakening and broadening of peaks resulting from the chain periodicity. These periods are clearly seen in figs.5.3 and 5.5 at about 1, 2 and 3  $\text{\AA}^{-1}$  for the isotactic order; for the syndiotactic order at  $\approx 1.5$  and  $\approx 3^{-1}$ , (as observed in figs.5.3 - 5.5).

These also appear for random oriented chains but only for the higher chain lengths and their powder averages are then weaker and broader (figs.5.6 and 5.7). If we denote the averaging by a pair of brackets  $\langle \dots \rangle$  we can then say that the calculated functions  $\langle F_M \rangle$ ,  $\langle |F_M|^2 \rangle$  and  $\langle |F_M|^2 \rangle - \langle F_M \rangle^2$  describe [eq.(5.11)] the scattering of a glassy material, which consists of molecules of one, two, three, six, twelve monomers regularly connected to form a chain segment. These chain segments are randomly oriented as a whole and, in principle, ordered or disordered on the sites  $\mathbf{R}_j$ ,  $\mathbf{R}_k$  from eq.(5.12). If they are perfectly disordered, the scattering of the segments of the chain is described by the term  $\langle |F_M(\mathbf{Q})|^2 \rangle$ . If there is order, the intermolecular interference decreases rapidly at large angles and the pattern tends towards that of a molecular gas as we already discussed in connection with eqs.(5.11)- (5.12). This order would otherwise modulate the diffuse scattering described by  $N(\langle |F_M(Q)|^2 \rangle - \langle F_M(Q) \rangle^2)$ . If one plots the diffuse scattering alone as  $N(\langle |F_M(Q)|^2 \rangle - \langle F_M(Q) \rangle^2)$  for the different lengths of chain segments one gets the results of fig.5.8 for the selectively deuterated samples.

Fig.5.8 shows that the diffuse scattering in the main region of the pattern weakly depends on the number of monomers in the chain segments and also not strongly on the isotactic or syndiotactic arrangement. This is the previously mentioned behavior of a molecular gas. Only in the region of small  $Q$  ( $< 1.0 \text{ \AA}^{-1}$ ) a strong scattering (a peak begins to appear) arises if the randomly oriented chain segments are long. This comes from the fact, that for long chains the bundles become cylindric and the spherical average gives is broader in  $\langle F_M^2 \rangle$  than in  $\langle F_M \rangle^2$ . To understand this behavior recall that in this approach the scattering by polymers begins with perfect disorder. Then we increase the order by joining in isotactic or syndiotactic order with more and more monomers. The resulting scattering, if it results only from one or two monomers, gives a nearly flat scattering as a function of  $Q$  with not much modulation. The scattering by one monomer shows always only a broad peak at about 3  $\text{\AA}^{-1}$  which remains about the same with increasing correlated chain length. This implies that the scattering of the molecular gas does not strongly depend on the size of the respective molecules, if it is related to the same units, namely the monomer unit. The results arise only from the structure of the monomer. Shifts of the position of this peak in  $Q$  can give information about the bond length in the monomers. This does not depend on the tacticity, therefore one sees it at  $Q \approx 3^{-1}$  both in the syndiotactic and isotactic forms (figs.5.6 and 5.7). The averaged periodicity peaks appearing with longer chains is the feature that varies in these figures and shows up as narrow peaks superimposed on the broad peak originating from the monomer. Then, with higher chain lengths all samples begin to show a peak arising at  $Q$  about 0.5 - 0.6  $\text{\AA}^{-1}$ . This peak does not yet come with 6 monomers but it appears for chain lengths of 12 and 18 monomers in the HH sample. Here we have a strong deviation of a sphere and this results from the spherical averaging of this cylindrical form. The length of 6 monomers corresponds to the grain size which was found by the powder approach. But the comparison of the measurements with the calculations (fig.5.9) shows that the former are stronger modulated also at other than those small  $Q$  values. For some samples the measured curves in fig.5.9 show even nearly no scattering at small  $Q$ . The pure amorphous scattering calculated for a single chain, given in fig.5.8 for the selectively deuterated samples, does not fully describe the results. None of these curves is perfect: if one part fits well, then there is always another part of it which does not. For example the peak in the HH sample at 1.3  $\text{\AA}^{-1}$  with the syndiotactic chains of twelve or eighteen monomers does not have the right height and does not show the peaks at smaller  $Q$ . The DH sample shows the best agreement. With chain length of six monomers the scattering from the syndiotactic chain shows the same height and width of the peak at 0.6  $\text{\AA}^{-1}$  as the calculated one but the second peak does not agree: it is smeared out in the calculations and well separated in the measurement. Also the trough at 2  $\text{\AA}^{-1}$  is deeper in the

experimental results.

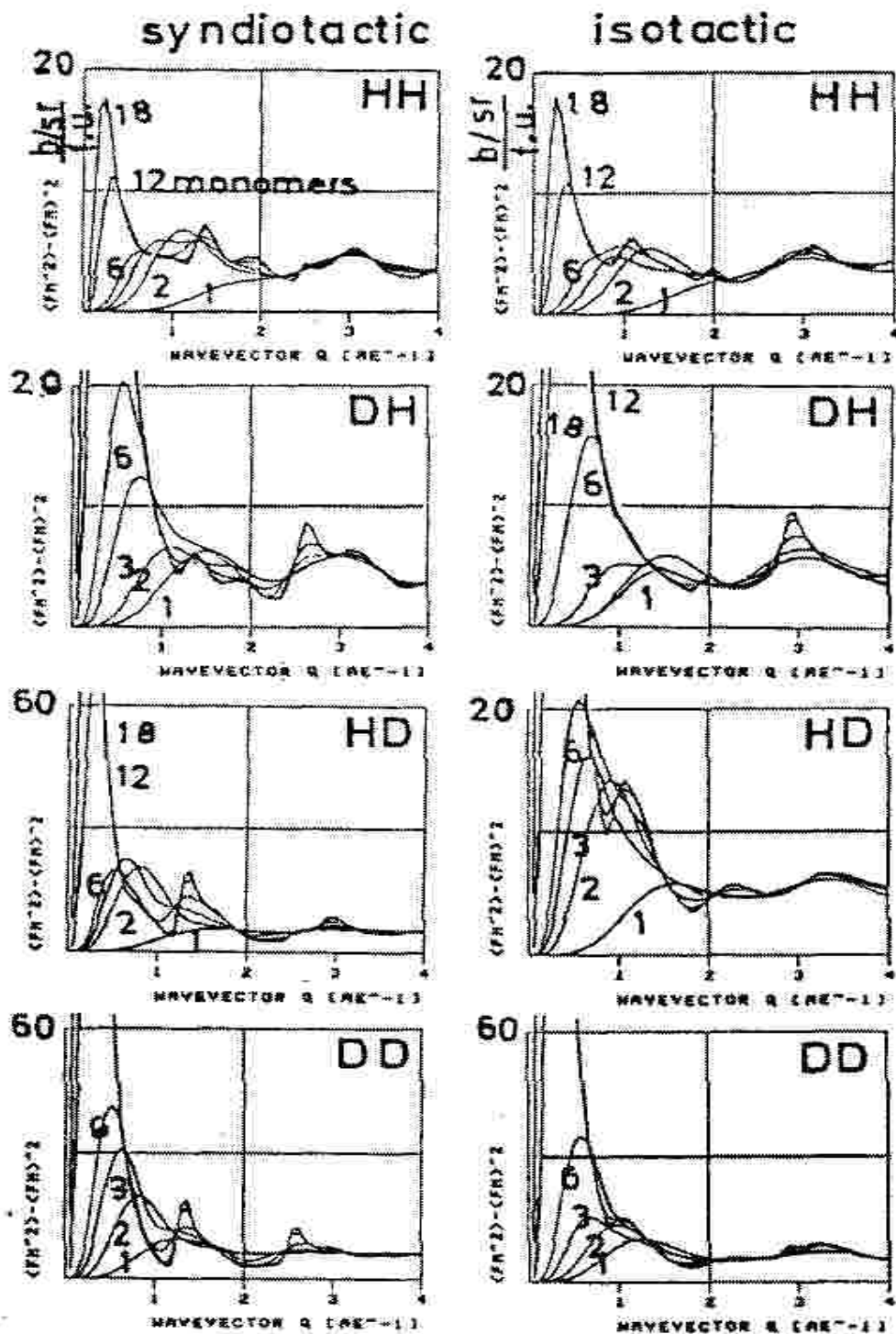


Figure 5.8: Diffuse scattering  $N(\langle F_M^2 \rangle - \langle |F_M|^2 \rangle)$  for arrangements of one, two, three, six, twelve and eighteen monomers in chain pieces of isotactic and syndiotactic order for selectively deuterated polystyrene.

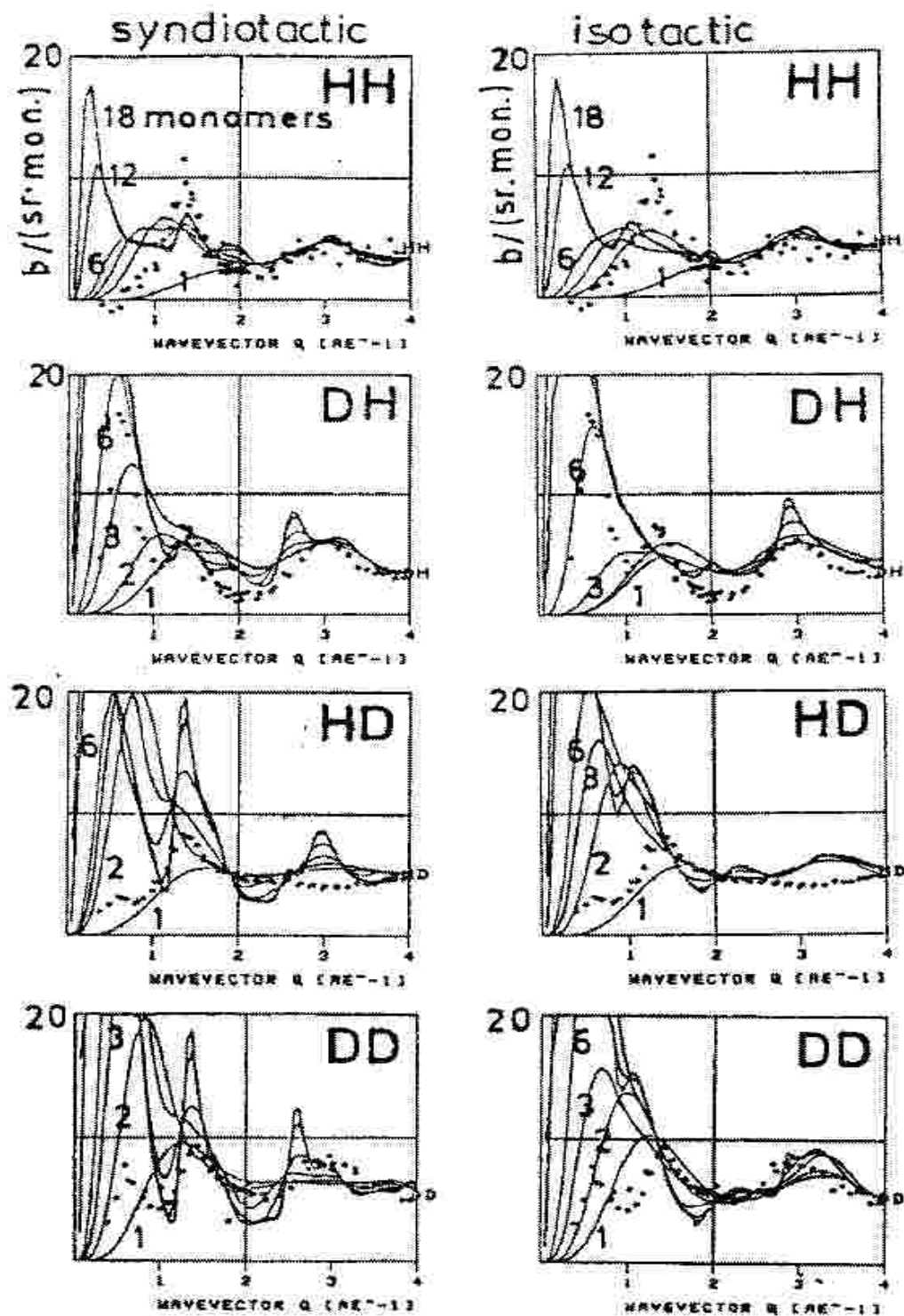


Figure 5.9: Comparison of the diffuse scattering of fig.5.8 for arrangements of chain pieces of one, two, three, six, twelve and eighteen monomers of syndiotactic and isotactic order for selectively deuterated polystyrene with the measurements corrected for the multiple scattering (dots).



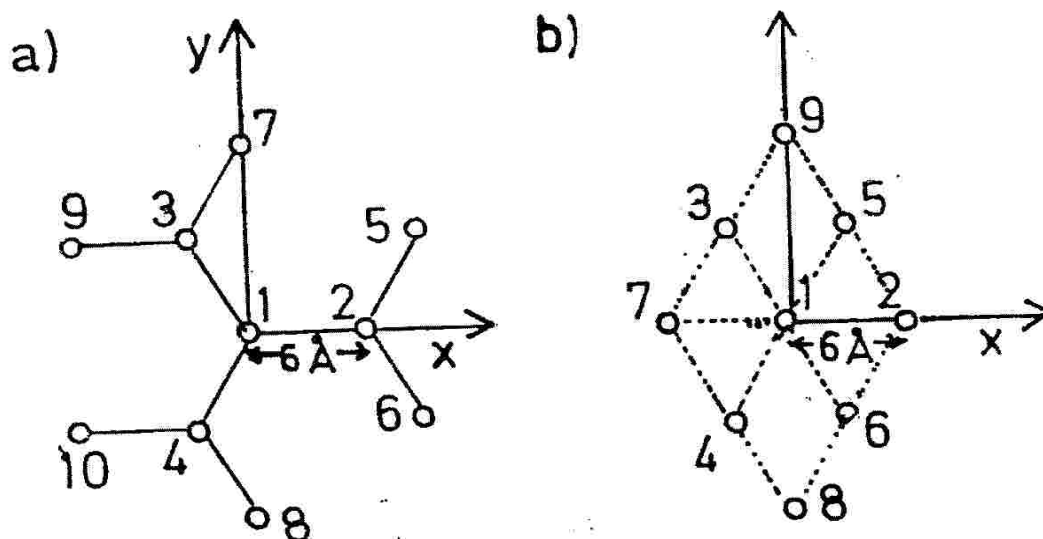


Figure 5.10: Sketch of the arrangement of the chains for the calculations of the diffuse scattering a) for four, six and ten parallel chain segments for three nearest neighbors, b) for seven and nine parallel chain segments for hexagonal dense packing.

The most serious disagreement occurs for the HD and the DD samples. The scattering curves can not be understood at all as due to single chains randomly oriented and randomly distributed. They show small peaks where the single chain calculations show very high peaks and they are more structured than the calculated diffuse scattering for the lower chain lengths.

This is what one obtains without any short range order. If one is satisfied with such an agreement one can sum up by saying that there is only random chain orientation present in the samples. It will be shown that with some short range order the agreement is better and that for all selectively deuterated samples with the same structure.

We can now attempt to join a few parallel chains, six monomers long, together in bundles to calculate the diffuse scattering from an arrangement which simulates a grain. The single grains obtained are then completely randomly arranged. With the 20 Å grain size found before we can arrange ten chains with three nearest neighbor chains as shown in fig.4.3a. If each chain comprises of six monomers we would have to calculate the scattering from units comprising sixty monomers, which is still achievable within reasonable computing times. We have done this for the chain arrangement of fig.5.10a taking different chain lengths in order to see the dependence on the number of monomers in each chain. With the numbering given there we calculate the diffuse scattering for different bundles comprising four, six and ten parallel chains: with chain length six monomers for four parallel chains, with chain lengths one, three, six monomers for six parallel chains and with one, six, nine monomers for ten parallel chains. This is shown in fig.5.11 for isotactic chains.

For the syndiotactic chain configuration we calculated the  $Q$ -dependence of the diffuse scattering for four, six and ten bundled chains. For four parallel chains we calculated it with chain lengths of one, two, and six monomers, for six parallel chains with one and six monomers and for ten parallel chains with six and eight monomers. The results are given in fig.5.12.

These calculated curves for the loosely arranged chains of fig. 5.10a do not show a strong dependence on the chain length in contrast to those obtained for the hexagonal densely packed chains of fig. 5.10b. The loosely packed chains with three nearest neighbors show for one monomer "chain length", i.e. only as a plane distribution of monomers, nearly the same diffuse scattering as

that of a packing of the longer chains. The only changes are in the range of up to  $1\text{\AA}^{-1}$ , which for the larger bundles of six or ten chains are very small. The one monomer long "chains" are really no chains but the bundles of four, six or ten "chains" correspond to the next higher dimension of an arrangement in comparison to the linear arrangement of one single chain (fig.5.8). It represents a plane arrangement, whereas in fig.5.8 we had linear arrangements that are randomly oriented and randomly distributed.

All curves of figs.5.11 and 5.12 show high peaks at  $0.6\text{\AA}^{-1}$  of the same form as we observe for the DH, HD and DD samples, the two latter are even higher than for DH. For these samples the measured curve has only a small blip or a very low peak. The HH sample should in this case also show a modulation of the peak at 1 to  $1.3\text{\AA}^{-1}$ , which is also not found.

To see also the behavior in the case of the hexagonal dense packing, fig.5.13 gives the results of the calculations for bundles of seven and nine chains with hexagonal dense packed syndiotactic chains in the arrangement of fig.5.10b where the numbering and the distances used are given. Here one can see for all samples a strong dependence of the scattering in the range of up to  $1\text{\AA}^{-1}$  on the chain length. For loose packing this region of sensitivity may have fallen in a smaller Q-region, because the respective distances  $r_{ik}$ , eq. (5.15), are larger there.

The scattering shows again a high peak at about  $0.6\text{\AA}^{-1}$  for one monomer "chain length" as before (but here dense packed monomers in the plane). This high peak depends now strongly on the chain length. Fig.5.13 shows that this peak lowers at a length of 4 monomers and even more with 6 monomers for the bundle of seven chains. With nine chains one can see a similar tendency but it seems to lower here only with higher chain lengths. In the case of seven chains each comprising ten monomers a very high peak appears at  $0.3\text{\AA}^{-1}$ , which is an artefact from the cylindrical form as discussed above.

Figs.5.11-5.13 present the interesting behavior of the scattering in the transition from only one dimensional order along the chains (figs.5.8 and 5.9) to growing order in three dimensions. This is achieved by adding more and more chains of different lengths, from one to six or nine monomers to parallel bundles. This is done for isotactic ordered chains (fig.5.11) and for syndiotactic ordered chains (fig.5.12) for three nearest neighbors and for syndiotactic chains for hexagonal dense packing (fig.5.13). These curves represent the diffuse scattering of different amorphous structures. A further generalization of this approach could only be a treatment of a mixture of different sizes of the ordered regions and with this a mixture of different degrees of amorphous scattering. (This will be treated in chapter 6 on page 83 which, somewhat tentatively, describes a real polymer as a combination of short range order and random chain orientation.) The increasing order results in an increasing height of the observed peaks, always normalized to the scattering from one monomer, and a narrowing of the peaks and an increased number of peaks. The explicit shape function is not necessary here, since it is already included by the basic assumption that the pattern is calculated for only a finite number of monomers. This explains the narrowing of the peaks by the increased number of monomers when these are taken into account.

Since we have normalized our measurements and our calculations to one monomer, we can compare the intensity of the pattern and the number of observed peaks, their positions and their width with the measured ones to get information about distance between chains, number of chains and the way of arrangement of the underlying structure.

### 5.3 Comparison with measurements

Figs.5.14 and 5.15 represent the different curves of figs.5.11 to 5.13 and figs.4.9 and 4.10 together with the measured points in the whole region of Q up to  $4\text{\AA}^{-1}$  (in the third column only to  $2\text{\AA}^{-1}$ ) for the sake of comparison with the above results.

Figs.5.14 and 5.15 can also serve to compare the calculations of the different models. Comparison of the grain size broadened spectra of figs.4.9 and 4.10 with the results of powder averaged scattering

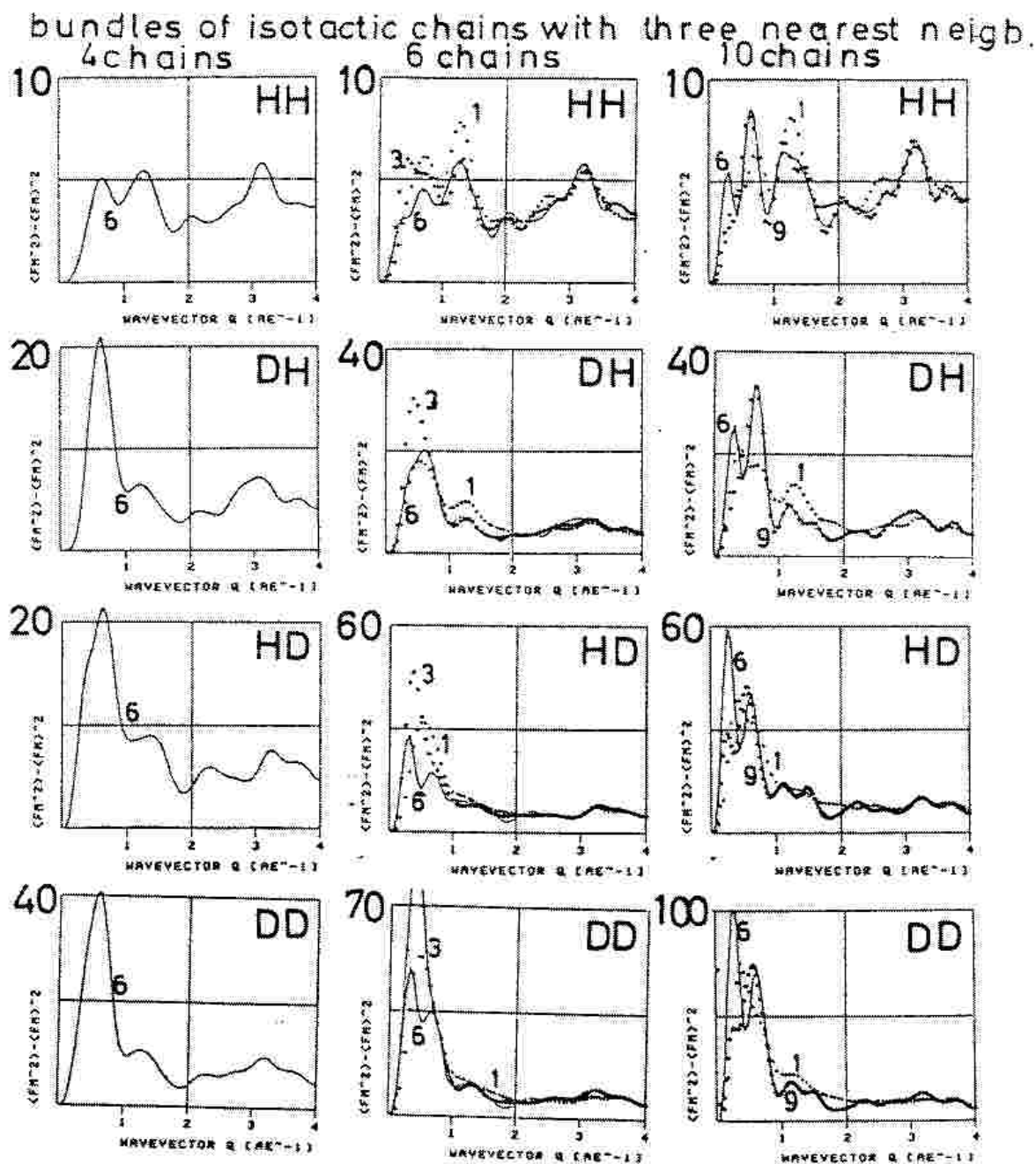


Figure 5.11: Results of calculations for the selectively deuterated chains with chain pieces of six isotactically ordered monomers (continuous line) for bundles of four, six and ten parallel chains in the arrangement of fig.24a with three nearest neighbors. For bundles of six chains crosses give curves for one monomer and circles for 3 monomers. For ten chains circles give curves for 9 monomers. These are given to show the dependence on the "chain length".

of bundles of four, six, ten chains comprising six and nine monomers for the loosely packed chains and the hexagonal densely packed chains in figs.5.11 to 5.13 shows, that the 20 Å grain size and the four chain bundles show many common features. Note that the  $Q$  scales are different. In figs.5.14 and 5.15 they are all drawn in comparison with the measurements. Both frames show two

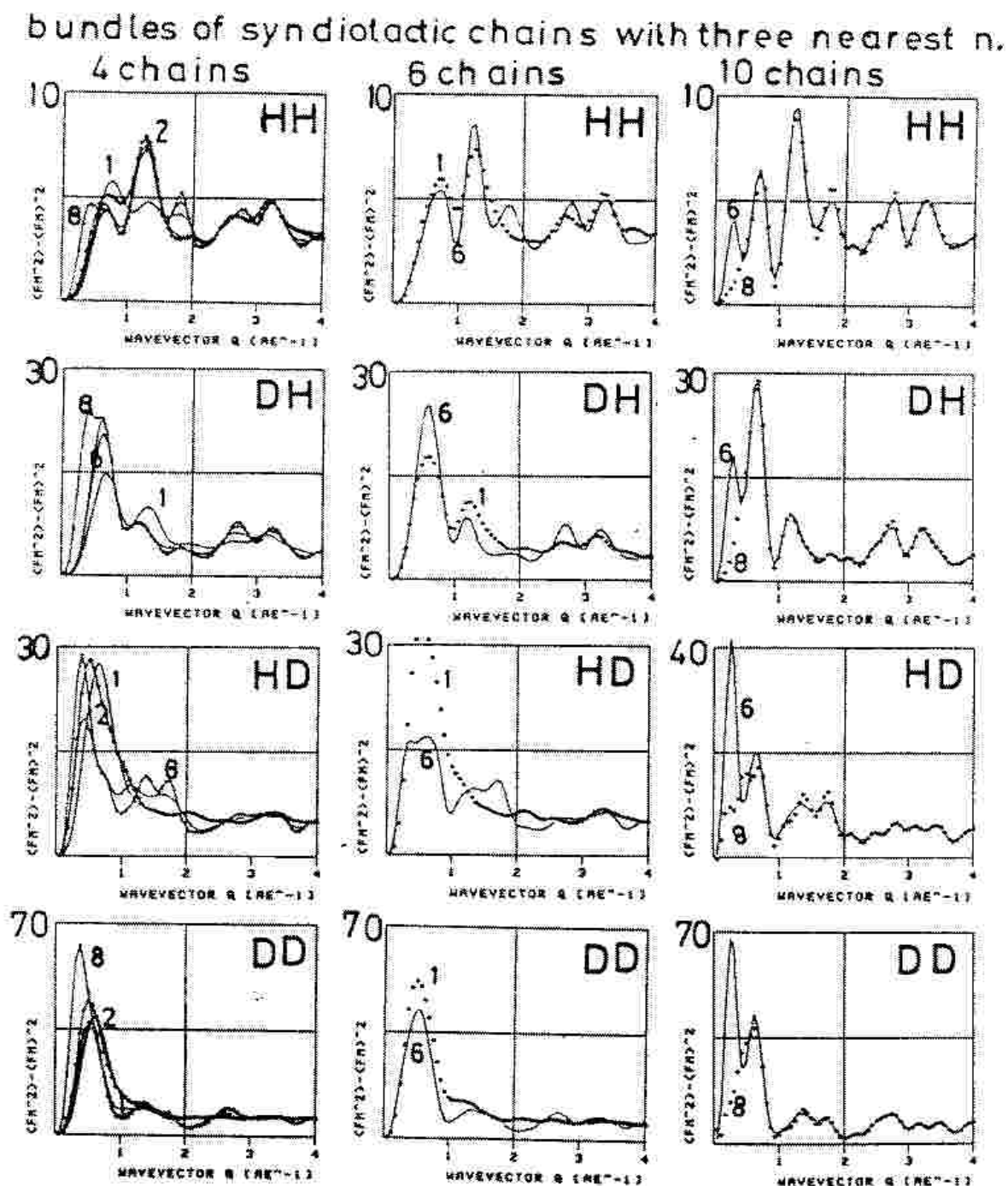


Figure 5.12: Results of calculations for the selectively deuterated chains with chain pieces of six syndiotactically ordered monomers (continuous line) for bundles of four, six, and ten parallel chains in the arrangement of fig.5.10a. For four chains the curves for 1 to 8 monomers are given (no big change). For six chains circles show also the results for 1 monomer and for ten chains the circles show the results for 8 monomers (no strong dependence above  $0.3 \text{ \AA}^{-1}$ ).



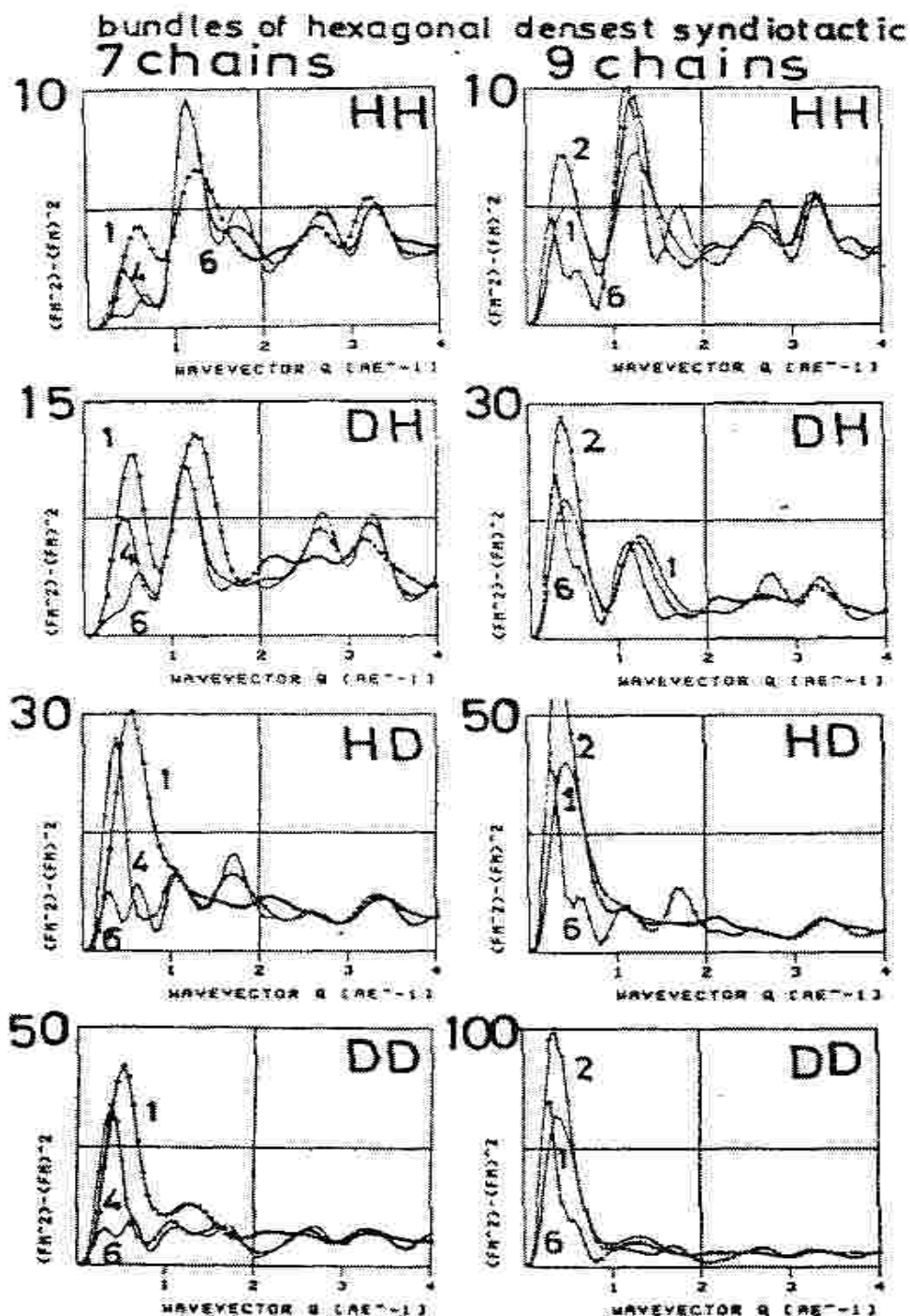


Figure 5.13: Calculations for HH,DH,HD and DD for hexagonal densely packed (fig.5.10b) parallel syndiotactic chains with bundles of seven and nine chains with length of 1 (circles), 4 (crosses) and 6 (continuous line) monomers for seven chains and 1 (continuous line), 2 (crosses) and 6 (crosses x) monomer chain lengths. A strong dependence on chain lengths is visible in the region about  $0.6 \text{ \AA}^{-1}$ .

broadened peaks for all samples which in the ring deuterated samples show reversed intensities in the both cases. This is also the case in figs.4.9 and 4.10 with the structure of hexagonal dense packing. Remember that the latter was invented to avoid peaks at smaller  $Q$  in the isotactic sample case. The loosely packed chains of fig.5.10a show peaks at small  $Q$  values for all samples. The hexagonal dense packed bundles (fig.5.10b) do not show such peaks at small  $Q$  values. But even with ninety monomers we still do not obtain spectra with narrow lines. The more monomers are included in the calculation the more features at the higher angles develop and the peaks at the low  $Q$ -values decrease, but by an oscillatory process in the lowest peak (at about  $0.3 \text{ \AA}^{-1}$  for the loosely packed case and at about  $0.6 \text{ \AA}$  for the dense packing).

Now we want to compare the calculated with the measured curves. The first observation is that in the higher  $Q$ -region above  $2 \text{ \AA}^{-1}$  the diffuse scattering does not strongly depend on the number of monomers and chains included in the calculations. This we saw already from the results obtained for different chain lengths in figs.5.8 and 5.9. It is just a consequence of the  $\langle F_M \rangle$  acting as an average form factor for the remaining peaks: it is so narrow and so low at higher  $Q$  that there are no intense peaks possible above about  $2 \text{ \AA}^{-1}$ . This is only an alternate way of saying that the structure of the scattering units does not manifest itself at  $Q > 2 \text{ \AA}^{-1}$  or that the calculated diffuse scattering results from chains acting as a molecular gas of monomers. This also remains true for parallel chains. But one feature is very interesting: one obtains for all samples in this higher  $Q$  region above  $2 \text{ \AA}^{-1}$  the right intensity without any arbitrary assumptions which shows that our calculations are correct. We emphasize that the dimensional units [b/sr/monomer] are the same in the calculated and measured curves, so that one can compare the calculated curves quantitatively with the measurements. The data in figs.5.14 and 5.15 is not parametrized or brought into line with the use of 'fudge factors'. The figures compare calculated and measured curves. They show just the absolute value as measured and corrected for multiple scattering for the measured curves and the value as it is calculated for the theoretical curves. This shows the strength of having an internal calibration. We can even use the results to renormalize the results of the DD sample, which does not have the right incoherent scattering corresponding to pure D content. The necessary renormalization in fig.5.14 and 5.15 shows that there must be a content of about 2.6 % hydrogen.

In the case of the chain deuterated sample DH the peaks come mainly from the chains, because these have the strongest coherently scattering deuterated atoms D. Then the pattern would mostly be determined by the bundle of 10 parallel chains with a distance smaller than  $6 \text{ \AA}$  with three nearest neighbors as sketched in fig.5.10 on page 72 in the column a). In the case of isotactic chains the large distances in this sample yield peaks with smaller  $Q$ . These are not so well regularly present to give all the high peaks of the calculations of fig.5.14 on page 78 (DH sample, ten chains), they only show up in the peaks at  $0.6 \text{ \AA}^{-1}$  and  $1.6 \text{ \AA}^{-1}$ . The peak at  $0.6 \text{ \AA}^{-1}$  is already weaker and that at  $0.3 \text{ \AA}^{-1}$  has disappeared showing just the effect of short range order, i.e.  $0.3 \text{ \AA}^{-1}$  corresponds to a distance of  $42 \text{ \AA}$  where we already know that we have no real periodicity of this size. In the case of syndiotactic chains the agreement is nearly perfect, only the peak at  $Q=3 \text{ \AA}^{-1}$  does not show up in the measurement. This can be understood by considering paracrystallinity, which is the best description of the short range order in this materials. The third column in fig.5.14 shows the results of grain size in the powder pattern for syndiotactic chains and isotactic chains as given by Greis et al.[10] and in fig.5.15 on page 79 for the hexagonal dense packing. The latter does not fit at all for the DH sample. It really seems to have another packing of chains than the HH, HD and DD samples. But remember that for the DH sample the randomly oriented chain itself gives already good agreement as seen in fig.5.9 on page 71. The resulting structure must also be consistent with the resulting structures of the other samples. One has to assume that selective deuteration will not change the structure if everything else remains the same. And we show that it is possible to obtain the same structure for all samples. Would we not have the full palette of the selectively deuterated samples, the conclusion would be quite definite because everything seems plausible. But since we also have the other measurements, we have to see further. If we do not get

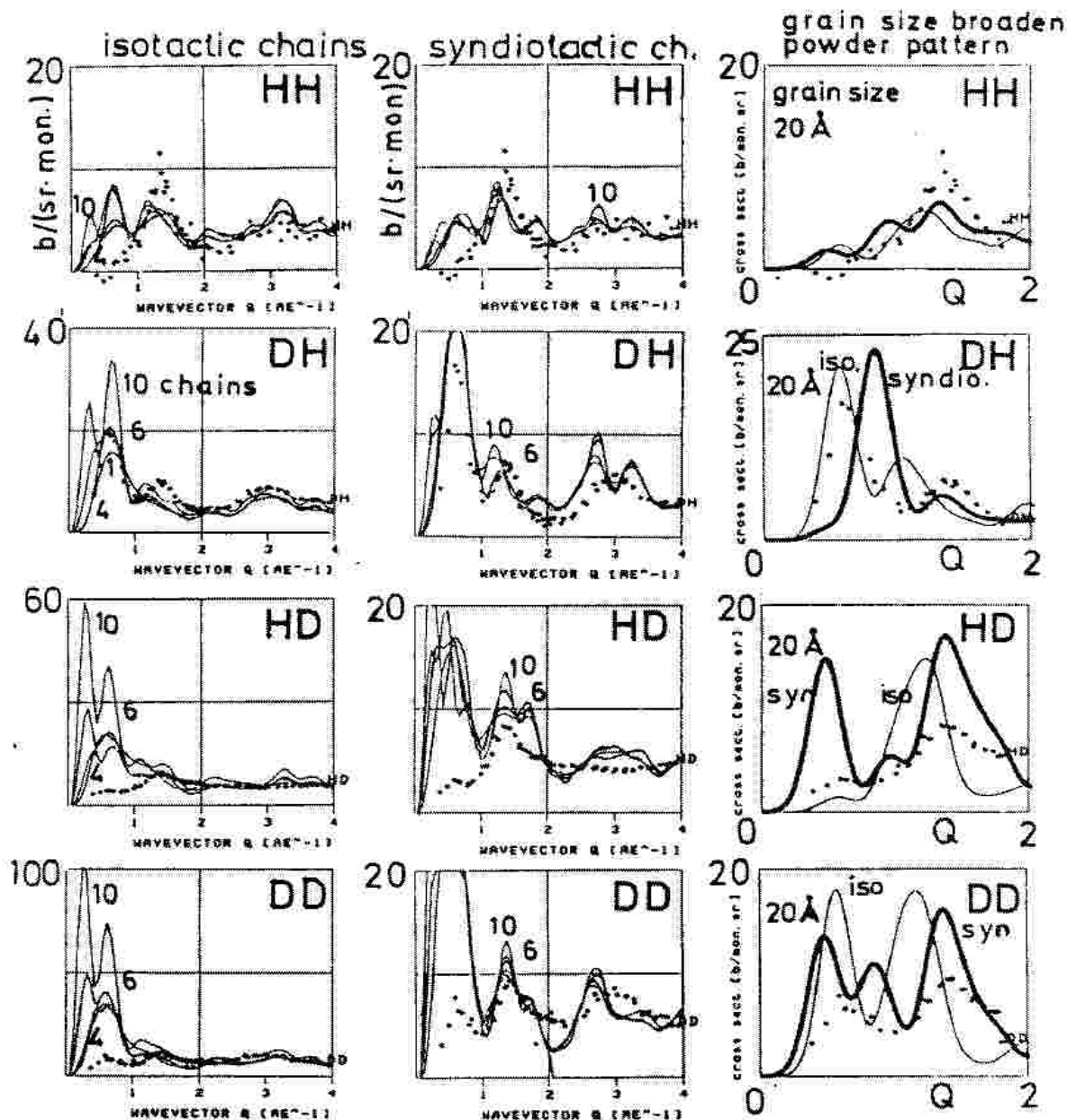


Figure 5.14: Measured points for the HH,DH,HD and DD samples (circles) compared with calculated diffuse scattering by spherical averaging over the respective chain assemblies on the same scales. The numbers on the solid lines give the number of parallel chain pieces of six isotactically ordered (first column) and syndiotactically ordered (second column) monomers in a bundle, spherically averaged as a whole. The third column gives the comparison of the measured points with the powder pattern of fig.4.9 for grain size of  $20 \text{ \AA}$  for isotactic and syndiotactic chains for the structure of Greis et al.

the same conformation for all atactic samples the resulting description is not the right description. We observed in fig.5.13 on page 76 that in the hexagonal dense packing the peak at  $0.6 \text{ \AA}^{-1}$  is very sensitive to small changes in this packing. This must give the possibility to find a common structure for all the samples.



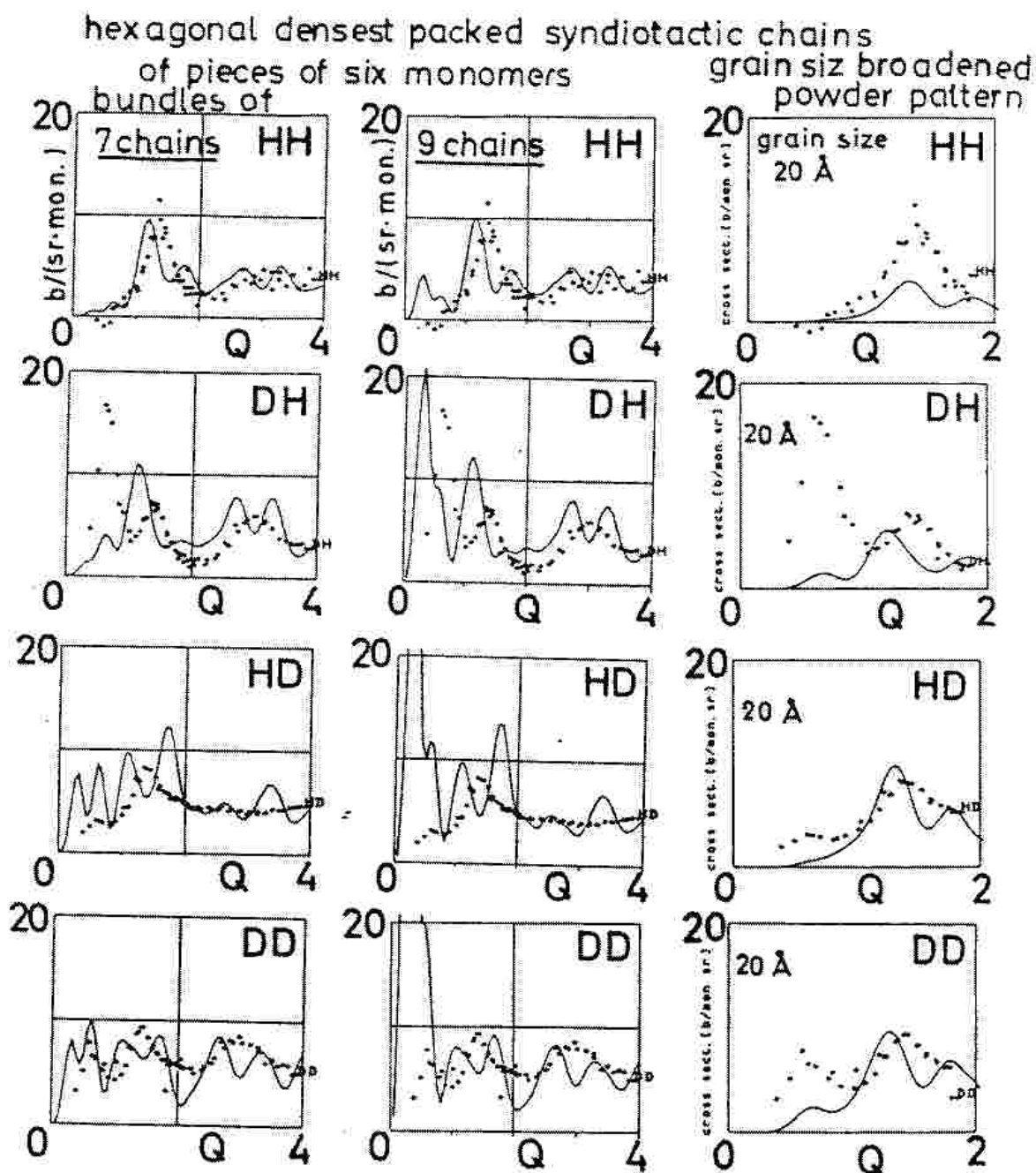


Figure 5.15: Comparison of the measured curves with the calculations of fig.5.13 for bundles of seven and nine hexagonally densely packed parallel syndiotactic chains of 6 monomers. The third column gives the comparison with the powder pattern for hexagonal dense packing with a grain size of 20 Å of fig.4.10.

In the HH, HD and DD material where the peaks result mainly from the rings, (as shown in fig.5.14 with the theoretically regularly arranged chains with the D-substituted rings as the most intense coherent scatterer), the calculation presented in figs. 5.11 on page 74 and 5.12 on page 75 gives high scattering in a Q region, where the measurement shows no scattering. One could think that those peaks totally disappear in our samples because in the atactic sample there



is no correlation between the benzene rings (which of course is the definition of atacticity). But also some correlation between the chains is visible which corresponds to a dense packing of six to ten parallel chains showing the beginning of the peaks as a small blip. But for these samples the third column of fig.5.15 on page 79 gives an interesting hint: there the denser packed hexagonal structure with 20 Å grain size gives nearly perfect agreement with the measurement and also in both samples HD and DD. This result also indicates that there the paracrystallinity with dense packing of chains gives the peaks found in the measurement. The first column of fig.5.14 on page 78 shows that the calculated scattering for the dense hexagonally packed chain bundles displays no peaks in the respective region in good agreement with the measurements.

For the HH sample the syndiotactic chain with two monomers gives again the whole diffuse background which shows up at the large  $Q$  values. The peak at about  $1.33 \text{ Å}^{-1}$  seems somewhat stronger than the calculated one for the isotactic structure but agrees perfectly for the hexagonally dense packed syndiotactic chains with seven to nine chains included in the bundle. In fig.4.11 on page 53 the scattering seems higher but there it must be corrected for double scattering of the incoherent flipped part. Correcting this gives also perfect agreement especially with the bundles of syndiotactic chains in the second column of fig.5.15. The crystalline powder pattern of figs.4.9 on page 51 and 4.10 on page 52 in the third column of fig. 5.14 and the second column of fig.5.15 with a grain size of 20 Å is also in good agreement as well as for the isotactic and for the syndiotactic structure for all arrangements: that of Greis et al.[10] with the looser packed structure and the dense packed structure of fig.4.10 on page 52. This shows only that for the HH sample these structures are not very different, one needs really the selective deuteration to find the right structure.

It is now clear from this calculation that the peak at  $3 \text{ Å}^{-1}$  results mainly from regular distances inside the monomer, and if this peak is shifted as seen in figs.4.11 on page 53, 5.14 on page 78 and 5.15 on page 79 it again may imply that the chains are deformed by the dense packing. These are the same in isotactic and syndiotactic structures and cause the peaks in the spectra (calculated for one and two monomers), to appear more or less pronounced in the measurements on all samples.

Since the scattering results only from six monomer chain lengths, in this diffuse scattering only the first peak from the chain periodicity, clearly visible in fig.5.9 on page 71 for high chain lengths appears in the measurements. The peak at higher  $Q$  does not appear clearly developed. This first peak indicates that the syndiotactic tacticity of the chains preferentially contributes to the peaks.

For the higher regions of  $Q$  ( $> 2 \text{ Å}^{-1}$ ) the scattering can be understood as diffuse scattering from a molecular gas of the monomers. This can even be used to renormalize the scattering from the DD sample for its hydrogen content, i.e. for its imperfect deuteration. In the HH and DH samples it became clear from fig.5.9 on page 71 that the random orientation of a single chain cannot give the details of the scattering pattern in the whole region. For complete agreement one has to assume at least a bundle of chains. For HD and DD we observed previously that they must have another chain packing what reiterates that it can only be understood by parallel chain segments - a short range order. A single chain shown in fig.5.9 on page 71 does not provide any details of the observed pattern. This shows that to understand many details of the observed measurement one really has to include parallelly arranged chains; i.e. one can not understand the scattering pattern with randomly oriented single chains only. Again, as observed previously, there are many features of the calculated intensities which correspond very well to the measured ones, but the correspondence is not entirely complete. But now the reasons for the deviation can be clearly understood. It would have been very difficult to find all these details from a pure treatment of the results of the scattering as resulting from a paracrystalline material. But all these details are parts of a paracrystalline description. Thus it becomes always clearer that for a complete description a paracrystalline description of the underlying polymer structure is needed.

Summing up we can say that there is good agreement between the measurements and calculations for the syndiotactic chain with hexagonal dense packing with about 6 Å distance between the chains. Only the DH sample shows very good agreement with the looser packed chains of the

structure of Greis et al.[10]. The peak at lower  $Q$  is a very prominent indicator of this order: this follows clearly from all our calculated curves. The DD and HD samples have no indication of such a strong peak with only a small blip (even if the calculated structures with the packing of three nearest neighbors should have this peak and provided they have the same coordination number of neighboring chains). This seems a very clear indication of the denser packing of chains for these samples. From this we conclude that we cannot use the generally used supposition, that the selectively deuterated polymer samples even made from the same beginning materials, have the same coordination (isostructural supposition). But in the chapter of the partial structure factors we need this supposition! However we had to seek a solution which would attribute the peak of the DH sample to the denser packing, because the behavior of the other samples can only be understood in terms of the densely packed chains. Moreover this corresponds also to the results for the isotactic sample IHH. It is not understandable why the packing should change by selective deuteration on the chain and not by selective deuteration on the rings. We found a way out of this problem - as we observed in fig.5.13 on page 76 - which is the sensitive dependence of the scattering in the  $Q$ -region of about  $0.6 \text{ \AA}^{-1}$  on the chain length. This also shows then very strongly that the chain length must be at least six monomers with bundles comprising at least seven chains. The effect seems to be less dependent on the number of monomers, if the bundles are larger and the chains longer. This indicates a higher degree of short range order or larger ordered regions.

The shifts of the peaks in fig.5.14 are not a serious problem. They are just caused by a change of the average distance, which is easily corrected in the case of the bundles. Therefore we did not require these to agree in our calculations. We prefer to have all curves obtained on the same assumptions so that they can be compared with one another.

We did not include the isotactic IHH sample in the above discussion, because it shows clearly crystalline order and allows a more exact analysis for all contributions. In the next section we analyse the data in the light of the results which can be obtained from a combination of powder pattern and random chain orientation, which yields an excellent analysis for the IHH sample and a good understanding of the features of the atactic samples.



## Chapter 6

# Real polymer and paracrystallinity. Description of the amorphous state.

### 6.1 a) Isotactic Material

We saw in figs. 4.7 on page 49 and 4.8 on page 50, that the scattering pattern from the isotactic sample has narrow peaks which can be understood as due to slightly disturbed hexagonal dense packed chains with a grain size of 100 Å in the a-b plane with a correlated chain length in c-direction of 80 Å. There two questions remained open, namely why the intensities do not fit and where the diffuse background comes from. In this section we deal with these, previously delayed, problems.

As indicated in chapter 4 on page 39 concerning the crystalline powder pattern, in the case of crystalline regions one should at least expect transition regions of lower order. Therefore as a first trial we will look for a combination of short range order and randomly oriented chains. It will become clear afterwards that randomly oriented chains are not necessarily needed in the samples. Regions possessing different paracrystalline order can account for all those transition regions in the isotactic and the atactic material. In the isotactic sample we find the grain size with 30 Å with higher disorder. This is the only transition region that is needed. The whole of an atactic sample corresponds loosely to the part of the transition regions in the isotactic sample with preserved short range order.

Looking at fig.4.8 on page 50 b, we see the measured peaks and their simulation by calculation. Their width is such, that the calculation shows no overlap of the peaks. Hence one can subtract the peaks from the measured pattern and fit them separately. The remaining measured pattern (with the peaks subtracted) represents a smooth curve, which still does not look like the curves due to randomly oriented chains of isotactic material comprising three monomers as stiff parts (fig.5.8 on page 70). The remaining maximum at  $1.33 \text{ Å}^{-1}$  (fitted by line 2 in fig.6.1) corresponds more to a somewhat ordered region like the one that is responsible for the peaks but with smaller grain size. Comparison with fig.4.10 on page 52, first column yields the grain size corresponding to 20 to 30 Å.

A guess of a percentage of the calculated cross sections of these different contributions is needed to simulate the measured curves: one gets 33% of hexagonal densely packed isotactic chains with 100 Å grain size across the chains and 80 Å along the chains, 50% of hexagonally dense packing with 30 Å grain size and 33% of scattering arising from two randomly oriented monomers. This gives nearly the complete picture as evident from fig.6.1 on page 84 where the respective curves are presented. We recall here that we have subtracted the contribution of the double flip scattering (for an estimate see fig.3.3 on page 34). If one would not subtract it, then 100% of amorphous single chain scattering would not be sufficient to understand even the unstructured background scattering, which would give serious problems at low Q. One has also to remember, that this corrected double

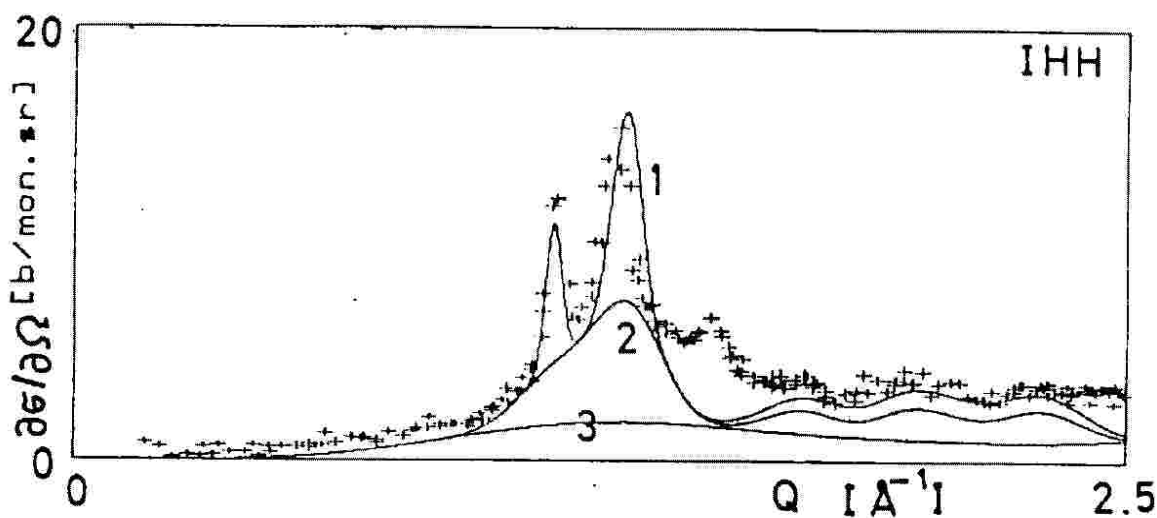


Figure 6.1: Plot of the different calculated contributions which could describe the observed scattering from the isotactic sample marked by crosses. Here 33% with grain size 200 Å, 50 % with grain size 30 Å, 33% with single chains of two monomers randomly oriented and distributed. The lines in the figure display these different parts: 1=part with 200 Å, 2=part with 30 Å, 3=diffuse part of two monomers.

flip scattering is lost in the incoherent part, which is used as standard, so that the normalization has to be corrected also for this loss. This is all accounted for in fig.6.1 on page 84.

The remaining differences are the hole at the third peak and the fact that the whole scattering needed to describe the measurements is 16% too high. This could perhaps also be clarified if one would invest more time. To indicate how much time already at this stage was spend, we remark that the calculation of one curve with 128 points for the 90 monomer assembly took 10 hours CPU time on a VAX8650. This shows that to arrive at the present result is not trivial at all considering the many curves needed to understand this behavior.

But there is yet another reason why better agreement was not attempted. We were forced to broaden the peaks at higher  $Q$  because the calculated curves of fig.4.8 on page 50 have several well pronounced peaks, but the measurements do not. We broadened those peaks assuming a grain size of 20 Å. They appear as a flat intensity in fig. 6.1 on page 84. But this is only artificial. If grain size is the reason for peak broadening, all peaks would then have the same width when plotted over  $Q$ . This corresponds to a convolution with the same shape function. Only an anisotropy in the grains can give different widths but not of a type which systematically increases with  $Q$ . The measurement shows that not only the second peak is broader but that with increasing  $Q$  the width of the peaks increases and they finally disappear. This points towards another cause: the broadening is caused by disorder. Such a behavior is described by the paracrystallinity. But we do not observe a clear and clean-cut paracrystalline behavior, because the two differently correlated regions which we described by different grain sizes would be difficult to be found if one would have resorted to the formalism of paracrystallinity already in the beginning. Perhaps the diffuse background scattering of curve 3 in fig.6.1 resulting from two randomly oriented monomers can also be understood as due to the paracrystallinity so that the discrepancy of the 16% too high percentage could disappear in this way. The features of two "grain sizes" disturb a simple paracrystalline evaluation because they assume a mixture of two preferential distributions of chain distances, which are superimposed on each other and have to be powder averaged in this work. In addition the lack of low  $Q$  peaks and the fact that the peaks at higher  $Q$  are more densely spaced is not a simple behavior and it

is supposed, that one has already sorted out all these by applying usual crystallographic methods. The lack of low Q-peaks results from a smaller diffracting unit and the peaks at higher Q more densely spaced results from two dimensional paracrystallinity.

This has necessitated the way we have taken to understand as much as possible the two extremes : crystalline order and total disorder in order to prepare the paracrystalline approach. Looking back, the whole evaluation guided us directly to the paracrystallinity concept beginning from perfect crystalline order and subsequently relaxing this order or beginning from single monomers and constructing always more ordered chains. The approach persued became clear in figs.4.7 and 4.8 on page 50. There we had to include disorder in the chain positions to obtain all of observed peaks. However it was still done in a regular manner i.e. in each crystal cell the disorder was the same, and it had no influence on the peak width.

The further interpretation of the results as due to paracrystallinity will unveil further properties of the short range order, namely the width of the probability distribution of the distances between nearest neighbors and the interaction radius and the measure of disorder  $\Delta/\langle a \rangle$  (description see below) for all samples studied. This allows us to determine whether the above described grain size is the limiting factor for the broadening of the reflections or interaction radius and disorder.

In a paracrystal we have a mean distance  $\langle a \rangle$  between nearest neighbors and a bell shaped probability distribution function  $H_1(x)$  giving the probability of finding any particular distance between neighbors with  $\int H_1(x)dx = 1$  and  $\langle a \rangle = \int x H_1(x)dx$  (see fig.6.4 For example one can get  $H_1(x + \langle a \rangle) = \frac{1}{\Delta\sqrt{2\pi}} \exp(-\frac{1}{2} \frac{x^2}{\Delta^2})$  a Gaussian with the width  $\Delta$  governed by the degree of order in the object as a whole. As this is valid for each neighbor one gets from this the probability distribution function of the second neighbor  $H_2(x)$  by the convolution  $\int H_1(x')H_1(x-x')dx' = H_2(x) = H_1 \otimes H_1$  and this can be repeated yielding  $H_m(x) = H_1 \otimes H_1 \otimes H_1 \otimes \dots H_1$ . The average distance of the mth chain is  $\int x H_m(x)dx = m\langle a \rangle$ . Using these functions instead of the usual sharp  $\delta$ -functions in the case of long range order one can now write the distribution function of the whole crystal. This represents a probability distribution with increasing width at each next point with an average distance  $\langle a \rangle$  between each two neighboring points or chains, representing a periodic distribution with separations  $\langle a \rangle$ . If this is extended to two dimensions then one has correspondingly also an average distance  $\langle b \rangle$  in this other direction. The paracrystalline description allows even to have directions where the distances are well-defined as for example the chain periodicities. In addition it allows for the treatment of shifts and bends, rotations and other irregularities of the chain molecules, but to get this type of information measurements should be made on preferentially oriented chains as found, for example, in fibers. The Fourier transform of such a distribution function is also a periodic function with increasing width of the peaks corresponding to the Fourier transform of  $H_m(x)$  (see fig.6.3). For the above assumed Gaussian one gets

$$\begin{aligned} |F(Q)| &= e^{-2\pi^2 Q^2 \Delta^2} \\ |F_m(Q)| &= |F|^m = e^{-2\pi^2 Q^2 \Delta^2 m} \end{aligned} \quad (6.1)$$

i.e. the width increases in the m-th order with  $\sqrt{m}$ :

$$\Delta_m = \Delta\sqrt{m}.$$

The peaks disappear if  $H_m$  becomes so broad that it attains half its peak value at half of the distance between two peaks i.e. at  $x = \langle a \rangle/2$ . The number of visible peaks M is reached if  $e^{-y} = \frac{1}{2}$  which one gets from

$$y \approx 0.7 = \frac{1}{2} \left( \frac{\langle a \rangle}{2} \right)^2 \frac{1}{(M\Delta^2)} \quad (6.2)$$

and then

$$M = \frac{1}{(2.5\Delta/\langle a \rangle)^2} \quad (6.3)$$

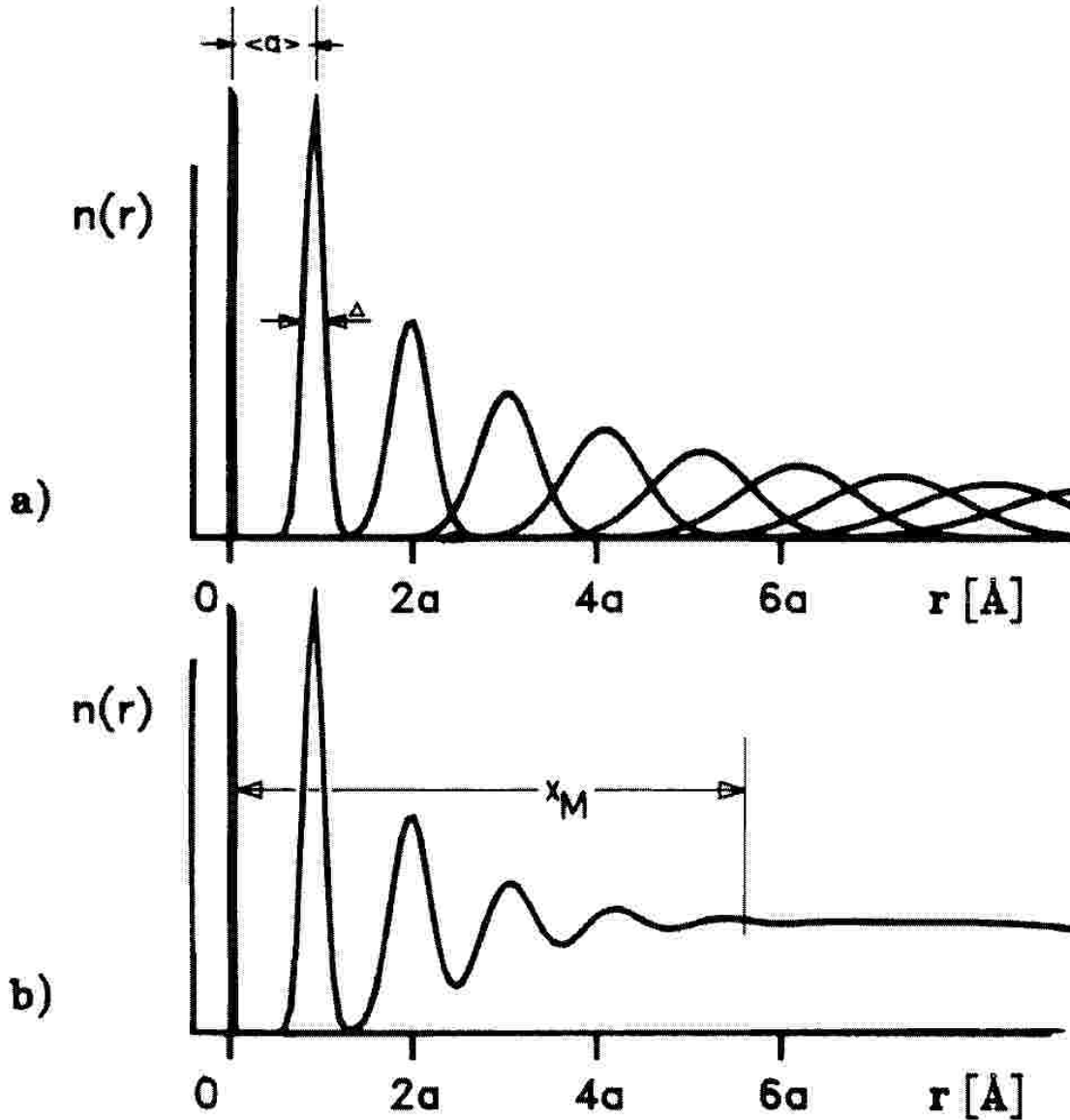


Figure 6.2: Distance distribution of nearest neighbors, next nearest neighbors etc. in a paracrystal. Width  $\Delta$ , average distance  $\langle a \rangle$  between chains and interaction region  $x_M$

and the interaction radius  $x_M$  is given by

$$x_M = M \cdot \langle a \rangle. \quad (6.4)$$

The relation between the peak width  $\Delta Q$  and the width of the distribution of the distances in object space is given by an equation

$$\Delta Q = \frac{2\pi}{\langle a \rangle} \pi^2 h^2 \left( \frac{\Delta}{\langle a \rangle} \right)^2 \quad (6.5)$$

with  $h$ =order of the peak. The derivation of this relation can be found in reference [20].

Interpreting the measurements of the isotactic polystyrene IHH as resulting from paracrystalline order we know the width  $\Delta Q$  of the first peak at  $Q=0.6 \text{ \AA}^{-1}$  and the average distance  $\langle a \rangle$  for this



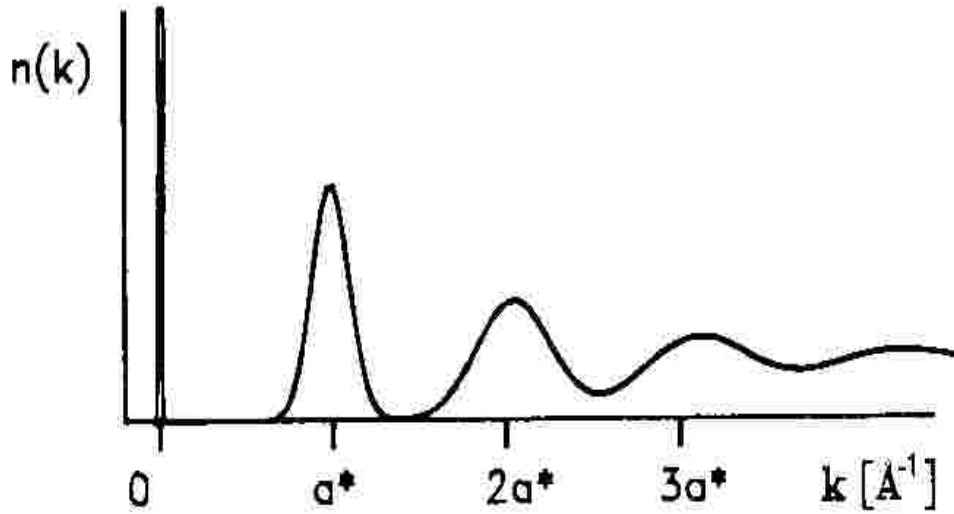


Figure 6.3: Fouriertransform of the distance distribution of fig.6.2

peak i.e.  $\langle a \rangle = 5.5 \text{ \AA}$  and  $\Delta Q = 0.06 \text{ \AA}^{-1}$ . Using the above relations 6.2-6.5 we obtain a width of the distribution of  $\Delta = 0.4 \text{ \AA}$  and an interaction radius  $x_M$  of  $166 \text{ \AA}$ . This is slightly larger than the grain size of  $100 \text{ \AA}$  found previously, which implies that in this case both grain size and paracrystallinity may contribute simultaneously to the peak width. This also clarifies why the peaks become broader and disappear with increasing  $Q$ . The measure of disorder is  $\Delta/\langle a \rangle = 0.4/5.5 = 0.073$  i.e. 7% disorder in this sample. This describes a part of the sample which shows the narrow peaks. Since we know that the second peak originates from the  $c$ -direction (along the chains axes) we could interpret the broadening of the peaks as caused by bending of the chains. However this peak has a mixture of Miller indices and the powder averaging and shifts along the chains have also a broadening effect on it. Therefore we did not try to evaluate this broadening separately.

The remaining broad peak at  $1.3 \text{ \AA}^{-1}$  with  $\Delta Q = 0.46 \text{ \AA}^{-1}$  corresponds to the average distance  $\langle a \rangle = 4.83 \text{ \AA}$ , the width  $\Delta = 0.91 \text{ \AA}$  and an interaction radius  $x_M$  of  $21.6 \text{ \AA}$ . The measure of disorder in this region is given by the ratio  $0.91/4.83 = 0.188$  i.e. 19%. Here we found the grain size of  $30 \text{ \AA}$ : the disorder is the limiting factor for the peak broadening but we still have a well defined short range order which gives a well defined peak.

The tail of the scattering at higher  $Q$  looks exactly as the smeared part of the broadened peaks of a paracrystal, so that the inclusion of amorphous scattering from single chains seems unnecessary and the abundant percentage of 16% can be expected to disappear. In order to test this hypothesis, it would be necessary to perform a model calculation of the paracrystalline description in order to compare the final intensities. This, however, goes beyond the scope of this paper.

In this way we have arrived at an exact description of the percentages and the degree of disorder of the different components in isotactic polystyrene - this is precisely what one calls a short range order. In the first part of this paper the peak width was fitted well with the determined grain size. What remained was the peak height which had to be understood by including the percentage of order. This was necessary, since the height of the calculated peaks was nearly three times too high. From this one could conclude (fig.6.1) that there is only 33% of grains comprising hexagonal densely packed chains with  $100 \text{ \AA}$  correlation length in the  $a$ - $b$  plane and  $80 \text{ \AA}$  correlation length in the  $c$ -direction. After subtraction of this scattering there remained a pattern which corresponds to the width  $30 \text{ \AA}$  with the hexagonal dense structure of figs.4.10 and 4.6 (see the "tabular description



of the grain size dependence”, figs.4.9 and 4.10). The integral over the part corresponding to the peak height of the broad peak imposed on the flat part gave 50% of intensity. Thus the second component consists of 50% of hexagonal densely packed chains with 30 Å grain size, where we cannot distinguish between a-b and c. Subsequently the third component is a diffuse part which we treated in a first attempt, as resulting from randomly oriented chains belonging to a sort of transition regions between the grains. This took another 33% of the scattering of randomly oriented chains comprising two monomers. The absolute units in our measurements and calculations allow a very simple procedure to find these percentages and put weight on these results. The percentages are the factors for the respective contributions calculated before.

The description in terms of paracrystallinity does not require such transition regions between grains and also yields a diffuse scattering by broadening of peaks outside the interaction region. This would redistribute the remaining 16% to the two other parts correspondingly giving finally 40% ordered and 60% transition regions. We got the measure of order in the two regions with a Gaussian width of 0.4 Å for the 5.5 Å average distance of the hexagonal densely packed chains giving the narrow peaks, and a width of 0.91 Å for the chain distribution giving the broad peak. The first corresponded to an average distance of 5.5 Å with a disorder of 7% and an interaction radius of 166 Å, the latter to an average distance of 4.83 Å with a disorder of 19% and an interaction radius of 21 Å. The grain sizes are of the same order of magnitude hence both types contribute to the result.

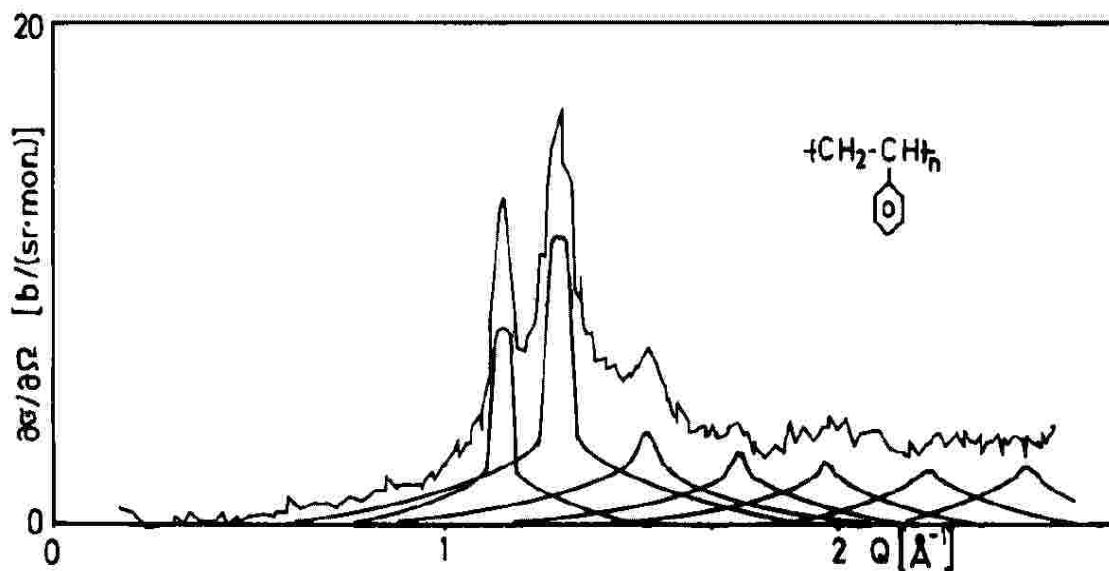


Figure 6.4: Evaluation with paracrystallinity

## 6.2 b) atactic material

In a follow-up paper [21] we discussed the effect of sulphonation on the structure of the isotactic polystyrene. There we demonstrate, that already a small percentage of 1.2 mol % of sulphonated groups destroys the order peaks and only the broader peak remains with the interaction radius of 21 Å. From this we can conclude that each kind of disorder along the chains is able to destroy the perfect conformation that gives narrow peaks: the atacticity is such a disorder. It is much weaker than the presence of the bulky sulphonation group of about 6 Å diameter. But already the conformation of hexagonal dense packing is disturbed by atacticity so that the average distances

between chains show a broader distribution of 10% to 30% of the distance (in the isotactic sample it was 7%).

As clear from the results obtained for the isotactic sample, also the data analysed of the atactic material cannot be understood in terms of randomly oriented chains alone. There also must be a component from regions where one has a grain size of about 20 Å with chains which are at the first glance packed like in fig.4.3a) but with a certain distribution of distances. This amounts to the isotactic structure of Greis et al.[10] but without the inversion symmetry and without the strong symmetry of the positions of the chains fulfilled also for the chains themselves. This seems to be implied in fig.4.11 for the DH sample. There one even does not need any contribution from random disorder of the chains, which we also found for the IHH sample. This is also valid for the DD sample provided its scattering is renormalized to the true proton content.

The scattering from the HH, HD and the DD samples is best described as resulting from another packing of the chains, namely the hexagonal dense packing of syndiotactic chain pieces with a preferential average distance of  $< 6$  Å, which we also found for the IHH sample but for isotactic chains. This fact, namely that DH has another packing than HH, HD and DD, does not make sense if one takes seriously the principle of isostructurality of selectively deuterated samples. There is a way to get rid of this other structure for the DH sample by the observed sensitivity of the scattering in the Q region of about  $0.6 \text{ Å}^{-1}$  to the chain length and the number of chains in the bundles. This then yields a peak of the observed height and width also with this dense packing. Hence we could find the same structure for all atactic samples, namely hexagonal dense packing of fig.5.10b.

Here we can search again how to relate these observations to the paracrystalline description. From the observed peak widths and the position of the different peaks in the different samples we can get the average distances  $\langle a \rangle$ , the widths  $\Delta$  of the distribution of these distances and the radius of interaction  $x_M$ . The DH sample shows a narrow peak at  $Q=0.60 \text{ Å}^{-1}$  with a width  $\Delta Q$  of  $0.34 \text{ Å}^{-1}$ . This corresponds to a average distance of  $\langle a \rangle=10.5 \text{ Å}$  which shows a width  $\Delta$  of the distribution of  $2.52 \text{ Å}$  corresponding to a disorder of 24% and gives an interaction radius  $x_M$  of  $29.1 \text{ Å}$ . This is larger than the grain size found therefore in this sample the grain size may be the limiting factor even if the degree of disorder is relatively high.

The HH sample has a peak at  $1.33 \text{ Å}^{-1}$  with a width of  $0.46 \text{ Å}^{-1}$ . This corresponds to a width of  $\Delta=1.29 \text{ Å}$  of the distribution function for the average distance of  $\langle a \rangle=4.71 \text{ Å}$ . The resulting interaction radius is  $x_M=10 \text{ Å}$ : disorder is responsible for the line broadening.

The HD sample shows a peak at  $3 \text{ Å}^{-1}$  with a width of  $0.60 \text{ Å}^{-1}$ . This corresponds to  $\langle a \rangle=2.09 \text{ Å}$  and  $\Delta=0.297 \text{ Å}$  giving a disorder of 14% and an interaction radius of  $16.55 \text{ Å}$ . The disorder is also primarily responsible for the line broadening. The size of  $\langle a \rangle$  seems to indicate that the peak is mostly coming from the periodicity along the chains, which are bent and rotated so that 14% disorder results. This corresponds to the use of the selective deuteration to distinguish different peaks with their preferred crystallographic directions using the powder pattern indices of fig.4.4 and the peak broadening of figs.4.9 and 4.10 to identify the different peaks.

Our observed results with the perdeuterated DD sample show, that our interpretation relies heavily on the exact hydrogen content. If the real differs from the assumed one, our results are wrong. To be sure about the hydrogen content, we intended to make a mass spectroscopy analysis of all the samples in order to fully rely on our interpretation. Since the diffuse gas scattering gives already a good test of it we finally skipped this test.

### 6.3 c) different definitions of amorphicity applied to our samples

Now we can draw some conclusions on the concept of amorphicity.

1. **1) One can assume that amorphous solids and liquids have structures characterised by an almost complete lack of periodicity and a tendency to "order" only in the sense that the atoms are fairly tightly packed together and show a statistical preference for a particular distance.** The result is a scattering curve showing nothing more than one or two broad maxima. This is exactly what we observe for the atactic chain molecules studied. This concept still admits short range order between chains. In a paracrystal with high disorder the "Bragg reflections" are like reflections of a mirror with a rough surface. The measure of disorder gives just a measure of this roughness of the "lattice planes". This roughness can broaden the reflected beam or can make it totally diffuse with no remaining definition of a plane. The latter is Hosemann's approach in his book [20] where the amorphous scattering is structureless.
2. **2) A second description assumes only randomly oriented chains, as we calculated in chapter 5 on page 57.** There we obtained a quantitative description for all our selectively deuterated polymers. Assuming a complete disorder one can already interpret the scattering at the higher angles, where the scattering comes from very small distances  $r_{ik}$  between atoms and planes, would they exist. It is clear that in the case of very small grains and paracrystalline order one can only obtain the information about intramolecular distances and this only about nearest neighbor atoms. These are the C-C distances and the C-H distances of 1.34 Å or 1.54 Å. Therefore in the region of  $Q > 2 \text{ Å}^{-1}$  one cannot get any information about order of the crystallites out of the amorphous or crystalline patterns. So the correspondance of the peak at  $Q=3 \text{ Å}^{-1}$  for one randomly oriented monomer (fig. 5.8) does not contain information about order of the crystallites, only about the bond lengths.
3. **3) A third definition of amorphicity is often applied in the analysis of the scattering pattern as follows: One takes the integral over the non peak-structured part and the integral over the peak-structured part as the measure of both parts, which one defines as the crystalline and amorphous ones.** But we got both parts much better for the IHH sample above in the stepwise procedure described in section 6.1 on page 83. This example shows that this definition of amorphicity loses essential information as there is still a broad peak coming from short range ordered regions of 20 Å, which this definition would include in the amorphous part.

## 6.4 CONCLUSIONS

The analysis of the scattering patterns from the polymer polystyrene in different selectively deuterated variants and in an isotactic variant shows that there is an order in the isotactic variant. This is not the crystal structure determined by Greis et al. [10] but a hexagonal dense packing of chains orthogonal to chain axes (directions), which corresponds just to paracrystallinity. The chains approach to less than 5.5 Å distance so that they overlap each other when viewed from the top of such a cell, which seems possible by avoiding the inversion symmetry of parallel chains, otherwise postulated in the structure of Greis. The correlation length is then 100 Å across the chains and 80 Å along the chains. The chains are also correlated along the chains by the helical grooves of the isotactic chains, giving a series of peaks in the scattering pattern with the third Miller index different from zero. The methods described above allow for a separation of three different portions, namely 33% densely packed chains with grain size 100 Å, 50% with a grain size of 30 Å and a part with random oriented chains comprising pieces of two monomers. The paracrystalline picture allows to avoid any part coming from randomly oriented chains and gives correspondingly 40% ordered domains with grain size 100 Å and 60% ordered domains with grain size 30 Å. The crystallographic method would show that the results postulate an affine deformation of the chains by elongation of

the isotactic unit from 6.65 Å to 9.65 Å and a compression of the chain diameter by a factor of  $\sqrt{3}/1.99$ .

The paracrystalline description shows then the degree of disorder of 7% in the 40% of more ordered regions of 100 Å width and 80 Å long chains with 0.4 Å width of the distance distribution with an average value of 5.5 Å and another 60% to 66% regions with higher disorder. This contributes to the unstructured amorphous scattering yielding the broadening of the peaks of higher order.

The above findings can seemingly be adapted to the DH sample by admitting only three nearest neighbor chains around one chain and so creating enough space for the atactic disorder. This would occur by selecting the conformation of the chains found in the crystal structure of Greis et al.[\[10\]](#) also for the isotactic material, but simultaneously one finds that the chains are nearer together than it corresponds to this crystal structure. This can be inferred from a shift of peaks in [fig.4.11](#). By this approach of the chains the chains again appear deformed, expanded along the chain and compressed across the chains. The results of calculations assuming an amorphous structure, with only chain pieces of a certain length and therewith only correlation along the chains do not agree with the measurements. It is clear that the measurement is better described with a grain size broadening or with at least six to ten parallel packed chains with some disorder. This could also be determined with the corresponding approximations of [chapter 5](#) on [page 57](#) and gave the same results. The resulting grains sizes of the atactic materials are 20 Å. We have also obtained the degree of disorder in the different samples and the interaction radius for a paracrystalline description of all samples.

This paper also describes a new technique used to obtain these results, namely polarization analysis with a multidetector. New methods to interpret the results are extensively described: crystallographic methods of structure plots, a procedure corresponding to a adaptation of the Rietveld refinement to chain molecules and the behavior of scattering in the transition from ordered to disordered state, the former being proportional to  $N^2$  the latter to  $N$ . It is also demonstrated how the paracrystalline picture can be applied to the understanding of powder patterns of isotactic and atactic polystyrene.

#### ACKNOWLEDGEMENT

We would like to thank Dr.Karl Hahn of the BASF, Anderson, USA for critical reading of the manuscript and making valuable suggestions.



# Bibliography

- [1] P.Gerlach, O.Schärpf, W.Prandl and B.Dorner, *Journal de Physique, Colloque C7*, 43, C7-151,(**1982**)
- [2] O.Schärpf,O., *Proceeding Series:Neutron scattering in the ninetieth*, p.85. Vienna: Int.Atomic Energy Agency **1985**
- [3] B.Gabrys, J.S.Higgins and O.Schärpf, *J.Chem.Soc.Far.Trans.I* 82, 1929 (**1986**)
- [4] P.J.Flory, *Statistical mechanics of chain molecules*, Interscience Publishers, New York **1969**
- [5] B.Gabrys, P.E.Tomlins, in:*Encyclopedia of Polymer Science and Engeneering* (eds. Mark-Bikales-Overberger-Menges) vol.15,p.25 (**1989**); M.B.Huglin, ed., *Light Scattering from polymer solutions*, Academic press, London **1972**
- [6] A.Eisenberg, *Macromolecules*, 3, 147 (**1970**) K.M.Mauritz, *JMS-Rev. Macromol.chem.phys.:* C28, 65-98 (**1988**)
- [7] A.Eisenberg and M.Pineri, Eds., *Structure and properties of ionomers*, NATO ASI series C198, D.Reidel, Dordrecht **1987**
- [8] G.Natta, *J.Polymer Sci.* 16, 143 (**1955**).
- [9] O.Schärpf, *Physica* B156&157, 631 (**1989**) O.Schärpf,*Physica* B156&157, 639 (**1989**)
- [10] O.Greis, T.Asano, J.Xu and J.Petermann, *Z.Kristallographie* 182, 58 (**1988**)
- [11] C.W.Bunn, E.R.Howells, *J.Polym.Sci.* 18, 307 (**1955**)
- [12] *International Tables for X-Ray Crystallography*, Th.Hahn (editor), Birmingham I. **1952,1962,1988**
- [13] Reinhard X. Fischer, STRUPLO (1984), Mineralogisches Institut der Universität, Am Hubland, D-8700 Würzburg, FRG
- [14] K.Yvon, W.Jeitschko, E.Parthe, *J.Appl.Cryst.* 10, 73 (**1977**)
- [15] A.Guinier, *X-Ray Diffraction*, W.H.Freeman, San Francisco **1963**
- [16] M.A.Krivoglaз, *Theory of X-ray and thermal-neutron scattering by real crystals*, Plenum press, New York **1969** p.129
- [17] H.M.Rietveld, *J.Appl.Cryst.* 2, 65 (**1969**)
- [18] B.K. Vainshtein, *Diffraction of X-rays by chain molecules*, Elsevier, Amsterdam-London-New York **1966**
- [19] Michele Vacatello, Do Y.Yoon, and Paul J.Flory, *Macromolecules* 23, 1993 (**1990**)

- [20] R.Hosemann, S.N.Bagchi, *Direct analysis of diffraction by matter*, North-Holland Publishing Company, Amsterdam **1962**.
- [21] O.Schärpf,B.Gabrys,D.Peiffer: Model Ionomers studied with spin-polarized neutrons using spin-polarization analysis. Chapter 4 in: Shulamith Schlick (edt.), *Ionomers, Characterization, Theory and Applications*. CRC Press New York **1995**.



## Chapter 7

# Application of methods used for partial structure factor determination.

### 7.1 The fundamental equations

The scattering of a polymer where we know the atomic coordinates of all atoms can generally be described by the scattering amplitude given by a sum of the phase related scattering lengths of all these atoms:

$$F(Q) = \sum_k b_k e^{-i\vec{Q} \cdot \vec{r}_k} \quad (7.1)$$

The scattered intensity is then generally given by the correlation function

$$I(Q) = \sum_{j,k} b_j b_k^* e^{i\vec{Q} \cdot \vec{r}_j} e^{-i\vec{Q} \cdot \vec{r}_k} \quad (7.2)$$

a relation which we already used in eq.5.8 on page 65. There we assumed the scattering units as the single monomers or a regular arrangement of monomers, which we described by a structure amplitude  $F_{M_j}$ , which was the phase corrected sum of the scattering lengths of the atoms in the monomer. Each of this parts was then spherically averaged .

In this chapter we take another approach. As we know from the first chapter, one has to expect a certain correlation between the monomers in a chain within the distance of the Kuhnlength (1.3.1.2 on page 6). With this assumption the chain behaves then like a freely jointed chain without correlations between the units with the Kuhn-bond-length. To take this into account we have to describe the polymer by units which have correlations and which we describe by correlation functions, and the rest of the polymer which consists of similar units but which have no correlations with each other. The scattered intensity can then be described by a spherical average of these units which are equally distributed with no preferred orientation within the scattering sample. As we have rings and chains of different deuteration, we can try to assume a description of the correlation within the Kuhnlength as a correlation between rings and rings, chains and chains, and a mixt term with correlation between rings and chains. We can expect to obtain the information of a coordination number of rings and chains.

The intensity is given by

$$I(Q) = \left| \sum_{\nu_{ring}^H} b_H e^{i\vec{Q} \cdot \vec{r}_{\nu_{ring}^H}} + \sum_{\nu_{ring}^C} b_C e^{i\vec{Q} \cdot \vec{r}_{\nu_{ring}^C}} + \sum_{\nu_{chain}^H} b_H e^{i\vec{Q} \cdot \vec{r}_{\nu_{chain}^H}} + \sum_{\nu_{chain}^C} b_C e^{i\vec{Q} \cdot \vec{r}_{\nu_{chain}^C}} \right|^2$$

$$= \overline{\left| \sum_j^{n'} (F_{ring}^j + F_{chain}^j) \right|^2} \quad (7.3)$$

$$= \sum_{j,k}^{n'} (F_{ring}^j + F_{chain}^j) (F_{ring}^k + F_{chain}^k)^* \quad (7.4)$$

$$= \begin{cases} \overline{n'^2 (F_{ring}^j + F_{chain}^j) (F_{ring}^j + F_{chain}^j)^*} = n'^2 \overline{|F_{ring}^j + F_{chain}^j|^2} & j=k \\ \overline{\sum_{j,k}^{n'} (F_{ring}^j + F_{chain}^j) (F_{ring}^k + F_{chain}^k)^*} = 0 & j \neq k \end{cases} \quad (7.5)$$

with overline indicating spherical average and

$$F_{ring} = \left( \sum_{\nu_{ring}^H}^{l'} b_H e^{i\vec{Q} \cdot \vec{r}_{\nu_{ring}^H}} + \sum_{\nu_{ring}^C} b_C e^{i\vec{Q} \cdot \vec{r}_{\nu_{ring}^C}} \right) \quad (7.6)$$

$$F_{chain} = \left( \sum_{\nu_{chain}^H}^{l'} b_H e^{i\vec{Q} \cdot \vec{r}_{\nu_{chain}^H}} + \sum_{\nu_{chain}^C} b_C e^{i\vec{Q} \cdot \vec{r}_{\nu_{chain}^C}} \right) \quad (7.7)$$

where  $l'$  indicates the range of correlation corresponding to the Kuhnlength.

As we do not know the coordinates of the correlated atoms within the Kuhnlength we try to determine this correlation by replacing

$$\overline{|F_{ring} + F_{chain}|^2} = \langle b_r^2 \rangle S_{rr}(Q) + \langle b_c^2 \rangle S_{cc} + 2\sqrt{\langle b_r^2 \rangle \langle b_c^2 \rangle} S_{rc} \quad (7.8)$$

In this way we arrive at a description of the scattering by partial structure factors, which here quite naturally is described by the averages  $\sqrt{\langle b_i^2 \rangle}$ . An overview of these methods can be found in [1] [2]. There the method is applied for alloys. The derivation of Faber and Ziman [3] in this case yields as factors the averages  $\langle \sum_i b_i \rangle$ . In our case we investigate something much more complicated and find other factors for this case. Taking the ring in the polystyrene monomer as one unit and the backbone atoms of the monomer as the other, we can try to determine structure factors of the rings alone, of the backbone parts alone and of a cross term of rings and backbones. We measure  $S^{HH}(Q)$ ,  $S^{DD}(Q)$ ,  $S^{HD}(Q)$  and  $S^{DH}(Q)$  for 80 different  $Q$  values. For each  $Q$  we have then the following system of equations

$$S^{DD} = \langle b_c^D \rangle^2 S_{cc} + 2\langle b_r^D \rangle \langle b_c^D \rangle S_{rc} + \langle b_r^D \rangle^2 S_{rr} \quad (7.9)$$

$$S^{DH} = \langle b_c^D \rangle^2 S_{cc} + 2\langle b_r^H \rangle \langle b_c^D \rangle S_{rc} + \langle b_r^H \rangle^2 S_{rr} \quad (7.10)$$

$$S^{HD} = \langle b_c^H \rangle^2 S_{cc} + 2\langle b_r^D \rangle \langle b_c^H \rangle S_{rc} + \langle b_r^D \rangle^2 S_{rr} \quad (7.11)$$

$$S^{HH} = \langle b_c^H \rangle^2 S_{cc} + 2\langle b_r^H \rangle \langle b_c^H \rangle S_{rc} + \langle b_r^H \rangle^2 S_{rr} \quad (7.12)$$

Three of these equations give always a solution for each  $Q$ . This gives then partial functions  $S_{rr}$ ,  $S_{cc}$  and  $S_{cr}$ . From these three partials these three measured curves then follow strictly. The fourth structure factor not used to determine the partial structure factors should then follow with the same partials. This is exactly the intention to determine the partial structure factors. But unfortunately this is not at all the case if one uses the averages  $\langle b_i \rangle$  as in the derivation of Faber Ziman. If one uses the method described in [1] p.99, by a fit of parameters of an overdetermined system, the structure factor  $S^{HH}$  gets so much weight that this determines the form of all the partial structure factors. One could think that the ring and the chain part of the monomer are not point scatterers but they are themselves scatterers with a molecular form factor, as determined in

Table 7.1: Values used for the determination of the partials

C	D			H	
$\sigma_{coh}^C = 5.554 \text{ b}$ $b_{coh}^C = 0.66484 \cdot 10^{-12} \text{ cm}$	$\sigma_{coh}^D = 5.697 \text{ b}$ $b_{coh}^D = 0.6674 \cdot 10^{-12} \text{ cm}$			$\sigma_{coh}^H = 1.7599 \text{ b}$ $b_{coh}^H = -0.37423 \cdot 10^{-12} \text{ cm}$	
	HH $10^{-12} \text{ cm}$	DD $10^{-12} \text{ cm}$	DH $10^{-12} \text{ cm}$	HD $10^{-12} \text{ cm}$	f.u
$\langle \sum_i b_i \rangle_{ring}$	2.11789	-	2.11789	-	6C+5H
	-	7.32604	-	7.32604	6C+5D
$\langle \sum_i b_i \rangle_{chain}$	0.20699	-	-	0.20699	2C+3H
	-	3.33188	3.33188	-	2C+3D
$\langle b_{monomer} \rangle$	2.32488	10.65792	5.44366	7.53303	
$\langle \sqrt{\sum b_i^2} \rangle_{ring}$	1.8309	2.208888	1.8309	2.208888	
$\langle \sqrt{\sum b_i^2} \rangle_{chain}$	1.142002	1.4900647	1.4900647	1.142002	
$\langle b^2 \rangle - \langle b \rangle^2$	-0.7486	-106.492	-24.127	-50.563	$10^{-24} \text{ cm}^2$
$\langle b^2 \rangle$	4.6565	7.09948	5.5726	6.1834	$10^{-24} \text{ cm}^2$
$\langle b \rangle^2$	5.4051	113.59	29.70	56.747	$10^{-24} \text{ cm}^2$

5.2 on page 64. This gives again other results but does not solve the problem of the incompatibility of the four measured structure factors.

There are even in the case of simple alloys two different possibilities of evaluation of the total structure factors: The already mentioned Faber-Ziman [3] definition and the Bhatia-Thornton [4] definition. In the Bhatia-Thornton way one looks for the change in the Laue diffuse scattering of an alloy with concentration  $c_A$  of one component and the scattering length  $b_A$  and  $b_B$  of the components. This is a Q-independent scattering  $c_A(1 - c_A)(b_A - b_B)^2$  in the case of no short range order and no deformation. If the sample shows short range order or deformation by size effects of the atoms this Laue diffuse scattering shows a structure. Just by the selection of the factors in the system of equations one can then determine this concentration fluctuation  $S_{CC}$ . The results have to be interpreted in different way: Bhatia-Thornton gives  $S_{NN}$  correlations between density fluctuations,  $S_{CC}$  correlations between concentration fluctuations,  $S_{NC}$  correlations between density and concentration fluctuations. The  $S_{CC}$  describes the correlation which is observed in the structure of the Laue diffuse scattering. The system of equations in this case is not so symmetric as in the Faber Ziman description, but it is again symmetric if one uses the formulation with the Laue description:

$$I(Q) = \langle b_i \rangle^2 S_{NN} + 2\langle b_i \rangle \sqrt{c(1 - c)}(b_A - b_B) S_{NC} + c(1 - c)(b_A - b_B)^2 S_{CC} \quad (7.13)$$

From the partial structure factors the partial distribution functions  $g_{\mu\nu}(r)$  can be derived by Fourier transformation. From the distribution function  $g(R)$  we obtain the coordination numbers  $Z$  i.e. the mean number of nearest neighbours in a shell between  $R_i$  and  $R_j$  by

$$Z = \int_{R_i}^{R_j} 4\pi R^2 \rho_0 g(R) dR \quad (7.14)$$

In the same way one gets the partial coordination numbers  $Z_{\mu\nu}$  from the partial distribution functions. The partial coordination numbers finally yield the Warren-Cowley short range order parameters. In view of all these possibilities it is very interesting to be able to find the partial structure factors for the rings and chains.

## 7.2 Application to the polymers

If one uses instead of the  $\langle b_i \rangle^2$  the expressions  $\langle \sqrt{\sum_i b_i^2} \rangle^2$  and divides each line of the equation by the factor on  $S_{cc}$  one can interpret each line as a function  $y=f(x)$  where  $f(x)$  is a parabola with the partial structure factors as parameters:  $y = S_{cc} + 2xS_{rc} + x^2S_{rr}$ . This gives a system of four equations with three unknown parameters, an over determined system which can be solved by a parabola fit .

$$y_1 = \frac{S^{DD}}{\langle b_c^D \rangle^2} = S_{cc} + 2 \frac{\langle b_r^D \rangle}{\langle b_c^D \rangle} S_{rc} + \left( \frac{\langle b_r^D \rangle}{\langle b_c^D \rangle} \right)^2 S_{rr} = S_{cc} + 2x_1 S_{rc} + x_1^2 S_{rr} \quad (7.15)$$

$$y_2 = \frac{S^{HD}}{\langle b_c^H \rangle^2} = S_{cc} + 2 \frac{\langle b_r^D \rangle}{\langle b_c^H \rangle} S_{rc} + \left( \frac{\langle b_r^D \rangle}{\langle b_c^H \rangle} \right)^2 S_{rr} = S_{cc} + 2x_2 S_{rc} + x_2^2 S_{rr} \quad (7.16)$$

$$y_3 = \frac{S^{DH}}{\langle b_c^D \rangle^2} = S_{cc} + 2 \frac{\langle b_r^H \rangle}{\langle b_c^D \rangle} S_{rc} + \left( \frac{\langle b_r^H \rangle}{\langle b_c^D \rangle} \right)^2 S_{rr} = S_{cc} + 2x_3 S_{rc} + x_3^2 S_{rr} \quad (7.17)$$

$$y_4 = \frac{S^{HH}}{\langle b_c^H \rangle^2} = S_{cc} + 2 \frac{\langle b_r^H \rangle}{\langle b_c^H \rangle} S_{rc} + \left( \frac{\langle b_r^H \rangle}{\langle b_c^H \rangle} \right)^2 S_{rr} = S_{cc} + 2x_4 S_{rc} + x_4^2 S_{rr} \quad (7.18)$$

with the average defined by  $\langle b_i \rangle = \sqrt{\sum_i b_i^2}$ . We derived this relation above. The reason for this could be the fact that the different atoms in the rings and chains can have many orientations inside the solid polymer so that the phase information averages out and the minus sign does not play a role. The best parabola fit of this system one gets by the solution of the system of the following three equations

$$\begin{pmatrix} N & [x] & [x^2] \\ [x] & [x^2] & [x^3] \\ [x^2] & [x^3] & [x^4] \end{pmatrix} \cdot \begin{pmatrix} S_{cc} \\ S_{rc} \\ S_{rr} \end{pmatrix} = \begin{pmatrix} [y] \\ [xy] \\ [x^2y] \end{pmatrix} \quad (7.19)$$

with  $[x] = \sum_i x_i$ ,  $[x^2] = \sum_i x_i^2$ ,  $[x^2y] = \sum_i x_i^2 y_i$  etc.. If one does this for each detector angle one gets the curves of the partial structure factors of fig.7.1. To see how good the fit is, we first want

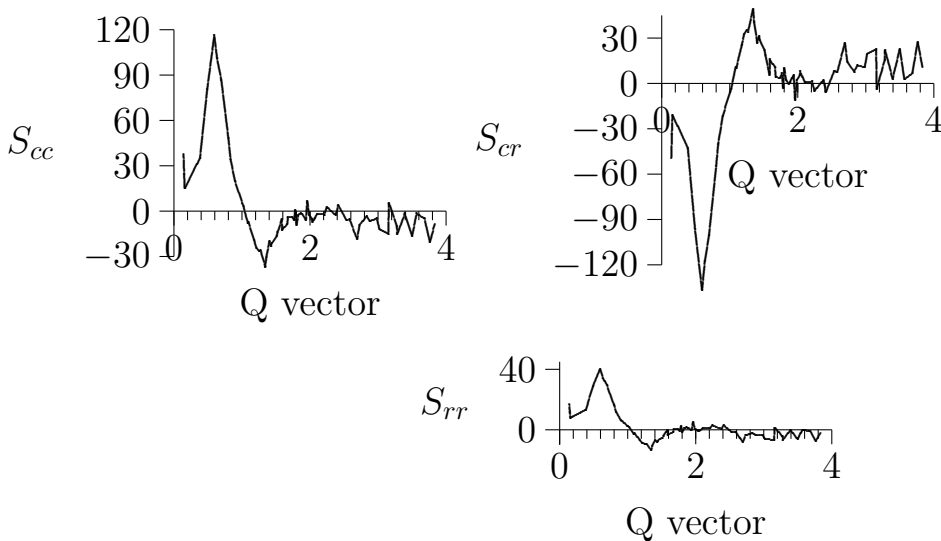


Figure 7.1: Partial structure factors for the correlation of the chain part, the ring part which each other and with themselves  $S_{cc}$ ,  $S_{rr}$ ,  $S_{rc}$

to see how the partial structure factors allow to represent the measured curves. This can be seen

in the figures 7.2. This figures show that HD and DH is very well reproduced, also HH is fairly well reproduced. The fully deuterated sample is not so well reproduced which may come from the problem we had already during the measurement, that the sample was not really fully deuterated but contained some hydrogene (about 2%). So we have corrected for this, but it seems also to have influenced the spectrum, which we of course cannot correct. This method finally seems to be the strongest method to treat the wide angle scattering of polymers.

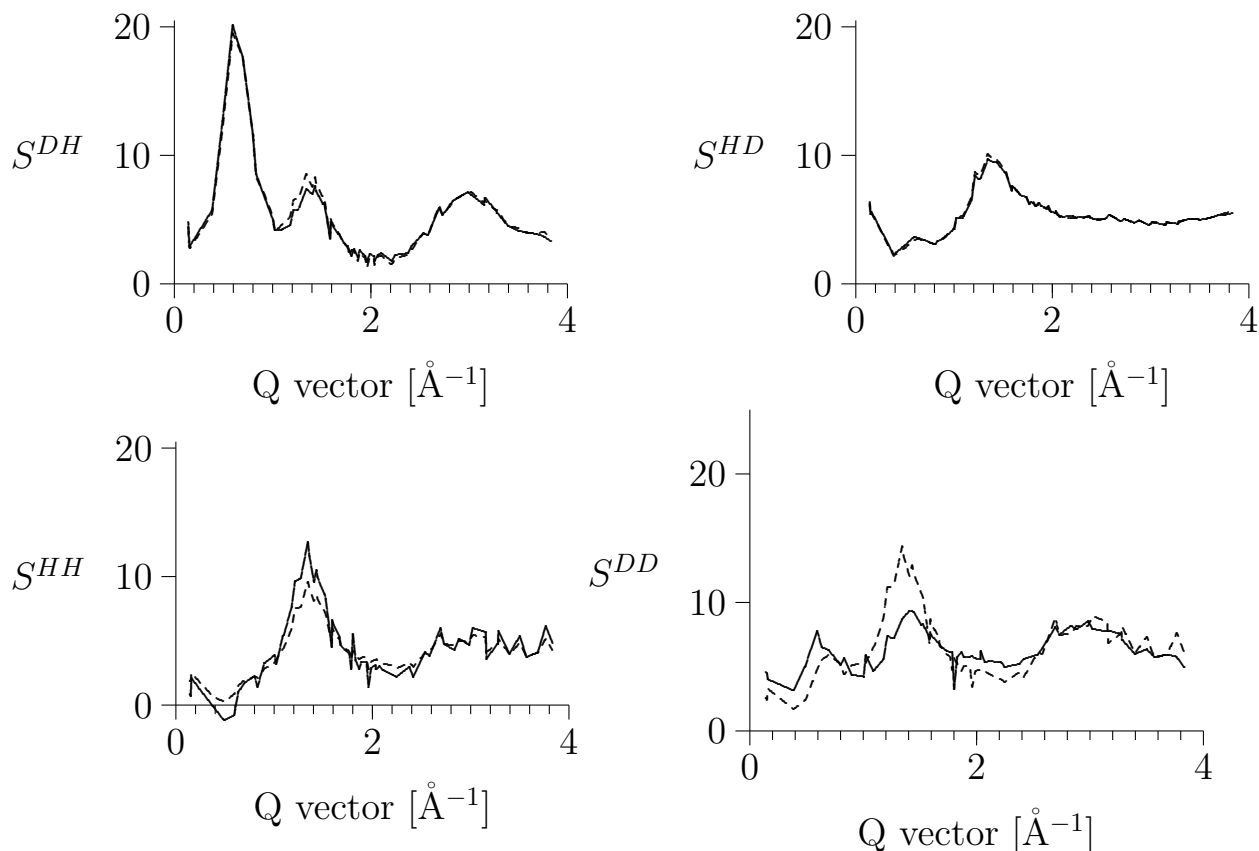


Figure 7.2: Structure factors  $S^{DH}$ ,  $S^{HD}$ ,  $S^{HH}$  and  $S^{DD}$  calculated with the partial structure factors of fig.7.1 (dashes curves) compared with the measured curves (solid lines)

### 7.3 Discussion of the results

The partial structure factors of fig.7.1 have now to be Fourier transformed to be able to say something about the coordination numbers of rings and chains. But one can already see that the high peak at  $0.6 \text{ \AA}^{-1}$  results from a high correlation of the chain parts of the monomer and a strong anticorrelation of these chain parts with the ring parts in a distance of  $2\pi/0.6 \approx 10.5 \text{ \AA}$ . In this radius also the rings are correlated with rings but this correlation is not so strong than that of the chains (see the curve for  $S_{rr}$  in fig.7.1). The peaks at  $1.35 \text{ \AA}^{-1}$  show that in a distance of  $r = 4.6 \text{ \AA}$  the chains are anticorrelated and there is higher probability to find the other element as  $S_{cr}$  has there a maximum, and the  $S_{rr}$  and the  $S_{cc}$  are there negative. At  $3 \text{ \AA}^{-1}$  the function  $S_{rc}$  has a broad positive maximum (approximately  $1 \text{ \AA}^{-1}$  wide), which is not very high. This says that at  $r = 2.1 \text{ \AA}$  the chain members have a sharp value of correlation, which is to be expected, as this is the distance of the chain members in the backbone. To get the quantitative probability one has to Fourier transform this and use eq.7.14. All this seems very probable as these distances are within the Kuhn-segment length, which is the length where the bond angles and the excluded

volume effect hinder the freely jointed chain behaviour in the strongest way. This forces then the observed correlations.

## 7.4 Spherical Fourier Transform

To get the full quantitative information from these partial structure factors they must be Fourier transformed. For this we define two Fourier pairs

$$\Phi(k) = k \cdot i(k) \quad (7.20)$$

$$f(r) = r[\rho(r) - \rho_0] = \frac{G(r)}{4\pi} \quad (7.21)$$

$$\text{which are connected by} \quad (7.22)$$

$$\Phi(k) = 4\pi \int_0^\infty f(r) \sin kr dr \quad (7.23)$$

$$f(r) = \frac{1}{2\pi^2} \int_0^\infty \Phi(k) \sin kr dk = \frac{1}{4\pi} G(r) = r\rho_0(g(r) - 1) \quad (7.24)$$

$$4\pi r^2 \rho(r) = 4\pi r^2 \rho_0 + \frac{2r}{\pi} \int_0^\infty ki(k) \sin(kr) dk \quad (7.25)$$

$$\rho(r) = \rho_0 g(r) \quad \text{local number density} \quad (7.26)$$

$$\rho_{ij}(r) = c_j \rho_0 g_{ij}(r) \quad (7.27)$$

$$G_{ij}(r) = 4\pi r \left[ \frac{\rho_{ij}}{c_j} - \rho_0 \right] = 4\pi r \rho_0 (g_{ij}(r) - 1) \quad (7.28)$$

$$A_{ij}(r) = c_j [4\pi r^2 \rho_0 + r G_{ij}(r)] = 4\pi r^2 c_j \rho_0 g_{ij}(r) \quad (7.29)$$

$$= \text{radial density function Rdf} \quad (7.30)$$

$$Z_{ij} = \int_{R_{low}}^{R_{upper}} A_{ij}(r) dr \quad \text{coordination number} \quad (7.31)$$

where i,j can be r or c (ring or chain). In this way we determine

$$G_{cc}(r) = \frac{2}{\pi} \int_0^\infty Q[S_{cc}(Q) - 1] \sin(Qr) dQ \quad (7.32)$$

$$= \frac{1}{\pi} \sum_{i=1}^n (S_{cc}(Q(i)) - 1)(Q(i)^2 - Q(i-1)^2) \sin(Q(i)r) \quad (7.33)$$

$$G_{rr}(r) = \frac{1}{\pi} \sum_{i=1}^n (S_{rr}(Q(i)) - 1)(Q(i)^2 - Q(i-1)^2) \sin(Q(i)r) \quad (7.34)$$

$$G_{cr}(r) = \frac{1}{\pi} \sum_{i=1}^n (S_{cr}(Q(i)) - 1)(Q(i)^2 - Q(i-1)^2) \sin(Q(i)r) \quad (7.35)$$

In this way we get the pair correlation functions  $G_{cc}(r)$ ,  $G_{rr}(r)$  and  $G_{cr}(r)$ , shown in fig.7.3 as solid lines. If one uses the convergence factor  $\exp(-\alpha Q(i)^2)$  with  $\alpha = 0.2$  (see [5]) the dotted lines in fig.7.3 are obtained. This convergence factor is used to get rid of oscillations resulting from the truncation at a finite  $Q$ . However the strong oscillations with a period of about 2.5 Å around the solid line are not resulting from the truncation but they result from the broad peak around  $Q=3$  Å<sup>-1</sup> i.e. they follow really from the measurement. But using the convergence factor one can see clearer another oscillation with a longer period. By Fourier back transform of this it can be seen that the convergence factor suppresses the peak at 3 Å<sup>-1</sup> in the original data and by this gets rid of the narrower oscillations, which really shows that these do not result from truncation.

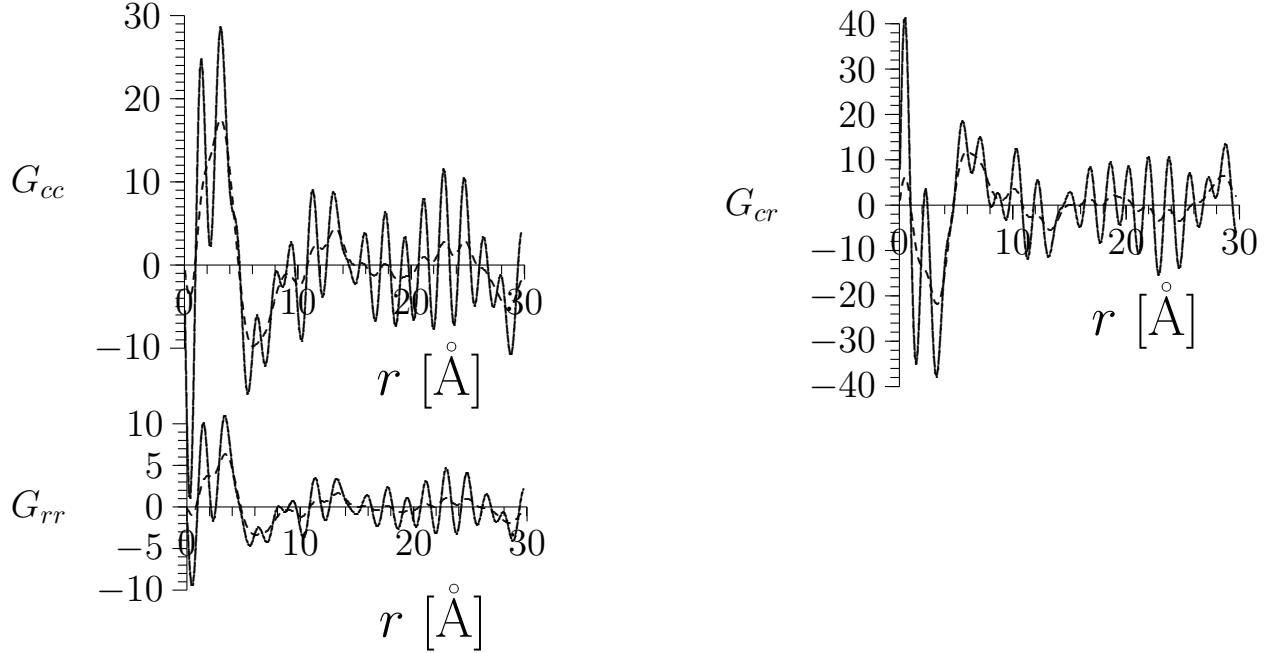


Figure 7.3: Partial correlation functions  $G_{ij}(r)$  as spherical Fourier transform of the partial structure factors  $S_{ij}(Q)$ . The solid lines are the simple Fourier transforms without convergence factor, the dotted lines are those with a convergence factor  $\exp(-\alpha Q^2)$  with  $\alpha = 0.2$ .

Table 7.2: Coordination numbers in the first, second and third coordination shell for  $\rho_0 = 0.037$

shell	$Z_{cc}$	$Z_{rr}$	$Z_{cr}$	random
0-4.5 Å	13.38	9.3	0.04	7.2
	1.86	1.89	0.005	
4.5-11 Å	86.7	93.3	107.6	96.5
	0.90	0.90	1.12	
11-15 Å	166.9	163.3	155	161
	1.034	1.04	0.96	

For the radial density functions (see fig.7.4)

$$\text{Rdf}(r) = c_j[4\pi r^2 \rho_0 + r G_{ij}(r)] = c_j 4\pi r^2 \rho_0 g_{ij}(r) \quad (7.36)$$

$$\text{Rdf}_0 = 4\pi r^2 \rho_0 c_j \quad (7.37)$$

the average density  $\rho_0$  is needed. The monomer of polystyrene is  $C_8H_8$  with the molecular weight of  $8 \cdot 12.011 + 8 \cdot 1.008 = 104.152$ . The mass density of polystyrene is  $1 \text{ g/cm}^3$ . This corresponds to  $1/104.152 = 9.6014 \cdot 10^{-3} \text{ mol cm}^{-3} = 5.7829 \cdot 10^{21} \text{ monomer cm}^{-3} = 5.7829 \cdot 10^{-3} \text{ monomer Å}^{-3}$ .

?for  $G_{cr}(r)$  one sees that  $\rho_0$  cannot be smaller than 0.037, otherwise the radial density function 7.36 would become negative for small  $r$ . One sees also, that the parabola 7.37 intersects the radial density function 7.36 at the radius 4.5 Å, 11 Å and 15 Å. Interpreting these ranges as coordination shells we can then determine  $Z_{ij}$  using the integrals over the radial density functions. In this way we obtain the values tabulated in table 7.2.

## 7.5 Maximum entropy method to determine the $g_{ij}(r)$

We follow here Daniell et al. [6] We want to determine the pair correlation functions  $g_{ij}(r)$  of an amorphous solid, which describes the statistics of the separations of the ring and chain parts of



the monomers in a polymer chain or between chains. The measurement yields  $S(Q)$  with  $Q = (4\pi/\lambda) \sin \vartheta/2$ ,  $\vartheta$ =scattering angle and  $\lambda$ =wavelength of the neutrons.  $S(Q)$  is related to  $g(r)$  by

$$S(Q) = 1 + \frac{4\pi\rho}{Q} \int_0^\infty R[g(R) - 1] \sin QR dR \quad (7.38)$$

$\rho$  is the density of the material. This equation has an analytic solution as we have seen before  $Q[S(Q) - 1]$  and  $R[g(R) - 1]$  are Fourier sine transforms of each other. But for this we need  $S(Q)$  for all  $Q$  up to infinity. The limits are the angular resolution of the detector and the limited range of  $Q$  by the wavelength and of the scattering angles. The maximum  $Q$  determines the resolution in  $R$  and the  $\Delta Q$  determines the maximum  $R$ .

Maximum entropy method can select these values independently of the experiment. But one has to define a proper probability density. A function that can become negative is not such a probability density. For a spherical sample of radius  $a$  with  $n$  atoms per unit volume we have

$$n = \frac{3}{4\pi a^3} \int_0^a 4\pi R^2 g(R) dR \quad (7.39)$$

If we use  $p(R) = 3R^2 g(R)/(a^3 n)$  we can fulfill the normalization condition of probabilities  $\int_0^a p(R) dR = 1$ . In the absence of data the simplest assumption is  $g(R)=1$  and we get the entropy

$$S = - \int p(R) \log \frac{p(R)}{m(R)} dR = - \frac{3}{na^3} \int R^2 g(R) \log \frac{R^2 g(R)}{eR^2} \quad (7.40)$$

We have to determine in our inverse problem  $R^2 g(R)$  with a prior proportional to  $R^2$  and get  $g(R)$  by dividing at the end by  $R^2$ .

We have to discretise the problem to apply the computer. We have to fix  $Q_{max}$  greater than the largest value of  $Q$  in the experiment and  $\Delta Q$  less than the smallest resolvable difference in  $Q$ . The first is fixed by the wavelength of the neutrons. The second by the resolution. To discretise the above equation we cut off the integral at  $R_{max} \gg 1/\Delta Q$ , introduce  $\Delta R \ll 1/Q_{max}$  and replace the integral by a sum:

$$S(Q) = 1 + \frac{4\pi\rho}{Q} \Delta R^2 \sum_\nu \nu [g_\nu - 1] \sin \nu Q \Delta R \quad (7.41)$$

with  $R = \nu \Delta R$  and  $g(\nu \Delta R) = g_\nu$  and  $\nu$  an integer. We must evaluate this sum for each  $Q$  for which we have a measured  $S(Q)$ .

Now we want to apply the maximum entropy method of Collins [7] also used by Sakata et al. [8]. For this we determine iteratively for each  $R$  an improved  $g(R)$  (or for each  $\nu$  an improved  $g_\nu$  by

$$g_{new}(R) = g_{old}(R) \exp \left[ \lambda \sum_{i=1}^n \frac{(F_{obs}(Q_i) - F_{calc}(Q_i))}{\sigma^2(Q_i)} \sin Q_i R \right] \quad (7.42)$$

with  $n$ =number of  $Q$ -positions of the measurement.  $F_{obs}(Q_i)$  is:

$$F_{obs}(Q_i) = S(Q_i) - 1 + \frac{4\pi\rho_0}{Q_i} (\Delta R)^2 \sum_\nu^{R_{max}/\Delta R} \nu \sin \nu Q_i \Delta R \quad (7.43)$$

$\sigma^2(Q_i)$  is the error squared of the measurement and

$$F_{calc}(Q_i) = \frac{4\pi\rho_0}{Q_i} (\Delta R)^2 \sum_\nu^{R_{max}/\Delta R} \nu g_\nu \sin \nu Q_i \Delta R \quad (7.44)$$

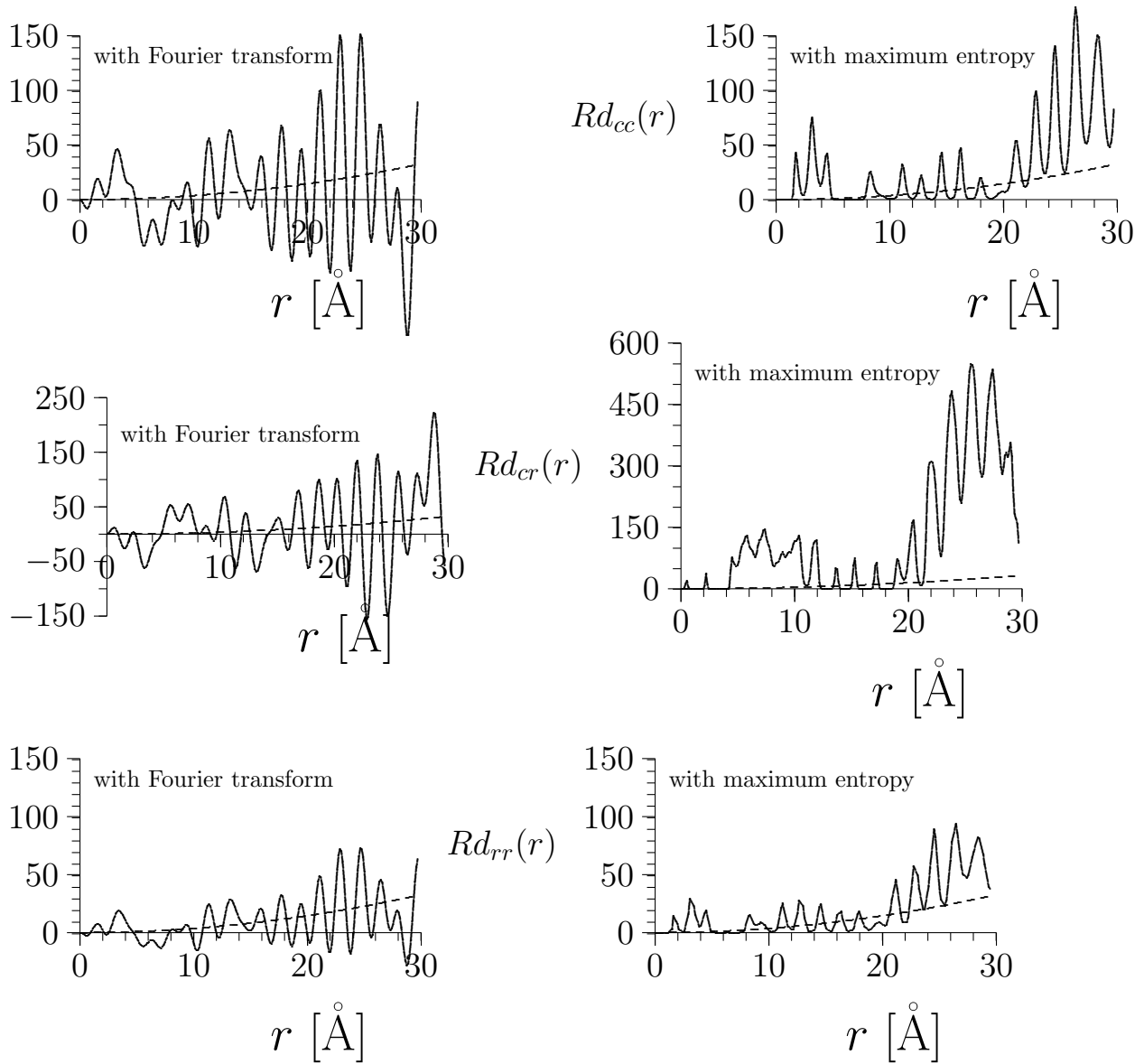


Figure 7.4: Plot of the radial density functions without (dotted) and with short-range order (solid lines), with Fourier transform (left) or with maximum entropy method (right)

## 7.6 Conclusions



# Bibliography

- [1] J.B.Suck, D.Raoux, P.Chieux, C.Riekkel, Methods in the Determination of Partial Structure Factors of Disordered Matter by Neutron and Anomalous X-Ray Diffraction, World Scientific, Singapore 1993.
- [2] J.M.Ziman, Models of Disorder, The theoretical physics of homogeneously disordered systems. Cambridge University Press, London 1979
- [3] T.E.Faber, J.M.Ziman, Phil.Mag. **11** (1965) 153
- [4] A.Bhatia, T.E.Thornton, Phys.Rev.B **2** (1970) 3004
- [5] B.E.Warren, X-Ray Diffraction, Addison-Wesley, London 1968
- [6] G.J.Daniell, J.A. Potton in Maximum Entropy and Bayesian Methods, ed.J.Skilling, Kluwer Academic Publishers, London 1988 p.151-162
- [7] D.M.Collins, Nature **298** (1982) 49-51
- [8] M.Sakata, R.Mori, S.Kumazawa, M.Takata, J.Appl. Cryst. **23** (1990) 526-534



## Chapter 8

# Neutron small angle scattering on selectively deuterated polystyrene with polarization analysis.

Otto Schärpf,ILL, Barbara Gabrys,Brunel Univ.,London and Dennis G. Peiffer,EXXON REC

### 8.1 Measurement

For all measurements the D7 instrument at the Institut Laue Langevin, Grenoble equipped with a polarization analysis option was used. Fig.3.1 on page 31 shows its general lay-out. The small angle scattering set-up with spin analysis is shown schematically in fig. 3.2 on page 32. We emphasize the small angle scattering was carried out simultaneously with the wide angle measurement. The small angle apparatus consists of one analyzer with supermirrors [5] arranged horizontally lying also in a horizontal magnetic field arranged near the sample. This allows an angular range of  $90^\circ$  to be "scanned" by measuring simultaneously with 16 detectors of 1.2 cm width at a 1.68 m distance from the sample. This corresponds to an angular resolution of  $0.01 \text{ \AA}^{-1}$  for the incident wavelength of  $5.72 \text{ \AA}$ .

In an actual experiment the neutrons doubly focused by a triple pyrolytic graphite monochromator are subsequently polarized vertically with a bender type supermirror polarizer [5] as shown in fig.3.1 on page 31. The neutrons subsequently traverse a Mezei-type flipper, which serves to change the polarization direction of the neutrons relative to the magnetic guide field. After scattering by the sample the neutrons are detected by an array of detectors equipped with supermirror analyzers which transmit neutrons with only spin up component. In order to distinguish between the coherent  $\sigma_{coh}$  and the incoherent scattering  $\sigma_{inc}$  as described below, the measurement is carried out by alternating the spin-flip and non-spin-flip modes and counting the respective neutrons separately. In this way it is possible to measure separately the scattering of neutrons which are flipped by the scattering process in the sample e.g. neutrons scattered by the nuclear spin of the proton. This spin-flip scattering is incoherent and its cross-section for each polymer sample is known. The specific values calculated for each polymer sample are given for in table 3.4. In this way an internal calibration for each sample is obtained since the incoherent scattering is isotropic and only this cross section is measured in the spin-flip mode. The non-spin flip mode measures the sum of the coherent scattering, 1/3 of the incoherent scattering and the isotope related part of the incoherent scattering. Therefore the coherent part of the scattering  $\sigma_{coh}$  can be determined. If one relates  $\sigma_{coh}$  after subtraction of the background and correction for finite flipping ratio [6] to the incoherent scattering  $\sigma_{inc}$ , one gets an absolute calibration of the coherent scattering in barn/formula unit. In the discussion that follows we shall see how important this calibration is and

why it is very useful. Normally neutron scattering without polarization analysis cannot separate these components and therefore one has to resort to subtracting arbitrarily assumed backgrounds whereas using spin polarization analysis both coherent and incoherent scattering can be separated experimentally. Subsequently the coherent scattering component can be directly determined using the previously determined incoherent part as an internal calibration, which otherwise must be determined in a separate measurement using an incoherent scattering standard (e.g. vanadium, water).

The finite flipping ratio for small angle scattering was measured with a strong small angle scattering Vycor glass sample which scatters without flip. Quartz was used to determine the flipping ratio at wide angles. The number of flipped neutrons transmitted in this case as compared to those transmitted without flip yields a finite flipping ratio,  $R = (I^\uparrow/I^\downarrow)$ , because of the imperfection of the polarizer. Typically, this ratio is approximately 30 to 40.

The fully deuterated sample has only a small  $\sigma_{inc}$  and shows a behavior deviating from the other samples, i.e. showing much less scattering than the others. The simplest reason for this behaviour is the contamination by water. This would give the wrong internal calibration standard, which would be in reality much higher due to an amount of absorbed water or hydrogen. To exclude this possibility, we also made a vanadium calibration measurement for both the small and wide angle scattering. Our measurements show that such 'contamination' was not the problem because the modulation with  $Q$  of the scattering intensity was much less than expected (see further discussion further).

Due to the geometry of our instrument the ideal sample shape should be cylindrical for wide angle scattering and flat for small angle scattering. This is due to the fact that it is hard to correct for the form of the sample if one has a standard scatterer of another form. There are no sharp limits. We tested the behaviour for some samples using both geometries. Cylindrical and flat sample geometries gave similar results if a) the measurement was related to the internal calibration, and b) the measured transmission (given in table 3.4 was of the order of 80%-90%). Due to multiple scattering a sample with the transmission of 68% showed the behaviour presented in fig.3.3 on page 34: This confirms the well-known fact that multiple scattering has a tendency to flatten out the scattering curve. To avoid this effect the amount of material in some samples in the incident beam was reduced in order to obtain higher transmission values and thus diminishing the multiple scattering.

## 8.2 Results and interpretation of the small angle scattering.

The next essential step is to investigate the relation of the wide-angle scattering results to the observed small angle scattering. There one could expect to obtain information on bigger units of the whole chain as for example the radius of gyration or the shape of the scattering units (spheres, ellipsoids, thin cylinders, flat disks) by Guinier plots, the specific surface area of the sample as a "powder" by Porod plots, and we can inspect the behaviour of the Kratky and Zimm plots for our samples. We also pose a question whether we can learn something from differences in the small angle scattering of the selectively deuterated samples. As we go to smaller  $Q$  values, the single monomers are no more resolved and the apparatus sees larger and larger units, where the monomers are more and more point-like, the sum of the scattering lengths of their atoms yielding a total contribution to their scattering. Since our wide-angle results demonstrate that instead of independent chains we have domains of regularly arranged pieces of chains, we cannot claim, that our small angle scattering results show properties of independent chains. Especially we cannot get any information over the whole chain length, because for this the resolution of the simple small angle set-up included in D7, of only 1.68 m length and detectors of 1.2 cm width at  $\lambda = 5.715$  Å, is not good enough. At this wavelength we get as the smallest  $Q$  value  $0.01 \text{ Å}^{-1}$  with a step  $\Delta Q$  between adjoining detectors  $\Delta Q = 0.01 \text{ Å}^{-1}$ . Logically one should not wonder if the radius



of gyration, which we obtain, is much smaller than normally quoted in the literature for the chain as a whole. For example,  $R_g \approx 0.275\sqrt{M_w}$  Å as quoted by Higgins and Stein [15], which should give  $R_g = 213$  Å in our case for the HH sample or 399 Å for the DH sample. A rough estimate of a diffraction pattern that could give information about such a size takes the scattering object just as a diffracting slit yielding a width in  $Q$  of  $2\pi/R_g$  corresponding to a half width of the scattering pattern of  $0.0295$  Å<sup>-1</sup> for the HH sample or  $0.016$  Å<sup>-1</sup> for the DH sample. Such a half width is not in the range of the above described set-up on D7 (fig.3.2 on page 32). However, Rawiso gives  $R_g = \sqrt{17}$  Å for a chain cross section model for polystyrene [16], which would lie well in the  $Q$  range accessible to us. We measured the samples also using D11 (see fig.8.3 on page 111 and 8.5 on page 115) which has a much better resolution and gives additional information.

Certainly, there are many effective interference effects between the chains, which we do not want to discuss here. Our aim is to test the set-up used here for the first time on a sample giving intense small angle scattering and to get a description of the small angle scattering observed by some characteristics of the curves, to see what sort of changes one observes after the selective deuteration, the heat treatment, and especially the sulfonation. We describe the observed curves by the customary plots (Guinier, Kratky, Porod and Zimm) and extract the respective characteristic values from these plots, without enquiring too much about the sense of these values. This approach is rewarding: we find a lot of interesting connections, which are easily overseen if one looks only for the confirmation of a model or a problem long discussed and not yet resolved. As before, we will not be guided by investigations of other workers but more by new possibilities offered by a new instrument. Our major criterium is the internal consistency rather than consistency with observations of others: the latter we cannot control here. But we measured the same samples also on the instrument D11, to see, whether the results are consistent also with results on this instrument.

### 8.2.1 General outline

The origin of the small angle scattering [16] originates from the fact that in forward direction all atoms in a solid scatter in phase, no matter how they are arranged in the  $r$ -space. This arrangement in space is termed the disposition function  $Z(\mathbf{r})$ . As it is conventional in crystallography to assume that the atoms fill the whole space, the disposition function fills the whole space and its Fourier transform is infinitely sharp and is described by a true  $\delta$ -function. Convolution of the shape function  $S(\mathbf{Q})$  with a  $\delta$ -function leaves the shape function unchanged and so one measures in the small angle scattering the shape function

$$I_0(\mathbf{Q}) \stackrel{Q \approx 0}{=} k|S(\mathbf{Q})|^2 \quad (8.1)$$

$k$  being proportional to  $\langle F_M(Q) \rangle^2$  different for the selectively deuterated samples,  $I_0(\mathbf{Q})$  is the intensity of the scattering. Thus small angle scattering enables us to determine the shape of the scattering regions from the  $|S|^2$  curves independently of the degree of order in these regions. If the degree of order is low then  $S(\mathbf{Q})$  is zero for wide angle scattering. If the order is crystalline then the shape factor is reproduced at any crystalline reflection i.e. it must be convoluted with the  $\delta$ -functions corresponding to the crystalline reflections. On the contrary the  $\langle F_M \rangle^2$  is a factor, it is not convoluted with the  $\delta$ -function but only multiplied with it. The function  $\langle F_M(Q) \rangle^2$  does not at all describe the small angle scattering what is evident from fig.8.1, where the measured small angle scattering is given for the four samples HH,DH,HD,DD in the  $Q$  range  $0.01 - 0.2$  Å<sup>-1</sup> compared with the respective curves of  $\langle F_M \rangle^2$  for the syndiotactic chain calculated for up to 12 monomers. From figs.5.6 -5.7 on page 68 we know that  $\langle F_M(Q) \rangle^2$  is broader for fewer monomers. This function  $\langle F_M(Q) \rangle^2$  has the effect of a form factor like the magnetic or electronic form factors of the atoms. Normally in the small angle scattering region it can be assumed constant. But if there are units or

domains of 14 monomers and more,  $\langle F_M(Q) \rangle^2$  already changes in the respective region as seen in fig.8.1.

### 8.2.2 Guinier plots

$\langle F_M \rangle^2$  represents a structure factor (eq.5.14), in which the structure of the monomer and the scattering lengths of the single atoms in the monomer are contained, and it is just this factor, by which the scattering of the differently deuterated samples HH,DH,HD,DD should differ, if the supposition of isostructurality is fulfilled. Fig.8.2 shows the Guinier plots of the thus reduced (by division through  $\langle F_M(Q) \rangle^2$ ) measured curves, i.e. the measurements given in fig.8.1 in barns/(sr · monomers) is now given by the logarithm of a dimensionless number as a function of  $Q$ , which should be the same in all samples, if the morphology in the small angular region is the same.

To understand the sense of this dimensionless number we have to remember, what one gets by extrapolation of  $I(Q)$  to  $Q=0$  in the Guinier plot. Since in our case the intensity is given by

$$\langle I(Q) \rangle \stackrel{Q \rightarrow 0}{=} \langle N \rangle \langle F_M(Q) \rangle^2 \quad (8.2)$$

division gives

$$\frac{\langle I(0) \rangle}{\langle F_M(0) \rangle^2} = \langle N \rangle \quad (8.3)$$

i.e. one obtains the average number of monomers  $\langle N \rangle$  which contribute to the scattering [17] p.36 and p.71 ss. In this way the Guinier plots provide two important quantities: the slope of the curves gives the radius of gyration  $R_g$  and the information whether there is only one  $R_g$  (or not), and the extrapolation to  $Q \rightarrow 0$  gives the number of monomers which contribute to the scattering with the respective radius of gyration. It is somewhat akin to the Zimm plot, which uses a similar procedure to obtain the chain length contributing to the respective part of the scattering (application to our data see section 8.2.4 on page 115). It is immediately obvious from fig.8.2 that the measured data

Figure 8.1: Observed small angle scattering curves ( $\partial\sigma/\partial\Omega$ ) for the 4 samples HH,DH,HD,DD together with the curves of  $\langle F_M \rangle^2$  calculated for 14 monomers.

cannot be described by straight lines, which means one has not a simple scatterer with one  $R_g$  but it has at least two different radii of gyration, one giving the intensity in the lower  $Q$  regions and one contributing to the higher  $Q$  region. This corresponds to the two different correlation lengths which we found in the wide-angle scattering, one for the observed crystalline interference by the parallel ordering of the chains in the ab-plane, the other one in the c direction for the chain periodicity. The polydispersity (giving a distribution of  $R_g$ 's) in our samples DH,HD,DD but not in HH (see table 3.4) does not play a role, as we do not see the whole chain anyway. Evaluation of the data plotted in figs.8.1 and 8.2 gives the results listed in table 8.1. The quantities  $\langle N \rangle$  are the respective intercepts and give the number of monomers contributing to the scattered intensity (eq.8.2). The D11 instrument is an instrument with a much better angular resolution. This measurement gives for HD the  $R_g=1072$  Å for the small  $Q$ -region and 250 Å for the largest  $Q$  region ( $Q=0.01$  Å<sup>-1</sup> in this case). These two measurements would show a very broad distribution of the radius of gyration ranging from 1072 to 13.5 Å. Extrapolation to  $Q \rightarrow 0$  yields  $\langle N \rangle = 110$ . It seems difficult to draw other consequences from this behaviour than the information that small angle scattering is not the adapted method for solid polymers.

The evaluation uses the formulas

$$\text{slope} = -\frac{R_g^2}{3} \log_{10} e \quad (8.4)$$

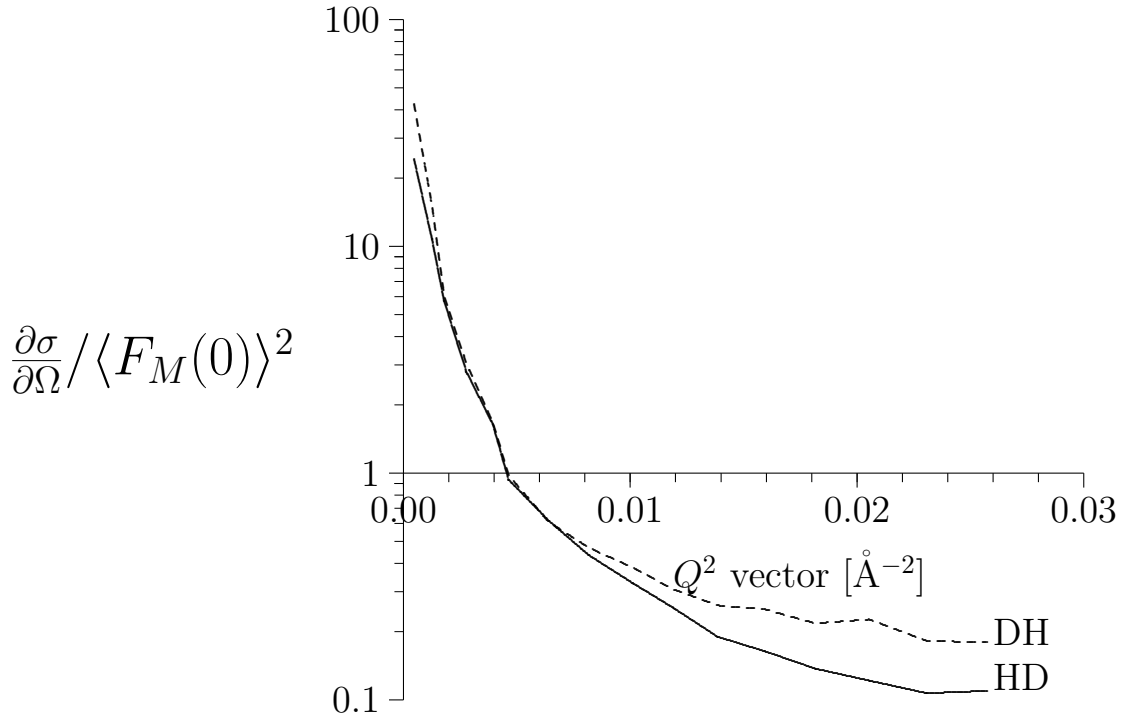


Figure 8.2: Guinier plots of  $\log(\partial\sigma(Q)/\partial\Omega/\langle F_M \rangle^2(0))$  over  $Q^2$  for samples DH and HD

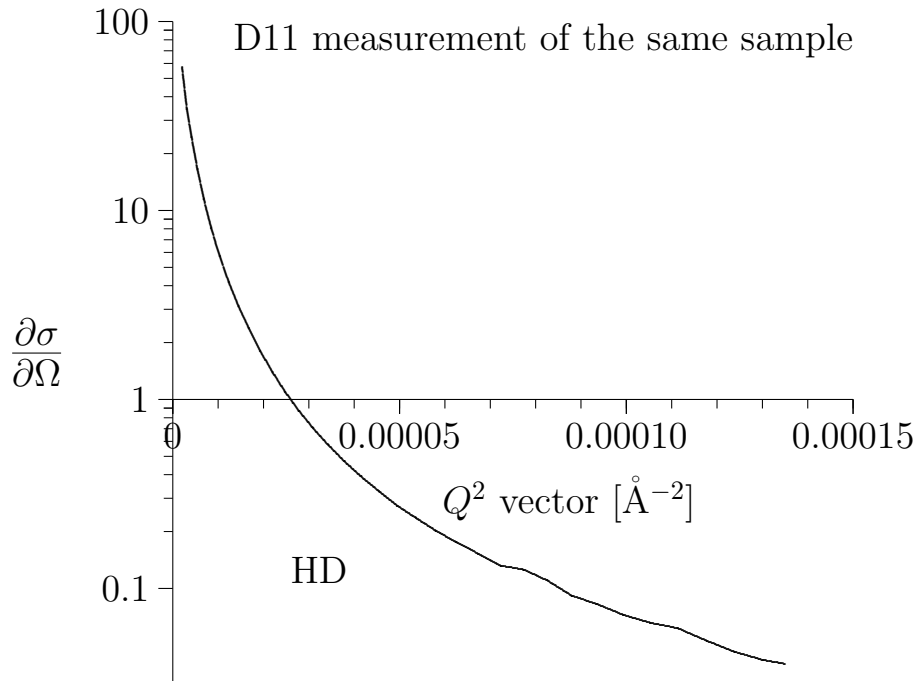


Figure 8.3: Measurement of the sample HD on the instrument D11 with a much better resolution. This says that the scattering looks the same in a much smaller scale. Fractal behaviour? Scaling?

$$R_g = \sqrt{\frac{3 \cdot \text{slope}}{\log_{10} e}} \quad (8.5)$$

$$= 2.628 \sqrt{\text{slope}} \quad (8.6)$$

The results presented in table 8.1 correspond very well to the results of the investigation of the

Table 8.1: **Results of the Guinier plot of the samples**

sample		$R_g$ small Q	$R_g$ larger Q	$\langle N \rangle$
HH	before	64.4 Å	8.5 Å	38.7
HH	after	65.2 Å	?	27.7
DH		49.3 Å	12.1 Å	76.1
HD		46.6 Å	13.5 Å	37.3
HD	D11 meas.	1075 Å	250 Å	110
DD		39.2 Å	12.5 Å	1.92

wide angular range (see preceding part). If we don not correct the DD sample for the hydrogen content but take the measurement as it is, we would get the following interpretation.

We found already that the diffuse scattering of two monomers describes the scattering from DD the best. Now we also find, that the small angle scattering in the region accessible for us comes only from correlations of, on the average, two monomers. If the radii of gyration for the HD, DH and DD samples are very close (table 8.1), then the difference in the intercepts (fig.8.2) yielding different  $\langle N \rangle$  must come from the changed number of monomers contributing in the average to the ordered domains with the measured  $R_g$ . If we assume that lower  $\langle N \rangle$  comes from the averaging process whereas the  $R_g$  comes from fewer ordered domains, in DD one would than have  $37.3/1.92 = 19.4$  times less ordered domains than in HD which has ordered domains in regions of the size of  $R_g$ , here around 45 Å. This implies that if HD would consist 100% from ordered domains then DD would be only 5% ordered; would HD be 20% ordered then DD would be only 1% ordered. (This example does not say that we really have a 100% ordered sample!). That would say the DD sample is practically an ideal Gaussian coil candidate with  $R_g \approx 298$  Å, scattering into a very small Q range inaccessible to our measurement. By comparison with the HD sample it scatters only little i.e. 1/20 into the wide angular region. All the other samples show ordered domains in the range of a domain size of up to 60 Å in the direction a packing of the chains and of 12 to 14 Å along the chains. This gives 5 to 6 monomers regularly arranged as we found exactly by diffractive methods in the wide angular scattering already. We were also able to explain, albeit qualitatively, the results of spin polarization analysis measurements on amorphous poly (methyl metacrylate) sample by assuming a short range order of 5 - 6 monomers [3]. These numbers correspond to flat discs which would give the above curved Guinier plot. In the light of these findings it is interesting to see the respective Kratky plots for the different samples, especially for DD. The big difference in the scattering from the DD sample with all the other ones which we believe to be due to the presence of hydrogen in the DD sample (this would destroy our calibration procedure) would in this case be caused by a higher amorphicity of this sample. We recall that in the wide-angle investigation of the amorphous background of DD we found the best agreement for the calculations of  $\langle |F_M|^2 \rangle - \langle F_M \rangle^2$  stacking up regularly two monomers.

A comment on another essential test is in order here. This experiment was aimed at claryfying a belief that the ionic clusters are destroyed by the presence of water which changes the position and shape of the monomer peak. For some samples we have compared spectra taken at room temperature with those after annealing for 24 hours at 115°C. The heating process was carried out in situ in a special furnace, the scattering was monitored continuously and nothing else was altered in the instrumental set-up. An example of such a measurement for the neutral HH sample is shown in figs.8.1 and 8.2. There are some small peaks visible at 0.09, 0.126, 0.16 Å<sup>-1</sup> before heating and at 0.063, 0.1, 0.135 Å<sup>-1</sup> after heating as described. The peaks observed become more pronounced by heating and they are shifted to smaller Q values. The interpretation of the maxima in the small angular region is not unique (cf.[17] pp.140-148), but they indicate a regularity corresponding to

these  $Q$  values, which change by heating. One can try to interpret it as a sort of long period. The corresponding long periods would be 69.8 Å, 49.8 Å and 39.3 Å before heating and 99.7 , 62.8 , and 46.5 Å after heating indicating an increase of "clusters" by heating, which sounds plausible. These sizes are of the same order as the larger radii of gyration which indicates a correlated arrangement of the observed crystalline microdomains. The small radius of gyration is not defined in the HH sample because of these peaks, which forbid to find a well defined slope in the wider angular part of low  $Q$  scattering in fig.8.2. The contribution  $\langle N \rangle$  of the monomer units to the parts with high  $R_g$  decreases simultaneously by the heating indicating an increase of the amorphous part.

The question which one asks in connection with ionomers is whether there can be found special structures like clusters with a long period, yielding maxima in the scattering curves. These peaks seem to have somehow similar properties as the so called ionomer peaks [18], but here they are found in samples where one has no ions . Such 'clustering' with a regular period seems to be also possible in the normal parent polymer and obviously cannot be due to an ionic charge in this case.

### 8.2.3 Kratky plots

The radius of gyration is a measure of the square of the end to end distance of the chain [19]. (see also chapter 1.3.1.1 on page 5)

$$\vec{r} = \sum_{i=1}^n \vec{\ell}_i \quad (8.7)$$

with  $\vec{\ell}_i$  = vector from the  $i - 1$  to  $i^{th}$  member of the chain. Then

$$r^2 = \sum_{i=1}^n \ell_i^2 + 2 \sum_{0 < i < j \leq n} \vec{\ell}_i \cdot \vec{\ell}_j \quad (8.8)$$

and  $r^2$  averaged

$$\langle r^2 \rangle = n\ell^2 + 2 \sum_{i < j} \langle \vec{\ell}_i \cdot \vec{\ell}_j \rangle \quad (8.9)$$

For a chain with  $\ell = |\vec{\ell}_i|$  fixed for all  $i$  and with all bond angles equally probable one gets  $\langle \vec{\ell}_i \cdot \vec{\ell}_j \rangle = 0$ . Hence

$$\langle r^2 \rangle = n\ell^2$$

and the radius of gyration

$$R_g^2 = \frac{1}{n+1} \sum_{i=0}^n s_i^2 = \frac{1}{(n+1)^2} \sum_{0 \leq i < j \leq n} r_{ij}^2 \quad (8.10)$$

with  $\vec{r}_{ij} = \vec{s}_j - \vec{s}_i$  with  $\vec{s}_i$  = vector of the atom number  $i$  in the system of inertia of the chain. For the above system with  $\langle r^2 \rangle = n\ell^2$  one obtains  $\langle r_{ij}^2 \rangle_0 = |j - i| \cdot \ell^2$  and therewith

$$\langle R_g^2 \rangle = \frac{\ell^2}{(n+1)^2} \sum_{0 < i < j \leq n} (J - i) \quad (8.11)$$

$$\frac{\langle R_g^2 \rangle_0}{n\ell^2} = \frac{1}{6} \frac{n+2}{n+1} \xrightarrow{n \rightarrow \infty} \frac{1}{6} \quad (8.12)$$

$$\langle R_g^2 \rangle = \frac{1}{6} \langle r^2 \rangle_0 \quad \text{for the freely jointed chain (Debye)} \quad (8.13)$$

If one assumes that the chain units are effectively point scatterers with the points corresponding to the scattering power  $\langle F_M \rangle^2$  for one monomer, then the structure factor of one chain is

$$\left. \frac{\partial \sigma}{\partial \Omega} \right|_{chain} = \frac{\partial \sigma / \partial \Omega}{\langle F_M \rangle^2} = F_{chain}(Q) = \frac{1}{N^2} \left| \sum_{j=1}^N e^{i\mathbf{Q} \cdot \mathbf{R}_j} \right|^2 \quad (8.14)$$

For an assembly of non-interacting chains, one obtains the average structure factor

$$\langle F_{chain} \rangle = \left\langle \frac{1}{N^2} \left| \sum_{j=1}^N e^{i\mathbf{Q} \cdot \mathbf{r}_j} \right|^2 \right\rangle \quad (8.15)$$

$$= \frac{1}{N^2} \sum_{i,j=1}^N \langle e^{i\mathbf{Q} \cdot \mathbf{r}_{ij}} \rangle \quad (8.16)$$

$$= \frac{1}{N^2} \sum_{i,j=1}^N e^{-Q^2 \langle r_{ij}^2 \rangle / 6} \quad (\text{isotropy}) \quad (8.17)$$

$$= \frac{1}{N} + \frac{2}{N} \sum_{k=1}^N \left(1 - \frac{k}{N}\right) e^{-Q^2 \langle r_k^2 \rangle / 6} \quad (8.18)$$

For a chain which is freely jointed  $\langle r_k^2 \rangle = k\ell^2$  and with

$$z = \frac{1}{6} Q^2 M \ell^2 \quad x = \frac{k}{N} \quad \frac{1}{N} \sum_{k=1}^N = \int_{1/N}^1 dx$$

one obtains for the structure factor of the chain

$$F_{chain}(Q) = D(Q) = 2 \int_{1/N}^1 (1-x) e^{-zx} dx + \frac{1}{N} \quad (8.19)$$

$$\approx 2 \int_0^1 (1-x) e^{-zx} dx = \frac{2}{z^2} (e^{-z} - 1 + z) \quad (8.20)$$

which goes back to Debye [20]. Finally

$$D(Q) = \frac{2}{Q^2 R_g^2} \left( e^{-QR_g} - 1 + QR_g \right) \quad (8.21)$$

with  $R_g = \frac{1}{6} N \ell^2$ , a relation which describes in a good approximation the scattering by real polymer chains.

On the basis of this equation the Kratky plot serves to determine  $R_g$  by plotting the product of  $Q^2$  with the scattering cross section  $\partial \sigma / \partial \Omega$  as a function of  $Q$ . This curve should show a plateau of the height proportional to  $2/R_g^2$  (see schematic curve 1.3 on page 13). Fig. 8.4 gives the Kratky plots of our samples DH, HD, DD and the two HH measurements. The extent of the plateaus in  $Q$  and the heights are the interesting parameters here. The supposition that there are no interchain correlations is certainly not fulfilled as discussed in the section on Guinier plots. Nevertheless we can use the plot and see, what it gives. Frequently one concludes from the presence of the plateau the existence of a Gaussian coil and excludes all other possibilities. In fig. 8.4 some plateau regions are clearly visible. We have both order and plateaus, which seems an apparent contradiction if one deduces the presence of a Gaussian coil from the existence of Kratky plateaus. Apparently there exist also other types of structure, which could cause a plateau. One can think of a generalised Kratky plot, which can be used to find  $Q$ -regions, where the scattering is a function of a certain power of  $Q$ , for example a power  $Q^{1/\nu}$  with  $\nu$  = excluded volume exponent as in Rawiso et al. [16].

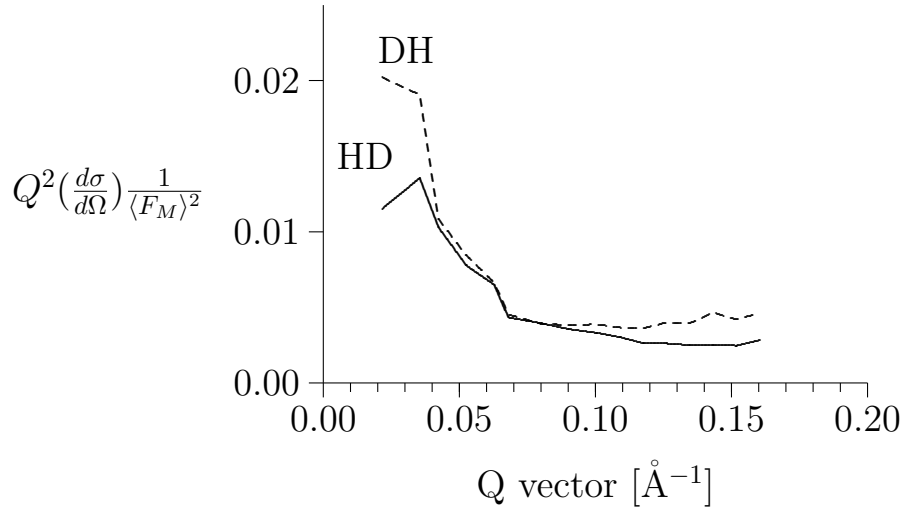


Figure 8.4: Kratky plots of the samples DH,HD measured with the set-up on D7

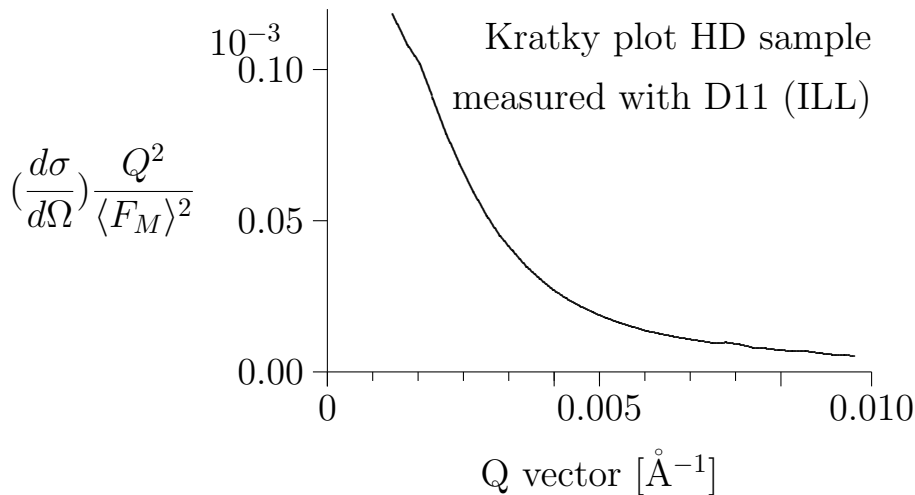


Figure 8.5: Kratky plot of the measurement of HD using D11 of the ILL. This shows, that in this region the chains cannot be regarded as scattering from a random coil . Normally atactic polystyrene is the school book example of a random coil, but this is valid in polystyrene in a theta solvent or the melt.

Rawiso et al. use also other models which give a plateau region in a generalized Kratky plot. Respective characteristic quantities for the usual Kratky plot are listed in table 8.2. We assume that the two clearly visible regions of different height in the Kratky plot correspond to two different plateaus and thus we get two different  $R_g$ 's, a small and a large one. Here the small one belongs to the small  $Q$  values contrary to the results from the Guinier plot. This comes from the fact, that the height of the plateau is proportional to  $2/R_g$  with the factor of proportionality equal to  $\langle N \rangle$ , the average number of monomers contributing to the small angle scattering. Assuming that  $R_g$  is the same as in the Guinier plots one gets a  $\langle N \rangle$ , which is also given in the table and which is also another than in the Guinier plots.

#### 8.2.4 Zimm plots

The Zimm plot uses a further evaluation of the Debye structure factor used in the Kratky plot. The Debye function  $D(Q)$  gives only the probability to find a segment of the **same** molecule (chain). Zimm extended this to the inclusion of the probability of finding a segment of a **different** molecule



Table 8.2: **Evaluation of the Kratky plots**

sample	$\frac{2}{R_g}$	$R_g[\text{\AA}]$ small Q	$R_g[\text{\AA}]$ larger Q	$V_{amorphous}$	$\langle N \rangle$
HH	no plateau	no plateau			
DH	0.004077	10	$22.15 \pm 4.6\%$	14.3 %	2.23
HD	0.002824	12	$26.61 \pm 7\%$	22.5 %	1.75
DD	0.0004695	36	$65.3 \pm 3.5\%$	89.8 %	0.60

(chain). This leads to an intensity formula of the form

$$I(Q) \propto n_W \left( \frac{\partial \sigma}{\partial \Omega} \right)_{monomer} \quad (8.22)$$

$$\propto [D(Q) + kD(Q)^2] \quad (8.23)$$

with  $D(Q)$  = Debye function , eq.(8.21). According to Zimm for small Q values this can be written in the form [21]

$$\frac{1}{n_W \left( \frac{\partial \sigma}{\partial \Omega} / \langle F_M \rangle^2 \right)} = \frac{1}{n_W} + \frac{1}{n_W} \frac{\langle R_g^2 \rangle_z}{3} Q^2 \quad (8.24)$$

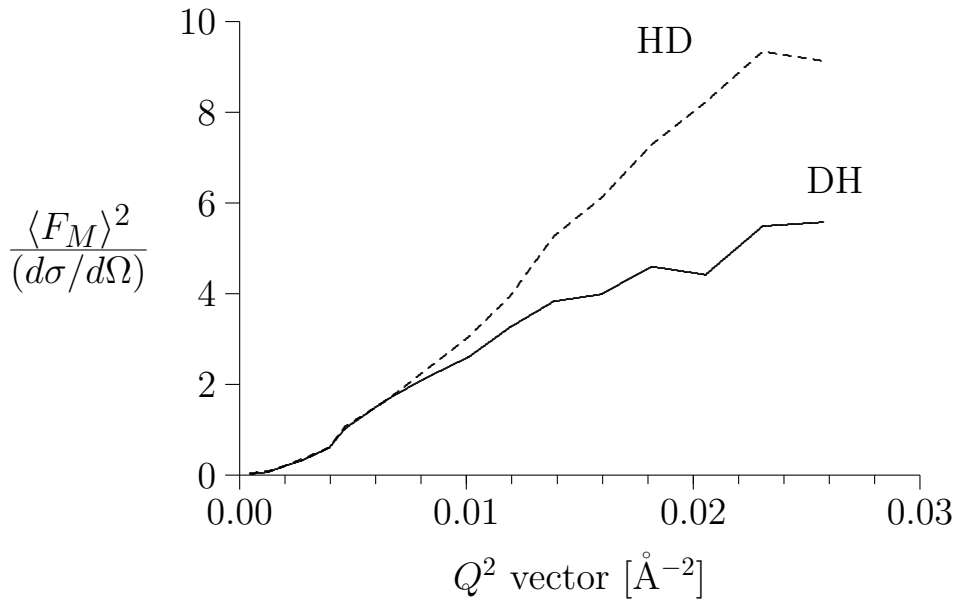


Figure 8.6: Zimm plots of the results for the samples DH,HD

By plotting the term  $(n_w(\partial\sigma/\partial\Omega)/\langle F_M \rangle^2)^{-1}$  as a function of  $Q^2$  one should get a straight line where the slope contains the z-average of the radius of gyration  $\langle R_g^2 \rangle_z$  and the value of the weight average of the polymerisation  $n_w$  from the extrapolation to  $Q^2 = 0$ . This is the Zimm plot shown in fig. 8.6 for the samples DH and HD. In table 8.3 the extrapolated values  $n_w$  of the small Q values and the  $\sqrt{\langle R_g^2 \rangle_z}$  for low and high Q are listed. Since Q is relatively high, one cannot expect a straight line in the whole range with the same slope also holding for the higher Q values [22]. For spheres, coils and rods one expects strong deviations from a straight line in the higher Q range, where an extrapolation to  $Q^2 = 0$  would give negative values. Only in the smaller angular region an extrapolation to  $Q=0$  is possible yielding  $n_w$ . We use again the slope in both regions to determine a  $\sqrt{\langle R_g^2 \rangle_z}$ . This will allow us to see, whether the sulfonation will change something. The  $R_g$  behave similarly as in the Kratky plot. In the Kratky plot one should also use the here determined  $n_w$

Table 8.3: Evaluation of the Zimm plots

sample	$\langle R_g \rangle_z$ low Q	$\langle R_g \rangle_z$ high Q	$n_W$
HH not	113.1 Å		19.75
HH heat			12.22
DH	130 Å	21 Å	42.46
HD	100 Å	36.4 Å	24.3
DD	58.6 Å	82.7 Å	1.52

to get the value of the  $R_g$  in the small Q region. But we let it as it is determined only from the Kratky plot, which does not allow to determine  $n_w$ . In the Kratky plot the  $R_g$  values in the small Q region would be too small also in the case of this correction.

The Zimm plot should be independent of the conformation of the chains, but what would this say in our case? The different slopes in the different Q regions certainly can again be correlated to the shape of the scattering units which can be either density fluctuations or the structure factor. The Zimm plot seems to give an average of them both, whereas the Kratky plot filters out the structure of the chain pieces, which are randomly distributed. The values from the Zimm plot correspond to those of the Guinier plot.

### 8.2.5 Porod plots

The Porod method determines the specific surface  $S_{sp}$  per unit volume, which allows to calculate the inner surface by the relation  $S = S_{sp} \cdot V$ . To determine  $S_{sp}$  one needs

$$K = \lim Q^4 I_{corr}(Q) = const. \quad (8.25)$$

To get this one plots  $I(Q)Q^4$  over  $Q^4$  (see fig.8.7):

$$\frac{\partial \sigma}{\partial \Omega}(Q) \xrightarrow{Q \rightarrow \infty} \frac{K}{Q^4} + U \quad (8.26)$$

U is determined from the slope of the straight line in fig.8.7 and K is the axis section. If the surfaces are not sharp but have a non sharp transition, one would have to use a damping function  $H^2(Q)$ . With the integral

$$Q_P = \int_0^\infty Q^2 \cdot (I(Q) - U) dQ \quad (8.27)$$

$$= \int_0^{Q_{max}} Q^2 (I(Q) - U) dQ + \frac{K}{Q_{max}} \quad (8.28)$$

because

$$\int_{Q_{max}}^\infty \frac{K}{Q^4} dQ = K \int_{Q_{max}}^\infty \frac{1}{Q^2} dQ \quad (8.29)$$

$$= \left[ -\frac{1}{Q} \right]_{Q_{max}}^\infty \quad (8.30)$$

$$= \frac{K}{Q_{max}} \quad (8.31)$$

and the relative part of the scattering units in the volume c one gets  $S_{sp}$  by:

$$S_{sp} = \pi c(1 - c) \frac{K}{Q_P} \quad (8.32)$$

The values  $U, K, Q_P$  and  $S_{sp}$  for the samples are given in table 8.4 as determined from the small angle scattering measurements. As we have no problem with an ambiguous subtraction of the incoherent background since we measure it with the spin flip method, we know that the  $U$  found here must arise due to the sample. It probably results from density fluctuations in the amorphous and crystalline phase, whose Fourier transform is given by  $U \cdot Q^4$  in nearly all our samples except HH after heat treatment, where one seems to have even a higher power of  $Q$  behaviour. But the number of points in our measurement is too small to allow more exact conclusions.

One conclusion, which can be drawn from these evaluations is that these density fluctuations in the HH sample change by the heating process of 24 hours.  $U$  becomes smaller. The Porod plots show also, that not only the HH samples have small peaks in the small angle scattering region, which changed by the heating. It reveals similar peaks also in the DD sample but not in the HD and DH samples. These peaks indicate a periodicity in these density fluctuations, which is strong in the HH sample and becomes stronger by the heat treatment. But it is also visible in the DD sample in the Porod plot.

It will be very interesting to see how the sulphonation in the ionomers changes this behaviour.

The Porod plot should extend over the whole  $Q$  range. As we have measured up to  $Q=3.8 \text{ \AA}^{-1}$ , we shall try to evaluate also the data of this whole range to obtain a feeling for the behaviour there by the respective parameters. The values can again be approximated by a straight line, even for HH. In this region one sees no difference between the different heat treatments for the HH samples. The DH and DD samples show strong deviations from the straight line similar to those of the HH sample in the small angle scattering region which correspond to the periodicities found above in the crystallinity interpretation, HH and HD do not show this so clear. The values obtained for  $U_{wide}$  are given in Table 8.4. Fig. 8.7 show for each sample the Porod plot  $Q^4(\partial\sigma/\partial\Omega)/\langle F_M(0) \rangle^2$  over  $Q^4$ , fig. 8.8 show it together with  $Q^4((\partial\sigma/\partial\Omega)/\langle F_M(0) \rangle^2 - U)$  over  $Q^4$ , to obtain the Porod invariant  $K$ , and with the function  $Q^2((\partial\sigma/\partial\Omega)/\langle F_M(0) \rangle^2 - U)$  for the determination of  $Q_P$ , and with the respective wide angular Porod plot again for each sample. In the wide angular region the above described method to determine  $K$ ,  $Q_P$  and  $S_{sp}$  does not work. There one would need  $\langle F_M(Q) \rangle^2$  as a function of  $Q$ .

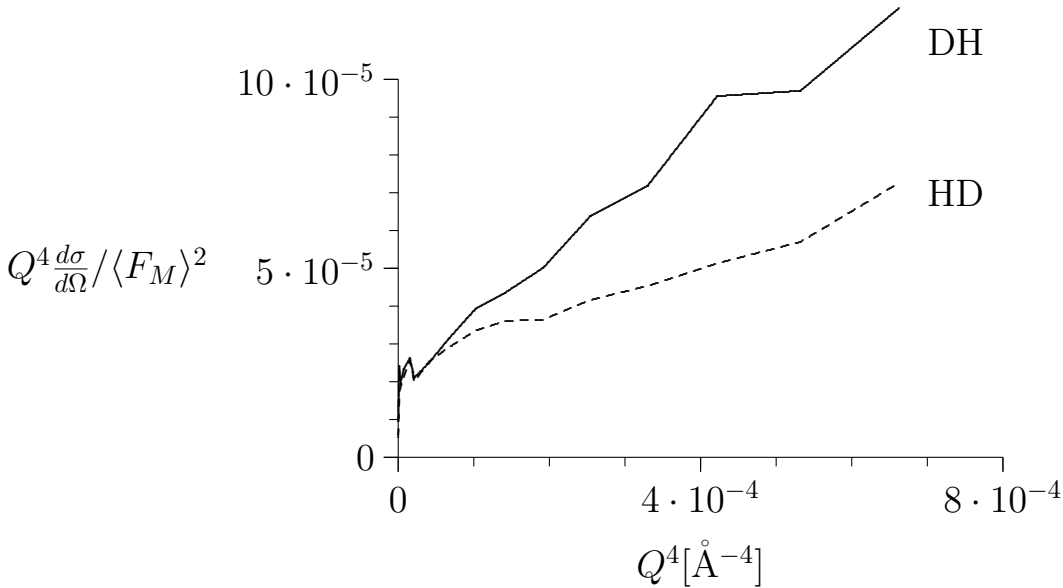


Figure 8.7: Porod plots of the results for the samples DH and HD

With this value of  $S_{sp}$  and the estimation of the crystalline regions given by  $1 - c_{amorph}$  of table 8.4 and the  $R_g$  for the height and radius of the cylinder from the Guinier plot, we can calculate the

Table 8.4: **Evaluation of the porod plots**

sample	U	K [Å <sup>-5</sup> ]	$Q_P$ [Å <sup>-4</sup> ]	$K/Q_P$ [Å <sup>-1</sup> ]	$c_{amorph}$ [%]	$S_{sp}$ [Å <sup>-1</sup> ]	$U_{wide}$
HH bef.	0.550						0.915
HH aft.	0.127						
DH	0.147	$0.228 \cdot 10^{-4}$	$1.65 \cdot 10^{-4}$	0.138	14.3	0.0532	0.136
HD	0.060	$0.252 \cdot 10^{-4}$	$1.82 \cdot 10^{-4}$	0.138	22.5	0.0757	0.095
DD	0.012	$0.377 \cdot 10^{-5}$	$2.49 \cdot 10^{-5}$	0.151	89.8	0.0435	0.022

surface to volume relation of the respective cylinders by

$$V_{sp}^{(theor)} = (1 - c_{amorph}) \frac{Area}{Volume} \quad (8.33)$$

$$= (1 - c_{amorph}) (R_{g1}^2 + R_{g1}R_{g2}) \frac{2\pi}{R_{g1}^2 R_{g2} \pi} \quad (8.34)$$

giving  $S_{sp}^{DD} = 0.011$ ,  $S_{sp}^{HD} = 0.074$ ,  $S_{sp}^{DH} = 0.088$ , which is not so far from what we got from the Porod plot.

### 8.3 Discussion

If not corrected for hydrogen content the interpretation would show quite clearly, why the differences with DD show other results than all the others. It would then come from the high part of DD which is amorphous, so that in the wide angle scattering the crystalline contributions are much too low in comparison to the other samples. It is also clear that the difference DH-HD is the most reliable, because the characteristics of these both samples obtained by small angle scattering are the most similar. The HH sample has a special behaviour in the small angular region in so far as the larger units giving small angle scattering seem to show some additional regularity. But globally (i.e. for the  $R_g$ 's and  $n_w$  values) it is not so different from the others, so that also these differences in the wide angular region are reliable. But to have such an amorphous sample as DD shows, that one has to be careful to generalize results obtained with one sample and say that atactic polystyrene is always amorphous or always crystalline.

Thus we have examined a complete set of well defined samples with a great variety of structural properties ranging from high degree of order in domains whose size we determined to perhaps strong amorphousness. This set of well characterized samples (no detectable incomplete deuteration or similar sources of error from the isotopic constitution) gave us the possibility to characterize them by neutron wide- and small-angle scattering in a very complete fashion. We have extracted many physical parameters, which can be compared to those obtained for the respective sulphonated samples.

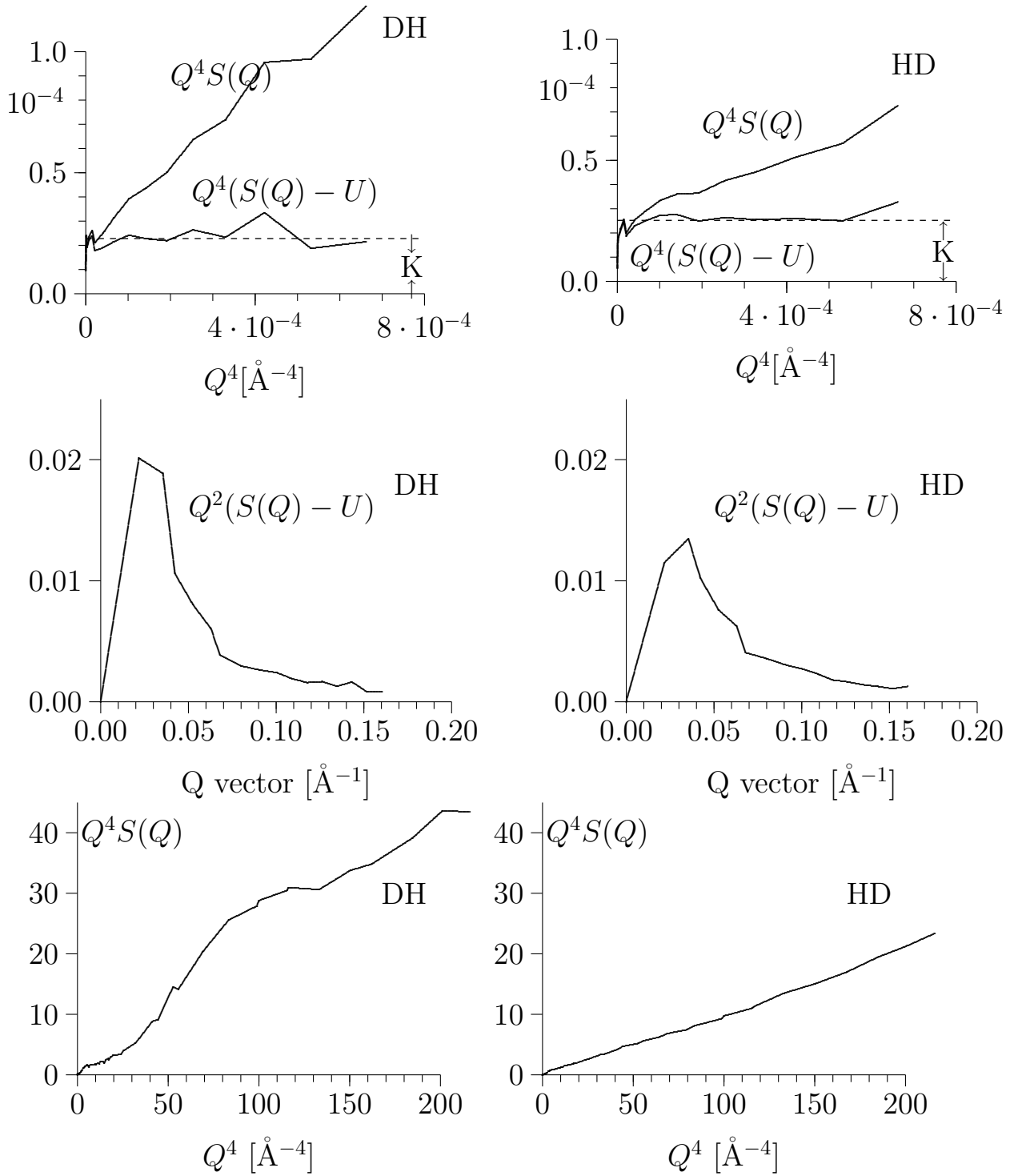


Figure 8.8: Porod plots  $S(Q)Q^4$  over  $Q^4$  in the small angular and wide angular region, plots of  $(S(Q) - U)Q^4$  over  $Q^4$ , plots of  $(S(Q) - U)Q^2$  over  $Q$  (for the integral  $Q_P$ ), only in the small angular region.

# Bibliography

- [1] A.Eisenberg, *Macromolecules*, 3,147(1970)
- [2] *JMS-Rev. Macromol.chem.phys.:*C28,65-98(1988)
- [3] B.Gabrys, J.S.Higgins and O.Schärfp, *J.Chem.Soc.Far.Trans.I* 82,1929(1986)
- [4] *The yellow book*, ILL(1988)
- [5] O.Schärfp,*Physica B*156&157,631(1989) O.Schärfp,*Physica B*156&157,639(1989)
- [6] O.Schärfp,O., *Proceeding Series:neutron scattering in the ninetieth*, p.85. Vienna: Int.Atomic Energy Agency 1985
- [7] O.Greis, T.Asano, J.Xu and J.Petermann, *Z.Kristallographie* 182,58(1988)
- [8] C.W.Bunn, E.R.Howells, *J.Polym.Sci.*18,307(1955)
- [9] *International Tables for X-Ray Crystallography*, Th.Hahn (editor), Birmingham I. 1952,1962,1988
- [10] Reinhard X. Fischer, *STRUPLO* (1984), Mineralogisches Institut der Universität, Am Hubland, D-8700 Würzburg, FRG
- [11] K.Yvon, W.Jeitschko, E.Parthe, *J.Appl.Cryst.* 10,73(1977)
- [12] B.K. Vainshtein, *Diffraction of X-rays by chain molecules*, Elsevier, Amsterdam-London-New York 1966
- [13] A.Guinier, *X-Ray Diffraction*, W.H.Freeman, San Francisco 1963
- [14] M.J.Buerger, *Vector space*, John Wiley, New York,London,Sydney 1967
- [15] J.S.Higgins and R.S.Stein, *J.Appl.Cryst.* 11,346(1978)
- [16] M.Rawiso, R.Duplessix and C.Picot, *Macromolecules* 20,630(1987)
- [17] A.Guinier and G.Fournet, *Small-angle scattering of X-rays*, John Wiley, New York 1955
- [18] A.Eisenberg and M.Pineri, Eds., *Structure and properties of ionomers*, NATO ASI series C198, D.Reidel, Dordrecht 1987
- [19] P.J.Flory, *Statistical mechanics of chain molecules*, Interscience Publishers, New York 1969
- [20] Debye, *Formel fuer Kratky plot*
- [21] Zimm, J. *Chem. Phys.*,16,1093(1948)
- [22] B.Gabrys, P.E.Tomlins, in: *Encyclopedia of Polymer Science and Engineering* (edts. Mark-Bikales-Overberger-Menges) vol.15,p.25 (1989); M.B.Huglin, ed., *Light Scattering from polymer solutions*, Academic press, London 1972





## Chapter 9

# Multiple scattering correction in polymer neutron scattering

### 9.1 Overview of methods for multiple scattering correction in neutron scattering

Models or in general theoretical predictions comprise always single scattering without absorption. Real measurements however cannot avoid multiple scattering and absorption. To be able to compare the latter with theoretical predictions the data evaluation has to include correction for multiple scattering and absorption. Often it is tried to experimentally eliminate multiple scattering effects. This is difficult if not impossible to do as multiple scattering effects are quite important even if the sample under study is as thin as is practically feasible. Thin sample experiments are considerably more expensive to perform than experiments using thicker samples. With lower counting rate experiments also background problems become more important. One is better off with somewhat thicker samples. Then one is in a position to take better quality data in a given time. These need then careful multiple scattering corrections but this would be needed in any case also for thin samples. Slaggie [1] and Bischoff [6, 7] have investigated multiple scattering as a function of sample thickness and have shown that to draw conclusions from an extrapolation to zero thickness can give erroneous conclusions. Sears [5] also demonstrates the well known result that insensitivity of the observed scattering per unit volume to changes in sample thickness is not a good test for the absence of multiple scattering. Neither is high sample transmission  $x$  (e.g.  $x=0.1$ ) in which case it depends much on the sample geometry (other for spherical (using the thumb rule of [3]  $\frac{1}{2}x^2 = 0.05$ ), but for a plane slab it is 0.16, or by use of absorbing spacers it is even 0.02, so such a thumb rule is of no use). There exist three reliable correction methods for multiple scattering.

#### 9.1.1 Method of Blech and Averbach

The simplest is that following Blech and Averbach [2] including only isotropic elastic double scattering in cylindrical samples. In this method a numerically calculated table published in [2] is used to correct for absorption and double scattering (see table 9.1). To obtain from a measured intensity  $I_{sample}^{exp}$  for the sample and  $I_{vanadium}^{exp}$  for vanadium the differential cross section in barn per sterad corrected for multiple scattering and absorption with the method of Blech and Averbach one can proceed in the following way. The sample must have the form of a cylinder. Then

$$\left(\frac{d\sigma}{d\Omega}\right)_{exp} = \frac{\sigma_{inc}^{vana}}{4\pi} \frac{(nR^2)_{vana}}{(\bar{n}R^2)_{sample}} \frac{A_{sample}^*(1 - \delta'_{sample})}{A_{vana}^*(1 - \delta'_{vana})} \frac{I_{sample}^{exp}}{I_{vana}^{exp}} \quad (9.1)$$

Table 9.1: **Coefficient  $\delta$  for secondary scattering**

R/h	$\mu R=0.1$	0.2	0.3	0.4	0.5	0.6	0.7	0.8	0.9
0.10	0.1049	0.1922	0.2657	0.3286					
0.12	0.1023	0.1878	0.2600	0.3212	0.2742				
0.14	0.1001	0.1841	0.2553	0.3157	0.3670	0.4118			
0.16	0.0981	0.1809	0.2512	0.3110	0.3616	0.4046	0.4422		
0.18	0.0963	0.1780	0.2475	0.3067	0.3570	0.3933	0.4349	0.4661	
0.20	0.0946	0.1752	0.2440	0.3028	0.3527	0.3947	0.4295	0.4585	
0.22	0.0931	0.1726	0.2407	0.2991	0.3488	0.3905	0.4250	0.4530	0.4751
0.24	0.0916	0.1701	0.2376	0.2955	0.3450	0.3866	0.4210	0.4486	0.4701
0.26	0.0902	0.1677	0.2345	0.2921	0.3413	0.2829	0.4172	0.4447	0.4657
0.28	0.0888	0.1654	0.2316	0.2887	0.3377	0.3792	0.4136	0.4411	0.4619
0.30	0.0895	0.1631	0.2287	0.2854	0.3342	0.3756	0.4100	0.4376	0.4586
0.40	0.0819	0.1536	0.2165	0.2715	0.3193	0.3605	0.3953	0.4239	0.4461
0.50	0.0768	0.1445	0.2044	0.2573	0.3036	0.3439	0.3785	0.4073	0.4303
1.00	0.0615	0.1174	0.1682	0.2143	0.2560	0.2937	0.3273	0.3571	0.3830
2.00	0.0425	0.0818	0.1181	0.1516	0.1825	0.2110	0.2370	0.2607	0.2820
3.00	0.0333	0.0644	0.0933	0.1203	0.1454	0.1687	0.1904	0.2103	0.2286
4.00	0.0277	0.0535	0.0778	0.1005	0.1218	0.1418	0.1604	0.1776	0.1936
5.00	0.0237	0.0460	0.0670	0.0867	0.1053	0.1227	0.1391	0.1543	0.1685

source: [2]

using  $\rho$ =density,  $N_L$ =Loschmidt number (number of particles per mol),  $M$ =molecular weight,  $c$ =concentration,  $\vartheta$ =scattering angle and

$$n = \rho \frac{N_L}{M} \quad (9.2)$$

$$\bar{n} = (1 - c)n_{host} + c \cdot n_{imp} \quad (9.3)$$

$$\sigma_s = \bar{\sigma}_{inc} + \bar{\sigma}_N + \bar{\sigma}_M \quad (9.4)$$

$$\bar{\sigma}_N = 4\pi c(1 - c)(\Delta b)^2 \quad (9.5)$$

$$\bar{\sigma}_M = 3\pi c(1 - c) \cdot 0.27(\Delta\mu_M)^2 \quad \text{for } H=0 \quad (9.6)$$

$$= 4\pi c(1 - c) \cdot 0.27(\Delta\mu_M)^2 \quad \text{for } H=H_{max} \quad (9.7)$$

$$\bar{\sigma}_{inc} = (1 - c)\sigma_{inc}^{host} + c\sigma_{inc}^{imp} \quad (9.8)$$

$$\sigma_t = \sigma_s + \sigma_a \quad (9.9)$$

$$\sigma_a(\lambda) = \sigma_a(\lambda_0) \cdot \frac{\lambda}{\lambda_0} \quad (\text{e.g. } \lambda_0 \text{ from Bacon's book is } 1.08 \text{ \AA} [3]) \quad (9.10)$$

$$\delta' = \frac{\sigma_s}{\sigma_t} \delta \quad (9.11)$$

$$\delta = \delta\left(\frac{R}{h}, \mu R\right) \quad \text{see table 9.1} \quad (9.12)$$

$$\mu = n \cdot \sigma_t \quad (9.13)$$

$$\sigma_{inc}^{vana} = 5.187 \text{ barn} \quad (9.14)$$

$$A^* = 1/A \quad (9.15)$$

$$A(\vartheta) = \exp[-(a_1 + b_1 \sin^2 \vartheta)(\mu R) - (a_2 + b_2 \sin^2 \vartheta)(\mu R)^2] \quad (9.16)$$

$$a_1 = 1.7133 \quad (9.17)$$

$$a_2 = -0.0927 \quad (9.18)$$

$$b_1 = -0.0368 \quad (9.19)$$

$$b_2 = -9.3750 \quad \text{source: [4]} \quad (9.20)$$

For  $I^{exp}$  one takes the measured count rate corrected for background as

$$I^{exp} = (N - N_{Cd}) - A(0) \cdot (N_{empty} - N_{Cd}) \quad (9.21)$$

### 9.1.2 Method of Sears

A second more sophisticated method is described by Sears [5]. This consists of an analytical method for a known  $S(Q, \omega)$ . He introduced this analytical method to give some physical understanding of the nature of multiple scattering and as a means for approximate estimates if multiple scattering is small. He uses integrals of the form

$$s_2(\mathbf{k}_0, \mathbf{k}) = \frac{n\sigma_0}{4\pi} \int d\Omega_1 d\epsilon_1 S(\mathbf{Q}_1, \omega_1) S(\mathbf{Q}_2, \omega_2) H_2(\mathbf{k}_0, \mathbf{k}_1, \mathbf{k}) \quad (9.22)$$

$$s_j(\mathbf{k}_0, \mathbf{k}) = \left\{ \frac{n\sigma_0}{4\pi} \right\}^{j-1} \int \int \dots \int d\Omega_1 d\epsilon_1 \dots d\Omega_{j-1} d\epsilon_{j-1} S(\mathbf{Q}_1, \omega_1) \dots S(\mathbf{Q}_j, \omega_j) H_j(\mathbf{k}_0, \dots, \mathbf{k}_{j-1}, \mathbf{k}_j) \quad (9.23)$$

for double scattering resp. j-fold scattering.  $\mathbf{k}_1$  (or  $\mathbf{k}_j$ ) is the momentum of the neutron in the intermediate state.

$$\begin{aligned} \mathbf{Q}_1 &= \mathbf{k}_0 - \mathbf{k}_1 & \omega_i &= \epsilon_{i-1} - \epsilon_i \\ \mathbf{Q}_2 &= \mathbf{k}_1 - \mathbf{k} & \mathbf{Q}_1 + \mathbf{Q}_2 &= \mathbf{Q} \\ \mathbf{Q}_i &= \mathbf{k}_{i-1} - \mathbf{k}_i & \sum_{i=1}^j \mathbf{Q}_i &= \mathbf{Q} \\ \omega_1 &= \epsilon_0 - \epsilon_1 & \omega_1 + \omega_2 &= \omega \\ \omega_2 &= \epsilon_1 - \epsilon \end{aligned}$$

The most difficult problem is the determination of  $H_2(\mathbf{k}_2, \mathbf{k}_1, \mathbf{k})$  or  $H_j(\mathbf{k}_0, \dots, \mathbf{k}_{j-1}, \mathbf{k})$  the second order or j order transmission factor, which depends on the form of the sample. In the paper [5] approximate procedures for an infinite plane slab, a thin slab, a thick slab, a sphere and a cylinder are derived and compared with results of Blech and Averbach [2]. He uses for this approximation that  $\delta = s_2(\mathbf{k}_0, \mathbf{k})/s_1(\mathbf{k}_0, \mathbf{k})$  is independent of  $\mathbf{k}_0$  and  $\mathbf{k}$  for a cylinder of radius r with the axis perpendicular to the scattering plane if  $a = 2\Sigma r \leq 1.6$  or for an infinite plane slab if  $a = \Sigma L \ll 1$ . This method allows to make simple predictions of certain geometries under the quasi-isotropic approximation. To show the sort of answers of Sears' method we show results for a cylindrical sample of diameter 2r and height d. This method yields an effective scattering function of

$$s(\mathbf{k}_0, \mathbf{k}) = H_1(\mathbf{k}_0, \mathbf{k}) [S(\mathbf{Q}, \omega) + \Delta \cdot R_2(\mathbf{k}_0, \mathbf{k})] \quad (9.24)$$

with

$$H_1(\mathbf{k}_0, \mathbf{k}) = 1 - \frac{16}{3\pi} n\sigma_s r + \frac{7}{4} (n\sigma_s r)^2 \quad (9.25)$$

the transmission

$$F(\mathbf{k}) = 1 - \frac{\pi}{2} n\sigma_s r + \frac{4}{3} (n\sigma_s r)^2 - \dots \quad (9.26)$$

$$\delta = \frac{\Sigma_2}{\Sigma} \left[ \frac{3}{4} \left\{ 1 - \cos \beta - I\left(\beta, \frac{2}{3}\Sigma d\right) \right\} + \frac{16}{9\pi^2 - 64} \left\{ \cos \beta - J\left(\beta, 2\left(\frac{3\pi}{4} - \frac{16}{3\pi}\right)\Sigma r\right) \right\} \right] \quad (9.27)$$

and

$$\Delta = \left( \frac{e^{2\delta} - 1}{2\delta} \right) - 1 \quad (9.28)$$

$$\Sigma = \Sigma_s + \Sigma_a \quad (9.29)$$

$$\Sigma_s = n\sigma_s \quad (9.30)$$

$$\Sigma_a = n\sigma_a \quad (9.31)$$

$$\tan \beta = \frac{2r}{d} \quad (9.32)$$

$$I(x, y) = \int_0^x \exp(-y \sec \theta) \sin \theta d\theta \quad (9.33)$$

$$J(x, y) = \int_x^{\pi/2} \exp(-y \operatorname{cosec} \theta) \sin \theta d\theta \quad (9.34)$$

$$R_2(\mathbf{k}_0, \mathbf{k}) \approx R(\mathbf{k}_0, \pi/2, \mathbf{k}) \quad (9.35)$$

$$R(\mathbf{k}_0, \pi/2, \mathbf{k}) = \frac{1}{2\pi} \int_0^{2\pi} d\phi_1 \int_0^\infty d\epsilon_1 S(\mathbf{Q}_1, \omega_1) S(\mathbf{Q}_2, \omega_2) \quad (9.36)$$

The numerical evaluation of this double integral is then all that is required to make a multiple scattering correction which is adequate for most purposes. Sears thinks that his approximate method represents a simple alternative to the Monte Carlo method for a sample partitioned with absorbing spacers and with high transmission in the plane of scattering.

### 9.1.3 Monte Carlo method

The most universal procedure for multiple scattering and absorption corrections are Monte Carlo programs, which were developed between 1970 and 1974 [6, 7] [8] [9]. We first describe the Monte Carlo program DISCUS [9] in a C version and compare it with the program of Copley [8]. Since none of these programs was initially developed for the correction of data from polarization analysis, we shall discuss simultaneously how Monte Carlo programs can be modified in a simple way to correct also data from polarization analysis.

## 9.2 Detailed description of a Monte Carlo program for multiple scattering correction

### 9.2.1 Some fundamental concepts of mathematical statistics

- Random variable: a variable which can assume more than one value (discrete or continuous range) but for which a value cannot be predicted.
- distribution of a random variable: gives the probability of a certain value (or a infinitesimal range of values)

$$g(u)du = P[u < u' < u + du]$$

- expectation value:  $E(f) = \int f(u)dG(u) = \int f(u)g(u)du$ 
  - with equipartition:  $E(f) = \frac{1}{b-a} \int_a^b f(u)du$
  - expectation of a variable u:  $E(u) = \int udG(u) = \int ug(u)du$
  - $E(cx + y) = cE(x) + E(y)$
- variance of a function or variable:  $V(f) = E([f - E(f)]^2) = \int [f - E(f)]^2 dG = E(f^2) - (E(f))^2$
- $V(cx + y) = c^2V(x) + V(y) + 2cE[(x - E(x))(y - E(y))]$
- Standard deviation = square root of variance
- covariance of x and y:  $E[(x - E(x))(y - E(y))]$

- correlation coefficient  $\rho(x, y) = \frac{E(xy) - E(x)E(y)}{\sqrt{V(x)V(y)}}$
- distributions:
  - discrete distributions: Poisson distribution  $P(r) = \frac{\lambda^r e^{-\lambda}}{r!}$
  - continuous distributions:
    - \* rectangular distribution:  $f(x) = \frac{1}{b-a}$
    - \* exponential distribution:  $f(x) = \lambda \exp(-\lambda x)$

### 9.2.2 Random number!generator

Monte Carlo method uses random numbers like those from the roulette in Monte Carlo. It seems to be a contradiction to generate random numbers by an arithmetic process. The random series generated by a arithmetic process is only pseudo random. It has the characteristic properties of real random series. We want to know

1. how to generate them
  - as fast as possible
  - without repetition
  - without correlation
2. which properties they have

#### 9.2.2.1 Generation of random numbers with rectangular distribution

One uses the uniform distribution of remainders of division. This one gets by

$$x_i = [ax_{i-1} + c] \bmod (m) \quad (9.37)$$

with properly chosen values a, c, m for a period of maximal length. This method is fast if the remainder is generated by the limitation of the bits in the computer after a multiplication with overflow. The multiplication can be replaced by arithmetic left shift corresponding to a properly chosen value m and the addition of c. If the numbers are properly selected the period can be  $\approx 2.1 \cdot 10^9$ . If the computer needs 2  $\mu$ sec for one random number, the series is repeating after 2000 seconds (see for examples [10], where a trick is described to avoid overflows in high-level languages.) One can gain CPU time if subroutines are avoided and the conversion into floating point number is avoided.

#### 9.2.2.2 Test for sequential correlation

Such a test is possible by filling a cubic lattice  $n(k_1, k_2, k_3)$  of  $L^3$  positions with three successive random numbers  $x_i$  in the following way. If for  $k_1 = 1 + x_i L$ ,  $k_2 = 1 + x_{i+1} L$ ,  $k_3 = 1 + x_{i+2} L$  the position  $n(k_1, k_2, k_3)$  is empty it will be filled, if it is already filled it remains filled. Such a process is binomial distributed and described by the probability of k successes with n trials given by

$$\binom{n}{k} p^k q^{n-k} \quad (9.38)$$

If the successes are uniformly distributed to  $L \cdot L \cdot L$  points with t repetitions one has 80000 trials with the probability  $p=1/(8000)$  for each position. This can be evaluated to show that less than one position should have no 1 after this process. Deviations of this show that the series is not uniformly distributed it has correlations. Marsaglia observed that random numbers from linear congruential generators fall mainly on hyperspaces. One can increase the number of hyperplanes by mixing two generators but one cannot avoid them.

### 9.2.3 Simulation of a trace of particles with collisions

Such a simulation can be applied for electrons in metals or semiconductors, atoms or molecules in a gas or liquid, which can itself be in rest or flowing, for ions in solution or in solids, for neutrons in the reactor or for neutrons in scattering experiments. Very often Monte Carlo programs are the only possibility of investigation of such systems, as they are not limited to certain geometries.

In this simulation we begin with incident particles, which are all parallel, have the same energy, have everywhere in the beam the same density (rectangular distribution). The sample has the form of a solid cylinder, plane slab (normal or inclined), or hollow cylinder. In such a sample

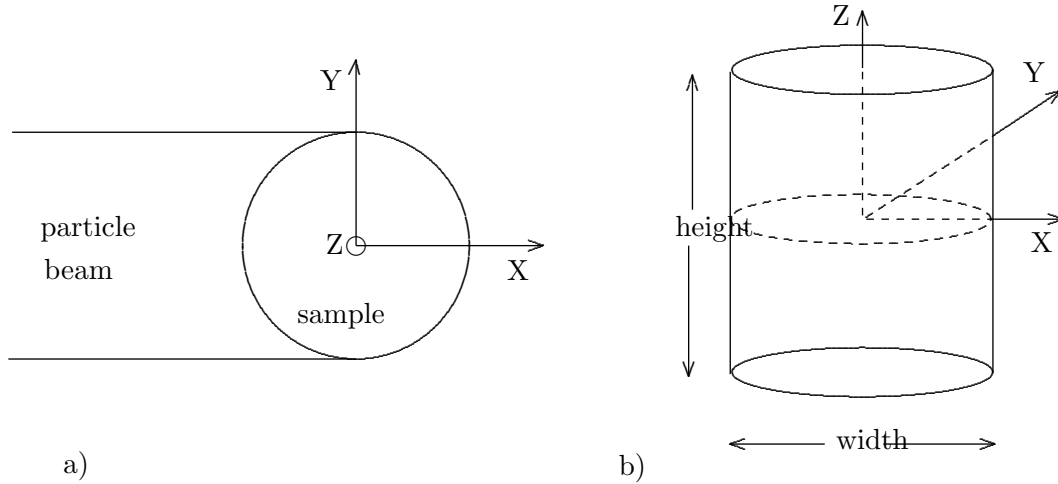


Figure 9.1: Geometry of the experiment, coordinates, sample size for cylindrical samples (hollow and solid)

neutrons are scattered not only once but twice and more. The scattering is also attenuated by absorption of neutrons. This is the result which is measured. What we look for is the law of single scattering. To be able to conclude this from the measurement we must be able to correct for multiple scattering and absorption for different  $Q$ ,  $\omega$  and spin. We have seen above that double scattering is essentially a convolution of the single scattering function with itself in  $Q$  and  $\omega$ . The result of such a convolution is a smoothed and flattened version of the single scattering function.

The following figures show some consequences of this smearing effect in  $\omega$ . Fig.9.2 shows single and double scattering in a simple model of an only incoherently scattering liquid. It shows that double scattering can become larger than single scattering, in a  $\omega$ -region where single scattering is weak. Fig.9.3 shows single scattering, double scattering and total scattering of a coherently scattering liquid, which shows in single scattering two maxima but in double scattering only one i.e. double scattering can show another pattern resulting from the broadening of the single peaks and the superposition of these broadened peaks. Absorption correction however only attenuates the peaks as is visible in fig.9.4, showing the effect of absorption for different absorption cross sections.

Some simple consequences from this behaviour can be drawn.

- If  $\sigma$  is neither  $Q$  nor  $\omega$  dependent (i.e. it is isotropic like it is in vanadium, then also multiple scattering is nearly isotropic. It is then also a relative constant fraction of the single scattering. Only the intensity of the incident beam is decreasing inside the beam as neutrons are scattered out of the beam on the way through the sample.
- If  $\sigma$  is anisotropic in  $Q$  or  $\omega$  then we do not have a constant fraction of the single scattering as multiple scattering. Then we can solve the problem

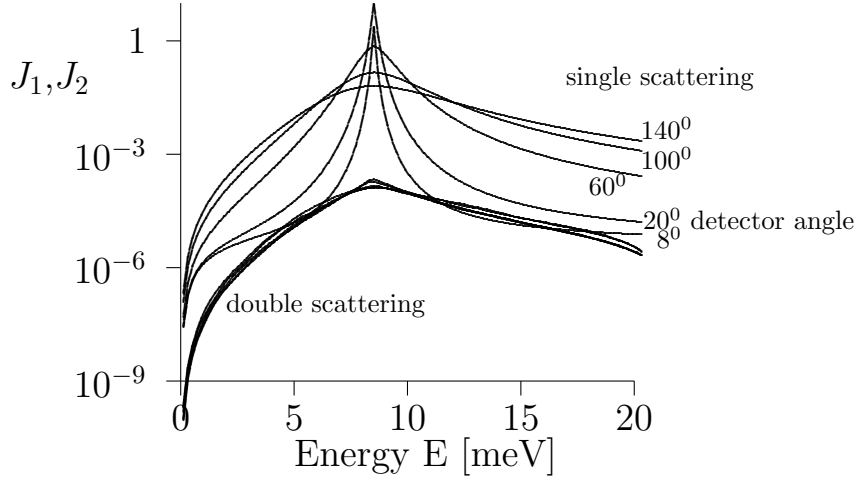


Figure 9.2: Single and double scattering in a simple only incoherently scattering model of a liquid with  $S_{inc}(Q, \omega)$  a Lorentzian with half width at half height  $DQ^2$

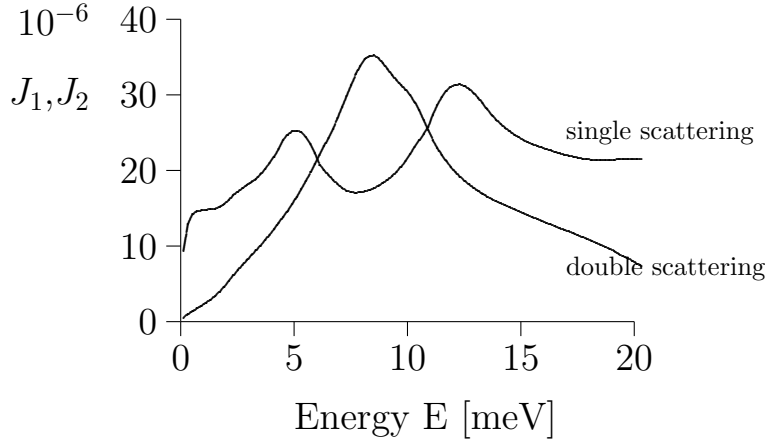


Figure 9.3: Double scattering compared with single scattering in a only coherently scattering liquid with  $S_{coh}(Q, \omega)$  given by the Lovesey model. It shows that double scattering can have a qualitative other pattern. Scattering angle  $8^\circ$ , cylindrical sample with diameter 1.4 cm, height 5 cm,  $\sigma_{abs} = 0.3b$ , wavelength  $\lambda = 3.1$  Å,  $\sigma_{coh} = 1.5b$ , calculated with the program in 9.3 on page 141

- either analytically by solution of the neutron transport equation [11] or as described by Sears (see 9.1.2 on page 125)
- or by Monte Carlo calculations as we want to describe here.

We want  $J_1^*$  = singly scattered neutrons, which we would observe if

1. there would be no absorption in the sample
2. after single scattering no further scattering would happen.

We determine  $J_1^*$ .  $J_1 \neq J_1^*$ , where  $J_1$  is the flux of singly scattered neutrons, as it is contained in the total flux, i.e. with losses by multiple scattering and absorption.

$J_1^*$  is compared to  $J_1 + J_2 + J_3 + J_4 = J_{total}$ . From this we form a correction factor

$$F_{corr}(Q, \omega) = \frac{J_1^*}{J_1 + J_2 + J_3 + J_4} \quad (9.39)$$

for the correction of the measured data to get the corrected  $J_1^{*measured}$ . This is done for every  $Q$  and  $\omega$ , i.e. also for inelastic scattering. For this one needs  $S'(Q, \omega)$  from  $\frac{d^2\sigma}{d\Omega d\omega} = \frac{\sigma_b}{4\pi} \frac{k}{k_0} S'(Q, \omega)$ .



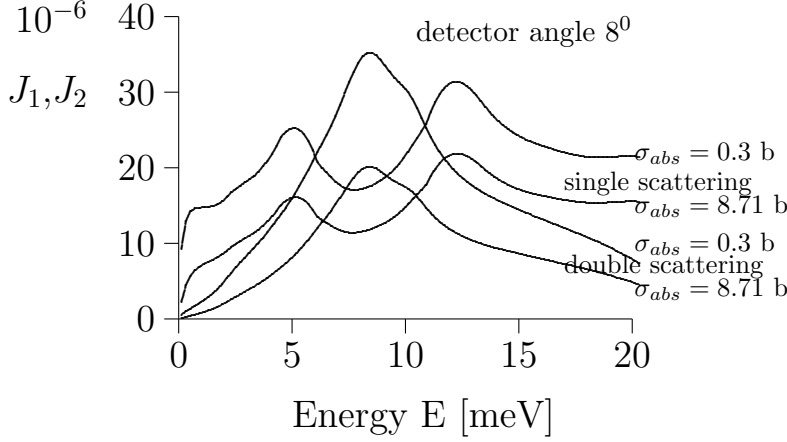


Figure 9.4: Effect of the absorption correction for samples of different absorption cross sections in a sample like that of fig.9.3. It shows that absorption only attenuates, it does not change the form of the pattern.

Generally we take  $S'(Q, \omega) = \frac{1}{\sigma_b} [\sigma_{coh} S(Q, \omega) + \sigma_{inc} S_s(Q, \omega)]$ . We need it only for  $\omega > 0$ , as  $S'(Q, -\omega) = e^{\frac{\hbar\omega}{kT}} \cdot S'(Q, \omega)$ . Our program only will be derived for  $S(|Q|, \omega)$  i.e. for isotropic  $Q$  dependence. It includes no model itself, one has to input a table of  $S(|Q|, \omega)$  and this for  $Q_{max} > 2k_0$  or better  $Q_{max} > 3k_0$ . There will be programs to write tables of  $S_{inc}(Q, \omega)$  and of  $S_{coh}(Q, \omega)$  using a model of a liquid for incoherent scattering (Nelkin-Ghatak model) and for coherent scattering (Lovesey model). An alternative method is to use the measured dynamic structure factors, which one can separate by polarization analysis and correct it by iteration.

## 9.2.4 Neutron histories

If one would proceed analogously to the real scattering process how it is in nature, one would loose many neutrons, which are not scattered or do not hit the detector. This would result in much lost computer time. To save this time one **forces** the neutrons all into a useful trace and corrects this force by proper statistical weights for the neutron. The same is then done after it arrived in the detector for the energy channels where the neutron will be forced to contribute to all energy channels. This is again corrected by a proper statistical weight. This is a very effective way to improve the variance of the method.

### 9.2.4.1 Neutron history in single scattering

1. **step.** Determine by random numbers the point where the neutron hits the sample

$$y = (2 \cdot rnd - 1) \cdot \frac{width}{2} \quad (9.40)$$

$$z = (2 \cdot rnd - 1) \cdot \frac{height}{2} \quad (9.41)$$

$$x = -\sqrt{\frac{width^2}{4} - y^2} \quad (9.42)$$

We suppose here that the neutron density is constant over the beam cross section. Then the probability is constant over the beam cross section and we can directly use the random number generator with rectangular distribution.

2. **step.** We determine the distance  $ab=D$  of the point of incidence to the boundary of the sample (see fig.9.5, if the original direction of the particle is conserved. This is done by using

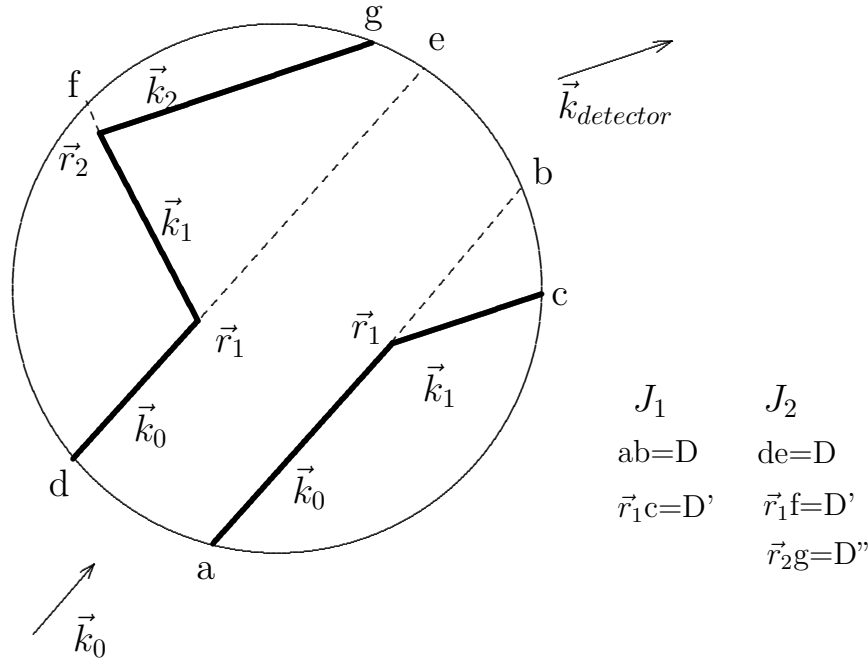


Figure 9.5: Geometry of the single and double scattering

the subroutine DIST (see 9.3 on page 142).

- 3. step.** We determine the coordinates of the first event in the sample after the travel distance  $\ell = L5$  with the random number

$$L5 = -\frac{1}{N\sigma} \ln(1 - rnd(1 - \exp(-N\sigma D))) \quad (9.43)$$

This follows from the fact that the travel distances  $\ell$  in the sample have the exponential probability density  $P(\ell)$

$$P(\ell) = \frac{N\sigma \exp(-N\sigma\ell)}{1 - \exp(-N\sigma D)} \quad (9.44)$$

with the denominator resulting from the condition that the event should happen within the sample with the probability  $p=1$ , i.e. it must be  $\int_0^D P(\ell)d\ell = 1$ . With the random number  $rnd$  between 0 and 1 as probability  $P(\ell)$  one can determine  $\ell$  from equation 9.44, which results in  $L5$  (see 9.43). This shows also an example how one can get a random number  $L5$  with exponential distribution from a random number with uniform distribution. The role of the subroutine RONE on 9.3 on page 143 is to determine the point where the neutron hits the surface and the distance  $l5sav$  to the first event point. The total cross section  $\sigma$ , which depends on the neutron energy, as the absorption changes proportional to the wavelength, is determined in the subroutine NEWV(V5) on 9.3 on page 141, which determines also the mean free path  $mfsav$  for the corresponding energy. V5 is the modulus of the wave vector of the neutron, which can change in an inelastic process. The mean free path for the incident energy is stored in VMFP0.

- 4. step.** We assume that the event at  $L5$  is a scattering event with the probability  $\frac{\sigma_{scatter}}{\sigma_{total}}$ .
- 5. step.** After this (first) scattering in the case of single scattering the neutron is forced to fly into the direction of the detector. We need the probability of this process. For the direction of

the detector one determines the resulting scattering vector  $Q$  and the scattering probability using  $S'(Q, \omega)$  by interpolation of a table of this function.

#### 9.2.4.2 Probability that the neutron arrives in the energy channel $\omega$ of the detector in angle $\vartheta$

The neutron which arrives in the energy channel  $E = E_0 + \omega$  in the detector with the angle  $\vartheta$  has then finally the probability

$$W_N(E) = A_1 \cdot B_1 \cdot C_1 \cdot D_1 \quad (9.45)$$

$$A_1 = 1 - \exp(-N\sigma(k_0)D) \quad \text{for forcing the first event on the way D} \quad (9.46)$$

through the sample to be within the sample

$$B_1 = \frac{\sigma_{scatter}(k_0)}{\sigma_{total}(k_0)} \quad \text{for forcing the first event to be scattering} \quad (9.47)$$

and not something else contained in  $\sigma_{total}$ ,  
like absorption,...

$$C_1 = \frac{\partial^2 \sigma(\vec{k}_0 \rightarrow \vec{k}_1)}{\partial \Omega \partial \omega} \frac{1}{\sigma_{scatt}(k_0)} \quad \text{because we forced the neutron at } \vec{r}_1 \quad (9.48)$$

into the solid angle 1 about the direction  $\vec{k}_1$   
with energy change  $\omega = \frac{\hbar}{2m}(k_1^2 - k_0^2)$

$$D_1 = e^{-N\sigma(k_0)D'} \quad \text{because we forced the neutron to escape} \quad (9.49)$$

i.e. to fly to the boundary of the sample  
without another event

The single scattering without absorption  $J_1^*$  is determined with the same procedure but with  $\sigma_{absorption} = 0$  and the factor  $D_1 = 1$  of eq.(9.49), because in this ideal case there cannot be another event on the way  $D'$ .

#### 9.2.4.3 Double and n-fold scattering

This process uses the same procedure as before but it includes a second event in the case of double scattering and n-1 other events in the case of n-fold scattering.

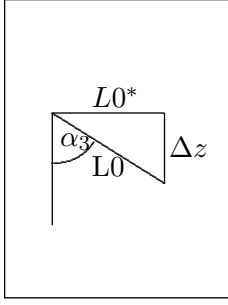
1. determine with random numbers the point where the neutron hits the sample. Here we have uniform distribution.
2. determine the point of the first event. This is exponential distribution.
3. determine  $Q$  and  $\omega_2$  uniformly distributed in  $Q, \omega$  space (but see the remarks 3 on page 137) and calculate new  $k_1$ .
4. determine  $D'$  along  $\vec{k}_1$  to the sample boundary and find the second event point  $\vec{r}_2$  within the sample (exponential distribution).
5. force the neutron into the detector and in the different energy channels.

Herewith we get the probability of the doubly scattered neutron  $W'_H(E)$

$$W'_H(E) = A_2 B_2 C_2 D_2 E_2 F_2 \quad (9.50)$$

$$A_2 = 1 - \exp(-\Sigma D) \quad (9.51)$$





$$L0^2 = (L0^*)^2 + (\Delta z)^2 \quad (9.62)$$

$$\frac{\Delta z}{L0^*} = \cot \alpha_3 \quad (9.63)$$

$$L0^2 = (L0^*)^2 (1 + \cot^2 \alpha_3) \quad (9.64)$$

$$= (L0^*)^2 \left(1 + \frac{\cos^2 \alpha_3}{\sin^2 \alpha_3}\right) \quad (9.65)$$

$$= (L0^*)^2 \frac{1}{\sin^2 \alpha_3} = \frac{(L0^*)^2}{m^2} \quad (9.66)$$

Figure 9.7: Sideview of scattering geometry of solid cylindric sample

the direction along the flight path. This depends on the sign of  $u_3$ . If  $u_3 < 0$  then one has to compare with

$$\frac{-\left(\frac{height}{2} + z\right)}{\cos \alpha_3} \quad (9.67)$$

and if  $u_3 > 0$  then one has to compare with

$$\frac{\left(\frac{height}{2} - z\right)}{\cos \alpha_3} \quad (9.68)$$

see fig.9.8. In the program in section 9.3 on page 142 the corresponding variable is RLsav. This results in the subroutine for the determination of the distance of the event point (x,y,z)

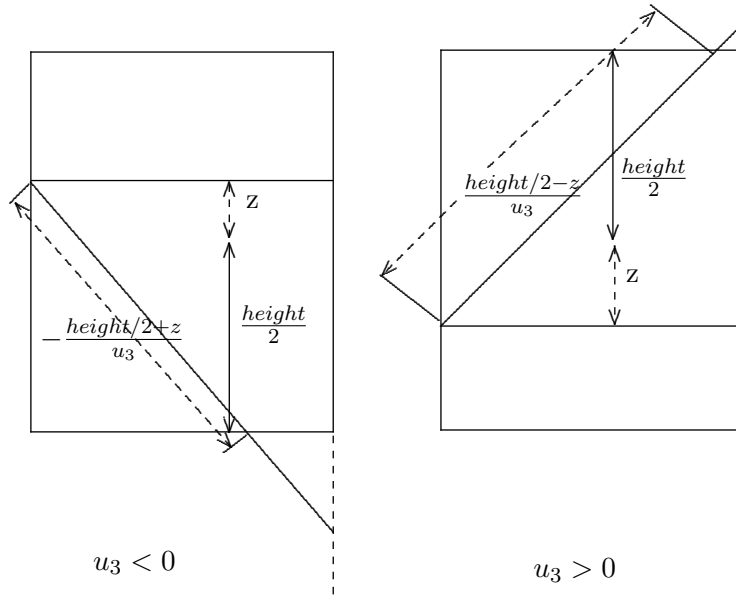


Figure 9.8: Is the way through the bottom or top area shorter than through the curved surface of the cylinder?

from the boundary of the solid cylindric sample, if the neutron has the direction with the unit vector  $(u_1, u_2, u_3)$  given in the program DIST on 9.3 on page 142, case: 2.

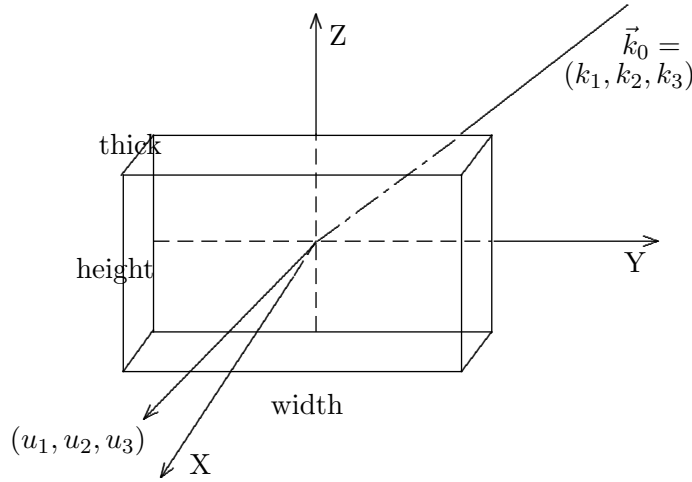


Figure 9.9: Coordinates if the sample is a flat plate

2. **Hollow cylinder** In the case of a hollow cylinder one has to look whether the neutron path traverses the hole in the cylinder and if this is the case one has to subtract the path length within this hole. In this case the program has the form given in the subroutine DIST on 9.3 on page 142, case: 3.
3. **Finite flat plate** In the case of a finite flat plate we choose the coordinate system as indicated in fig. 9.9. The x-axis is defined as perpendicular to the face of the sample bathed by the incident neutron beam. Two of the sample faces are defined by the equations  $x=0$  and  $x=\text{thick}$ . The other two faces are assumed to be perpendicular to the other two coordinate axes according to fig. 9.9. In case of oblique incidence onto the flat slab we have to select the wave vector of the neutrons  $(k_1, k_2, k_3)$  correspondingly. for flat slab geometry neutrons are considered to be incident on all of the face  $x=0$  (and only that face).  $k_1$  must then always be  $> 0$ . To find the distance of the first event point from the boundary of the sample we have to determine the distance of three surfaces in the way as it is done in figure 9.8 and take the smallest one. This results in a program given in the program DIST on 9.3 on page 142, case: 1.

#### 9.2.5.2 Different problems connected with $S(Q, \omega)$

1. **How to include elastic scattering by SIGSS(I).** The sample can scatter elastically and inelastically or quasi elastically. The elastic scattering can even be strongly modulated like a powder pattern. Think for example of hydrogen dissolved in a polycrystal. In such a case the elastic scattering can be described by SIGSS(I) which corresponds to:

$$\sigma_{scat}(q) = \sigma_{inc} + \sigma_{coh} \left( 1 + \int_{\Omega} (q) \frac{S(Q)}{4\pi} d\Omega \right) \quad (9.69)$$

$$= \sigma_{inc} + \sigma_{coh} \cdot (1 + SQPC(I)) \quad (9.70)$$

SQPC(I) can be a powder pattern normalized in such a way that the real intensity is related to the number density DENS and the cross section  $\sigma_{coh}$ , which is the coherent cross section of the inelastic scatterer, whose scattering behaviour is given by  $S(Q, \omega)$ . This cross section then determines the mean free path of the neutron in the direction  $q$ . The respective calculations are performed in the subroutine NEWV(V5) by quadratic interpolation of SIGSS(I), which is stored in the program in logarithmic form. It must be given in the same Q-step width DQsav

as the  $S(Q, \omega)$ . The number of steps is independently given by N2, which can be for example 200. One can use for SQPC(I) a measured powder pattern or one can use a description of the pattern by short range parameters ALPC1=-0.1364, ALPC2=-0.1464, ALPC3=-0.0022, and a formula describing the short range order scattering. An example can be

$$\begin{aligned} SPCT(I) = & 0.8833 * (1.0 + \frac{4.0 * ALPC1}{(Q(I) * 1.206)} * \sin(Q(I) * 1.206) + \\ & + (\frac{2 * ALPC2}{Q(I) * 1.715} * \sin(Q(I) * 1.715) + \\ & + \frac{8.0 * ALPC3}{Q(I) * 2.020} * \sin(Q(I) * 2.010)) \end{aligned} \quad (9.71)$$

This must still be normalized using the number density fraction and the cross section fraction if it has to be described by the same effective number density DENS as the inelastic scatterer. For the interpolation the values of SIGSS(I) at values of the neutron momentum  $k(I)$  nearest to the neutron momentum are  $k(I) < k < k(I+1) < k(I+2)$  have to be found similar to fig.9.12. The value of  $\ln(\text{sig}1)$ , which one needs, is then assumed to lie on the quadratic curve  $Ak^2 + Bk + C$ , which passes through the points  $\ln(\text{SIGSS}(I))$ ,  $\ln(\text{SIGSS}(I+1))$ ,  $\ln(\text{SIGSS}(I+2))$ . If  $k < k(1)$  then  $\text{sig}1 = \text{SIGSS}(1)$ , if  $k > k(N2)$  then  $\text{sig}1 = \text{SIGSS}(N2)$ .  $\text{sig}1 = \text{sig}1 + \text{sig}a * \text{kinc} / V5$  and the mean free path is simply  $\text{mfsav} = 1 / (\text{DENS} * \text{sig}1)$ . See program 9.3 on page 141 and 9.3 on page 146.

2. **Weight factor**  $\frac{S(Q, \omega)}{\langle S(Q, \omega)Q \rangle}$ : As we do not sample  $\Omega$  but  $Q$  we do not use  $\frac{\partial^2 \sigma}{\partial \Omega \partial \omega}$  but  $\frac{\partial^2 \sigma}{\partial Q \partial \omega}$ . As only  $S(Q, \omega)$  is normalized to 1 and can be used as a probability, we have to determine the normalization factor for the really used procedure.

$$\frac{\partial^2 \sigma}{\partial Q \partial \omega} = \frac{\partial^2 \sigma}{\partial \Omega \partial \omega} \frac{d\Omega}{d\theta} \frac{d\theta}{dQ} \quad (9.72)$$

$$\propto \frac{k_1}{k_0} S(Q, \omega) \cdot 2\pi \sin \theta \cdot \frac{Q}{2k_0 k_1 \sin \theta} \quad (9.73)$$

$$\propto S(Q, \omega) Q \quad \text{for constant } k_0 \quad (9.74)$$

which follows from the relations

$$Q^2 = k_0^2 + k_1^2 - 2k_0 k_1 \cos \theta \quad (9.75)$$

$$Q \frac{dQ}{d\theta} = 2k_0 k_1 \sin \theta \quad (9.76)$$

$$\frac{dQ}{d\theta} = \frac{Q}{2k_0 k_1 \sin \theta} \quad (9.77)$$

$$d\Omega = 2\pi \sin \theta d\theta \quad (9.78)$$

This shows that we finally use  $S(Q, \omega)Q$  instead of  $S(Q, \omega)$  as the distribution function and we have to normalize thus our final values by dividing it by the  $\int S(Q, \omega)Q dQ d\omega$ .  $S(Q, \omega)$  is in this case the effective function resulting from the superposition of the coherent and the incoherent part weighted with the respective cross sections.

The Monte Carlo method allows a simple way to determine this integral. The basic theorem of Monte Carlo integration is that if one picks N random points  $x_1, \dots, x_N$ , uniformly distributed in a multidimensional volume V and determines the function  $f(x_i)$  at these points, the arithmetic mean over the N points [12, 10]

$$\langle f \rangle \equiv \frac{1}{N} \sum_{i=1}^N f(x_i) \quad (9.79)$$



$$\langle f^2 \rangle \equiv \frac{1}{N} \sum_{i=1}^N f^2(x_i) \quad (9.80)$$

gives the integral of the function over the multidimensional volume by

$$\int f dV \approx \langle f \rangle V \pm V \sqrt{\frac{\langle f^2 \rangle - \langle f \rangle^2}{N}} \quad (9.81)$$

As we determine in any case  $S(Q, \omega)$  at random points  $Q$  we have just to sum all values of  $QS(Q, \omega)$  determined in this way and divide by the number of sampling points, to get the normalization which we need. It is not done for each energy channel as these are not randomly selected but it is sorted into channels of equal width. Only at the scattering process before we sort into the energy channels we sum up for each neutron and each detector  $Q7(Nplx) = Q7(Nplx) + Q \cdot S(Q, \omega)$ . At the end we use this to normalize the result by dividing through this sum. In the triple scattering case we have to divide this sum by two to get the normalization as we have then picked double as many random points, correspondingly at quadruple scattering a factor of three, as we will for each process always begin from the first scattering add then again values to the integral at the second scattering and again at the third scattering.

**3. Why uniformly distributed  $Q$  and  $\omega$  sample for  $J_2$  ?** If one proceeds strongly analogously to the natural scattering process then one should use only few neutrons in the region where  $S(Q, \omega)Q$  is small and many where it is large. Then statistics is high in the region where  $S(Q, \omega)Q$  is high and bad where it is low. Second scattering would then be good for quasi-elastic quasi-elastic scattering but bad for inelastic quasi-elastic and very bad for inelastic inelastic processes. Selecting the first  $Q, \omega$  uniformly distributed then one gets uniform precision in the whole specular region.

**4. Determination of  $Q$  and  $\omega$  with uniform distribution** Select a random  $Q$  by

$$Q = (Q_{max} - (DQ + Q_{min})) \cdot rnd + DQ + Q4 \quad (9.82)$$

then we select a random  $\omega$  as a channel number by

$$N_\omega = (int)[(2 \cdot \omega_{max} - 1) \cdot rnd + 1] \quad (9.83)$$

This determines the angle  $\vartheta$  of possible new directions on a cone with apex angle  $\vartheta$  (see fig.9.10) by

$$\hbar\omega = \frac{\hbar^2}{2m}(k_1^2 - k_0^2) \quad (9.84)$$

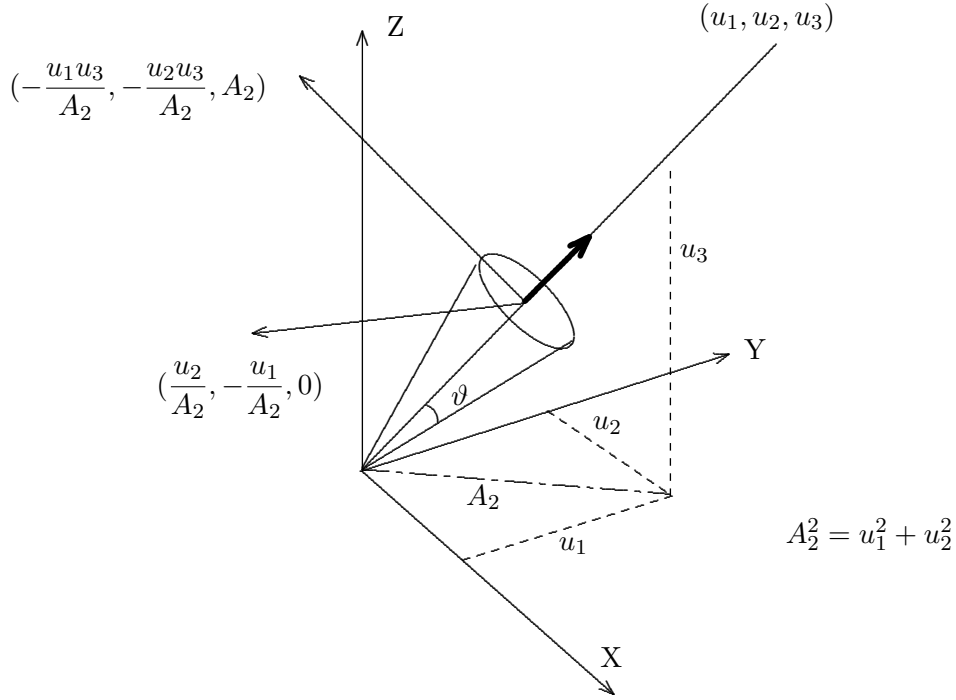
$$k_1^2 = k_0^2 + \frac{2m}{\hbar}\omega \quad (9.85)$$

$$Q^2 = k_0^2 + k_1^2 - 2k_0k_1 \cos \vartheta \quad (9.86)$$

If the original direction is given by the unit vector  $(u_1, u_2, u_3)$  we obtain a new orthonormal coordinate system with  $z'$  in the  $(u_1, u_2, u_3)$  direction and  $(-\frac{u_1 u_3}{A_2}, -\frac{u_2 u_3}{A_2}, A_2)$  as  $x'$  axis and  $(\frac{u_2}{A_2}, -\frac{u_1}{A_2}, 0)$  as  $y'$  axis.  $A_2^2 = u_1^2 + u_2^2$ .

Out of this possible directions we select one final direction by determining a  $\varphi$  randomly out of an uniform distribution using

$$\varphi = 2 \cdot \pi \cdot rnd \quad (9.87)$$

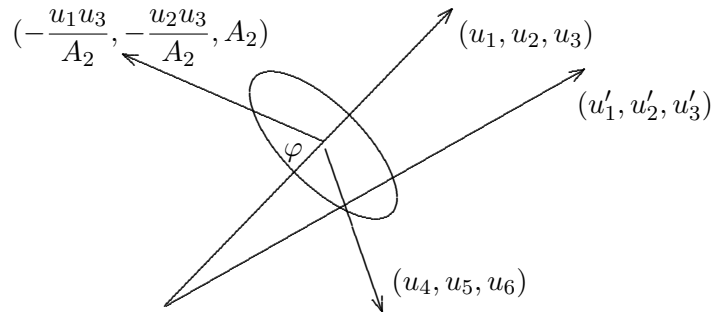
Figure 9.10: Visualization of the angle  $\vartheta$  and the coordinate system to determine  $\varphi$ 

with the random number  $rnd$ . This gives a vector (see figure 9.11)

$$\begin{pmatrix} u_4 \\ u_5 \\ u_6 \end{pmatrix} = \cos \varphi \begin{pmatrix} -\frac{u_1 u_3}{A_2} \\ -\frac{u_2 u_3}{A_2} \\ A_2 \end{pmatrix} + \sin \varphi \begin{pmatrix} \frac{u_2}{A_2} \\ -\frac{u_1}{A_2} \\ 0 \end{pmatrix} \quad (9.88)$$

Finally we get the new neutron direction as the vector

$$\begin{pmatrix} u'_1 \\ u'_2 \\ u'_3 \end{pmatrix} = \cos \vartheta \begin{pmatrix} u_1 \\ u_2 \\ u_3 \end{pmatrix} + \sin \vartheta \begin{pmatrix} u_4 \\ u_5 \\ u_6 \end{pmatrix} \quad (9.89)$$

Figure 9.11: How  $\varphi$  is determined

**5. Determination of  $S(Q, \omega)$  by quadratic interpolation from a table.** We need a fast process to obtain many  $S(Q, \omega)$  values for very different  $Q, \omega$ , which we can get from a table by quadratic interpolation from a table of logarithms of  $S(Q, \omega)$ . The value we need is then calculated by exponentiation. This is done by the program SINT(WPR, Q) 9.3 on page 144.

The logarithmic values in the table are  $I(Q_1)$ ,  $I(Q_2)$  and  $I(Q_3)$  at the table positions  $Q_1, Q_2$  and  $Q_3$  (see fig.9.12). If  $Q$  is between  $Q_1$  and  $Q_2$ , we determine

$$u = \frac{(Q - (Q_1 - 1) \cdot DQ - Q_{min})}{DQ} \quad (9.90)$$

$$2 \cdot A = (I(Q_1, \omega) - 2 \cdot I(Q_2, \omega) + I(Q_3, \omega)) \quad (9.91)$$

$$2 \cdot B = (-3 \cdot I(Q_1, \omega) + 4 \cdot I(Q_2, \omega) - I(Q_3, \omega)) \quad (9.92)$$

$$C = I(Q_1, \omega) \quad (9.93)$$

$$S(Q, \omega) = \exp(A \cdot u^2 + B \cdot u + C) \quad (9.94)$$

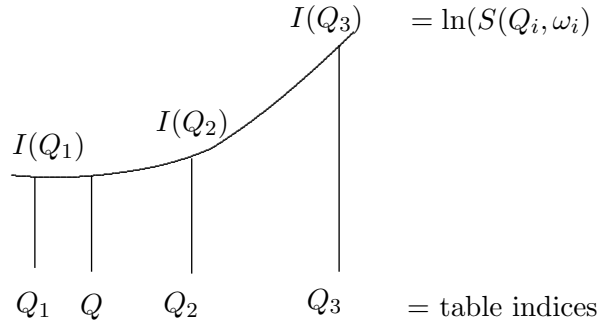


Figure 9.12: For quadratic interpolation of the logarithm of  $S(Q, \omega)$ . If  $Q$  or  $\omega$  are beyond the bound of the array for  $Q$  and  $W$ , the values of  $S(Q, \omega)$  are put to zero. The table is stored as the logarithms at the beginning of the program. The size of the table must be so that  $(NQ-1)DQ+Q_{min} > 3k_0$  with  $k_0 =$  incident wave vector.

### 9.2.5.3 Monte Carlo program with spin dependent scattering

We distinguish coherent and incoherent scattering. The incoherent scattering is scattering where phase relations do not play a role, either because they are lost in the scattering process (nuclear spin incoherent scattering) or because they average out (isotope incoherent scattering). In tables one finds the total cross sections for coherent  $\sigma_{coh}$  and incoherent  $\sigma_{inco}$  scattering. Inelastic scattering is described by the dynamical structure factors, also for coherent and incoherent scattering  $S_{coh}(Q, \omega)$  and  $S_{inco}(Q, \omega)$ . The coherent and the isotope incoherent scattering have no influence on the spin of the neutron. The nuclear spin incoherent scattering flips the spin with the probability  $\frac{2}{3}$ . In this way the incoherent scattering exchanges neutrons between the channel of the flipped neutrons and the unflipped neutrons. The more often a neutron is scattered the more it is then depolarized. Four fold scattering is much less polarized than single scattering etc. (See fig.9.13)

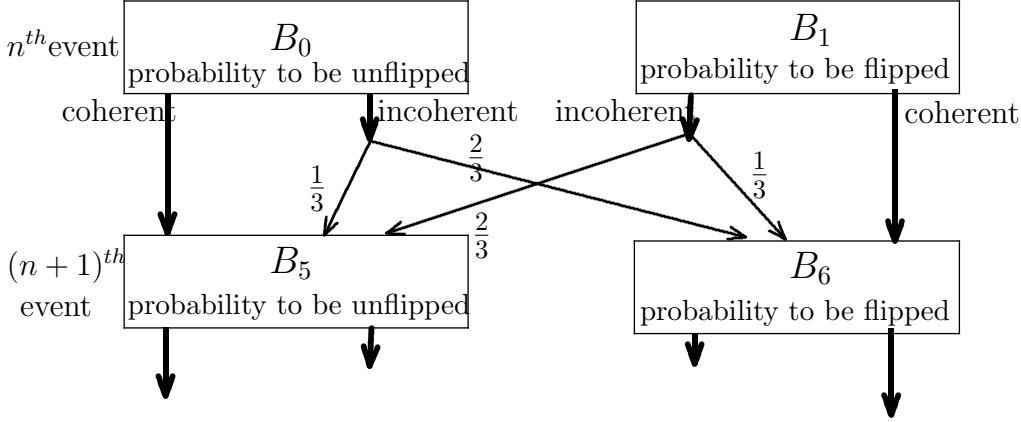
### 9.2.5.4 How one can determine a standard deviation?

The energy channels have a common neutron history and are therefore statistically not independent. Then the standard deviation cannot be determined from the variance of neighbouring points.

**Initially:**  $B_0=1, B_1=0$

probability to scatter coherently:  $p_{coh} = \frac{\sigma_{coh}}{\sigma_T} \cdot Q \cdot S_{coh}$

probability to scatter incoherently:  $p_{inc} = \frac{\sigma_{inc}}{\sigma_T} \cdot Q \cdot S_{inc}$



**After this process:**

$$B_5 = p_{coh} B_0 + p_{inc} \left( \frac{1}{3} B_0 + \frac{2}{3} B_1 \right)$$

$$B_6 = p_{coh} B_1 + p_{inc} \left( \frac{1}{3} B_1 + \frac{2}{3} B_0 \right)$$

Figure 9.13: To describe the spin flip behaviour of the scattering process with coherent and spin incoherent scattering

It could be determined by running the program with another random sequence. One can also in a further array sum up the squares of the  $W_H(E)$  and with this determine the variance for each channel. One needs

$$S(I, Nplx) = \sum_{numberofneutr.} W_H(E) \quad (9.95)$$

$$S_2(I, Nplx) = \sum_{numberofneutr.} W_H^2(I) \quad (9.96)$$

We get

$$\Delta S(I, 0) = \pm \sqrt{(S_2(I, 0) - S(I, 0)^2 / nrun1) / (nrun1 - 1) / nrun1} \quad (9.97)$$

$$\Delta S(I, 1) = \pm \sqrt{(S_2(I, 1) - S(I, 1)^2 / nrun1) / (nrun1 - 1) / nrun1} \quad (9.98)$$

With higher multiplicities one has to include the normalisation factor  $P9=Q7(Nplx)$  2 on page 136. For  $Nplx > 1$   $Nplx-1$  is the multiplicity of the scattering. For  $Nplx > 1$  one determines the error by

$$\Delta S(I, Nplx) = \sqrt{\frac{s^2}{n}} = \frac{nrun2}{P9} \sqrt{\frac{(S_2(I, Nplx) - S^2(I, Nplx))}{nrun2}} (nrun2 - 1) nrun2 \quad (9.99)$$

For different  $Nplx > 1$  the  $P9$  is given by

$$Nplx = 2 \quad P9 = Q7(Nplx) = \langle S(Q, \omega) \cdot Q \rangle \quad (9.100)$$

$$Nplx = 3 \quad P9 = \frac{Q7(3) \cdot Q7(3)}{4nrun2} \quad (9.101)$$

$$Nplx = 4 \quad P9 = \frac{Q7(4)Q7(4)Q7(4)}{27 \cdot nrun2 \cdot nrun2} \quad (9.102)$$

### 9.3 Example Monte Carlo multiple scattering program in C.

```

#include <stdio.h>
#include <string.h>
#include <math.h>
#include <stdlib.h>
#include <malloc.h>
#include <fcntl.h>
#include <sys\ types.h>
#include <sys\ stat.h>
#include <io.h>
#include <conio.h>
#include "nrutil.h"
#define NP1 41
#define NP2 4

static float    xsav,ysav,zsav,width,height;
static float    thick,siga,sigs,sigt,mfsav,DLsav;
static float    DENS,Kinc,l5sav,b0sav,b1sav,Qmin;
static float    DQsav,NQmax,L2,L3,I5,K5;
static float    sigs1,sigt1,VMFP0;
static float    **SI,**SK,*SIGSS;
static int      igeom;
static long     N2;

void NEWV(float V5)
{

    float  SIGA1,A,B,C;
    double dummy,U;
    long int  IV5;

    SIGA1=siga*Kinc/V5;
    IV5=(int)(V5/DQsav);
    if (IV5<N2) goto drei;
    sigs1=(float)exp(SIGSS[N2]);
    goto zwei;
drei:  if (IV5>0) goto eins;
        sigs1=(float)exp(SIGSS[1]);
        goto zwei;
eins:  if (IV5>(N2-2)) IV5=N2-2;
        U=(V5-IV5*DQsav)/DQsav;
        A=(SIGSS[IV5]-2*SIGSS[IV5+1]+SIGSS[IV5+2])/2;

```

```

        B=(-3*SIGSS[IV5]+4*SIGSS[IV5+1]-SIGSS[IV5+2])/2;
        C=SIGSS[IV5];
        dummy=A*U*U+B*U+C;
        sigs1=(float)exp(dummy);
zwei:    sigt1=sigs1+SIGA1;
        mfsav=1/DENS/sigt1;
        return;
}

```

```

void DIST(float P1, float P2, float P3)

```

```

{
    float A1,A2,A3,L1,L7,L8;
    double dummy,Y1,dummy1;
switch(igeom) {
    case 1:
        if (P1<0) L1= -xsav/P1;
        if (P1==0) L1= (float)1.0e+06;
        if (P1>0) L1= (thick-xsav)/P1;
        if (P2<0) L2= (-width/2-ysav)/P2;
        if (P2==0) L2= (float)1.0e+06;
        if (P2>0) L2= (width/2-ysav)/P2;
        if (P3<0) L3= (-height/2-zsav)/P3;
        if (P3==0) L3= (float)1.0e+06;
        if (P3>0) L3= (height/2-zsav)/P3;
        L8=L1;
        if (L2<L8) L8=L2;
        if (L3<L8) L8=L3;
        DLsav=L8;

        break;
    case 2:
        A1=xsav*P1+ysav*P2;
        A2=P1*P1+P2*P2;
        A3=width*width/4-xsav*xsav-ysav*ysav;
        dummy= A1*A1+A2*A3;
        DLsav= (-A1+(float)sqrt(dummy))/A2;
        if (P3<0) L8= (-height/2-zsav)/P3;
        if (P3==0) L8=(float)1.0e+06;
        if (P3>0) L8=(float)(height/2-zsav)/P3;
        if (L8<DLsav) DLsav=L8;

        break;
    case 3:
        A1=xsav*P1+ysav*P2;
        A2=P1*P1+P2*P2;
        A3=width*width/4-xsav*xsav-ysav*ysav;
        dummy= A1*A1+A2*A3;
        L1 = (-A1+(float)sqrt(dummy))/A2;
        L2 = (float)0.0;
        L3 = (float)0.0;
        dummy = sqrt(A2);

```

```

        Y1 = (ysav*P1- xsav*P2)/dummy;
        Y1 = fabs(Y1);
        if (Y1 > thick/2) goto first;
        if (P1*xsav+P2*ysav > 0) goto first;
        L2=(float)(2*sqrt(width*width/4-Y1*Y1)/dummy);
        DLsav = L1-L2;
        dummy1=xsav*xsav+ysav*ysav-Y1*Y1;
        L3=(float)((sqrt(dummy1)-sqrt(thick*thick/4-Y1*Y1))/dummy);
        if (P3<0) L7= (-height/2-zsav)/P3;
        if (P3>0) L7= (height/2-zsav)/P3;
        if (P3 == 0) L7= (float)1.0e+06;
        if (L7<L1) DLsav=L7-L2;
        if (L7<L3) goto third;
        if (L7<(L2+L3)) goto secon;
        goto fourth;
secon:    DLsav=L3;
          goto second;
third:    DLsav=L7;
second:   L2=(float)0.0;
          goto fourth;
first:    DLsav=L1;
          if (P3<0) L8= (-height/2-zsav)/P3;
          if (P3==0) L8=(float)1.0e+06;
          if (P3>0) L8=(float)(height/2-zsav)/P3;
          if (L8<DLsav) DLsav=L8;
fourth:
          break;
          }
        return; }

void RONE(float U1, float U2, float U3, float K1, float K2, float K3)
{

    void    DIST(float P1, float P2, float P3);
    long c=RAND_MAX;
    float rara;
    double dummy;
        rara=rand();
        rara=rara/c;
        ysav = width * (2 * rara - 1) / 2;

        rara=rand();
        rara=rara/c;
        zsav = height * (2 * rara - 1) / 2;

        dummy= width * width /4 - ysav * ysav;
        xsav = (float)(-sqrt(dummy));
        if (igeom == 1) xsav=0;
        DIST(U1,U2,U3);
        dummy=DENS * DLsav * sigt;
        b0sav=(float)(1-exp(-dummy));

```



```

    b1sav=(float)0.0;

    rara=rand();
    rara=rara/c;
    dummy=1-rara*b0sav;
    l5sav=(float)((-VMFP0)*log(dummy));
    b0sav=b0sav/sigt;
    if (igeom==1) L2=0;
    if (igeom==1) L3=0;
    if (l5sav<L3) L2=0;
    xsav=xsav+(l5sav+L2)*K1;
    ysav=ysav+(l5sav+L2)*K2;
    zsav=zsav+(l5sav+L2)*K3;
    return;
}

void SINT(int WPR,float Q)

{
    int IQ0,IQ1,IQ2;
    double U,A,B,C;

    if (Q<Qmin) {
        I5=0;
        K5=0;
    } else {
        IQ0=(int)((Q-Qmin)/DQsav+1);
        if (IQ0>NQmax) {
            I5=0;
            K5=0;
        }
        else { if (IQ0>NQmax-2) IQ0=(int)(NQmax-2);
        IQ1=IQ0+1;
        IQ2=IQ0+2;
        U=(double)(Q-(IQ0-1)*DQsav-Qmin)/DQsav;
        A=(double)(SI[IQ0][WPR]-2*SI[IQ1][WPR]+SI[IQ2][WPR])/2;
        B=(double)(-3*SI[IQ0][WPR]+4*SI[IQ1][WPR]-SI[IQ2][WPR])/2;
        C=(double)SI[IQ0][WPR];
        I5=(float)(exp(A*U*U+B*U+C));
        A=(double)(SK[IQ0][WPR]-2*SK[IQ1][WPR]+SK[IQ2][WPR])/2;
        B=(double)(-3*SK[IQ0][WPR]+4*SK[IQ1][WPR]-SK[IQ2][WPR])/2;
        C=(double)SK[IQ0][WPR];
        K5=(float)(exp(A*U*U+B*U+C));
        }
    }
    return;
}

```

```

void main(void)

```

```

{
    float K1,K2,K3,M1,M2,M3,M4,M5,M6,DW,Qmax;
    float U1,U2,U3,U4,U5,U6,Z1,Z2,Z3,flag;
    float E1,T,hoverT,T1,T2,T3,T4,T5,T9,H0;
    float D,PI,sigic,sigco,sigcot,siga0,A2,K,Q2max;
    double XX,YY,O2;
    float Winc,Wmax,W5,W,P5,V5,C5,Q,Q2,Q3,Q6;
    float B5,B6,phi,B3,B2,B,B4,V6,dummy;
    int IDet,W5PR,Nw,Ndet,WPR,frstdet,Detstp,N0PR;
    int Mulmx,Nrun1,Nrun2;
    int Nplx,Iplx,Iel,I1PR,I,M7,W9PR,NNeutr,i,k,result;
    float **V,**S,**F,*Q1,*QSsum,*A9,*SQPC;
    long nrl,nq1h,nq2h,nd1h,nd2h,ns1h,ns2h,nv1h,nv2h,I7,J;
    long c = RANDMAX;
    float rara,W3,F1,F2,O1,O3,O4,O5,O6,O7,S3;
    static double Vinit[NP1][NP2]= {
0.000, 0.000, 0.000, 0.000,    0.380, 0.050, 0.048, 0.079,    0.480, 0.060, 0.050, 0.100,
0.570, 0.130, 0.060, 0.100,    0.670, 0.115, 0.064, 0.101,    0.770, 0.156, 0.100, 0.120,
0.860, 0.124, 0.106, 0.143,    0.960, 0.177, 0.158, 0.180,    1.050, 0.193, 0.168, 0.236,
1.140, 0.191, 0.200, 0.274,    1.240, 0.194, 0.217, 0.289,    1.330, 0.220, 0.251, 0.355,
1.420, 0.298, 0.324, 0.495,    1.520, 0.322, 0.437, 0.558,    1.610, 0.443, 0.585, 0.767,
1.700, 0.638, 0.852, 1.037,    1.790, 1.016, 1.245, 1.387,    1.880, 1.670, 1.843, 1.740,
1.970, 2.688, 2.134, 1.841,    2.060, 2.757, 2.043, 1.728,    2.140, 1.945, 1.565, 1.418,
2.230, 1.351, 1.235, 1.210,    2.320, 1.047, 1.040, 1.070,    2.400, 0.863, 0.903, 0.976,
2.480, 0.792, 0.779, 0.882,    2.890, 0.700, 0.750, 0.800,    3.190, 0.800, 0.784, 0.846,
3.340, 0.930, 0.927, 0.974,    3.410, 1.050, 0.960, 1.026,    3.540, 1.111, 0.957, 1.007,
3.610, 1.120, 0.952, 1.000,    3.740, 1.120, 0.974, 1.047,    4.140, 1.034, 1.098, 1.139,
4.240, 1.027, 1.080, 1.033,    4.290, 0.986, 1.060, 1.138,    4.420, 0.905, 1.034, 1.078,
4.500, 0.881, 1.000, 0.966,    4.540, 0.883, 0.980, 1.007,    6.000, 1.000, 1.000, 1.000,
9.990, 1.000, 1.000, 1.000,    100.0, 1.000, 1.000, 1.000, };

    /* FILE *fh2; */
    nrl=1;
    nv1h=41;
    nv2h=4;
    ns1h=105;
    ns2h=5;
    nd1h=80;
    nd2h=80;
    nq1h=64;
    nq2h=10;
    N2=10;
    SI=matrix(nrl,nd1h,nrl,nd2h);
    SK=matrix(nrl,nd1h,nrl,nd2h);
    V=matrix(nrl,nv1h,nrl,nv2h);
    S=matrix(nrl,ns1h,nrl,ns2h);
    F=matrix(nrl,ns1h,nrl,ns2h);
    Q1=vector(nrl,nq1h);
    QSsum=vector(nrl,nq2h);
    A9=vector(nrl,nq2h);
    SIGSS=vector(nrl,N2);
    SQPC=vector(nrl,N2);

```

```

for (i=1;i<=41;i++)      {
    for (k=1;k<=4;k++)    {
        V[i][k]=(float)Vinit[i-1][k-1];
    }
}
for (i=1;i <=N2;i++)      {
    SQPC[i]=0;
    /*here one can give a powder spectrum
    or something similar determining
    a cross section dependence on Q (see 1 on page 135)
    One has to increase the dimension N2*/

    sigic=(float)0.0;      /*SIG icoh in barn*/
    sigco=(float)2.0;      /*SIG coh in barn*/
    for (i=1;i<=N2;i++)    {
        SIGSS[i]=sigic+sigco*(1+SQPC[i]);
        SIGSS[i]=(float)log(SIGSS[i]);
    }

    result=scanf("%d",&Ndet); /* number of detectors */
    if (result==0) Ndet=8;    /*allows to enter Ndet by a file with <<*/
    frstdet=1;               /*number of first detector*/
    Detstp=1;                /*step */
    igeom=2;                 /*1=flat plate, 2=cylinder, 3=hollow cylinder */

/* if ((fh2=fopen("C:/ARBEIT/MCDEV/SQT468.DAT","r"))==0) /* In case you want */
    nerror("datafile sqt468 not found\n"); /* to read V[i][k] from */
for (k=1;k<=41;k++)      { /* a file you can use */
    for (i=1;i<=4;i++)    { /* code similar to this */
        fscanf(fh2,"%f", &V[k][i]);
    } /*
/* for (i=1;i<=41;i++)    {
    printf("%1.2f\ t%1.3f\ t%1.3f\ t%1.3f\ n", V[i][1],V[i][2],V[i][3],V[i][4]);
} */

Nrun1=1000;               /* number of neutrons for single sc.*/
Nrun2=5000;               /* number of neutrons for multiple */
width=(float)1.4;         /*width in cm or outer diameter of cyl. */
height=(float)5.0;        /*height in cm*/
thick=(float)0.4;
/* thickness of plate or inner diameter of hollow cyl.*/
E1=(float)125.0;          /*Einst energ*/
T=400;                    /*Temperat of sample*/
siga=(float)0.3;          /*SIGABS*/
siga0=siga;               /* store siga locally during reduced scattering calc. */
Qmin=(float)0.00001;      /*Qmin */
DQsav=(float)0.2;         /*DQ in A-1*/
NQmax=60;                 /* NQ */
DW=(float)0.2;            /*DW in meV */
Nw=60;                    /* NW */
DENS=(float)0.04007;      /*DENS */
Kinc=(float)2.0268;        /* modulus of Kinc */

```

```

K1=1; /* KX */
K2=0; /* KY */
K3=0; /* KZ */
A9[1]=8; /* angles of detectors */
A9[2]=20;
A9[3]=40;
A9[4]=60;
A9[5]=80;
A9[6]=100;
A9[7]=140;
A9[8]=160;
A9[9]=2;
Mulmx=2; /* Mulmx= total number of scatters*/
D=(float)0.5; /*Diffusion constant in sodium */
PI=(float)3.141593;
I5=0;
K5=0;
for (I7=1;I7<=nd1h;I7++) {
    for (J=1;J<=nd2h;J++) {
        XX=I7*DQsav+Qmin;
        XX=XX*XX*D*D;
        YY=J*DW*J*DW+XX*XX;
        SI[I7][J]=(float)(XX/YY/PI);
    }
}
T9=(float)(9.32214*T/600);
/* 9.322=kT/M for sodium, M=molecular mass in g*/
for (i=1;i<=NQmax;i++) {
    W3=Qmin+(i-1)*DQsav;
    for (k=1;k<=41;k++) {
        if (W3>=V[k][1]) I1PR=k;
    }
    F1=V[I1PR][2]; /* sodium 400 K */
    F2=V[I1PR+1][2]; /* sodium 800 K */
    S3=(F2-F1)/(V[I1PR+1][1] - V[I1PR][1])*(W3-V[I1PR][1])+F1;
    O1=T9*W3*W3/S3;
    O2=W3*3.3;
    O3=(float)(1-3*sin(O2)/O2-6*cos(O2)/O2/O2+6*sin(O2)/O2/O2/O2);
    O4=3*T9*W3*W3+E1*O3;
    O2=O4-O1;
    O5=(float)(.5*sqrt(PI)/sqrt(fabs(O2)));
    for (J=1;J<=Nw;J++) {
        O6=(J-1)*(J-1)*DW*DW;
        O2=(J-1)*DW*O5*(O6-O4);
        O7=(float)(S3/4*O1/O5/(O2*O2+(O6-O1)*(O6-O1)));
        SK[i][J]=O7;
    }
}

```

```

/* for (J=1;J<=Nw;J++)      {
    for (i=1;i<=NQmax;i++)    {
        printf("%f\ n%",SK[i][J]);
    }
}                               */

for (J=1;J<=Nw;J++)          {
    for (i=1;i<=NQmax;i++)    {
        if (SK[i][J] <=0) { SK[i][J]=(float)(-20.0); }
        else { SK[i][J]=(float)log(SK[i][J]); }

        if (SI[i][J] <=0) { SI[i][J]=(float)(-20.0); }
        else { SI[i][J]=(float)log(SI[i][J]); }
    }
}

IDet=firstdet;
H0=(float).481902;              /* 2m/h [A-2(meV)-1] */
Qmax=(float)((NQmax-1.00001)*DQsav+Qmin);
hoverT=(float)(11.6027/T);      /* h/(2pi kT) */
anf0: Winc=(float)(Kinc*Kinc/H0);

    printf("%s\ t", "Detector Nr.");
    printf("%d\ t", IDet);
    printf("%s\ t", "with angle ");
    printf("%1.3f\ n", A9[IDet]);

Wmax=(Nw-1)*DW+Winc;
K=(float)sqrt(K1*K1+K2*K2+K3*K3);
K1=K1/K;                        /* unit vector */
K2=K2/K;                        /* direc. of neutron */
K3=K3/K;
Iel=(int)(Winc/DW+1);
siga=siga0;

for (I=1;I<=5;I++)              {
    QSsum[I]=0;
}

Z1=(float)cos(PI/180*A9[IDet]); /* unit vector */
Z2=(float)sin(PI/180*A9[IDet]); /* in detector dir.*/
Z3=0;
B=K1*Z1+K2*Z2+K3*Z3;
T5=(float)(180/PI*acos(B));      /* sattering angle T5 */

for (I=1;I<=ns2h;I++)           {
    for (J=1;J<=ns1h;J++)        {
        S[J][I]=0;
        F[J][I]=0;
    }
}

```

```

/* loop for reduced, single, double, and higher multiple scattering */

for (Nplx=0;Nplx<=Mulmx;Nplx++)
{
    V5=Kinc;
    if (Nplx< 1)      { siga=0.0;
                       }
                       else
                       { siga=siga0;
                       }

    NEWV(V5);
    sigt=sigt1;
    sigs=sigs1;
    sigcot=sigs1-sigic;
    xsav= -width/2;

/* cylinder case: zero in center, radius=width/2 */
    if (igeom==1) xsav=(float)0.0;
    ysav=0;
    zsav=0;
    U1=K1;
    U2=K2;
    U3=K3;
    DIST(K1,K2,K3);
    VMFP0=mfsav;
        if (Nplx<=1)  {   NNeutr=Nrun1;
                       }   else {   NNeutr=Nrun2;
                       }

/* here the new neutrons begin */

for (N0PR=1;N0PR<=NNeutr;N0PR++)
{
    anf:   V5=Kinc;
           U1=K1;
           U2=K2;
           U3=K3;
           RONE(U1,U2,U3,K1,K2,K3);
    if (Nplx<2) goto anf3;
        Iplx=Nplx-1;
    anf1:   M7=0;
           /* Now for double and higher scat. we select */
    anf2:   M7=M7+1;
           /* a (Q,W) with uniform distribution*/
    if (M7>1000) goto anf;
        rara=rand();
        rara=rara/c;
        Q=(Qmax-(DQsav+Qmin))*rara+DQsav+Qmin;
        W5=(float)(2*Nw-1);
        rara=rand();
        rara=rara/c;

```

```

W5PR=(int)(W5*rara+1);
W=(float)(W5PR-Nw)*DW;
P5=V5*V5+H0*W;
if (P5<0) goto anf2;
P5=(float)sqrt(P5);
C5=(P5*P5+V5*V5-Q*Q)/2/V5/P5;
if (C5-1>0) goto anf2;
if (C5+1<0) goto anf2;
WPR=(int)(abs(W5PR-Nw)+1);
SINT(WPR,Q);
if (W<=0)
{
K5=(float)(K5*exp(-hoverT*W));
I5=(float)(I5*exp(-hoverT*W));
}
QSSum[Nplx + 1]=QSSum[Nplx + 1]+Q*(sigic*I5+sigco*K5)/(sigic+sigco);
B5=Q*(sigco*K5*b0sav+sigic*I5/3*(b0sav+2*b1sav));
B6=Q*(sigco*K5*b1sav+sigic*I5/3*(b1sav+2*b0sav));
b0sav=B5;
b1sav=B6;
rara=rand();
rara=rara/c;
phi=rara*2*PI;
B3=(float)sqrt(1-C5*C5);
B2=C5;
if (U3>=1)
{
U1=(float)(B3*cos(phi));
U2=(float)(B3*sin(phi));
U3=B2;
} else {
A2=(float)sqrt(1-U3*U3);
U6=(float)(cos(phi)*A2);
U4=(float)(-cos(phi)*U3*U1/A2+sin(phi)*U2/A2);
U5=(float)(-cos(phi)*U3*U2/A2-sin(phi)*U1/A2);
U1=B2*U1+B3*U4;
U2=B2*U2+B3*U5;
U3=B2*U3+B3*U6;
}
V5=P5;
NEWV(V5);

```

**/\*We found a the neutron direction (U1,U2,U3), modulus V5 \*/**

```

DIST(U1,U2,U3);
B4=(float)(1-exp(-DENS*DLsav*sigt1));
rara=rand();
rara=rara/c;
l5sav=(float)(-mfsav*log(1-rara*B4));
b0sav=b0sav*B4/sigt1;
b1sav=b1sav*B4/sigt1;
xsav=xsav+l5sav*U1;

```



```

        ysav=ysav+l5sav*U2;
        zsav=zsav+l5sav*U3;
        Iplx=Iplx-1;
if (Iplx>0) goto anf1;
anf3:   V6=V5;
        DIST(Z1,Z2,Z3);
if (Nplx==0) DLsav=(float)0.0;

/* Loop over positive energy transfers */

for (WPR=1;WPR<=Nw;WPR++)
    {
        W=(WPR-1)*DW;
        V5=(float)sqrt(V6*V6+H0*W);
        NEWV(V5);
        Q6=V5*Z1-V6*U1;
        Q2=V5*Z2-V6*U2;
        Q3=V5*Z3-V6*U3;
        Q=(float)sqrt(Q6*Q6+Q2*Q2+Q3*Q3);
if (Q>Qmax) continue;
        SINT(WPR,Q);
        if (WPR==1)
            { flag=sigcot-sigco;
              }
            else {
              flag = 0;
            }
        B5=(float)(exp(-DENS*DLsav*sigt1)*V5/V6/4/PI);
        B6=(float)(exp(-DENS*DLsav*sigt1)*V5/V6/4/PI);
        B5=B5*((sigco*K5+flag)*b0sav+sigic*I5/3*(b0sav+2*b1sav));
        B6=B6*((sigco*K5+flag)*b1sav+sigic*I5/3*(b1sav+2*b0sav));
        W5=V5*V5/H0;
        W5PR=(int)((W5-Winc)/DW+Iel+0.5);
if (W5PR>ns1h) continue;
        S[W5PR][Nplx+1]=S[W5PR][Nplx+1]+B5;
        F[W5PR][Nplx+1]=F[W5PR][Nplx+1]+B6;
    }

/*C Loop over negative energy transfers */

if (Nw<=1) goto schluss;
for (WPR=2;WPR<=Nw;WPR++)
    {
        W= -(WPR-1)*DW;
        P5=V6*V6+H0*W;
if (P5<=0) continue;
        V5=(float)sqrt(P5);
        NEWV(V5);
        Q6=V5*Z1-V6*U1;
        Q2=V5*Z2-V6*U2;

```

```

Q3=V5*Z3-V6*U3;
Q=(float)sqrt(Q6*Q6+Q2*Q2+Q3*Q3);
if (Q>Qmax) continue;
SINT(WPR,Q);
B5=(float)(exp(-DENS*DLsav*sigt1)*V5/V6/4/PI);
B6=(float)(exp(-DENS*DLsav*sigt1)*V5/V6/4/PI);
B5=B5*(sigco*K5*b0sav+sigic*I5/3*(b0sav+2*b1sav));
B6=B6*(sigco*K5*b1sav+sigic*I5/3*(b1sav+2*b0sav));
B5=(float)(B5*exp(-hoverT*W));
B6=(float)(B6*exp(-hoverT*W));
W5=V5*V5/H0;
W5PR=(int)((W5-Winc)/DW+Iel+0.5);
if (W5PR>ns1h) continue;
S[W5PR][Nplx+1]=S[W5PR][Nplx+1]+B5;
F[W5PR][Nplx+1]=F[W5PR][Nplx+1]+B6;
    }
    }
schluss;
    }

W9PR=Nw+Iel;
for (I=1;I<=W9PR-1;I++)
    {
        W=(I-Iel)*DW+Winc;
        P5=(float)sqrt(H0*W);
        Q2=(Kinc*K1-P5*Z1);
        Q3=(Kinc*K2-P5*Z2);
        Q6=(Kinc*K3-P5*Z3);
        Q2=Q2*Q2+Q6*Q6+Q3*Q3;
        Q=(float)sqrt(Q2);
        M1=S[I][1]/Nrun1;
        M2=F[I][1]/Nrun1;
        M3=S[I][2]/Nrun1;
        M4=F[I][2]/Nrun1;
        M5=S[I][3]/QSSum[3];
        M6=F[I][3]/QSSum[3];
if (QSSum[4]==0) goto finis;
        T1=S[I][4]*4*Nrun2/QSSum[4]/QSSum[4];
        T2=F[I][4]*4*Nrun2/QSSum[4]/QSSum[4];
if (QSSum[5]==0) goto finis;
        dummy=QSSum[5]*QSSum[5]*QSSum[5];
        T3=S[I][5]*27*Nrun2*Nrun2/dummy;
        T4=F[I][5]*27*Nrun2*Nrun2/dummy;
if (M1==0.) continue;
finis:  printf("%2.7f\t",W);
        printf("%2.7f\t",Q);
        printf("%e\t",M1);
        printf("%e\t",M2);
        printf("%e\t",M3);
        printf("%e\t",M4);
        printf("%e\t",M5);

```

```

        printf("%e\t",M6);
if (QSsum[4]==0) goto fin1;
        printf("%e\t",T1);
        printf("%e\t",T2);
if (QSsum[5]==0) goto fin1;
        printf("%e\t",T3);
        printf("%e\t",T4);
fin1:   printf("\ n");
        }

IDet=IDet+Detstp;
if (IDet<Ndet+frstdet) goto anf0;
printf("%s\t", "width=");
printf("%2.3f\t",width);
printf("%s\t", "height=");
printf("%2.3f\t",height);
printf("%s\t", "Einsteinen.=");
printf("%3.3f\t",E1);
printf("%s\t", "sigic=");
printf("%2.3f\t",sigic);
printf("%s\t", "sigco=");
printf("%2.3f\t",sigco);
printf("%s\t", "sigabs=");
printf("%2.3f\t",siga);
printf("%s\t", "densty=");
printf("%1.4f\t",DENS);
printf("%s\t", "DQ=");
printf("%1.3f\t",DQsav);
printf("%s\t", "NQmax=");
printf("%1.3f\t",NQmax);
printf("%s\t", "DW=");
printf("%1.3f\t",DW);
printf("%s\t", "Nw=");
printf("%d\t",Nw);
printf("%s\t", "Kinc");
printf("%1.5f\t",Kinc);
printf("%s\t", "igeom=");
printf("%d\t",igeom);

free_matrix(SI,nrl,nd1h,nrl,nd2h);
free_matrix(SK,nrl,nd1h,nrl,nd2h);
free_matrix(S,nrl,ns1h,nrl,ns2h);
free_matrix(F,nrl,ns1h,nrl,ns2h);
free_matrix(V,nrl,nv1h,nrl,nv2h);
free_vector(Q1,nrl,nq1h);
free_vector(QSsum,nrl,nq2h);
free_vector(A9,nrl,nq2h);
free_vector(SIGSS,nrl,N2);
free_vector(SQPC,nrl,N2);
}

```

This program contains all modules which you can use to build a program after your own wishes. For example one could construct a program with a liquid in a container, the container described by a hollow cylinder with elastic scattering given by SIGSS(I), the liquid by a solid cylinder and the scattering described by  $S_{coh}(Q, \omega)$  and  $S_{inc}(Q, \omega)$ . The Code can certainly be simplified by a routined programmer. But normally one has then to buy it and can only run it on one machine or similar conditions. This program you can improve yourself and change it after your wishes.

# Bibliography

- [1] E.L.Slaggie in IAEA Symposion on neutron thermalisation and reactor spectra, Michigan, Sm 96/53 (1967) p.311
- [2] I.A. Blech, B.L.Averbach, Phys.Rev. **137** (1965) A1113
- [3] Bacon, Thermal neutron scattering, 3rd edition, Oxford 1979
- [4] A.W.Hewat, Acta Cryst. **A 35** (1979) 248
- [5] V.F.Sears, Advances in Physics **24** (1975) 1-45
- [6] F.G.Bischoff, Ph.D. Thesis, Rensselaer Polytechnic Institute 1970
- [7] F.G.Bischoff, M.L.Yeater, W.E.More; Nuc. Science and Eng. **48** (1972) 266
- [8] J.R.D.Copley Comp. Phys. Commun. **7** (1974) 289
- [9] M.W.Johnson, DISCUS, a computer program for the calculation of multiple scattering effects in inelastic neutron scattering experiments, AERE-R7682, Harwell, Oxfordshire 1974.
- [10] W.H.Press, S.A.Teukolsky, W.T.Vetterling, B.P.Flannery, Numerical Recipes in C, Cambridge University Press 1994.
- [11] Egelstaff, Poole, Experimental Neutron thermalization, Pergamon 1969, appendix.
- [12] J.M. Hammersley, D.C. Handscomb, Monte Carlo methods, Methuen & Co, London, John Wiley & Sons New York 1964
- [13] E.D. Cashwell, C.J. Everett, A practical manual on the Monte Carlo Method for random walk problems, Pergamon Press, New York 1959



## Chapter 10

# On the question of the origin for a spherical average in scattering experiments

### 10.1 Abstract

When calculating the scattered intensity from a system in which the scattering units are randomly orientated (such as in glasses or polymers), the scattering is partly due to pair correlation between different scattering units. This pair correlation function is determined by the probability of the relative separation of the centers of the two scattering units. The dependence of the scattering on the choice of the scattering unit center is determined by details of the scattering experiment.

### 10.2 Introduction

The investigation of the arrangement of atoms by scattering experiments (neutrons, X-rays) is a powerful tool for determining the details of a wide variety of systems on an atomic scale. As pointed out by van Hove [1] the scattering intensity is determined by correlation functions. It is the Fourier transform in space and time of the pair correlation function which determines the scattering vector and energy dependence of the scattered particles.

A large number of scattering systems consist of a random collection of scattering units (e.g. glasses, polymers) where to a first approximation, each scattering unit itself can be considered as a rigid structure while the relationship between various scattering units is determined by the properties of the system. Consider  $N$  atoms with positions given by  $\mathbf{r}_i$  with  $\mathbf{r}_i$  also being a function of time. The scattering intensity of this collection of atoms is determined by

$$I = \sum_{i,j} b_i b_j e^{i\mathbf{k} \cdot (\mathbf{r}_i - \mathbf{r}_j)} = \left| \sum_i b_i e^{i\mathbf{k} \cdot \mathbf{r}_i} \right|^2 \quad (10.1)$$

where  $\mathbf{k}$  is the scattering vector and  $b_i$  is the scattering strength of the  $i$ th atom. (The formulation here is given in terms of a neutron scattering experiment). The sum in equation 10.1 is carried out over all atoms of the system.

The atoms of a given scattering unit can be grouped together. Taking the center of the  $\nu$ th

---

<sup>0</sup>first published in: K.U.Neumann, O.Schärpf, K.R.A.Ziebeck, Physica B **180** & **181** (1992) 817

scattering unit to be given by  $\mathbf{R}_\nu$ , the scattered intensity takes the form

$$I = \left| \sum_{\nu} \left( \sum_{i \in SU_{\nu}} b_i e^{i\mathbf{k} \cdot (\mathbf{r}_i - \mathbf{R}_{\nu})} \right) e^{i\mathbf{k} \cdot \mathbf{R}_{\nu}} \right|^2 \quad (10.2)$$

with the sum over  $\nu$  being carried out over all scattering units in the system. It has to be noted that the scattering unit center  $\mathbf{R}_\nu$  is arbitrary and it is not yet fixed by any physical considerations. The scattering unit is now described by a scattering unit structure factor which has the form

$$F_{\nu}(\mathbf{k}, \mathbf{R}_{\nu}) = \sum_{i \in SU_{\nu}} b_i e^{i\mathbf{k} \cdot (\mathbf{r}_i - \mathbf{R}_{\nu})} \quad (10.3)$$

In terms of this structure factor the scattered intensity can be written as

$$I = \sum_{\nu, \nu'} F_{\nu}(\mathbf{k}, \mathbf{R}_{\nu}) \cdot F_{\nu'}^*(\mathbf{k}, \mathbf{R}_{\nu'}) e^{i\mathbf{k} \cdot (\mathbf{R}_{\nu} - \mathbf{R}_{\nu'})} \quad (10.4)$$

The scattering intensity in 10.4 is evaluated in a two stage process. First, the scattering strength of a single scattering unit is determined, and second the total scattering is obtained by summing over all the scattering units of the system.

For a scattering system such as molecules in solution, the orientation of the scattering units is random. Therefore an average has to be carried out over all possible orientations of the scattering units. With the spherical average indicated by a bar, this results in

$$\begin{aligned} I &= \sum_{\nu} \overline{|F_{\nu}(\mathbf{k}, \mathbf{R}_{\nu})|^2} \\ &+ \sum_{\nu, \nu', \nu \neq \nu'} \overline{F_{\nu}(\mathbf{k}, \mathbf{R}_{\nu}) \cdot F_{\nu'}^*(\mathbf{k}, \mathbf{R}_{\nu'})} e^{i\mathbf{k} \cdot (\mathbf{R}_{\nu} - \mathbf{R}_{\nu'})} \\ &= N \left( \overline{|F_{\nu}(\mathbf{k}, \mathbf{R}_{\nu})|^2} - \left| \overline{F_{\nu}(\mathbf{k}, \mathbf{R}_{\nu})} \right|^2 \right) \\ &+ \left| \overline{F_{\nu}(\mathbf{k}, \mathbf{R}_{\nu})} \right|^2 \sum_{\nu, \nu'} e^{i\mathbf{k} \cdot (\mathbf{R}_{\nu} - \mathbf{R}_{\nu'})} \end{aligned} \quad (10.5)$$

Two averages appear in 10.5, namely  $\overline{F_{\nu}^2}$  and  $\overline{F_{\nu}}^2$ . Evaluating the averages with the assumption that all orientations are equally likely and that the orientations of different scattering units are not correlated, results in

$$\begin{aligned} \overline{F_{\nu}(\mathbf{k}, \mathbf{R}_{\nu}) \cdot F_{\nu'}^*(\mathbf{k}, \mathbf{R}_{\nu'})} &= \sum_{i, j \in SU_{\nu}} b_i b_j \overline{e^{i\mathbf{k} \cdot ((\mathbf{r}_i - \mathbf{R}_{\nu}) - (\mathbf{r}_j - \mathbf{R}_{\nu}))}} \\ &= \frac{1}{4\pi} \sum_{i, j \in SU_{\nu}} b_i b_j \int_0^{\pi} d\theta \sin \theta \int_0^{2\pi} d\phi e^{ik|\mathbf{r}_i - \mathbf{r}_j| \cos \theta} \\ &= \sum_{i, j \in SU_{\nu}} b_i b_j \frac{\sin k|\mathbf{r}_i - \mathbf{r}_j|}{k|\mathbf{r}_i - \mathbf{r}_j|} \end{aligned} \quad (10.6)$$

$$\begin{aligned} \overline{F_{\nu}(\mathbf{k}, \mathbf{R}_{\nu})} &= \sum_{i \in SU_{\nu}} b_i \overline{e^{i\mathbf{k} \cdot (\mathbf{r}_i - \mathbf{R}_{\nu})}} \\ &= \sum_{i \in SU_{\nu}} b_i \frac{\sin k|\mathbf{r}_i - \mathbf{R}_{\nu}|}{k|\mathbf{r}_i - \mathbf{R}_{\nu}|} \end{aligned} \quad (10.7)$$

It has to be pointed out that the averaged scattering unit structure factor has an explicit dependence on the center of the scattering unit. The center which appears in  $\overline{F_{\nu}}$  can be shown



to be the point around which the scattering unit is rotated for the calculation of the spherical average. Different choices of  $\mathbf{R}_\nu$  result in different average structure factors. As the averaged scattering unit structure factor determines the intensity of short range order reflections (which, for the existence of long range order between scattering units results in Bragg reflections) the effects of  $\mathbf{R}_\nu$  are physically observable. The question arises as to which point  $\mathbf{R}_\nu$  should be chosen for the evaluation of the spherical average.

In addition to the scattering vector dependence of the scattering, the intensity will also be a function of energy transfer to or from the probing particle. While the  $\mathbf{k}$  dependence of the scattering is determined by spatial correlations, the  $\omega$  dependence is related to the Fourier transform in time of the correlation function [1, 2].

The question of the scattering unit center and the time resolution of the experiment with which the system is probed are intimately connected. It is argued here that for some experiments the proper choice of the scattering unit center is given by the "scattering center" (similar to the center of mass in mechanics) of the scattering unit with the scattering center defined as

$$\mathbf{R}_\nu^c = \frac{\sum_i b_i \mathbf{r}_i}{\sum_i b_i} \quad (10.8)$$

The significance of this point is readily identified by investigating the average scattering unit structure factor. It can be shown that only for this reference point, the average is carried out without allowing interference to occur between the various configurations of the scattering unit in the angular average. It is argued that this reference point has to be chosen whenever the angular motion of the scattering units takes place on a time scale which is outside the time window of the experiment.

The  $\omega$  range of the neutron scattering experiment is determined by experimental factors such as the energy of the neutron and the temperature of the system. These energy scales limit the possible energy gains and losses in the scattering experiment and they are related by the detailed balance factor. In addition the uncertainty principle relates the uncertainty in  $\omega$  as given by  $\Delta\omega$  to the lower limit in time  $\Delta t$  with  $\Delta\omega \cdot \Delta t \approx 1$ . This imposes a lower limit time resolution of  $\Delta t \approx 1/\Delta\omega$  on the experiment. It is pointed out that it is the time scale of rotations in the scattering units in the spherical average 10.7 which determines the evaluation of the average. If the rotations of the scattering units take place on a time scale longer than  $\Delta t$ , the average has to take into account the phases of the scattered waves. For glasses and polymers the time scale of rotation is much longer than the instrumental time resolution  $\Delta t$ , and consequently the average has to be carried out using 10.8 as the point of rotation of the scattering unit in 10.7 [3]. This choice insures that the average is carried out without interference between the various positions of the scattering unit in the spherical average.

### 10.3 Discussion

The investigation of the dependence of the averaged scattering unit structure factor has led to the conclusion that the choice of the scattering unit center  $\mathbf{R}_\nu$  will determine the experimentally observable intensity in scattering experiments. While it is naively expected that this point should be determined solely by the properties of the system under investigation, a more detailed analysis reveals that it is related to the details of the experiment with which the system is probed. The experimental setup determines the time window in which interference effects are observable experimentally. For systems with a mismatch of system time window (as determined by the slow rotation of large scattering units) and the experimental time window, it is the experimental arrangement which determines  $\mathbf{R}_\nu$ . The scattering center of the scattering unit is identified as the only point for which no interference can occur in the averaging process 10.5.



# Bibliography

- [1] L. van Hove, Phys. Rev. 95 (1954) 249
- [2] K.R.A. Ziebeck, J.G. Booth, P.J. Brown, H. Capellmann, J.A.C. Bland. Z.Phys. B 48 (1982) 233
- [3] O.Schärpf, B.Gabrys, D.G.Peiffer. ILL-Report 90SC26T (1990)